

Magnetogenetic Control of Cellular Functions
using Biofunctionalized Magnetic Nanoparticles
Inside Living Cells

Dissertation

Presented to the department of Biology/Chemistry,
Osnabrück University
in partial fulfillment of the requirements of the degree of

'Doctor rerum naturalium'

Marie Kappen

Osnabrück

December 2022

Summary

Remote control of cellular functions using magnetic forces offers unique opportunities in fundamental research and biomedical applications. The intracellular application of functionalized magnetic nanoparticles (MNP) provides the possibility to spatiotemporally increase the concentration of specific target proteins and thus locally enhance protein interactions (space mode magnetogenetic control). These can be exploited for site-specific activation of signaling pathways, for instance by increasing reaction turnovers or by inducing phase separation. However, designing MNPs suitable for effective, unbiased manipulation of target proteins inside cells has remained challenging.

This work aimed to design biofunctionalization of MNPs for space mode magnetic manipulation of downstream signaling effector proteins at the plasma membrane and in the cytosol. For initial proof-of-concept experiments, application of previously established magnetic intracellular stealth MNPs based on natural ferritin (MagIcS) as a highly biocompatible protein cage were explored. As these exhibited limitations in terms of magnetic properties, a new MNP design was implemented based on a single-step surface coating of synthetic magnetic core nanoparticles with green fluorescent protein (GFP) fused to the iron binding site of Mms6 from magnetotactic bacteria (syMagIcS). In doing so, a stable biocompatible coating was created, which simultaneously enables site-specific recruitment of proteins of interest to the magnetic nanoparticle surface. The direct functionalization of synthetic magnetic cores yielded optimized magnetic properties and offers the possibility to customize core sizes and thus further enhance magnetic responsiveness. Exploiting the coherent functional design of MagIcS and syMagIcS, applicability for intracellular magnetogenetic use in space mode was explored at different levels. Efficient *in situ* MNP biofunctionalization with intracellular effector proteins by direct capturing via α GFP nanobodies was achieved and intracellular translocation by using magnetic field gradients was obtained for both types of MNP. Activation of G-proteins at the plasma membrane was achieved by magnetogenetic translocation of MNP-bound catalytically active region of GEF proteins, with syMagIcS clearly showing superior performance as compared to MagIcS. Furthermore, liquid-liquid phase separation of the intrinsically disordered protein Dvl2, which plays an important role in Wnt signaling pathways, was induced by space mode magnetogenetics. With this tool at hand, we aim to understand the activation and regulatory mechanisms of these signaling pathways in more detail and test hypotheses by manipulating the signaling activation. These proof-of-concept experiments highlight the exciting possibilities of space mode magnetic manipulation to explore the spatiotemporal regulation of cellular processes in living cells and open new avenues in regenerative medicine.

Contents

I. Introduction	1
1. Regulation of cellular functions	3
1.1. Principles of protein-protein interaction	4
2. Remote control of cellular functions	17
2.1. Optical control	18
2.2. Magnetic control	21
II. Aims	25
III. Strategy	29
3. Space mode magnetogenetic control of cellular functions	31
4. Engineering of nanoparticles for space mode magnetic remote control	33
4.1. Magnetic properties	35
4.2. Colloidal stability in aqueous solutions	39
4.3. Biofunctionalization	42
4.4. Intracellular nanoparticle diffusion	46
4.5. Engineered biofunctionalized magnetic nanoparticles	48
4.6. Magnetic devices for spatiotemporal control of magnetic nanoparticles	54
5. Model system - Small GTPases	57
5.1. Ras	59
5.2. Rac	64
5.3. The Role of Rho and Ras GTPases in Axon Growth, Guidance, and Branching	69
6. Model systems - Wnt signaling	71
6.1. Dishevelled	73
IV. Results & Discussion	77
7. Magnetic Remote Activation of small GTPase HRas using MagIcS	79
7.1. Non-fluorescent MNPs with intracellular stealth properties (xMagIcS)	79

7.2. <i>In vitro</i> MNP-GEF activity of biofunctionalized MNPs	80
7.3. Reengineered FRET biosensors for probing GTPase activation	82
7.4. Magnetic remote activation of the small GTPase HRas	86
8. Semi-synthetic Magnetic Intracellular Stealth Nanoparticles	89
8.1. Synthesis and <i>in vitro</i> characterization of maghemite core particles	91
8.2. One-step biofunctional coating of MCP	92
8.3. <i>In vitro</i> characterization of syMagIcS	93
8.4. <i>In cellulo</i> characterization of syMagIcS	96
8.5. Functionalization and site-specific targeting	102
9. Magnetic remote activation of small GTPase Rac1 using syMagIcS	107
9.1. <i>In cellulo</i> MNP-GEF activity	108
9.2. Magnetic remote activation of Rac1	110
9.3. Cellular response resulting upon magnetic remote activation of Rac1	113
10. Magnetic Remote Manipulation of LLPS to activate Wnt signaling pathway	117
10.1. Characterization of Dvl2 liquid-liquid phase separation	119
10.2. Magnetic remote manipulation of Dvl2 liquid-liquid phase separation	125
11. Conclusion	135
V. Appendix	141
12. Materials and methods	143
12.1. Biofunctionalized magnetic nanoparticles	143
12.2. <i>In vitro</i> MNP characterization	147
12.3. <i>In cellulo</i> experiments	148
13. References	151
14. Abbreviations	185
15. Acknowledgements	189
16. Curriculum Vitae	191
17. Declaration	193

I Introduction

1 | Regulation of cellular functions

Cellular functions are regulated in time and space. Cells are continuously sensing their environment and further process the collected information via signaling pathways. This enables the cell to respond to environmental changes at the cellular level and to control cellular functions such as migration, cell division and cell death. These cellular responses are enabled by the ability to sense physical changes and chemical signals, and to process these external signals. The extrinsic signals are diverse, such as chemical messengers (e.g. hormones, neurotransmitters, growth factors), mechanical forces, electrical impulses, light, and changes in pH or temperature.¹⁻⁶ This signal, mediated by a specific receptor, stimulates an intracellular transduction process. The signal transduction consists of the reception of a signal, the transduction of the signal via effector molecules, and results in a cellular response, e.g. altered metabolism, gene expression, or cell shape (see Fig. 1.1).⁶⁻⁸

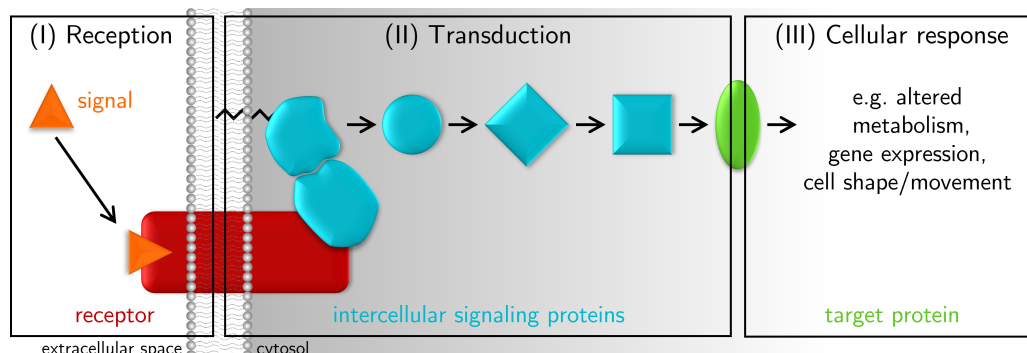


Figure 1.1.: **Schematic illustration of the key stages for signal transduction.** The signal transduction consists of the reception of a signal, the transduction of the signal, and the resulting cellular response.

Cells are equipped with a limited number of signaling pathways for signal transduction, the specificity of which depends on the strict spatiotemporal regulation of signaling molecules. Crucial for cellular information processing is the regulation of protein concentration in space and time and thus the availability of interaction partners and the site-specific control of protein-protein interactions. In this context, both the spatial control of signaling components and their activities at specific subcellular locations as well as the temporal control through precise timing of different reaction dynamics, e.g. transient, persistent or oscillatory, is crucial.⁹⁻¹³ Cellular mechanics that control changes in localized protein concentration, and thereby regulate cellular functions, include scaffold recruitment and release of signaling pathway components, translocation of transcription factors from the cytosol to the nucleus, release of mitochondrial proteins into the cytosol, and endocytic recycling of

plasma membrane proteins.^{12,14–16} Abnormal activation or disruption of signaling pathways can cause a variety of cellular dysfunctions, resulting in diseases, such as cancer.^{17–24}

The ability to interfere and manipulate cell signaling and signal transduction, and thereby to remotely control cellular functions provides a powerful tool for numerous applications in basic research as well as exciting prospects in biomedicine.²⁵ This allows, for example, testing the hypothesis of activation mechanisms or the development of new therapeutic approaches. In order to be able to control cellular functions, it is important to understand how their regulation takes place. This allows to identify where the decisions for the initiation of cellular functions are triggered, which further stations and switches are passed through and at which sites intervention is possible and which are suitable targets to manipulate regulation in a targeted manner.

1.1. Principles of protein-protein interaction

In the cell, proteins and other biomolecules form a highly complex interaction network, called the interactome. Signaling pathways are part of this complex network that transmits and processes information. This enables the maintenance of homeostatic equilibrium or a spatial and temporal response to stimuli in order to make decisions for cellular responses.^{26–33} Protein-protein interactions are influenced by biophysical properties, such as the concentration of the interaction partners, the affinity for each other, and also the availability and accessibility of the interaction partners. The interaction between two interaction partners can be described thermodynamically using the law of mass action. In equation 1.2 the interaction of two partners A and B for forming a complex AB is described, with association rate constant (k_a) and dissociation rate constant (k_d).



The equilibrium dissociation constant (K_D) and the concentrations of the interaction partners are key factors to determine the concentration of the complex. Thus, the regulation of the protein concentration is crucial for the control of the signaling pathways.³⁴

$$K_D = \frac{[A]_{eq}[B]_{eq}}{[AB]_{eq}} \quad (1.2)$$

with

$$K_D = \frac{k_d}{k_a} \quad (1.3)$$

For the interaction kinetics, k_a and k_d are important to describe the rate of association and dissociation of the complex. The equilibrium dissociation constant (K_D) is often used for quantifying the binding affinity. The relation of the rate constants to K_D is shown in equation 1.3. Equilibrium concentrations are indicated by square brackets ($[]_{eq}$).³⁵ Protein-protein interactions can be permanent and form a stable protein assembly, but they can also have a transient character and be temporally constrained, dynamically changing in response to intrinsic and extrinsic stimuli.^{27,33,36} In addition, a large fraction of protein-protein interactions are defined by spatial constraints. Protein-protein interactions can be regulated by protein relocalization to specific cellular structures, such as membranes, nucleus, and cytoplasm, or organelles. The initialization and signaling response are often spatially located at different cellular regions.³⁷⁻⁴⁴ Besides concentration and thus interaction with other biomolecules, environmental conditions such as temperature, redox conditions, osmolarity have an influence on protein activity.⁴⁵

Common mechanisms for controlling protein activity include covalent modification and allosteric regulation. Thus, post-translational modifications (PTMs) are an important component of cellular signal transduction. Examples of PTMs include the addition of chemical functional groups (e.g. phosphoryl, alkyl, glycosyl, and acyl groups) or small proteins (e.g. ubiquitin, SUMO), or altering the chemical properties of amino acids through oxidation, deimination, and deamidation.^{46,47} In signaling pathways, phosphorylation represents the most common type of covalent modification. In this process, protein kinases catalyze the transfer of terminal phosphate from ATP to an amino acid of the protein. Target amino acids for phosphorylation are mainly amino acids with a hydroxyl group in their side chain: tyrosine, threonine and serine.^{6,46,47} The addition of the negatively charged phosphate can lead to a conformational change that can increase or decrease the activity of the target protein. In addition, phosphorylation can also serve as a docking site for interaction partners or a marker for proteosomal degradation. Reversibly, phosphatases cleave the phosphate group on amino acids.^{6,8} The duration of the phosphorylated state is significant for the signaling response. Many of the proteins phosphorylated in signal transduction are themselves protein kinases, so activation results in a phosphorylation cascade.^{6,48}

Protein structures are not rigid. Proteins undergo a spectrum of conformational changes from their initial folding to their degradation. The functionality of proteins is based on reversible, dynamic conformations for their activity and interaction with other molecules.^{26,26,45,49} Conformational changes that regulate protein activity can be inter-domain or intra-domain conformational changes. In inter-domain conformational changes, the structurally ordered domain itself undergoes no to little structural changes, and is modulated through steric blocking, e.g. by autoinhibitory domains. Intra-domain conformational changes can range from structural order-disorder transitions locally near active sites to structuring of intrinsically disordered domains due to binding to interaction partners.⁴⁹ In addition to structured proteins, such as enzymes, transmembrane proteins,

and signaling domains, intrinsically disordered proteins (IDPs) and regions (IDRs) perform crucial biological functions, particularly in regulation of signaling pathways and cellular processes, including the regulation of transcription, translation, and the cell cycle. As signaling and regulatory proteins and regions, IDPs or IDRs often cooperatively interact intra- or intermolecularly with or act as nodes in protein interaction networks.^{50,51} IDRs lack a stable secondary and tertiary structure due to fewer aromatic and aliphatic amino acids. These aromatic and aliphatic amino acids typically form the core of folded domains, resulting in a single folded, energetically favorable structure. In contrast, IDRs adopt various energetically similar favorable conformations.^{13,51–58}

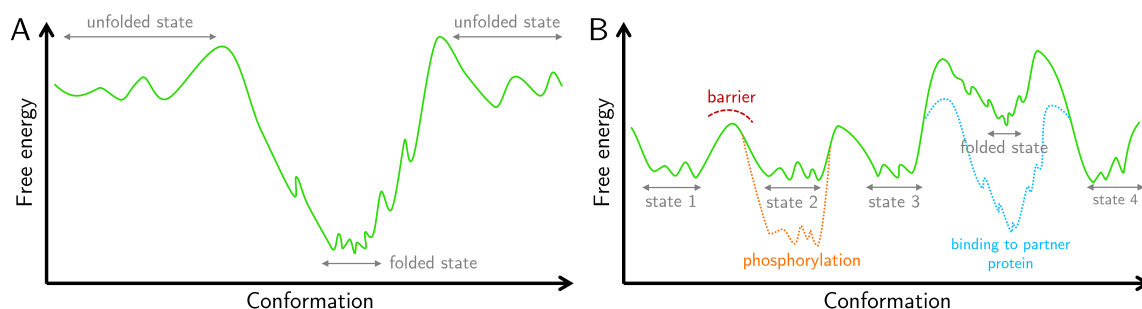


Figure 1.2.: (A) Schematic diagram of the free energy of a folded protein. The folded state consists of an ensemble of structurally related states. (B) Schematic diagram of the free energy of a hypothetical intrinsically disordered protein. Four disordered (unfolded) states in free solution separated by shallow energy barriers for rapid exchange. Multiple shallow minima and no dominant overall minimum indicate high structural flexibility. Post-translational modifications such as phosphorylation may stabilize one of the states relative to the others. A folded state is present in the energy landscape but is stabilized only upon binding to a partner protein. Adapted from Bhattacharya et al. 2019.⁵⁹

Their properties enable IDPs to regulate cellular signaling processes. IDRs can be partially ordered by binding to an interaction partner. The energetic barriers between bound and free states are low due to the lack of a stable structure, allowing IDRs to act as reversible, highly sensitive sensors.^{51,59,60} IDRs of signaling and regulatory proteins often contain multiple conserved sequence motifs for interaction with nucleic acids or proteins. This, along with some degree of flexibility, allows them to interact promiscuously with multiple targets and thus act as a central hub in signaling networks. IDPs support the dynamic assembly of ternary and higher-order complexes and the integration of different signaling pathways.^{51,61} The transient and dynamic interaction of IDPs with partners results in a dynamic regulatory network in which IDPs exchange binding partners and compete for binding to key hub proteins, which are often present in limited quantities. Post-translational modifications of IDPs and variation of pathway components through alternative mRNA splicing allow for fine-tuning of these interactions and orchestration of signaling.^{51,60}

1.1.1. Signal transduction

The reception and processing of signals is mediated by different receptors, which can be divided into two categories: intracellular receptors and cell surface receptors. In contrast to intracellular receptors, in the case of cell surface receptors the signal molecules (ligands) do not have to pass through the plasma membrane, they can also be large and hydrophilic molecules.⁴⁸

Membrane-anchored cell surface receptors include for example ligand-gated ion channels, enzyme-linked receptors, and protein-coupled receptors.⁴⁸ Ligand-gated ion channels regulate the ion flux across cell membranes. The activity of these channels is regulated by the binding of a ligand to the channel. The reaction is rapid and takes a few milliseconds. The membrane-spanning hydrophilic channel allows ions to pass through the membrane without contacting the hydrophobic core of the phospholipid bilayer.^{48,62,63} Enzyme-linked receptors are linked to enzymes, which they activate, or act as enzymes themselves when activated. In terms of structure, the class of enzyme-linked receptors is heterogeneous. They consist of a single-pass transmembrane protein with an extracellular ligand-binding site and an intracellular catalytic domain or enzyme-binding site, usually protein kinases.^{48,64} Binding of the ligand to the extracellular domain activates or inhibits enzyme activity, and the duration of the reaction is on the order of minutes to hours. Many enzyme-coupled receptors have tyrosine kinase activity. Often, binding of the ligand results in a conformational change of the receptor subunit to the active kinase form. This leads to autophosphorylation or phosphorylation of tyrosine residues on specific proteins, which initiates a downstream signaling cascade, resulting in a cellular response.^{48,64} Binding of the ligand to the extracellular region of a protein-coupled receptor leads to activation of the associated protein resulting in downstream signaling. Stimulation of protein-coupled receptors leads to responses that last seconds to minutes.^{48,62,63} Upon activation, enzyme- and protein-coupled receptors transduce a signal into the inside of the cell. In the process, cascades of intracellular signaling proteins are activated. Some of these signaling proteins transduce, amplify, or propagate the signal. Other signaling proteins integrate signals from different signaling pathways. In this process, these signaling proteins often behave as switches by being transiently activated by phosphorylation or GTP binding. Modular binding domains of signaling proteins allow the formation of functional signaling complexes and thus complex protein assemblies in signaling networks.⁴⁸

G proteins represent a common signaling hub and act as molecular switches.⁴⁸ G proteins can switch between an inactive guanosine diphosphate (GDP)-bound and active guanosine triphosphate (GTP)-bound form.⁶⁵⁻⁶⁷ Upstream guanine nucleotide exchange factors (GEFs) activate G proteins by catalyzing the exchange of GDP for GTP. The intrinsic ability to hydrolyze GTP to GDP is enhanced by GTPase-activating proteins (GAPs).^{6,65} G proteins include trimeric G proteins and monomeric G proteins, also called small GTPases. Trimeric

G proteins consist of a α -, β - and a γ -subunit, small GTPases consist of a single polypeptide that forms a subunit analogous to the α -subunit of trimeric G proteins.^{48,68,69} Trimeric G proteins are involved in protein-coupled receptor signaling. G protein-coupled receptors (GPCRs) are a class of cell surface receptors, with common structure and signal transduction mechanism.^{6,65} GPCRs consist of a peptide with seven membrane-spanning regions and are associated with a trimeric G protein.^{48,62,63} Upon GPCR signaling, the receptor functions as a GEF. Binding of the ligand to the extracellular region of the receptor results in activation of the G protein and thus dissociation of the α -subunit from the $\beta\gamma$ -subunit complex. Both the α -subunit and $\beta\gamma$ -subunit complex interacts with and activates several downstream effectors, usually an enzyme or ion channel.^{6,48,65-67} This effector activation can, in the case of the ion channel, alter the ion permeability of the plasma membrane or, in the case of the enzyme, alter the concentration of one or more intracellular mediators resulting in the initiation of a signaling cascade.⁴⁸ Small GTPases function as molecular switches in signal transduction from activated cell surface receptors, for example receptor tyrosine kinases (RTKs), to intracellular targets.^{70,71} The signaling pathways in which G proteins are involved are paradigmatic for signaling pathways controlled by switches of PPI. Their function as molecular switches and their localization at the plasma membrane make G proteins a suitable site for intervening in signaling pathways for remote control of cellular functions. Using optical and magnetic remote control, proteins can be translocated and concentrated site-specifically to the plasma membrane, enabling and enhancing interactions (see Chapter 2). By recruiting GEFs or GAPs, or their catalytically active segments, G proteins can be switched in a controlled manner, resulting in remote control of signaling pathways and thus cellular functions with high spatiotemporal resolution.⁷²⁻⁷⁵

In cellular signal transduction, the signal is transmitted through a complex network with numerous connective nodes. The signaling pathways are not independent in the cell. Most signaling pathways interact with each other through so-called crosstalk. Already in the first step of signal transduction, many receptors interact with multiple effector pathways. Examples include the interaction of RTKs with, respectively the Ras/Raf/MAPK pathway, the phosphatidylinositol 3-kinase pathway, and with phospholipase C γ , or the interaction of the α -subunits and the $\beta\gamma$ -subunit complex of G-proteins with several downstream effectors. The network is equally branched at the level of small GTPases, which can be regulated by a variety of GEFs and GAPs. GEFs and GAPs themselves often interact with many downstream effectors, regulating the activity of multiple signaling pathways, and by protein kinases and protein phosphatases, which are activated by different receptors and have many substrates.^{27,67,76-78} Furthermore, signal transduction is regulated by inhibition or feedback motifs. Negative feedback loops can stabilize the signaling state, limit the maximum signal output and delay the signal response. Positive feedback loops can amplify the output signal, accelerate or delay the timing of the signal response, and create bistable switches. This can generate spatiotemporal activation profiles that regulate signaling pathways and thus cellular decisions.^{27,79,80} Interactions can be promoted by cooperative

processes such as allostery and configural preorganization. One measure of cooperativity is the Hill coefficient.^{81,82} These are only a few examples to illustrate how branched and complex the signal path network is.

1.1.2. Liquid–liquid phase separation

Protein interactions leading to the assembly of multicomponent protein complexes play a crucial role in signal transduction. If the cooperativity of the assembly process increases, driven by multivalent transient interactions, this can lead to liquid-liquid phase separation (LLPS). Recently, signaling complexes with highly dynamic behavior and properties of liquid-liquid phase separation (LLPS) have attracted intense research interests, especially as a widespread mechanism of spatiotemporal regulation of biological processes.^{13,20,83–89} The concept of LLPS-mediated signal transduction is hypothesized to be involved in many signaling pathways. For example, LLPS of Axin and dishevelled (Dvl) was identified in the Wnt signaling pathway that is crucial for development.^{90–92} LLPS of proteins in the nephrin/Nck/N-WASP pathway is involved in actin filament assembly^{93–95} and LLPS of SOS to induce Ras signaling in the LAT-GRB2-SOS pathway was characterized.⁹⁶ LLPS rely on multivalent protein interactions which are often mediated by intrinsically disordered proteins or proteins with intrinsically disordered regions.⁵² The IDPs/IDRs are frequently found in signaling relevant scaffold proteins. This suggests phase separation as a widespread mechanism of signal transduction.^{51,84,97}

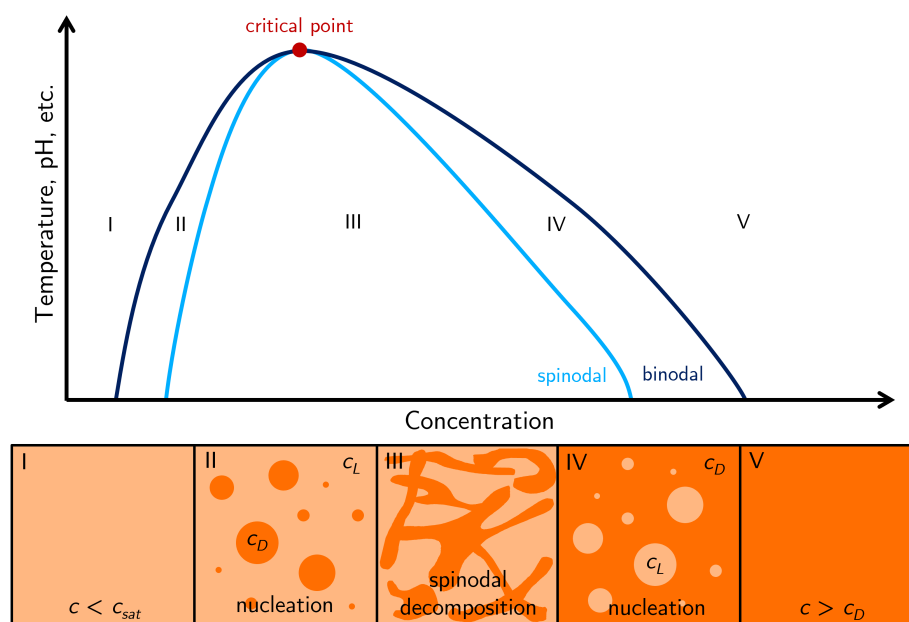


Figure 1.3.: **Schematic phase diagram of LLPS.** Outside the coexistence line (dark blue) there is the one-phase regime and inside the two-phase regime, consisting of a light phase (with concentration c_L) and a dense phase (with concentration c_D). Within the spinodal line (light blue) the system is unstable and undergoes segregation by spinodal decomposition. Adapted from Alberti et al. 2019.⁹⁸

During LLPS, macromolecules in solution condense into a dense phase that coexists with a dilute phase. This process depends on the concentration and identity of the macromolecules, as well as on the environmental conditions. Environmental conditions include temperature, pH, salt type and concentration, other solutes, and macromolecular crowding. The dependence of LLPS on these factors is illustrated in Figure 1.3 in the schematic phase diagram.^{88,98–100} There are two regimes in the diagram, the single-phase and the two-phase regime, which are separated by the binodal coexistence line. LLPS occurs above the saturation concentration (c_{sat}), the concentration threshold above which the system demixes into a light phase (with concentration c_L) and a dense phase (with concentration c_D). Above the critical point, no phase separation exists. On a horizontal line, the concentrations of the two phases (c_L and c_D) are constant, only the volume fractions change. In the region of instability the transition occurs by spinodal decomposition within the spinodal line.^{88,98–102} Liquid-liquid phase separation is characterized by spherical liquid droplets in solutions, except for spinodal decomposition. These liquid droplets have the ability to fuse. Another critical criterion is that molecules are mobile to transfer between the light and dense phases. This mobility of molecules can be detected by fluorescence recovery after photobleaching (FRAP).^{56,98} LLPS can undergo further phase transitions (Fig. 1.4). Deep in the two-phase regime of the phase diagram, the condensates can transition to a gel-like, also called glassy state.^{98,103} The glassy state exhibits irregular morphology and incomplete FRAP recovery. From the liquid and gel-like state, condensates can further mature and transition to a fibrous state. This transition is usually irreversible, requiring high salt concentrations or denaturants for initiation.^{56,98} Abnormal phase transitions of condensates to a solid state are associated with certain neurodegenerative diseases, including β -amyloid peptide and tau protein in Alzheimer's disease, TDP-43/FUS in amyotrophic lateral sclerosis (ALS), and huntingtin protein in Huntington's disease.^{89,99,104–107}

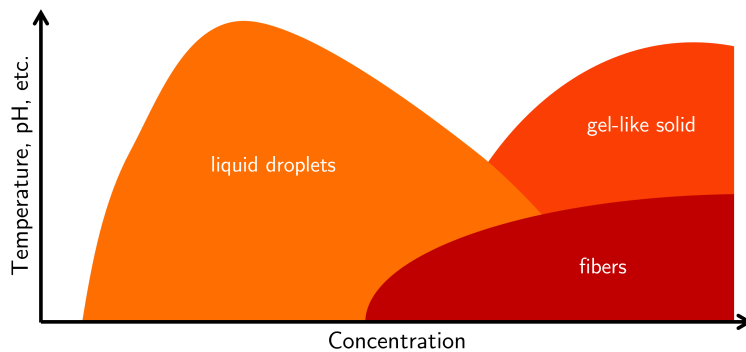


Figure 1.4.: **Schematic phase diagram of LLPS, gel-like solid and fibers.** Adapted from Shin et al. 2017.⁸⁸

Phase transition is a thermodynamic process. A system always strives for the lowest energy state as the most thermodynamically favorable energy state. The free energy of a system is composed of entropic and enthalpic contributions. According to the 2nd Law of thermodynamics, the system strives for the maximum entropy.^{56,58,98} The Flory-Huggins theory has been used to describe LLPS of polymer solutions. This lattice model, developed

by Paul Flory and Maurice Loyal Huggins, describes in simplified terms the thermodynamics of polymer solutions. Polymers dissolve in a solvent if this reduces the Gibbs energy of the system, meaning that the change in Gibbs energy (ΔG_{mix}) is negative, which is composed of the enthalpy of mixing (ΔH_{mix}) and entropy of mixing (ΔS_{mix}) at a given temperature (T).¹⁰⁸

$$\Delta G_{mix} = \Delta H_{mix} - T\Delta S_{mix} \quad (1.4)$$

Thus, a solution with uniformly distributed biomolecules is energetically favored which counteracts phase separation. However, for biomolecules that possess energetically favorable interactions, the additional enthalpic free energy can compensate for the entropic penalty. In this case, phase separation can happen leading the system toward less disorders. Also in this context, the higher the biomolecule concentration, the lower the entropic penalty. Above the critical saturation concentration (c_{sat}), the additional free energy from the biomolecule interactions equals the entropic penalty due to reduced disorder. Phase separation thus occurs at these critical conditions that the interactions are strong enough to drive LLPS but weak enough to prevent aggregation. Complementing the Flory-Huggins theory, the sticker and spacer model describes the interplay and pattern of regions that form specific interactions, the stickers, alternating with space between them.^{56,58,98,109,110}

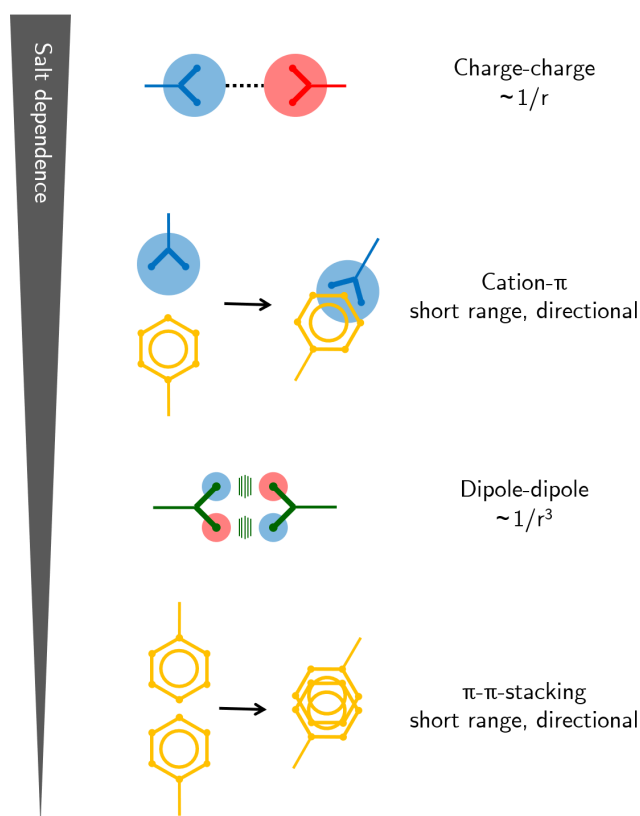


Figure 1.5.: **Molecular interactions to drive LLPS and their interaction ranges.**
Adapted from Brangwynne et al. 2015.¹¹¹

LLPS is driven by an interplay of different types of non-covalent interactions, such as electrostatic Coulomb interactions or van der Waals forces including the Keesom interaction between two dipoles, the Debye interaction between a dipole and an induced dipole, the London dispersion interaction between two induced dipoles, the cation- π interaction between a monopole (cation) and a quadrupole (π -system), or the π - π stacking interaction between two π -systems.^{58,112–116} These types of interactions give rise to weak, multivalent protein-protein and protein-RNA interactions, which are an important molecular driving force of phase separation.⁸⁸ Changes in environmental conditions such as temperature, pH, and ionic changes, as well as changes in reactive oxygen species and hydrogen bonding affect LLPS. In Figure 1.5, different types of interactions of amino acid residues and their dependence on salt are shown.^{111,117}

Multivalency of interactions promote the LLPS of proteins. These weak, transient interactions between proteins are mediated by repeats of interaction domains. This can be protein-protein interactions (e.g. SH3 domains that can bind to proline-rich motifs) or protein-RNA interactions (e.g. through zinc finger domains, RNA recognition motifs, or nucleic acid binding domains).^{52,56,86,88,98,117} In addition to interactions in structured domains, extended regions of low complexity can mediate multi-interactions. As previously described, IDRs are particularly abundant in proteins involved in cellular regulation and signal transduction.^{13,51–58} Motifs driving LLPS include prion-like domains, which are rich in polar, uncharged amino acids such as asparagine, glutamine, serine, and tyrosine, and RGG domains, which are rich in arginine and contain RGG boxes. These motifs mediate interactions with RNA. Aromatic residues particularly phenylalanine (F) and tyrosine (Y), often form a pattern on the sequence and can mediate cation- π and π - π stacking interactions.^{52,56,98,111,118,119} Furthermore, the lack of a secondary structure makes IDRs particularly susceptible to post-translational modifications controlling LLPS through the addition of functional groups or subtler chemical changes.^{46,47}

PTMs are able to influence interactions and thereby regulate LLPS. PTMs involved in LLPS include phosphorylation, acetylation, ubiquitination, and methylation.^{13,117} Phosphorylation enables a rapid and reversible response to stimulation changes. Addition of a negative charge to an amino acid through a phosphate group can enhance both electrostatic attraction and electrostatic repulsion, thus enhancing or inhibiting LLPS. Furthermore, phosphorylation can provide a binding site for partner proteins and thus drive LLPS. Acetylation regulates LLPS by neutralizing charged amino acids, which inhibits LLPS. Also inhibiting LLPS is methylation. Reversible methylation can strongly neutralize electrical properties of proteins and inhibit electrostatic action. In the case of ubiquitination, the multivalent binding potential of the ubiquitin molecule promotes LLPS.^{117,120–123}

The cytosol is a complex solution containing a variety of macromolecules, such as proteins, nucleic acids, and polysaccharides. Concentrations of them vary with cell type and organism

which can reach a combined concentration of up to 400 mg ml^{-1} and occupy up to 30 % of the cell volume.^{52,99,124} This crowded environment inside the cell has an influence on LLPS. The excluded volume theory shows one aspect of the effect of crowding on biomolecular structure and dynamics. Depending on the size of the molecules, the excluded volume locally increases the concentration of biomolecules. Crowding can also increase the interaction of diverse biomolecules, which can lead to co-condensation that promotes LLPS. In addition, repulsive forces between dissimilar biomolecules can reduce solubility and lead to segregation in LLPS. Furthermore, client proteins influence LLPS behavior, such that monovalent clients are slightly destabilizing by dilution, while multivalent clients provide cross-linking.^{13,52}

When a protein involved in LLPS is membrane bound, phase separation occurs at the plasma membrane. Within this pseudo-two-dimensional LLPS, components can be included or excluded by the LLPS and thus enriched or depleted, resulting in clustering and co-compartmentalization at the plasma membrane (see Fig. 1.6).⁸⁴ This enables and enhances interactions that can induce signal transduction. The membrane dwell time of constituent proteins has been shown to be much higher in phase-separated regions than in surrounding regions of the membrane. It has been proposed that reduced diffusion leads to amplification of signaling, through a process resembling kinetic proofreading, which favors reactions that are slow and multistep.^{86,96} For example, Case et al. showed that dwell time depends on cluster stoichiometry, and that stoichiometry of regulatory proteins can control actin assembly.⁹⁴ Huang et al. show that the longer dwell time enables kinetic proofreading in receptor-mediated activation of the small GTPase Ras. The Ras-GEF SOS is autoinhibited in the cytosol and is activated upon membrane recruitment. The autoinhibition release involves structural rearrangements of the protein at the membrane, which results in a delay between initial recruitment and activation and is enabled by the extended dwell time.⁹⁶

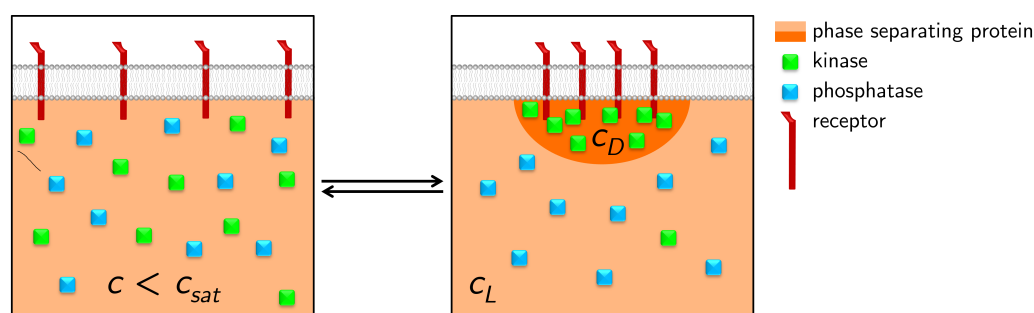


Figure 1.6.: **Schematic illustration of pseudo-two-dimensional LLPS.** If a protein involved in LLPS is membrane-bound, phase separation occurs at the membrane, resulting in clustering and co-compartmentalization. Components can be included or excluded by the LLPS, and thus enriched or depleted. The schematic shows the enrichment of kinases that phosphorylate the receptor and the exclusion of phosphatases. Adapted from Chong et al. 2016.⁸⁴

In addition to signal transduction by clustering or co-compartmentalization, LLPS can perform other functions in cells (Figure 1.7). The increased concentration of compo-

nents in a condensate can promote protein interactions and lead to accelerated biochemical reactions and increased enzymatic activity. However, the increase in concentration and associated viscosity can lead to slow diffusion within the droplet, thereby limiting turnover.^{83,86,95,98,112,117,122,125–127} On the other hand, an interaction component can also be excluded from the system, which can prevent a reaction or, if it is an inhibitory component, promote the reaction. Through LLPS, biomolecules can be separated into distinct subcellular condensates.^{83,86,95,98,112,117,122,126,127} Furthermore, LLPS can buffer the system: further increasing the concentration results in a larger volume fraction of the dense phase and a smaller volume fraction of the dilute phase with the same droplet and environmental concentration. Due to the increase in viscosity, condensates can exert mechanical forces. In addition, LLPS can be used as fast environment sensitive signaling valve for adaptively and reversibly tuning of biomolecule reactions. Since small changes in solution conditions, such as heat or pH stress, lead to a rapid phase transition, a fast signaling response can be achieved to adapt to the changed environment, especially when the system is balanced near to c_{sat} .^{83,98,112,117,122,126–128} Condensates formed by LLPS can serve as physicochemical and mechanical filters. By increasing viscosity, condensates can exert mechanical forces.^{83,98,112,117,122,126}

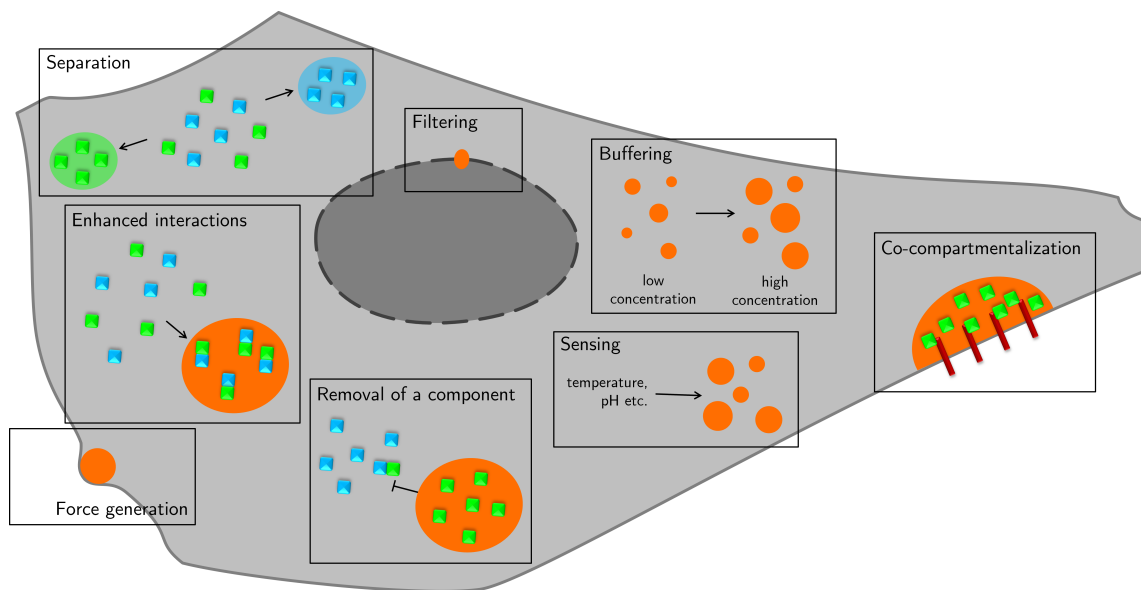


Figure 1.7.: **Schematic illustration of the functions of LLPS in cells.** Adapted from Alberti et al. 2019 and Feng et al. 2019.^{98,112}

In summary, cellular processes are triggered by weak interactions being modified and strengthened by multivalent interactions (e.g. by increased local protein concentrations) and post-translational modification. Cell signaling possesses different stages at which decisions are made and transmitted. Targets at the plasma membrane are of particular interest to control of cellular functions, as they can either be targeted from outside of the cell or intracellular components can be recruited to them. This offers the potential of manipulating the regulation of cellular functions, for example by remotely activating the receptor or channels, which receives and processes the external signal, or by translocating specific downstream components to the plasma membrane, such as GEFs, which activate downstream GTPases, resulting in the initiation of the signaling cascade. Another promising tool represents the control of LLPS, due to its sensitivity to protein concentrations, and due to the widespread role of LLPS in cellular functions, especially in the activation of signaling pathways.

2 | Remote control of cellular functions

The previous chapter has shown that processes are triggered by weak interactions being modified and strengthened by multivalent interactions and post-translational modification. Cell signaling offers potential and different targets for remote control of the regulation of cellular functions. For example, receptors or channels can be activated externally by stimulation with a ligand, by dimerization, or by other stimuli such as heat or force.^{129–134} In addition, certain downstream components can be recruited to the plasma membrane, which site-specifically increases the concentration and thereby the frequency of protein-protein interactions, for example a GEF, which activates GTPases and thus signaling cascades. However, the site-specifically increased concentration can also result in the induction of phase separation.^{25,56,72,73,75,135,136} Remote control technologies enable the targeted activation of signal transduction receptors to initiate the cascade and trigger cellular functions. Spatiotemporal regulation of protein functions is critical for the control and coordination of cellular functions.^{30,41,137–139} Spatiotemporal control of proteins allows signal transduction to be tackled at different stages, gaining fundamental understanding of the structure and dynamics of cellular signal transduction and regulation of cellular processes.^{56,136} This targeted subcellular manipulation and quantitative interrogation of signaling pathways provides molecular insights for understanding signaling pathways, which can be used in biomedical applications. A wide variety of cellular processes can be manipulated in this way, such as differentiation, gene expression, migration, outgrowth, or intracellular transport.^{25,140–146} In addition, remote manipulation of cellular functions over a longer period of time can be used for therapeutic approaches in regenerative medicine.^{25,147,148}

Numerous approaches have been developed to remotely control cellular functions. These include optical control and magnetic control as two exciting new interdisciplinary fields, which will be introduced further in the following part. Other approaches are based on electrical, mechanical and chemical control: Electrogenetics is based on the activation of voltage-gated receptors using electrical stimuli.¹³⁰ In mechanogenetics, mechanosensitive receptors are activated by means of physical stimuli, which have the advantage of having a high penetration depth into the tissue, such as focused ultrasound.¹³² Chemogenetics is based on engineered specific activation of a receptor or channel by means of a ligand, such as chemically inducible dimerization of FK506-binding protein (FKBP) and the FKBP-rapamycin-binding domain by rapamycin.^{129,131,133,134}

2.1. Optical control

First approaches of remote control of cellular processes were developed with caged compounds in cellular neurology. Caged compounds are biomolecules or ions that are encapsulated by chemical modification with a protecting group in an inactive form. The bond is photochemically labile, so exposure to light results in release and thus increased concentration of the biologically active molecule or ion. The release can be temporally and spatially defined, intracellular or extracellular, and amplitude or frequency modulated. This spatially and temporally controlled release and thus control over the interaction of biologically active components, for example with a receptor, enables targeted interference with and activation or deactivation of biological processes.^{149,150}

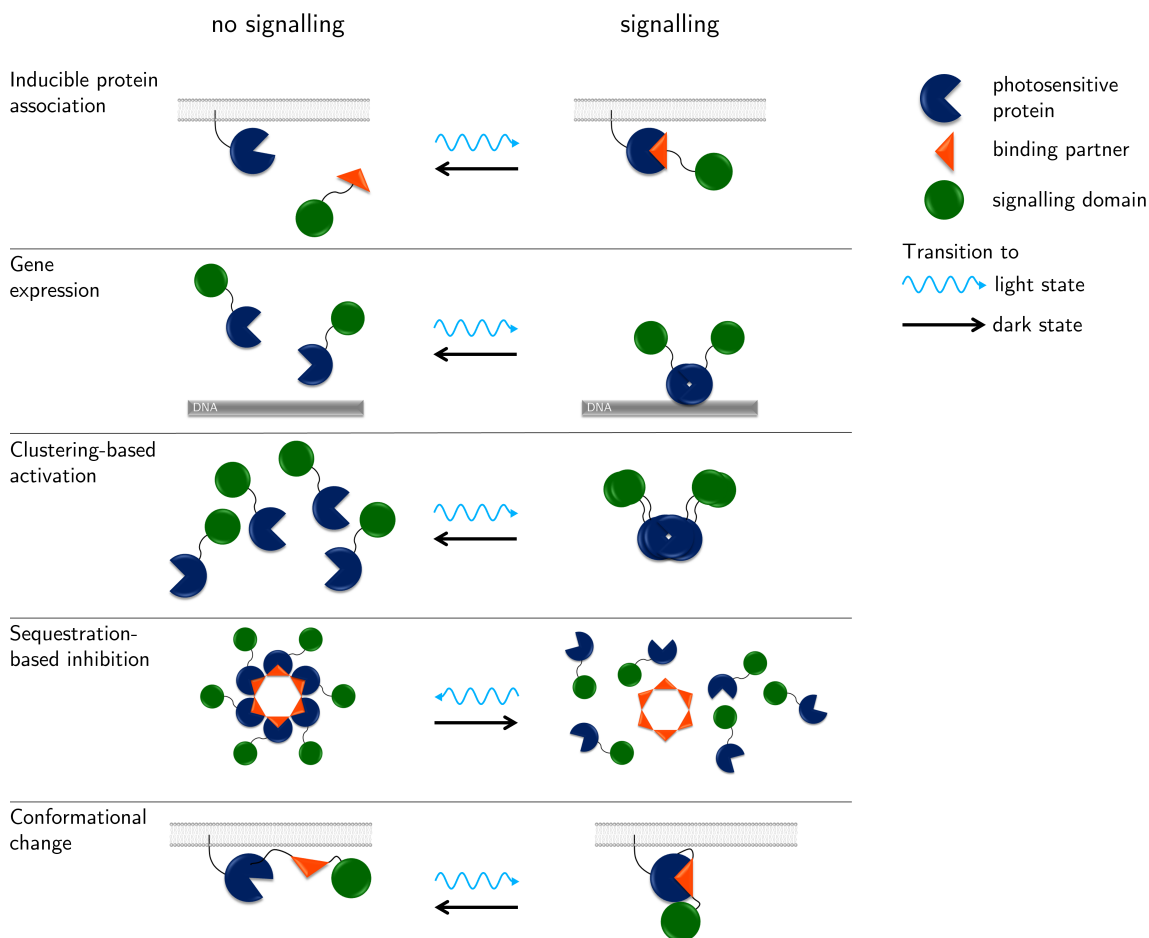


Figure 2.1.: **Different optogenetic strategies.** Optical stimulated signals induced by light (blue arrow) or in the dark (black arrow). Adapted from Tischer et al. 2014.¹⁵¹

These initial approaches were limited by the availability of the component at the target location. Therefore, the research field of optogenetics has developed. This non-invasive method uses genetically encoded proteins to stimulate interactions by light and thus site-specifically enrich components. Optogenetics provides a powerful and responsive tool for spatiotemporal control of molecular processes in living cells or organisms and allows to

study physiological processes at the single cell level by controlling protein activity patterns at the subcellular level.^{12,136,152} Heterodimerization can be used to recruit a signaling domain to its substrate^{151,153–155} or for targeted membrane recruitment^{156,157}. Homodimerization and heterodimerization can be used to recruit transcriptional activators or other DNA-modifying proteins to DNA to initiate gene expression.^{151,158} Proteins clustered by light can be used to increase the local concentration of signaling domains whose activity depends on density.^{151,159} In addition, signaling activity can be inhibited by removing the signaling proteins from the site of action. For this purpose, they will be recruited to cytosolic clusters or compartments so that they are no longer available for interaction with their upstream activators or downstream effectors.¹⁵¹ Furthermore, conformational change of light-sensitive proteins can be used to make a signaling domain accessible from an allosterically autoinhibited state (Fig. 2.1).^{145,151,160} Examples of optogenetic systems are light-sensitive ion channels, pumps, transporters, enzymes, and light-induced association and dissociation. This spatiotemporal control of the intensity and timing of the signals enables a quantitative understanding of the signaling pathway and functional mapping of the signaling network in living cells.^{146,147,153,161–163}

For reversible optogenetic systems, light-sensitive proteins are often used.¹⁵¹ Based on the light-sensitive Phytochrome B (PHYB) and phytochrome-interacting factor (PIF) system, Toettcher et al. developed an optogenetic approach to selectively activate intracellular signaling nodes to monitor signal transduction through the Ras/Erk mitogen-activated protein kinase (MAPK) cascade.¹³⁶ Exposure of the PHYB/PIF system to red light (650 nm) induces a conformational change within seconds, resulting in binding to PIF. Irradiation with infrared light (750 nm) leads to dissociation of this complex within seconds, in the dark it is stable for hours.^{151,164,165} Toettcher et al. demonstrated recruitment of the Ras-GEF SOS catalytic region (SOS_{cat}) to the plasma membrane by light stimulation, resulting in activation of Ras (for more information on small GTPases see Chapter 5). Switching between states within seconds allowed precise spatial and temporal control of activity. This allowed them to study dose-response curves and frequency-response curves of the pathway at the single cell level.¹³⁶ Cryptochrome 2 (CRY2) is an *Arabidopsis thaliana*-derived protein sensitive to blue light (405–488 nm), which uses ubiquitously expressed endogenous flavin functions as chromophore. Exposure to blue light within second leads to homo-oligomerization of the CRY2 protein and binding of its binding partner CIB1 (calcium and integrin-binding protein 1). Return to the initial state occurs within 5 min in the dark.^{151,155} De Beco et al. used CRY2-based optogenetics to investigate the mechanisms of spatial gradient formation of Rho GTPases during cell migration. Using patterned illumination, optogenetic activation of the small GTPases Cdc42 and Rac1 by recruiting the catalytic regions of their GEFs fused to CRY2 was obtained. Their results showed that the spatial gradients of Cdc42 and Rac1 determine the directionality and speed of cell movement, respectively.⁷² Similarly, Harris et al. succeeded in long-range optogenetically controlling axonal guidance in zebrafish motoneurons by targeting activation of the photoactivatable Rac1 protein.¹⁴¹ In addition to

these two-component approaches, which require stoichiometric tuning of both components, the one-component approach using BcLOV4, a LOV (light-oxygen-voltage) photoreceptor, was described for stimulation of the GTPases Rac1¹⁶⁶, RhoA29 and Cdc42⁷⁴, and Ras¹⁶⁷. Where Benman et al. showed temperature-dependent photoinactivation.¹⁶⁷ Shin et al. developed an optogenetic platform for dynamic modulation and spatiotemporal control of phase transitions in living cells. They induced LLPS both globally and subcellularly for several proteins with intrinsically disordered regions (FUS, DDX4, HNRNPA1) fused to CYR2. At the end, they observed both reversible activation cycles of LLPS and solid-like gels due to aging to irreversible aggregates by shifting the phase diagram.⁵⁶

Despite their great potential, optogenetic methods have some inherent disadvantages. First, optical manipulation techniques are not compatible with opaque probes, such as tissues.^{168–171} Second, the maintenance of a controlled spatial signaling pattern over long periods of time is a challenge due to the diffusion of photoactivated molecules.⁷³ In addition, the expression of genetically modified constructs is required, which complicates the biomedical application in cell therapies.¹³⁵ Importantly, light sources must be maintained in close proximity with the target sites. To overcome the limitation of penetrating deep into the tissue, for example, fiber-optic implants are used.¹⁷² Another promising approach is the use of upconversion nanoparticles (UCNP), which allow the use of tissue-penetrating near-infrared (NIR) light. By upconverting photons, they can absorb two or more incident photons of relatively low, deeper penetrating energy and emit a photon of higher energy. Thus, they can act as a light source for optical approaches.^{173,174}

2.2. Magnetic control

The use of biofunctionalized magnetic nanoparticles represents a promising approach to remotely control protein functions, and thus cellular processes.^{25,75,175} Because magnetic fields generally interact weakly with biological matter, they can penetrate tissue and offer great potential for an analogous approach to the plethora of optogenetic methods, with their limitations in, for instance, penetration depth.^{176,177} The magnetic control approach uses MNPs to apply thermal, mechanical, or biochemical stimuli. This is done, for example, by generating heat, applying mechanical forces, inducing clusters, or generating protein concentration gradients and thus biomolecular activity patterns.^{175,178–182}

The use of magnetic fields is non-invasive and penetration into tissues and, unlike optogenetics, does not require transparent samples.^{168–171} Thus, cellular functions and signaling pathways can be studied in living cells and tissues, which is of great advantage for biomedical applications. This offers the possibility of using remote magnetic control of cellular processes, such as targeted cell differentiation, migration or outgrowth, in innovative cell-based therapies, for example to treat neurological diseases.^{25,147} Another advantage is the ability to maintain concentration gradients over periods of minutes to hours. This is in contrast to optogenetic techniques, which are rapidly equilibrated by protein diffusion.⁷³ In addition to these limitations of optogenetics, which the magnetic approach overcomes, the range of functions is extended by the ability to exert forces or heat in a site-specifically at a subcellular level.^{25,73,168–171} The opportunity of *in vitro* functionalization of magnetic nanoparticles also offers an advantage over optogenetics since no genetic modification of the biological material is required.

Following optogenetics this field is often referred to as magnetogenetics.^{25,75,170,171,175,183} Although the magnetogenetic approach contains both genetically encoded and non-genetically encoded components, the term has become widely established due to its similarity to the optogenetic approach. The magnetogenetic approach consists of a genetically encoded cellular component which is tackled by the magnetic nanoparticles, such as a channel or receptor, and the nanoparticles themselves. Depending on the used nanoparticle system, these fulfill the definition ‘genetically encoded’ in a narrower or less narrow way. The nanoparticles can consist of genetically encoded proteins together with a magnetic component formed *in cellulo*. Examples include magnetosomes from magnetotactic bacteria or protein cages, such as ferritin, wherein a magnetic core can be encapsulated.^{144,178,184–186} However, the magnetic response of these purely genetically cored intrinsically magnetic particles is limited. Enhanced magnetic response is achieved by semi-synthetic approaches in which the magnetic component is formed under controlled conditions *in vitro*. For example, *in vitro* encapsulation in recombinant ferritin enables the formation of a superparamagnetic core.^{187–192} Further optimization of magnetic properties can be achieved by *in vitro* biocompatibilization and biofunctionalization of synthetic magnetic particles, e.g.

through protein coating or as in core-shell particles.^{135,168,193}

The applications of magnetic control by using magnetic nanoparticles can be classified in three categories (Fig. 2.2): The thermal mode, in which a thermal stimulus is exerted, the force mode, in which a mechanical force is exerted, and the space mode, in which a protein gradient is generated resulting in locally increased protein concentrations and a biochemical stimulus (e.g., increased reaction turnover, induction of liquid-liquid phase separation).

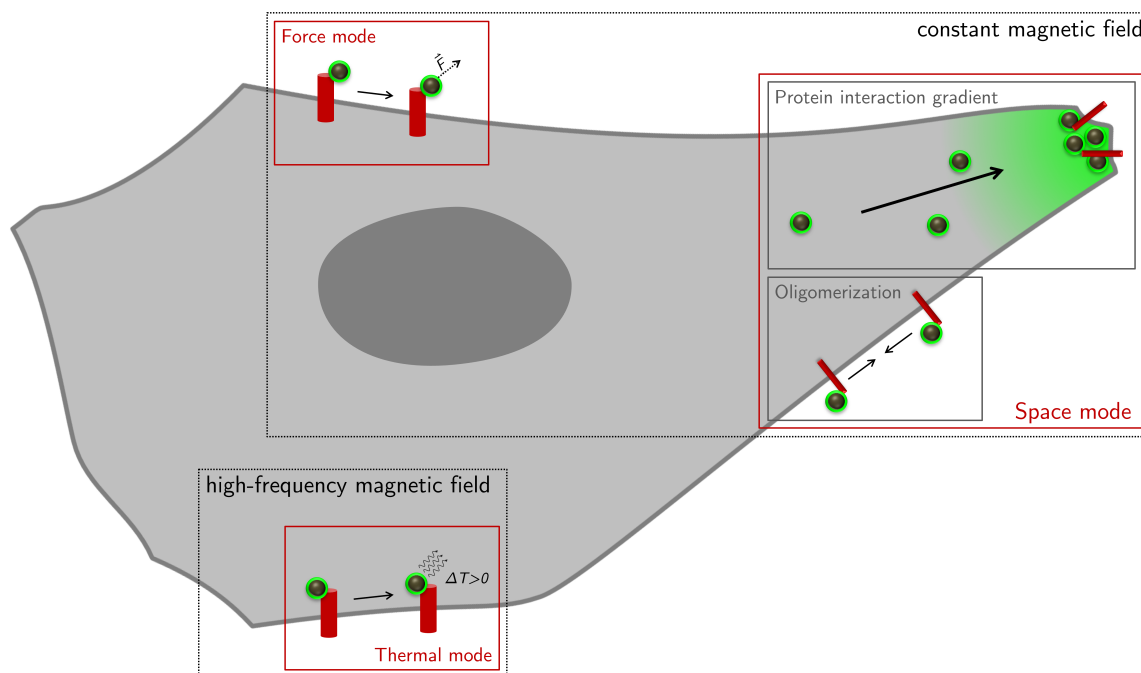


Figure 2.2.: **Schematic illustration of the different modes of magnetic control.**

Magnetic nanoparticles, depending on their size, shape, and magnetic properties, can convert the field stimulation into heat when exposed to a high-frequency magnetic field (thermal mode).^{194–196} The resulting hotspots can be used for efficient site-specific hyperthermia.¹⁹⁶ Furthermore, these hotspots can be used to specifically stimulate thermoreactive molecules, such as ion channels of the transient receptor potential (TRP) family.^{25,147} Magnetic nanoparticles can exert mechanical forces on the cell membrane attached to the cell surface or from cytosol (force mode). This can be used to study cell mechanical properties and mechano-transduction, the conversion of mechanical stimuli into electrical or biochemical signals, of membrane-associated complexes. Force can also be targeted by directly gating ion channels and acting on them by deflection or stretching.^{25,178,185} Early magnetogenetic studies with genetically encoded magnetic nanoparticles were examined by Meister using theoretical calculations.¹⁷⁷ Among the investigated approaches was the activation of a mechanosensitive cation channel reported by Wheeler et al. and activation of a temperature-sensitive membrane channel reported by Stanley et al.. Both channels were fused to ferritin, in one case to apply torsional and tensile forces using a static magnetic field, and in the other to generate heating using a high-frequency magnetic field.^{144,177,186}

Meister's calculations suggest that the forces and temperatures generated are not sufficient for channel activation and that the effects described cannot be explained by magnetic phenomena generated by genetically encoded magnetic nanoparticles.¹⁷⁷ This points out the limitations of genetically encoded magnetic nanoparticles and the need for improved magnetic properties. The magnetic properties of ferritin can be improved by *in vitro* encapsulation under controlled conditions, resulting in the formation of a superparamagnetic magnetite/maghemite ($\text{Fe}_3\text{O}_4/\gamma\text{-Fe}_2\text{O}_3$) core.^{187,188,190,191} However, this magnetic core is limited to a size of ~ 8 nm due to the protein cage.¹⁹⁷ More potential for improvement in size and magnetic properties is offered by the use of (semi-)synthetic nanoparticles.

Spatiotemporal manipulation of the concentration and spatial distribution of signaling molecules can control the biomolecular activity pattern (space mode). Early studies used MNPs to control membrane receptor oligomerization and thus activation. For this, MNPs were specifically bound to membrane receptors and a dipole-dipole interaction was generated by applying a static field for reversible clustering of MNP-receptor complexes and triggering intracellular signaling responses.^{25,198,199} In addition applying MNPs for intracellular control offers great potential for studying complex signaling pathways and subcellular organization. In this context, the biofunctionalized MNPs act as nano signaling actuators that can be translocated in the cytoplasm by magnetic field gradients. This results in formation of protein concentration gradients and thereby modulates protein interactions spatiotemporally to manipulate cellular processes. Using biofunctionalized MNPs, Hoffmann et al. controlled the *in vitro* assembly of microtubule fibers in *Xenopus laevis* egg extracts into asymmetric arrays of polarized fibers.²⁰⁰ The spatiotemporal control was achieved using Ran- and RCC1-functionalized MNPs, where functionalization with the upstream Ran-GEF RCC1 showed a larger effective range compared to functionalization with GTP-linked small GTPase Ran. The MNPs were ~ 120 nm in size, which does not allow free diffusion in the cytosol for a majority of cell types (see Chapter 4.4).^{201,202} Unfavorably, these MNPs exert forces on the crowded intracellular network. Using biofunctionalized 500 nm sized MNPs, Etoc et al. demonstrated site-specific activation of the small GTPase Rac1 resulting in remodeling of the actin cytoskeleton and formation of cell protrusion. To activate Rac1, the MNPs were functionalized with the DH and PH domains of the Rac1-GEF Tiam1, which are responsible for GEF activity, thus activation of the small GTPase.^{25,73,75,135,147} However, due to the use of 500 nm sized MNPs, it is unlikely that they acted in pure space mode, but also forces are exerted, resulting in a hybrid mode. Due to their size, the particles probably also exerted mechanical forces on the plasma membrane, and destructive forces on their way through the intracellular network.

The use of biofunctionalized magnetic nanoparticles offers the great potential of control at the submicrometer scale and thus control of thermal, mechanical, and biochemical stimuli at the subcellular level. This enables the study of cellular processes, such as signaling pathways, with high spatiotemporal resolution.

However, in addition to their great potential, for intracellular application, the complex cytoplasmic environment poses high requirements for the magnetic nanoparticles and their coating. The nanoparticles must be biocompatible, including colloidal stability, and exhibit stealth behavior in the cell to avoid inducing unwanted cellular reactions. The requirements are particularly stringent for a pure space mode. To enable this, the nanoparticles must be small enough to avoid exerting mechanical forces on the crowded cell interior and be able to diffuse freely in the cytosol. This is countered by the magnetic properties. Despite their small size, the particles must exhibit sufficient magnetic response to allow spatial remote control of the biofunctionalized nanoparticles. A small size, within the limits of superparamagnetism, also offers the advantage of immediate loss of magnetization when no magnetic field is applied. This prevents an unwanted magnetic force between the nanoparticles beyond the magnetic manipulation. In addition, site-specific functionalization of the nanoparticles is critical in order to perform the desired function. Ideally, this functionalization should be bio-orthogonal, which minimizes non-specific interactions and enables *in cellulo* functionalization. The development of functional-coated nanoparticles that fulfill these requirements represents the basic building block for intracellular applications of magnetic control.

II Aims

Aims

The spatially and temporally highly coordinated regulation of protein functions in the cell is a cornerstone enabling the high versatility and complexity of biological processes. Remote control of protein localization inside cells therefore offers tremendous potential for interrogating and manipulating biological processes by allowing targeted manipulation at different levels of these processes. In recent years, magnetogenetic manipulation has emerged as a promising tool offering high spatial and temporal resolution for remote control of cellular functions in tissues and organisms. However, the application of magnetic nanoparticles (MNPs) in living cells is still a critical challenge. These MNPs need to maintain their robust colloidal properties in complex biological environments, while their hydrodynamic diameter has to be small enough to ensure efficient cellular delivery of nanoparticles and maintain unhindered mobility in the cytoplasm. At the same time, high magnetic response, effective biocompatible surface passivation to minimize toxicity and recognition by cellular degradation machinery as well as biofunctionalization for selective and efficient conjugation with target proteins by *in situ* capturing in cells is required.

Focusing on the demanding requirements on MNPs for intracellular applications, this thesis aims to develop a toolkit and methodologies for magnetogenetic manipulation inside living cells. In first proof-of-concept experiments, the application of previously established magnetic intracellular stealth MNPs based on natural ferritin was investigated (Chapter 7). To overcome the limitations of these particles, a new generation of biocompatible nanoparticles was developed, which provides improved properties in terms of magnetic response and versatility of functionalization (Chapter 8). To ensure suitable biocompatible, biofunctional, and magnetic properties, a dense protein-based self-assembled coating for magnetic core particles is developed, which provides biocompatibility and colloidal stability in the complex and crowded biological environment of the cytosol. These MNPs were designed for *in situ* biofunctionalization by site-specific capturing to enable spatial reorganization of target proteins in the cytosol by magnetic field gradients. After *in vitro* and *in cellulo* characterizing and systematically optimizing properties and magnetic control of biofunctional MNPs, they were employed to established manipulation of cellular functions by altering local protein concentrations via magnetic forces (space mode magnetogenetics). To demonstrate the capabilities of this approach, complementary model systems were established: (I) activation of G-protein signaling at the plasma membrane by spatiotemporal control of catalytically active region of GEF proteins (Chapter 7 and 9), and (II) induction of liquid-liquid phase separation using effector proteins of the Wnt signaling pathway (Chapter 10) as a showcase.

III Strategy

3 | Space mode magnetogenetic control of cellular functions

The concept of magnetogenetic control in space mode is shown in Figure 3.1A. It consists of: I. The delivery of biofunctional-coated MNPs into the living cell, for example by microinjection. II. The intracellular, site-specific biofunctionalization of these particles with specific target proteins to generate a functional nano-signaling actuator. III. The controlled spatial translocation of the biofunctionalized MNPs by applying a magnetic field gradient to a desired location to manipulate specific cellular processes on a sub-cellular scale.

This controlled spatial translocation of biofunctionalized MNPs allows remote control of protein concentration at a subcellular level and maintenance of this protein gradient over a large time interval. This spatiotemporal increase in the concentration of specific target proteins results in local enhancement of protein interactions. Thereby, it offers the possibility of site-specific activation of signaling pathways by, for example, increasing reaction turnover or by the increased concentration leading to LLPS (Fig. 3.1B).

To demonstrate targeted remote control by locally increased reaction turnover, the small GTPases HRas and Rac1 were chosen as model systems. Rac1 belongs to the Rho family GTPases, which regulate and coordinate cytoskeleton remodeling by inducing polymerization of actin with Rac1 being mostly involved in the formation of protrusions.^{203–205} This enables convenient readout of activation by observing cytoskeleton remodeling and morphological changes. HRas plays a crucial role in various processes such as proliferation, differentiation, cell growth, embryogenesis, axonogenesis and neurotrophin signaling.^{206–212} The demonstration of the magnetic remote activation of the small GTPases HRas and Rac1 and the detection of the cellular response, is going to demonstrate the potential of biofunctionalized MNPs and the magnetic remote control approach for biomedical research.

The second model system is the canonical Wnt signal pathway, which demonstrates the potential of the particles and the magnetic remote control approach for basic research. The hypothesis of the activation mechanism was examined by the specific remote control. For this purpose, phase separation was induced by a locally increased protein concentration, accompanied by increased protein interaction. Moreover, this phase separation was located with high spatial precision near to the plasma membrane. These high requirements, on the one hand of remote temporal control via the LLPS, but also of site-specific localization at

the subcellular level, demonstrate the potential of precise remote spatiotemporal control of cellular processes.

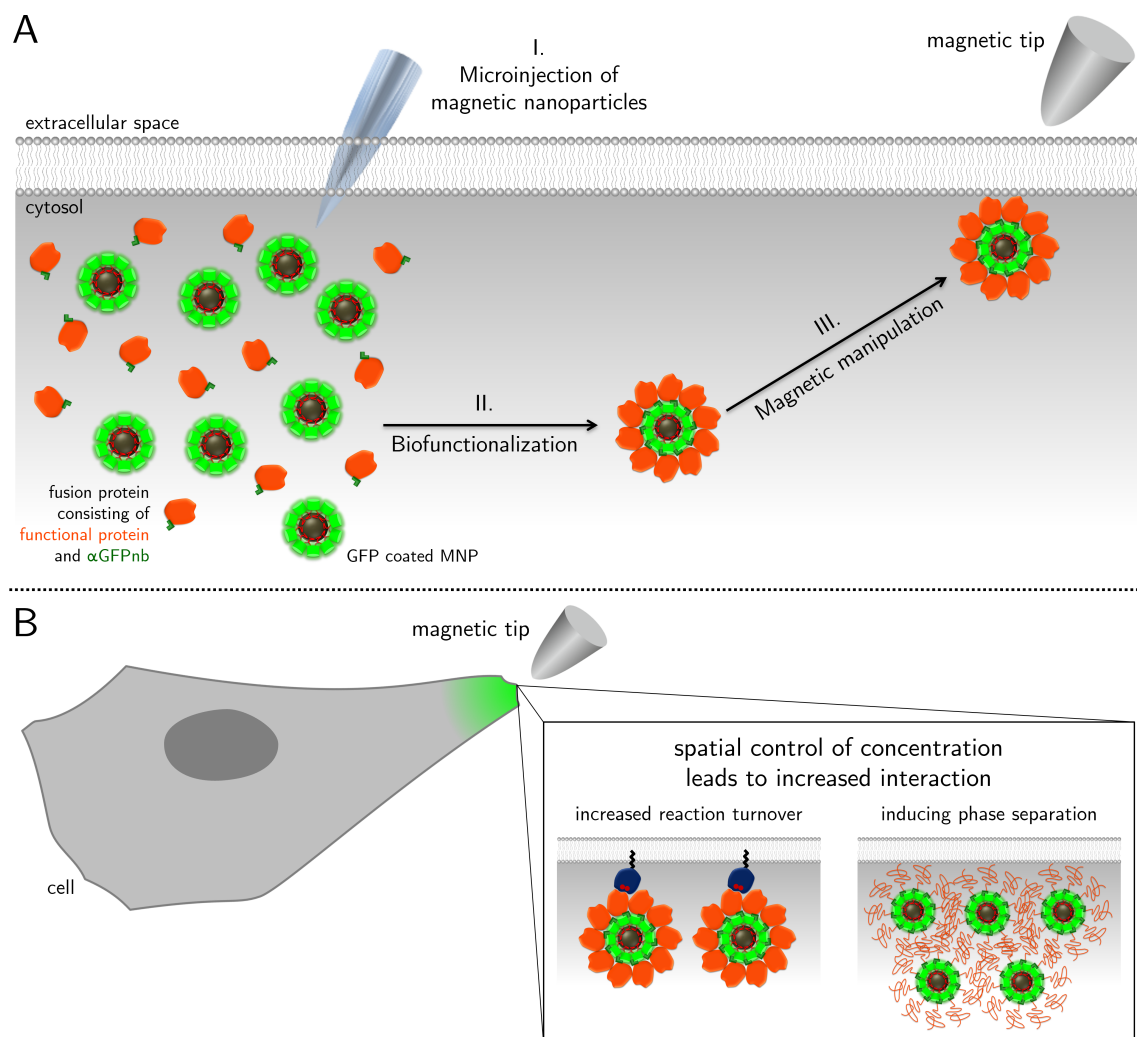


Figure 3.1.: **Concept of magnetogenetic control in space mode.** (A) I. Delivery of biofunctional coated magnetic nanoparticles (MNPs) into the living cell. II. Site-specific biofunctionalization with specific target proteins to generate a functional nano-signaling actuator. III. Controlled spatial translocation of the biofunctionalized MNPs by applying a magnetic field gradient to the target site. (B) Magnetic remote control of cellular processes by local increase in concentration. Increased concentrations result in a local increase of protein-protein interactions and thus (I) in locally increased reaction turnover or (II) in the induction of liquid-liquid phase separation.

4 | Engineering of nanoparticles for space mode magnetic remote control

Due to their small and controllable size, high biocompatibility and magnetic behavior, magnetic nanoparticles (MNP) and especially superparamagnetic iron oxide nanoparticles (SPION) are promising tools to be applied in biomedicine and basic biomedical research.²¹³ Since the early application of MNPs in cell separation using magnetically labeled antibodies^{214,215}, a broad field has opened up in biology and biomedicine¹⁸⁴. In addition to the evolving application of isolation and detection of cells using magnet-assisted cell separation (MACS)^{216–219}, applications include targeted and controlled drug delivery^{220–222}, magnetic resonance imaging (MRI)²²³, magnetic particle imaging (MPI)²²⁴, hyperthermia-based therapy^{225–228}, Lab-on-Chip technologies²²⁹, magnetic control of proteins and cellular functions^{75,179,230}, and regenerative medicine and tissue engineering²²⁹.

One nanometer (ancient Greek *νανος*, 'dwarf') corresponds to a billionth of a meter ($1 \text{ nm} = 10^{-9} \text{ m} = 10 \text{ \AA}$).²³¹ Figure 4.1 depicts the dimensions of typical globular protein, and the plasma membrane.

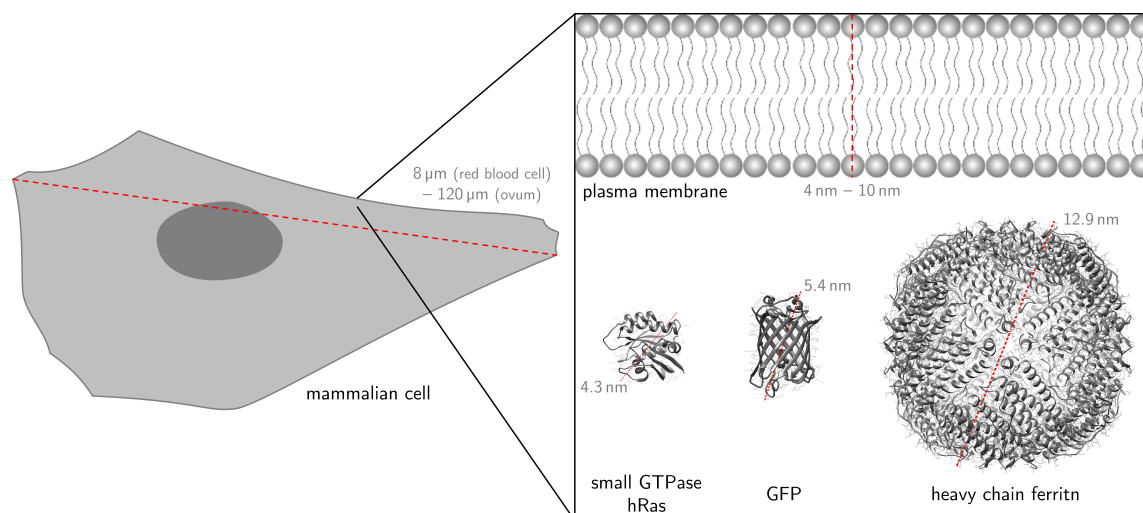


Figure 4.1.: **Schematic size comparison of different biomolecules.**⁴⁸ PDB entry Ferritin - 6m52, GFP - 3K1K, HRas - 5P21, created with UCSF Chimera.

According to ISO/TS 80004-2:2015, nanoobjects have at least one dimension in the nanoscale range, approximately from 1 nm to 100 nm; in the case of nanoparticles, all three dimensions are in the nanoscale range.²³² The upper limit depends on the size, up to which

size-related phenomena can occur, typically the limit is drawn at 100 nm.²³³ The lower limit of nanoparticle size is at the border of chemical clusters with a diameter of 1-2 nm and countable number of atoms, an example of such a cluster is the Au₅₅ cluster with a diameter of 1.4 nm.²³⁴ The chemical and physical properties of nanomaterials differ from the bulk materials of which they are composed. Nanomaterials have a large surface area in relation to their volume (usually in the range of $e\ 100\text{ m}^2\text{ g}^{-1}$ - $1000\text{ m}^2\text{ g}^{-1}$). The majority of the atoms are located on the surface (Fig 4.2). Atoms on the surface usually have fewer neighbors, so they have free/unsaturated bonds and thus partial charges on the surface. This increases the surface energy. The system strives to reduce the free surface energy, this can be done by forming bonds, surface relaxation or surface restructuring. Thus, surface functionalization, grafting, adsorption, homo- and hetero-agglomeration, reactivity, and interaction with the environment are influenced by the size and surface energy of the nanomaterial.²³⁵

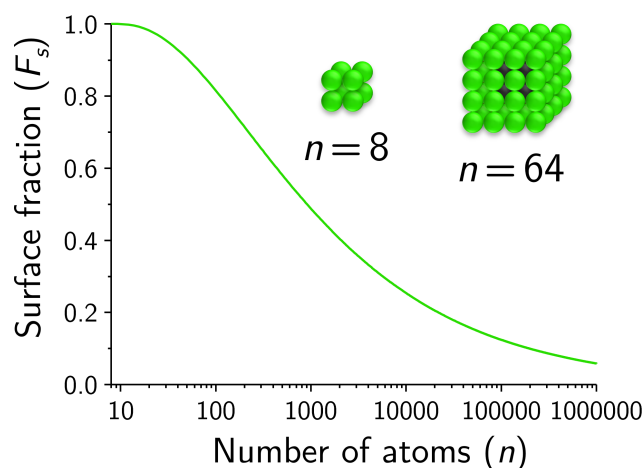


Figure 4.2.: **Fraction of atoms at the surface (F_s) of a material as a function of the number of atoms (n).**

Synthesis of nanoparticles follows two different approaches, using a bottom-up or top-down approach. In bottom-up processes, nanoparticles are built up from atomic, ionic or molecular precursors, in top-down processes, nanoparticles are produced from bulk materials by particleisation.^{234,236} Common synthesis methods for MNP include co-precipitation, thermal decomposition, hydrothermal synthesis, microemulsion/micelle synthesis, solvothermal synthesis, sonochemical synthesis, chemical vapor deposition, laser pyrolysis methods, and synthesis by microorganisms or bacteria.²³⁷⁻²³⁹

The most conventional method for the preparation of magnetite (Fe_3O_4), maghemite ($\gamma\text{-Fe}_2\text{O}_3$) and mixed ferrite (MFe_2O_4) nanoparticles is the coprecipitation of iron(III) and iron(II) or other metal salts (M(II)) in aqueous solution by adding a base.²³⁷⁻²³⁹ After the formation reaction



with $M = \text{Fe}^{2+}, \text{Mn}^{2+}, \text{Co}^{2+}, \text{Cu}^{2+}, \text{Mg}^{2+}, \text{Zn}^{2+}$ or Ni^{2+} .²³⁷ The size and shape of the MNP depend on the type of salt used, the ratio of iron(III) and M(II) ions, the reaction temperature, the pH value, the ionic strength of the medium and other reaction parameters (e.g. stirring speed, dripping rate of the basic solution). Magnetite nanoparticles are not highly stable in an aqueous environment and are oxidized to maghemite or dissolved in an acidic medium. For this reason, controlled oxidation to the more stable maghemite is often performed as a follow-up step. Better dispersibility in water can be achieved by subsequent acidification. The synthesis is characterized by high reproducibility and high yield ($> \text{kg}$), but the polydispersity is large compared to other methods. A controlled narrower size distribution can be achieved by the addition of organic stabilizing agents during synthesis or by post-sizing.^{237–241}

4.1. Magnetic properties

Magnetic manipulation requires high magnetic response of MNPs. Superparamagnetic iron oxide, magnetite and maghemite nanoparticles are suitable for use in nanomedicine.²¹⁸ They represent a compromise between good magnetic properties and very low toxicity.²⁴² In comparison, other magnetic nanoparticles, such as Co or FePt, have higher saturation magnetization and better magnetic behavior. However, their toxicity makes them less suitable for biomedical applications.^{218,229}

Rotating electrons in an atom have a magnetic orbital moment and a magnetic spin moment. These add vectorially to the magnetic dipole moment, which is typically given in the natural unit of Bohr magneton (μ_B). The Bohr magneton is the absolute value of the magnetic moment generated by an electron with orbital angular momentum quantum number $l = 1$ through its orbital angular momentum.^{243–246}

The unitless magnetic susceptibility describes the magnetizability due to the application of an external magnetic field. If the magnetic susceptibility takes negative values, this means a magnetization against the applied magnetic field and vice versa. In simple terms, the magnetic volume susceptibility χ_V is the constant of proportionality between the magnetization \vec{M} and the magnetic field strength \vec{H} .^{243–246}

$$\vec{M} = \chi_V \vec{H} \quad (4.2)$$

There is a simple relation to the relative magnetic permeability μ_r , which indicates permeability of matter to magnetic fields.^{243–246}

$$\chi_V = \mu_r - 1 \quad (4.3)$$

Here the permeability of a material is given in relative to the permeability of the vacuum

(μ_0) .^{243–246}

$$\mu_r = \frac{\mu}{\mu_0} \quad (4.4)$$

Materials can be classified based on their response to an applied magnetic field. There are five basic types of magnetism: diamagnetism, paramagnetism, ferromagnetism, antiferromagnetism and ferrimagnetism (Fig. 4.3).^{184,247}

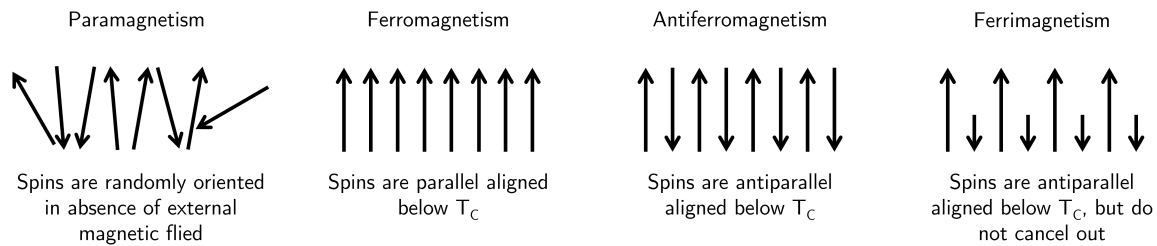


Figure 4.3.: **Different types of magnetism.** Diamagnetism is not shown. Adapted from Pekarsky et al.¹⁸⁴

All materials exposed to a magnetic field exhibit diamagnetism, where the atomic current loops generated by the orbital motion of electrons react to the external field. This produces a very weak repulsion, which can only be observed when no other form of magnetism is present, as these are much more potent. In materials in which the electron configuration of the atom are complete, i.e. each electron orbital must be fully paired, the electron moments annihilate so that only the weak reaction moment directed against the magnetic field remains. These materials are diamagnetic. Examples are noble gases, ionic and covalent compounds like quartz (SiO_2), NaCl , H_2O , metals like Zn or superconductors. Superconductors represent a perfect diamagnet ($\chi = -1$). Diamagnetic materials display negative magnetic susceptibility ($\chi < 0$) and low relative permeability ($0 \leq \mu_r < 1$).^{243–247}

In materials whose electrons are at least partially unpaired, other forms of magnetism occur. Paramagnetic materials, such as pyrite, O_2 , Al or Ti , have a combination of orbital and spin angular momentum greater than zero. The orientation of these magnetic moments is disordered, so that only a slight total magnetic moment of the material is present. The application of an external magnetic field leads to the alignment of the magnetic moments along the magnetic field and the magnetic susceptibility is slightly positive ($\chi \approx 0$), correspondingly the relative permeability $\mu_r > 1$.^{243–247}

Ferromagnetic materials have atomic magnetic moments, which are aligned. Ferromagnetic materials are exclusively metals, such as iron (Fe), nickel (Ni) and cobalt (Co) and special alloys. These have a very high relative permeability ($\mu_r \gg 1$, $\chi > 1$) and show a temperature dependence of χ (described by the Curie-Weiss law). Above a critical particle size, an energetically favorable division into domains takes place, the so-called Weiss domains. These domains have different spin orientations, which on a macroscopic scale lead to a

low net magnetic field of the sample. The superior order of the magnetic moments is in contrast to the disordered orientation in paramagnetic materials. If the atomic magnetic moments are present in an antiparallel arrangement and cancel each other, one speaks of antiferromagnetism, e.g. hematite ($\alpha\text{-Fe}_2\text{O}_3$), and of ferrimagnetism, e.g. magnetite (Fe_3O_4), maghemite ($\gamma\text{-Fe}_2\text{O}_3$), greigite (Fe_3S_4), if the magnetic moments do not cancel each other completely. Above the Curie temperature T_C , ferro-, antiferro- and ferrimagnetic materials show paramagnetic behavior. In this case, the thermal energy is sufficient for the previously arranged magnetic moments to rotate randomly, causing the long-range order to disappear.^{184,243–247}

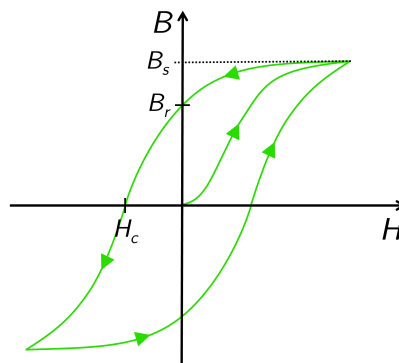


Figure 4.4.: **Hysteresis curve.** Magnetic flux density (B) as a function of the strength of the external magnetic field (H) with saturation flux density (B_s), coercive field strength (H_c), and remanence flux density (B_r). Adapted from Pekarsky et al.¹⁸⁴

In Figure 4.4 the magnetization curve of a ferro- or ferrimagnetic material is shown, which by means of the flux density B shows the course of the magnetization as a function of the field strength H . From the equation

$$B = \mu_r \mu_0 H \quad (4.5)$$

it follows that the relative permeability μ_r indicates the slope of the magnetization curve and the curve progression shows a dependence of the relative permeability μ_r on the field strength H . The flux density in the material initially increases strongly, then becomes progressively slower until the saturation flux density B_s is reached and all magnetic moments are aligned parallel to the external field. If the field strength H is now reduced, the curve describes a slower decrease, so that at the field strength $H = 0 \text{ A/m}$ a remanent flux density B_t can be detected, indicating that the material is magnetized. To remove the remanent flux density B_t a magnetic counter field with the coercive field strength H_c must be applied. Thus the magnetization curve shows a clear hysteresis. If this hysteresis is broad, one speaks of magnetic hard materials, which are suitable for permanent magnets. A narrow hysteresis indicates that the material has small remagnetization energy, suitable for electromagnets and fast switching. These materials are called magnetically soft.^{243–247}

In addition to the temperature, the particle size also has a critical influence on the magnetic behavior. On the one hand, the size and thus the volume is also relevant for the strength of the interaction of the nanoparticle with an external magnetic field. On the other hand, below a critical particle size, magnetic orientation is described by a single Weiss domain. The particles then consist of a single domain (single domain state). The critical size for the single domain state depends on the material. The magnetic field required for demagnetization (coercive field) decreases in this state. If the particle size is reduced further, some materials exhibit, dependent on the temperature, superparamagnetism (Fig. 4.5). Superparamagnetic particles have a fixed magnetic moment and no coercive force resulting in loss of magnetization due to removal of the external magnetic field. The net macroscopic magnetization is zero due to the random orientation of the particles without an external magnetic field. Due to high initial magnetic susceptibility, only small fields are required for magnetization. The critical particle size for superparamagnetism is 10 nm for cubic magnetite and 15 nm - 18 nm for maghemite. The small size and magnetic behavior, such as no permanent magnetization and fast response to external magnetic fields, of superparamagnetic nanoparticles make them exceedingly interesting for biomedical applications.^{184,218,229,247}

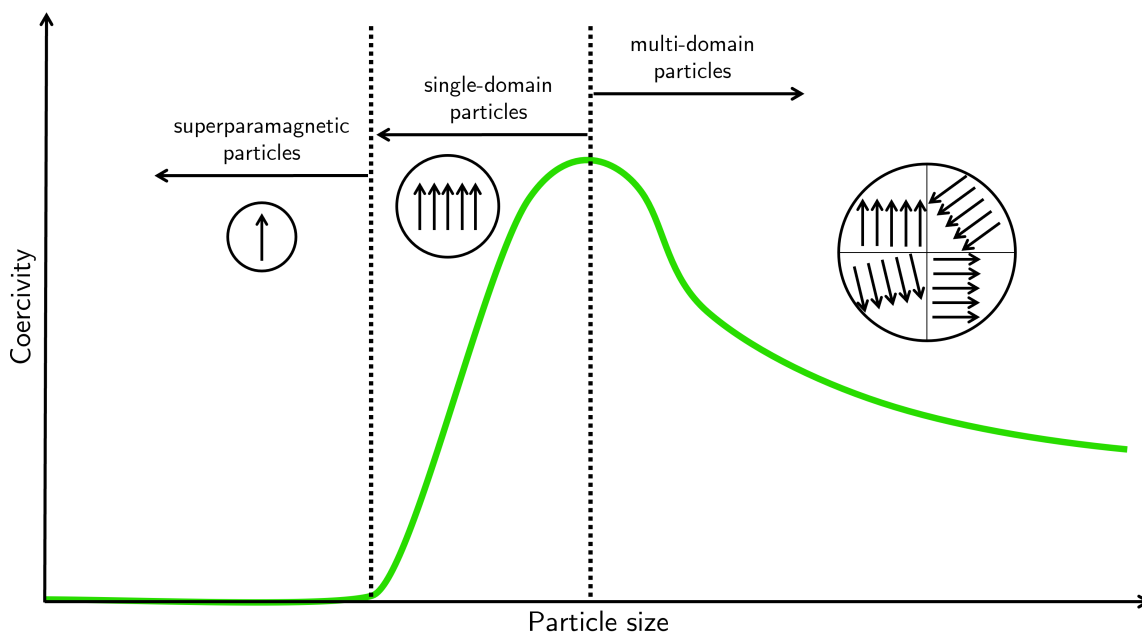


Figure 4.5.: **Schematic graph of coercivity as a function of particle size.** Adapted from Pekarsky et al.¹⁸⁴

4.2. Colloidal stability in aqueous solutions

As described previously, nanoparticles have a high surface energy due to their high surface-to-volume ratio, which enables strong intermolecular interactions. The determining interactions in aqueous solution are the long-range (up to approximately 10 nm) van der Waals interactions and electrostatic interactions, as well as short-range forces, such as hydration forces, hydrophobic, depletion forces, and steric forces. Magnetic forces also play a role for magnetic nanoparticles.^{248–251}

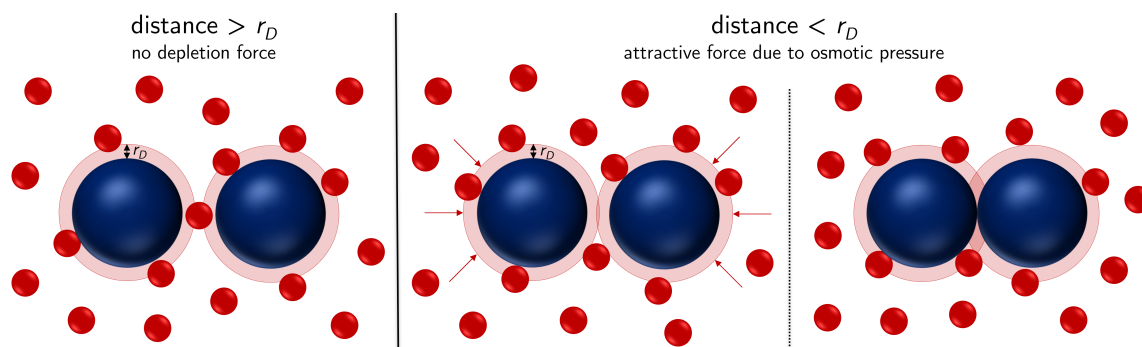


Figure 4.6.: **Scheme of depletion force.** Attractive force between large colloidal particles (blue) which occurs when they are suspended in a solution containing small solute particles (depletant, red), when the distance is smaller than the diameter of the depletant ($2 \times r_D$).

Depletion force is an attractive force between large colloidal particles which occurs when they are suspended in a solution containing small solute particles (depletant). This force is described in the Asakura-Oosawa model: A distance between two particles which is smaller than the diameter of the depletant ($2 \times r_D$) leads to the exclusion of the depletant from the interstitial space, resulting in an osmotic pressure exerted by the environment on the particles and an attractive force.²⁵²

When charged nanoparticles are dispersed in an aqueous, saline solution, their potential is counterbalanced by the attachment of ions and an electric double layer (EDL) is formed (Fig. 4.7). Within the so-called Stern-layer, these counterions are strongly bound. This layer surrounds a layer of loosely bound co- and counterions. The boundary of this relatively diffuse layer is called the slipping plane, and the potential at the boundary of this layer represents the ζ -potential.^{249–251,253} Typically, the values of the ζ -potential range from -100 mV to +100 mV and can be used as an indicator of colloidal stability. Nanoparticles with a ζ -potential between -10 mV and +10 mV are considered approximately neutral and with more than +30 mV or less than -30 mV are considered strongly cationic and strongly anionic and thus are considered colloidally stable.

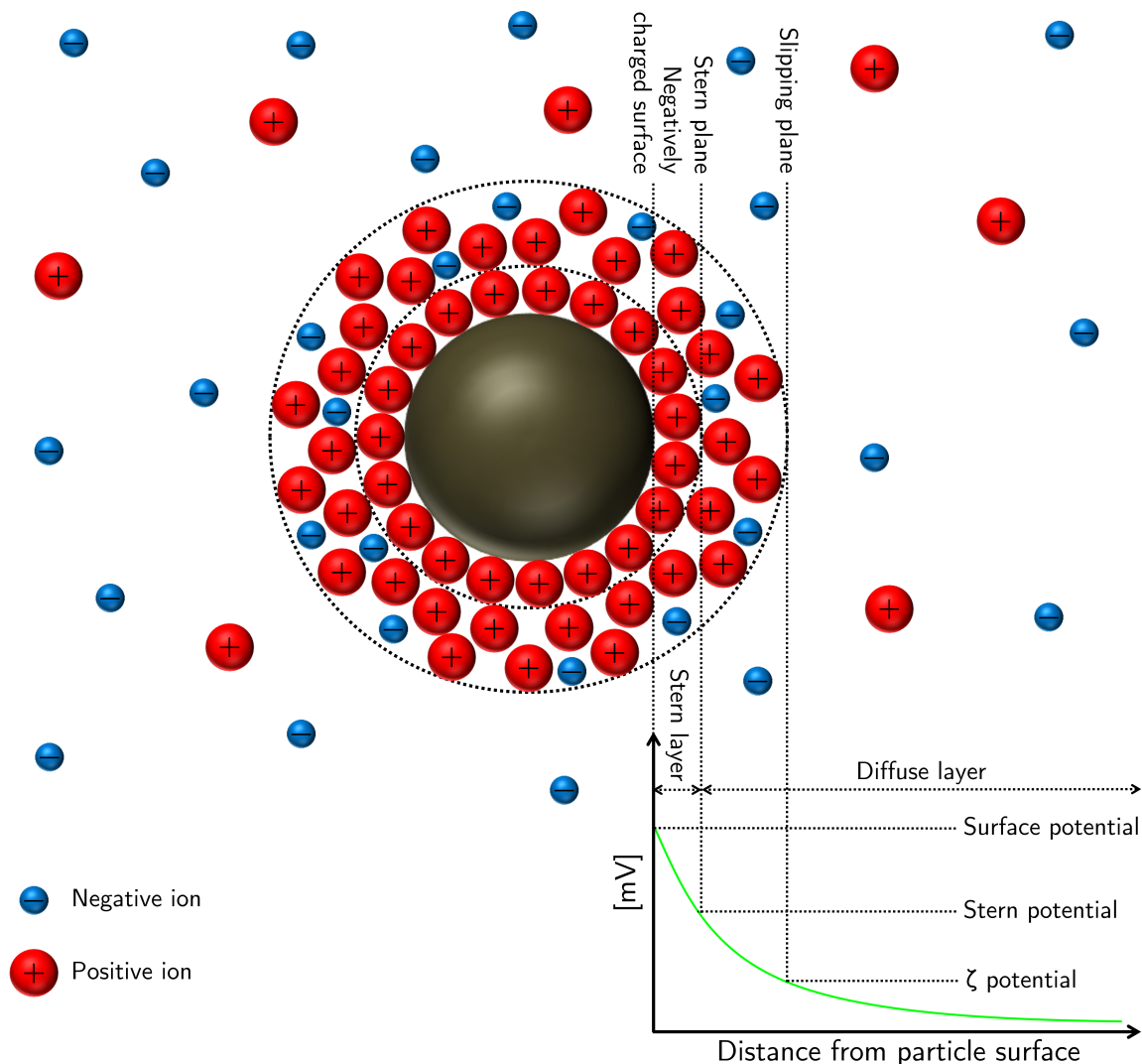


Figure 4.7.: **Scheme of the double layer of particles with a negatively charged surface in solution.** Adapted from Zhang et al.²⁵¹

Aggregation occurs when their particle surfaces are brought into contact by physical processes and short-range thermodynamic interactions that enable particle-particle adhesion. To understand the aggregation of nanoparticles under different conditions and to predict the colloidal behavior, the Derjaguin-Landau-Verwey-Overbeek (DLVO) theory is often used. This describes the energetic interactions in dispersions as a function of particle distance. Two approaching, like-charged, spherical particles and the resulting attractive van der Waals and repulsive electrostatic forces from the overlap between the electric double layers of the interacting surfaces are considered.^{251,254,255} In a simplified view, the thermodynamic surface interactions are obtained by summing the van der Waals and electric double layer interaction energies and considering whether the net interaction energy is negative (attractive) or positive (repulsive).^{251,254,255} The attractive van der Waals interactions occur in all types of atoms, molecules and ions and are relatively weak non-covalent interactions, which can be divided into three components: Interaction between two dipoles (Keesom

force), interaction between a dipole and a polarizable - induced dipole (Debye force) and between two polarizable molecules without permanent dipole moment - fluctuating dipoles (London dispersion interaction, often referred to as van der Waals force).^{248,251,254,255} The electrostatic interaction energy indicates the strength in electrostatic attraction or repulsion due to the formation of an electrical double layer (EDL) on the surface. The ionic strength determines the surface ionization and thickness of the electrical double layer. A low ionic strength allows the ion cloud to spread further, resulting in a high Debye length; high ionic strengths compresses the electrical double layer, resulting in a low Debye length.^{251,254,255}

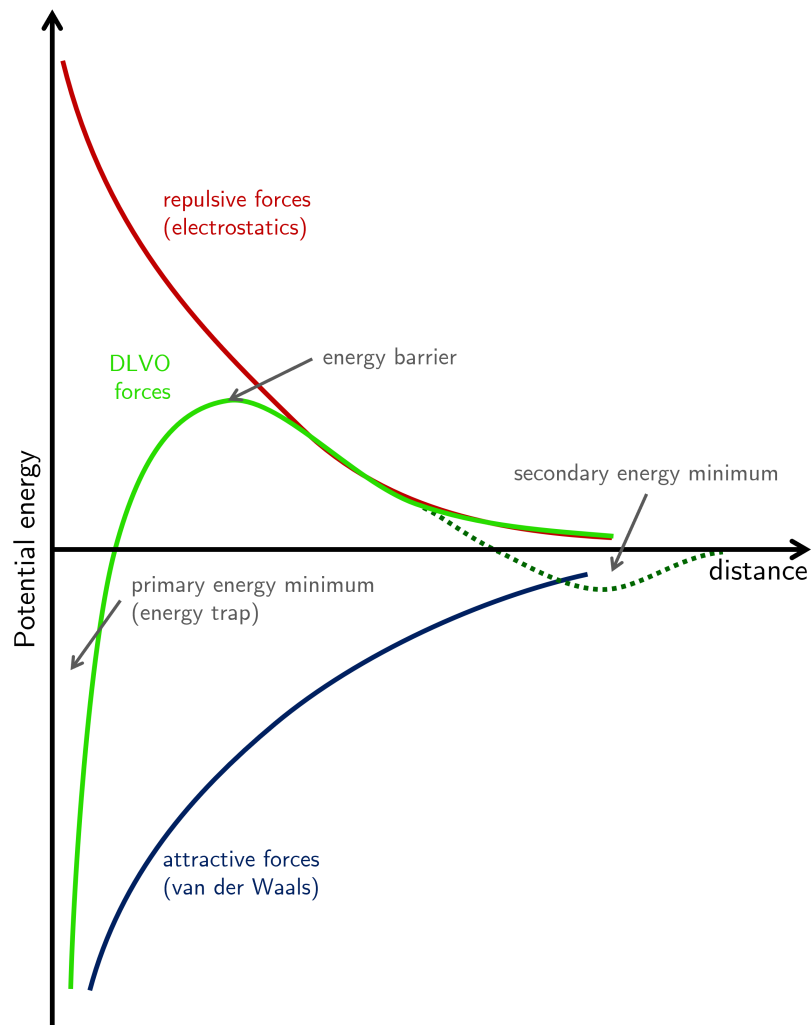


Figure 4.8.: **DLVO theory.** Potential energy as a function of the distance between two spherical particles.

If one considers the approach of two spherical particles (Fig. 4.8), the curve of the net interaction energy (DVLO force, light green curve) initially shows a positive peak, the so-called interaction energy barrier. Since the net interaction energy is dominated by repulsive forces, the particles do not aggregate. In order for the particles to contact each other, this energy barrier must be overcome. If this thermodynamic barrier is low enough, the distance can be further reduced, the net interaction energy becomes negative and the

particles enter the so-called energy trap. This is also called primary energy minimum and leads to an irreversible aggregation of the particles. The dark green dotted curve shows that there is the possibility of a secondary minimum, in which aggregation of the particles occurs. In contrast to the primary energy minimum, this aggregation is reversible and can be reversed by for instance shear forces.^{251,254,255}

4.3. Biofunctionalization

The use of nanoparticles in a biological environment, especially intracellular use, places great demands on biocompatibility, colloidal stability, and functionality. Tailored biofunctionalization of nanoparticles is a common tool to fulfill these requirements. Biofunctionalization achieves two main purposes: one is the biocompatible coating of the particles, in which toxicity is reduced and undesirable cell reactions are prevented, and the other is the functionalization of the particles with a functionally active component, for example, a functional protein, which mediates site specific interactions.

Biocompatibility, including colloidal stability, inhibition of protein corona formation, and prevention of undesired cell reactions, can be influenced by surface charge, hydrophobicity, and steric shielding of the particles.^{256–258}

Non-covalent functionalization utilizes electrostatic and hydrophobic interactions. These interactions offer ease of functionalization and a high binding rate. Another advantage is that neither the particle surface nor the biomolecules need to be modified. However, compared to covalent conjugation, stability is low, especially in complex biological fluids, and the amount and orientation of bound molecules is difficult to control.^{259–261} Adsorption of proteins via hydrophobic interactions can lead to denaturation through conformational changes and exposure of their internal region.²⁵⁹ Stable functionalization can be obtained through covalent bonds, which is very suitable for intracellular applications. Amine, thiol, or carboxyl groups are most commonly used in bioconjugation strategies for covalent bonding. Well-established *in vitro* bioconjugation strategies include NHS coupling reaction, maleimide coupling and click chemistry reaction, which can be carried out under mild conditions in aqueous solutions.^{259,262}

Functionalization of magnetic nanoparticles can be achieved by both organic and inorganic coatings. Organic coatings can provide functional reactive groups, e.g. hydroxyl groups, carboxyl groups, amino groups, or aldehyde groups. These coatings include small molecules, surfactants, polymers and biofunctional ligands.^{237–239} Small molecules and surfactants can be divided into three types: oil-soluble, water-soluble, and amphiphilic. The classic example of an oil-soluble functionalization is represented by oleic acid. Water-soluble iron oxide NPs can be obtained by adding small organic molecules, such as citric acid or

amino acids directly during the synthesis process, or oil-soluble functionalizations can be exchanged, here the ligand exchange reaction is a widely used method.^{237,239} Polymers can be irreversibly applied to the particle surface by chemisorption of the macromolecular chains or polymerization can be initiated on the particle surface. A commonly used method of functionalization is the replacement of the hydrophobic stabilizing ligands with hydrophilic bifunctional molecules, with an anchor group that binds efficiently to the surface and a hydrophilic moiety that imparts stability in aqueous media.^{237,238}

Widely used inorganic surface modifications of MNPs include coating with silica, controlled oxidation of the surface for passivation, and coating with noble metals. In the latter, coating with gold offers many advantages for further functionalization steps.²³⁹ Gold is able to form a covalent bond with sulfur. This allows functionalization with sulfur-containing organic molecules, usually mediated by the sulfhydryl group in thiols.²⁶³ The most widely used method for preparing functionalized iron oxide NPs is silica coating, which provides good biocompatibility, hydrophilicity, and stability, with a controllable shell thickness. In addition, silica coating offers the possibility of incorporating fluorescent dyes into the SiO₂ matrix, which increases its stability and efficiency of the dye. The application of a mesoporous shell, optionally with a protective boundary layer of thin non-porous silica, provides an increased surface area for further functionalization steps and pores for the adsorption of various drugs.^{238,239}

As evident by DLVO theory, one way to protect nanoparticles from aggregation is electrostatic stabilization. By applying electric charges to the nanoparticle surface, the repulsive electrostatic forces can be increased.^{249,264} Surface charge also affects interaction with charged cellular constituents and protein corona composition. Requião et al. studied the charge of 551,705 proteins from different organisms from *E. Coli* to *H. Sapiens*. This revealed more negatively charged sequences than positively charged sequences and the underrepresentation of extremely positively charged sequences in most proteomes, making the net charge slightly negative.^{257,265}

Another approach to increase biocompatibility is steric stabilization or steric shielding. This steric shielding prevents aggregation as well as undesired cell reactions, such as recognition by the immune system, and protein absorption. To obtain a shielded nanoparticle polymers or surfactants are bound to the surface. Poly(ethylene glycol) (PEG) and other intrinsically disordered polymers such as polyphosphate esters or the polypeptide repeats of proline-alanine-serine (PAS) are widely used. The gold standard is PEG, with high hydrophilicity and low toxicity. The grafting of PEG chains onto the particle surface is known as PEGylation.^{257,266–272}

In PEGylation, the hydrophilic and flexible properties of the chains in solution lead to a hydrated cloud. Due to their long disordered chains, PEG polymers have high confor-

mational entropy. When proteins encounter the PEGylated surfaces, they compress the chains. This leads to entropy loss and thus to a repulsive force opposite to the attractive force between protein and surface.^{266,267,269,273–275} An effective stealth effect depends on several parameters such as molecular weight, i.e. chain length, the density of the chains on the surface, and the conformation of the polymer. For efficient shielding against protein adsorption, a minimum molecular weight of 2 kDa is described.^{267,269} Efficient shielding also requires dense packing of the PEG chains and a complete, closed coating. Molecular weight and especially density also have an effect on polymer conformation. Low surface coverage leads to a large range of motion, this can result in the formation of the so-called mushroom conformation. The required range of motion depends on the chain length and the resulting radius of the mushroom conformation. In the mushroom conformation, the entropy of the chain as well as thickness of the stealth layer is reduced and thus the efficiency of the shielding. At high surface densities and a small available range of motion, the so-called brush conformation is formed, in which the chains are stretched out and have a higher entropy.^{267,276} At very high surface densities, the freedom of the PEG chains, their entropy, and thus the effectiveness of the shielding decreases.²⁶⁷ Binding of PEG to SPIONs has been shown to increase hydrophilicity and stability and decrease cytotoxicity.^{260,277} Often electrostatic and steric stabilization are used in combination to keep the nanoparticles in dispersion.^{249,278}

To specifically functionalize nanoparticles with proteins of interest (POI) *in vitro* and *in vivo* or to intracellularly recruit nanoparticles site-specifically to regions of interest (ROI), different targeting systems are used. This requires fast, selective and stable binding even under complex and reactive intracellular conditions. For this purpose, targeting systems well established for labeling with organic dyes can be used. Established targeting systems include the HaloTag²⁷⁹ and the SNAP-Tag^{280,281}, which belong to the so-called suicide proteins and form an irreversible covalent bond. These targeting systems are bio-orthogonal, so there are no unwanted endogenous interaction partners in the cell or medium.²⁸² The HaloTag consists of the HaloTag protein, which is based on the haloalkane dehalogenase DhaA from *Rhodococcus rhodocrous* engineered for covalent and rapid binding to the synthetic HaloTag ligand (HTL). The HaloTag protein (33.6 kDa) can be fused to the N- and C-termini of the POI and mediate binding of the POI to NPs functionalized with the HTL ligand. The SNAP-Tag (19.4 kDa) is based on the ubiquitous O-6-alkylguanylyltransferase, a mammalian DNA repair enzyme, which binds rapidly and covalently to the SNAP-Tag ligand.²⁸³ In particular, bio-orthogonality represents an important criterion for *in vivo* functionalization and *in vivo* targeting. In contrast, non-bio-orthogonal systems, such as streptavidin-biotin^{284,285} are only suitable for *in vitro* functionalization due to streptavidin being blocked by ubiquitously present endogenous biotin.

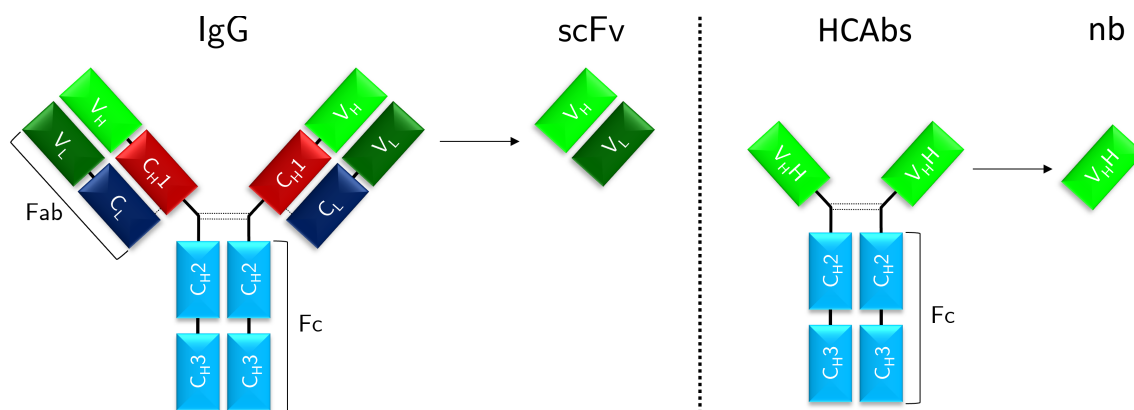


Figure 4.9.: **Schematic structure of immunoglobulin γ (IgG) antibody and heavy-chain antibody (HCAbs) and the derived single-chain variable fragment (scFv) and nanobody (nb).** Consisting of heavy (H) and light (L) chains with conserved (C) and variable (V) domains. (Fc: crystallizable fragment, Fab: antigen-binding fragment).²⁸⁶

Another advantageous targeting system is based on the green fluorescent protein (GFP) from *Aequorea victoria* and GFP-specific binding proteins, e.g. nanobodies and DARPin. In sera of camelids, in addition to immunoglobulin γ (IgG) antibodies (~ 150 kD) highly conserved in mammals, consisting of two identical heavy (H)-chain polypeptides folded into four domains and two identical light (L)-chain polypeptides folded into two domains, a special type of IgG antibodies called heavy-chain antibodies (HCAbs) are present. In conventional heterotetrameric antibodies, the sequence of the N-terminal domain of the H and L polypeptide chains is variable (variable domain, V_H and V_L, respectively); together, these form the variable fragment (Fv) that recognizes the antigen. The smallest intact functional antigen-binding fragment generated from conventional antibodies consists of these two domains, which are formed through an oligopeptide, this is called a single-chain variable fragment (scFv, ~ 25 kD). The remaining domains are more conserved (C_H and C_L, respectively). The first C_H domain, together with the C_L domain and the two variable domains, forms the antigen-binding fragment (Fab, ~ 50 kD). The last two C_H domains play a role in immune cell recruitment and effector functions and are referred to as the crystallizable fragment (Fc). The cameloid heavy chain antibodies lack the L-chain polypeptide and the first domain of the H-chain (C_{H1}). The H-chain of the homodimeric protein has a special variable domain (~ 15 kD) called V_{HH} (variable heavy domain of heavy chain antibodies) that binds the antigen and forms the structural and functional equivalent of the Fab fragment. This V_{HH} domain contains a complete antigen binding site and is the smallest functional antigen binding fragment, also called a nanobody (nb).^{286–288} α GFP nanobodies have been developed which bind with high affinity (down to submolar k_D) and specificity to GFP^{289,290}. Nanobodies can be genetically modified and fused to POIs. This fusion protein can be expressed in prokaryotic cells and *in vitro* purified in large amounts, as well as expressed in eukaryotic cells and bind intracellular GFP. This allows both *in vitro* and *in vivo* functionalization of the nanoparticles and site-specific targeting.²⁹¹

Disulfide bonds play a crucial role for thermal stability and correct and reversible folding of nanobodies.^{292,293} Therefore expression and folding from the reduced unfolded state in cytosol is a major challenge. The reducing conditions of the cytosol hinder the folding and stability of some nanobodies.²⁹²

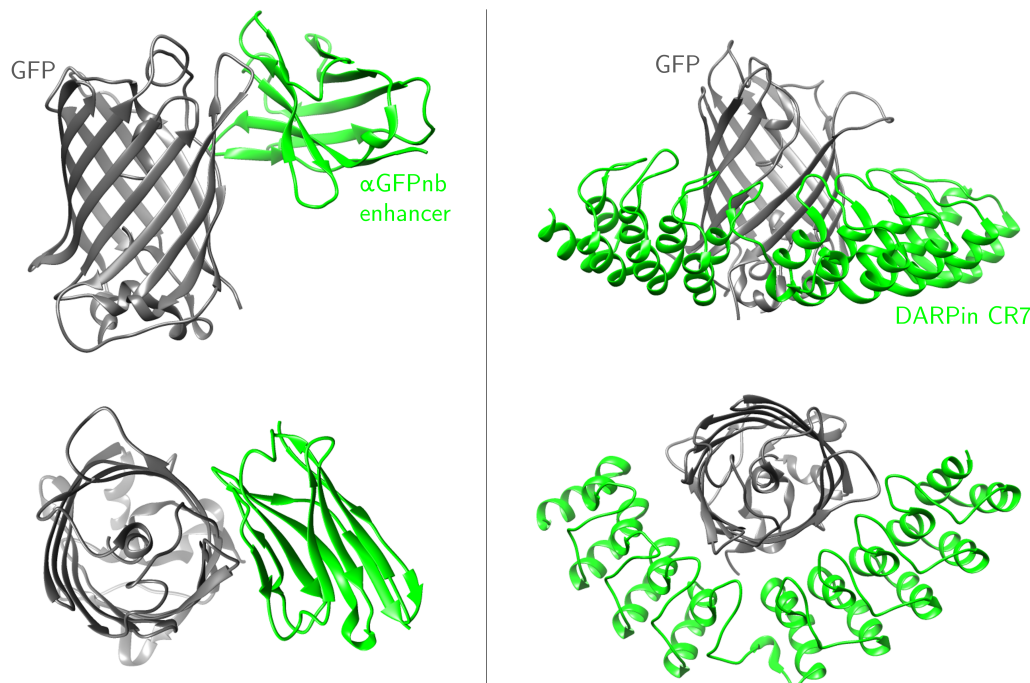


Figure 4.10.: **Crystal structure of the binding of nanobody and DARPins (both in green) to GFP (grey).** Side view and top view of the α GFP nanobody (PDB 3K1k) and DARPins CR7 (PDB 5MA5) is shown. Created with UCSF Chimera.

Ankyrin repeat proteins (DARPins) represent another type of binding proteins. These are artificial proteins, and the design avoids cysteines and thus disulfide bonds. DARPins exhibit high thermal stability and stability to denaturants. Their stable, elongated tertiary structure consists of at least 3 compactly layered repeats (3 repeats: ~ 10 kDa + ~ 4 kDa per repeat) consisting of a β loop followed by two antiparallel α helices. The outer, flanking ones are called capping repeats. DARPins can also be fused to POIs and produced in high yield, up to 30% protein of total cellular protein (up to 200 mg/l).^{286,294,295}

4.4. Intracellular nanoparticle diffusion

The cytoplasm of eukaryotic cells behaves like a two-phase poroelastic medium and consists of a liquid phase, the cytosol, and a solid phase, such as the cytoskeleton and organelles.²⁹⁶ The diffusion of nanoparticles is influenced by both the properties of the liquid phase and physicochemical properties of the substances dissolved in it, and the composition, geometry, and organization of the solid phase, especially the cytoskeleton.²⁹⁷ A crucial criterion for diffusion in the liquid phase is its viscosity. Studies showed 2-5 times higher viscosity of

cytosol compared to water.^{298,299} If the particle size is above the pore size of the cellular solid network, the diffusion of the particles is restricted. On short time scales, particles are hindered from diffusing by these barriers. On longer time scales, remodeling of the internal cellular structures allows the particles to move. Pore size depends on the cell type. The size of the actin meshwork of the plasmalemmal undercoat varies from approximately 30 nm to 230 nm. The compartment size of the actin meshwork in HeLa cells is 68 nm.^{201,202} Etoc et al. showed that the limit of hindered diffusion in HeLa cells for particles is below a size between 50 nm and 70 nm. Smaller and inert particles show Brownian diffusion without being hindered by obstacles. As the non-specific interaction of particles with intracellular components increases, diffusion slows down. The increasing interactions lead to longer immobilization times and subdiffusive behavior.²⁹⁷

4.5. Engineered biofunctionalized magnetic nanoparticles

4.5.1. MagIcS - Magnetic Intracellular Stealth Particles

In a previous work, Liße et al. engineered MagIcS based on the natural protein cage ferritin for magnetic remote control of GTPase activation.⁷⁵

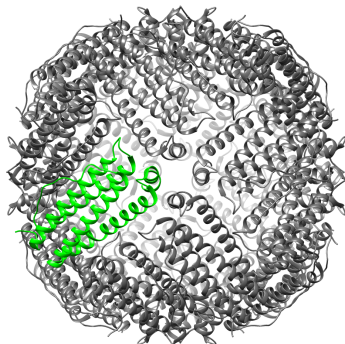
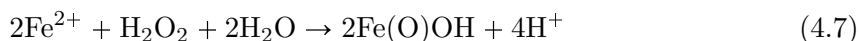
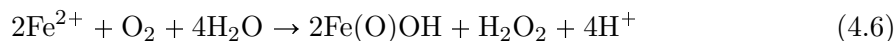


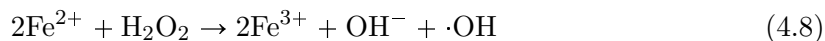
Figure 4.11.: **Crystal structure of human heavy chain ferritin (HCF).** One of the 24 subunits is highlighted in green. PDB entry 6m52, created with UCSF Chimera.

Ferritin is a ubiquitous protein in all life forms from archaea and bacteria to eukaryotes, with the exception of yeast. Ferritin (~ 450 kDa) consists of 24 subunits that self-assemble into a protein cage (Fig. 4.11). This protein cage has an outer diameter of ~ 12 nm and a cavity with a diameter of ~ 8 nm.^{184,192,300–302} Ferritin is found in extracellular and intracellular compartments, such as cytosol, nucleus and mitochondria. Ferritin is an iron storage protein and is able to store up to 4500 iron atoms in a compact and safe form. This storage can be re-available when needed, which renders ferritin as cellular iron reserve.^{184,192,301} Ferritin sequesters two ferrous iron ions (Fe^{2+}) at the ferroxidase center, converts it to ferric iron ions (Fe^{3+}), and stores this in the form of hydrous ferric oxide in the cavity of the protein cage. Both O_2 and H_2O_2 can be used in this oxidation with the latter being preferred (equations 4.6–4.7). This protects the cell from cell damage from metal toxicity by biomineralization into an inert form for storage. Secondly, it inhibits free radical production as it competes with the toxic Fenton reaction (equation 4.8), in which a hydroxyl radical and a hydroxide ion is released.^{184,192,300,301,303}

Ferritin ferroxidation:



Fenton reaction:

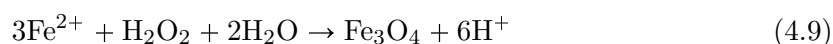


The ferritin subunits have a α -helix structure with strong helix-helix interactions. In eukaryotes, ferritin is composed of a heavy chain (HC, 21 kDa) and a light chain (LC, 19 kDa) arranged in tetrahedral symmetry. A dodecameric cage with dimeric intermediates is formed. The ratio of HC and LC is variable in different tissue types. Amphibians possess an additional type of ferritin, that of plants and bacteria is similar to HCF. The HC subunit involves a highly conserved catalytic ferroxidase center that binds and oxidizes ferrous iron ions. The LC subunit is involved in iron nucleation. When ferritin is present with empty protein cages, it is called apoferritin.^{184,192,301,303}

Ferritin has numerous properties that make it interesting for biotechnological and biomedical applications. Ferritin is highly biocompatible and low immunogenic.³⁰³ Functional peptides and proteins can be genetically fused to the ferritin subunit so that they are presented on the inner or outer surface of the protein cage. This allows efficient functionalization and site-specific targeting of proteins of interest or target regions.^{75,304} Ferritin has a highly symmetric structure with high thermal and chemical stability. Thus, the protein cage is stable over a relatively wide pH range and resistant to high temperatures of up to 85 °C, as well as to relatively high concentrations of many denaturants, such as urea. In addition, it is possible to selectively and reversibly disassemble the ferritin protein cage by exposing it to extreme pH conditions (pH 2-3, pH 10-12); a switch to neutral pH conditions thereafter results in self-assembly. The ferritin protein cage offers the possibility of loading and mineralization with a variety of metals as a reaction vessel separated from the environment.^{301,303}

What makes ferritin particularly interesting for biotechnological and biomedical applications is the possibility to obtain magnetoferritin *in vitro* (equation 4.9). The high stability at high concentrations and elevated pH values is used to synthesize a magnetic mineral core in apoferritin under controlled conditions. This can be obtained by slow oxidation at 60 °C - 65 °C and pH 8.5, resulting in the formation of a superparamagnetic magnetite/maghemite ($\text{Fe}_3\text{O}_4/\gamma\text{-Fe}_2\text{O}_3$) core.^{187,188,190,191}

Magnetoferritin:



Taking advantage of the unique properties of ferritin, Liße et al. fused monomeric EGFP (mEGFP) to the N-terminus of human heavy chain ferritin (HCF) to generate mEGFP::HCF protein cages. The densely coated mEGFPs provide highly stable GFP β -barrels. Moreover, GFP is used for both visualization and as a specific bio-orthogonal targeting motif for protein of interest fused to α GFP nanobodies. After encapsulating a magnetic core, by using the natural ferroxidase activity (equation 4.9), a magnetic nanoparticle with intracellular stealth properties (MagIcS) was obtained (Fig. 4.12). Characterization by analytical size exclusion chromatography (aSEC) and dynamic light scattering (DLS) revealed robust and

monodisperse cages. The small hydrodynamic diameter of (25.6 ± 0.3) nm without and (27.7 ± 1.1) nm with PEGylation enables free diffusion in the cytoplasm. TEM measurements show the *ex vivo* synthesis strategy yielded highly monodisperse core size of (7.1 ± 0.5) nm. After microinjection of PEGylated MagIcS into the cytoplasm of HeLa cells, a rapid homogeneous distribution was observed confirming the free diffusion in the cytosol. This homogeneous distribution remained stable over the 20 min observation period. In contrast, particles without PEGylation were detected by the intracellular degradation machinery, visible by the appearance of bright spots. Microinjection of the PEGylated MagIcS into HeLa cells expressing the autophagy marker mCherry::LC3B showed colocalization of these dots with autophagosomes. For HeLa cells expressing mitochondria-specific Tom20 fused with mCherry and α GFPnb, microinjection of PEGylated MagIcS showed rapid site-specific targeting to mitochondria.⁷⁵

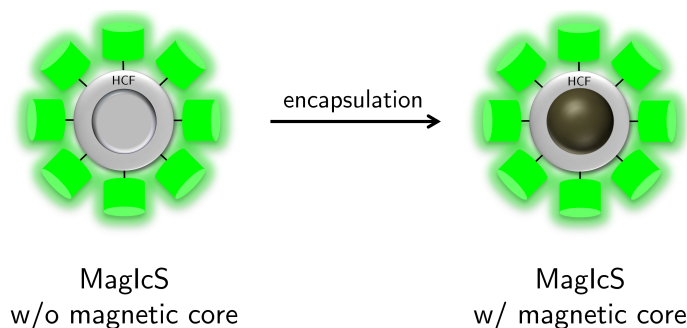


Figure 4.12.: ***In vitro* encapsulation of the magnetic core into the empty mEGFP::HCF fusion protein cage.** Under controlled conditions, the natural ferroxidase activity is used to synthesize a magnetic core into the protein cage.

Due to the limitation of the discrimination of color channels, non-fluorescent MagIcS ferritin has a key advantage for multicolor fluorescence experiments since the green fluorescence is often occupied by fluorescent reporters. For this purpose, in this thesis, a non-fluorescent MagIcS ferritin consisting of non-fluorescent GFP (mXFP, meGFP Y66F) fused to the N-terminus of human heavy chain ferritin (HCF) was generated. In the point mutation of meGFP Y66F, the tyrosine at position 66 known to constitute the GFP chromophore was replaced with phenylalanine, yielding the non-fluorescent mXFP.

4.5.2. syMagIcS - semi-synthetic Magnetic Intracellular Stealth Particles

Besides the advantageous properties, such as excellent biocompatibility, the MagIcS have certain limitations. The size of the magnetic core is limited to a maximum of 8 nm due to the fixed cage size. Furthermore, the protein cage consists of 24 identical subunits, or if a mixture of HCF and LCF is used, 12 identical subunits each. This puts a limit to the flexibility of functionalization and the control of the degree of functionalization. Intending to overcome the limitations, a new generation of biofunctionalized magnetic nanoparticles was

developed by using synthetic magnetic core particles. The synthetic cores can be obtained under optimized synthesis conditions with improved magnetic properties, thus removing the restriction due to natural ferridase activity. A larger size than 8 nm can be obtained which offers enormous potential for improving the magnetic properties as the volume increases cubically with the radius ($V = \frac{4}{3} \pi r^3$). Furthermore, versatile functionalizations could be provided by controlling the degree of functionalization. Besides these advantages, the new generation maintains the excellent biocompatibility and site-specific functionalization of MagIcS.

One-step functional coating of synthetic magnetic core particles (MCPs) is based on the high affinity iron oxide binding property of Mms6 protein from magnetotactic bacteria. Mms6 is a small protein (~6.5 kDa, 136 amino acids) found in magnetic organelles of magnetotactic bacteria, such as *Magnetospirillum magneticum* AMB-1 (i.e. magnetosomes). The magnetosomes serve as a biological compass needle for the bacteria, allowing them to align with the magnetic field of the earth and migrate along oxygen gradients in aquatic environments.³⁰⁵⁻³¹¹ The magnetosomes consist of an octahedral magnetite core surrounded by a phospholipid bilayer membrane with integrated proteins. The typical sizes of magnetosomes have a range of 35 nm - 120 nm.³⁰⁵⁻³¹¹

In 2003, Arakaki et al. described novel proteins tightly bound to the magnetosome core in *Magnetospirillum magneticum* strain AMB-1 (Fig. 4.14A). These proteins that bind strongly to magnetite are magnetosome membrane mineralization proteins (Mms5, Mms6, Mms7, Mms13).^{305,312} Among them, Mms6 is an amphipathic protein with a hydrophobic N-terminal part, adjacent a transmembrane helix and a hydrophilic C-terminal part. With the exception of the transmembrane helix, Mms6 is predicted to be intrinsically disordered due to the long leucine and glycine repeat sequence. This sequence is shared by Mms6 with MamD and MamG, which is also found in other proteins involved in biomineralization. The C-terminus (~3 amino acids) forms an α helix and consists largely of acidic (aspartic acid, glutamic acid) and hydroxyl-containing (serine, threonine) amino acids. This results in Mms6 being negatively charged at pH 7.5. The amphiphilic Mms6 self-assembles *in vitro* in aqueous solution into ~10 nm sized micelles of 20-40 subunits, with the hydrophilic C-termini on the micelle surface.^{308,309,312,313}

Biomineralization is a multi-step process. Initially, there is invagination of the cytoplasmic membrane and formation of a vesicle. These are aligned together with cytoskeletal filaments to form a linear chain. Followed by accumulation of iron ions in the vesicle mediated by transmembrane iron transporters. In the final step, nucleation and crystal growth of magnetite crystals occurs. In this process, the magnetosome associated proteins are involved in the local accumulation of iron concentration, the maintenance of reductive conditions, the mineralization by oxidation of iron, and in the reduction and dehydration of ferrihydrite to magnetite.³⁰⁶

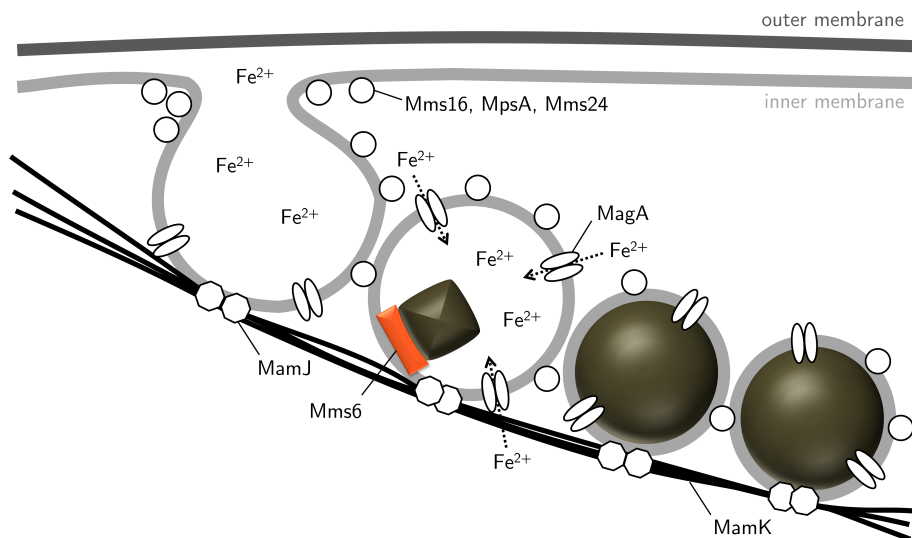


Figure 4.13.: **Scheme of the hypothesized mechanism of magnetosome biomineralization.** Based on Arakaki et al.³⁰⁶

Mms6 performs an important role in biomineralization by binding ferrous and ferric iron. The C-terminal part contains many aspartate and glutamic acids that can mediate this binding. In particular, DEEVE motif (residues 123-127) or the extension of DEEVELRD has been identified as the binding site. Studies revealed a significant structural change of the four acidic residues of the DEEVE motif in the binding of ferrous iron and it is suggested that especially the glutamic acid at position 125 and the carbonyl backbone between the glutamic acids at positions 124 and 125 mediate the binding of ferrous iron. The glutamic acids at positions 124 and 118 and the arginine at position 55 are assumed to be responsible for the binding of ferric iron. This indicates orthogonal binding sites of ferrous and ferric iron with specific conformation could promote magnetite formation.^{312,314}

Shipunova et al. have used this motif to functionalize magnetic nanoparticles with a versatile targeting system. They used a fusion protein composed of the C-terminal part of Mms6 and Barstar as the inhibitor of the ribonuclease barnase. Barstar and barnase bind rapidly and with high affinity ($k_{on} = 10^8 \text{ M}^{-1}\text{s}^{-1}$, $K_A = 10^{14} \text{ M}^{-1}$) and can thus be used for site-specific targeting.³¹⁵

Based on this, for a new generation of biofunctionalized magnetic nanoparticles, the efficient high-affinity binding of the iron-binding domain was used to create a dense mEGFP coating around a magnetic core particle. The usage of mEGFP protein provides multiple desired properties for MCP. Due to its β -barrel structure, mEGFP is robust and highly stable. Besides, mEGFP is highly biocompatible and it can be used for fluorescent visualization. Most prominently, the ability of site-specific functionalization by GFP-binding proteins with different affinities can tune the binding strength on GFP-coated MCP. For this purpose, a fusion construct consists of mEGFP, at its C-terminus the C-terminal iron-binding domain of the Mms6 protein (amino acids 112-133, Mms6 Δ N) and at its fused N-terminus His6-Tag

(H6) for purification, was produced and purified (Fig. 8.2B). Simply mixing the MCP with the fusion protein (H6::mEGFP::Mms6 Δ N) resulted in bio-functionalized semi-synthetic MNPs with intracellular stealth properties (syMagIcS) (Fig. 8.2C).

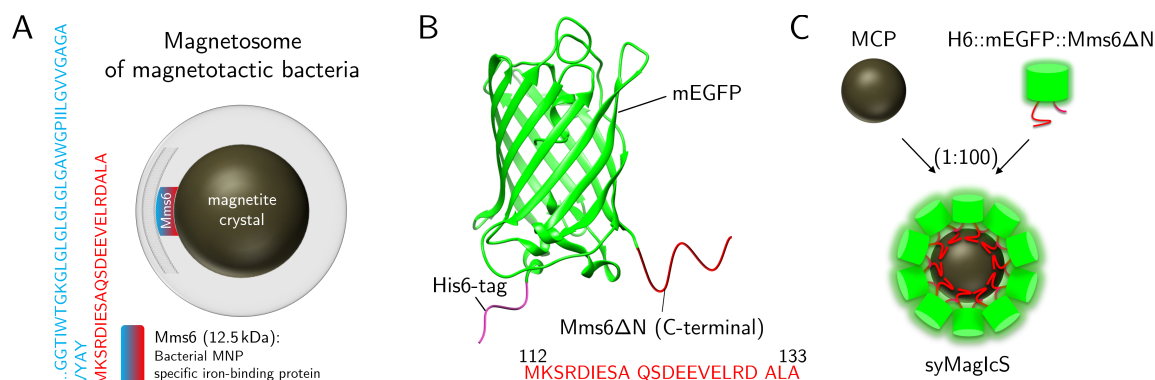


Figure 4.14.: **Genetic engineering of the coating protein for MCP biofunctionalization.** (A) Mms6 – bacterial magnetic particle specific iron-binding protein is part of the magnetosome membrane of magnetotactic bacteria. Based on Rawlings et al.³¹⁴ (B) Schematic model of H6::mEGFP::Mms6 Δ N based on a GFP crystal structure (PDB 3K1K). Mms6 Δ N is illustrated in red, mEGFP in green and the His6-Tag in magenta. (C) Coating MCP by mixing a 100-fold excess H6::mEGFP::Mms6 Δ N with MCPs.

Table 4.1.: Overview of MagIcS and syMagIcS properties.

	MagIcS	syMagIcS
	Ferritin-based MNP	Mms6-based MNP
Size	$d_{\text{hydro}} \approx 25$ nm	variable
Biocompatibility	natural ferritin cage, optional PEGylation	dense mEGFP-coating, optional PEGylation
Biofunctionalization	GFP/nanobody interaction	GFP/nanobody interaction
Multivalency	24 sites, limited controllable multivalency	highly controllable multivalency
Magnetic response	magnetic core ≤ 8 nm, superparamagnetic	synthetic magnetic core, superparamagnetic (\leq approx. 15 nm)
Preparation	<i>in vitro</i> encapsulation	one-step functional coating

4.6. Magnetic devices for spatiotemporal control of magnetic nanoparticles

Due to their small size, NP have a low magnetic moment (\vec{m}).

$$\vec{F} = \vec{\nabla}(\vec{m} \cdot \vec{B}) \quad (4.10)$$

For this reason, for a directed magnetic force (\vec{F}) and spatial control, a sufficient magnetic field gradient ($\vec{\nabla}\vec{B}$) acting on the nanoparticles is crucial.²⁴⁵ The strength of the magnetic field is responsible for the magnetization of the particles.

4.6.1. Magnetic tip

The magnetic tips for spatial manipulation were home-built. For this purpose, an iron string (0.1 mm diameter) was pulled in the flame of a Bunsen burner. The string was pulled slowly, resulting in two sharp extremities of 20 μm diameter, which were used as paramagnetic tips mounted on top of a small permanent magnet of neodymium iron boron N-52 (5 mm \times 2 mm \times 1 mm, magnetic poles axial over the length, HKCM, Eckernförde).

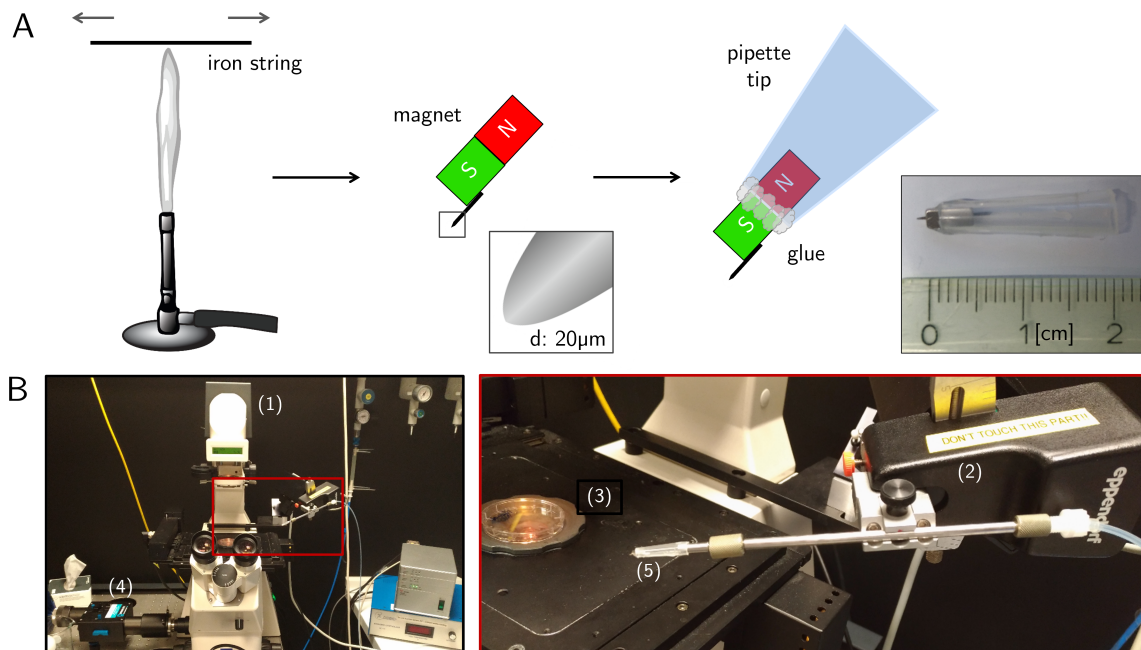


Figure 4.15.: **Fabrication of the magnetic tip and its application for magnetic manipulation.** (A) Tip fabrication and assembly: An iron wire is pulled over a Bunsen burner flame to yield a fine tip, which is attached to a magnet (Ni-45SH) and glued into a plastic pipette tip. This allows the magnetic tip to be attached to the micromanipulation apparatus. (B) Images of the microscope setup for the magnetic manipulation of human cells. (1) Microscope stand, (2) micromanipulator, (3) cell sample, (4) camera and (5) micromagnet attached to the micromanipulator.

4.6.2. Halbach Array

The application of the magnetic tip for magnetic control is limited to single cell experiments due to the need for positioning close to the investigated cells. To overcome this limitation, the aim was to develop a magnetic device that exerts a sufficiently strong magnetic gradient over an extended area to allow parallel investigation of multiple cells in a single experiment. For this purpose, a magnetic device based on the Halbach array developed by Klaus Halbach was constructed (Fig. 4.16A). The Halbach array is a special configuration of permanent magnets, which strongly enhances the magnetic field on one side and almost completely extinguishes it on the other side.³¹⁶ This results on the enhanced side in a magnetic field gradient that decreases strongly with its isomagnetic flux lines being relatively parallel to the array (Fig. 4.16B). It allows the application of a strong magnetic field gradient over a large area and at a certain distance from the sample. The magnetic device consists of a 3D-printed tray for the microscopy stage with an integrated Halbach array consisting of seven permanent magnets of neodymium iron boron N-52 (18 mm × 18 mm × 18 mm, HKCM, Eckernförde, Germany).

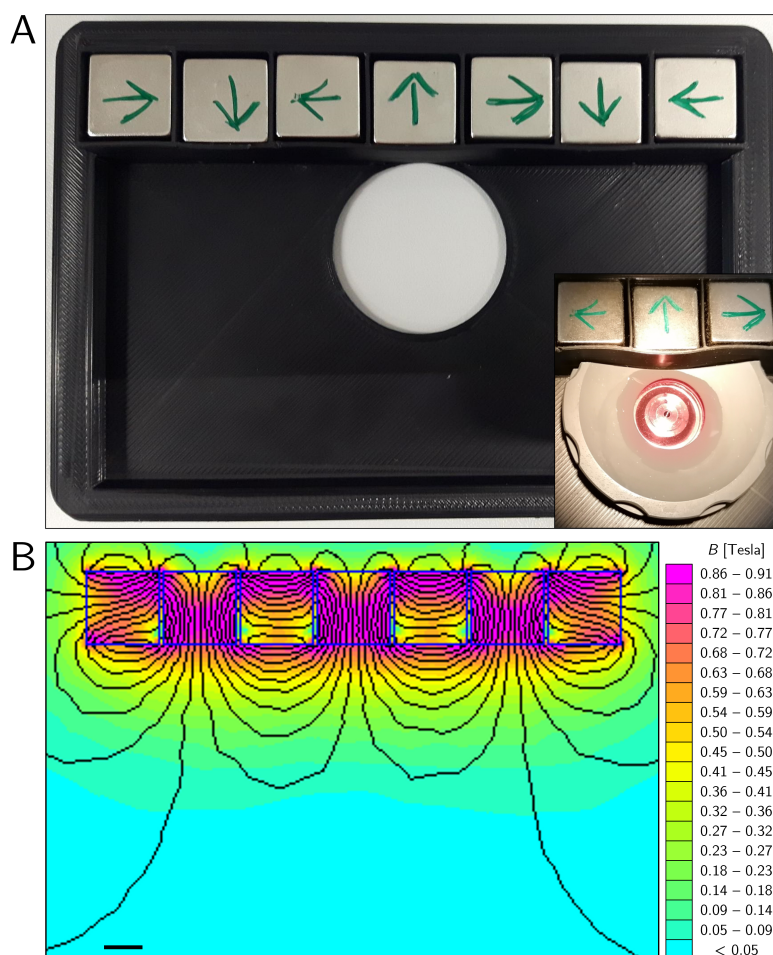


Figure 4.16.: **Magnetic device based on Halbach array.** (A) 3D printed tray for microscopy stage (Insert: sample holder). (B) Simulation of magnetic field strengths. Simulation was created with FEMM 4.2. Scale bar: 1 cm.

5 | Model system - Small GTPases

Small GTPases are molecular binary switches involved in a variety of processes of cell dynamics. They switch between an inactive GDP-bound state and an active GTP-bound state, in which downstream pathways are activated by the binding of effectors. Small GTPases have high-affinity binding for GDP and GTP and low intrinsic GTP hydrolysis activity. Switching between states is controlled by two major classes of regulatory proteins, guanine nucleotide exchange factors (GEFs) and GTPase-activating proteins (GAPs). GEFs promote the dissociation of the strongly bound GDP and GAPs catalyze the weak intrinsic GTPase function of small GTPases, which leads to the hydrolysis of GTP to GDP. In small GTPases that carry a farnesyl or geranylgeranyl group at their C-terminus, such as Ras, Rho and Rab GTPases, a cytosol/membrane alternation occurs in addition to the GDP/GTP alternation. This is controlled by guanine dissociation inhibitors (GDIs) and GDI-like proteins. These form soluble complexes with small GTPases by shielding their lipid.^{68,317–319} (Fig. 5.1)

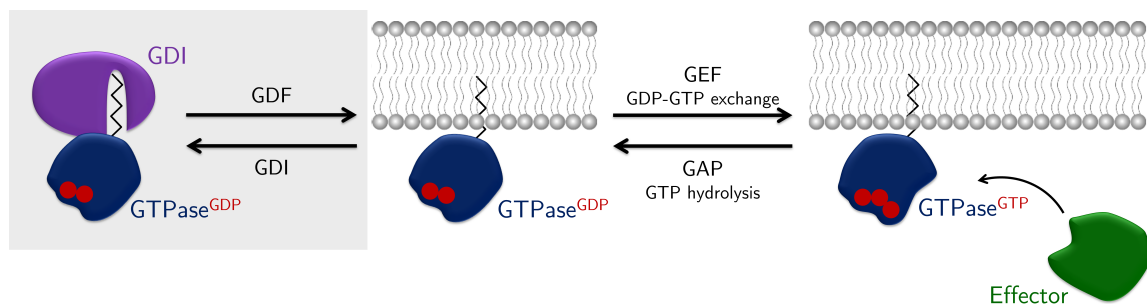


Figure 5.1.: **Schematic representation of the conformational switch between GDP-bound inactive status (centre) and GTP-bound active status (right) and inactive cytosolic state (left).** Adapted from Gray et al.³²⁰

The Ras superfamily consists of five major branches (Ras, Rho, Rab, Sar1/Arf and Ran), which are classified according to sequence and functional similarities. The Ras GTPase subfamily are signaling switches that are activated by extracellular stimuli and interact with catalytically diverse downstream effectors. They are involved in the regulation of cytoplasmic signaling networks that control gene expression and the regulation of cell proliferation, growth, differentiation and survival.^{317,321} Rho (Ras homologous) GTPases play an important role in regulating the cytoskeleton and vesicular traffic, in particular by controlling actin dynamics.^{68,322} The largest subfamily of small GTPases is Rab, which were first described as Ras-like proteins in the brain. Rab GTPases regulate intracellular vesicular trafficking and protein transport between different organelles of the endocytic and

secretory pathways, promoting vesicle formation and budding from the donor compartment, transport to the acceptor compartment, vesicle fusion and release of vesicle contents into the acceptor compartment.^{68,317} The Ras-like nuclear protein (Ran) regulates the nucleocytoplasmic import and export of RNA and proteins, the assembly of the mitotic spindle and the formation of the nuclear envelope and it is the most abundant small GTPase in the cell.^{68,317,323} ADP-ribosylation factor (Arf) family proteins play an important role in the regulation of vesicular transport, like the Rab proteins. In this process, they act as regulators in the formation of vesicle coats in various steps of the exocytic and endocytic pathways.^{68,317,324}

Due to the high-affinity GTPase/nucleotide interactions, the dissociation of GDP must be increased by GEFs to achieve efficient activation of small GTPases in cells. Despite their similar activation mechanisms, GEFs have distinctly different structures and specificity for small GTPases, which allows specific downstream signaling. Binding of the low-affinity GEF to the GDP-bound GTPase leads to the opening of the nucleotide-binding site of the GTPase and to the destabilization of the high-affinity GDP binding, thus stimulating the dissociation of the GDP. A high-affinity, binary, nucleotide-free GEF-GTPase complex is formed and due to the significantly higher concentration of free GTP than GDP in the cell, binding of a GTP occurs. The binding of the GTP leads to a conformational change, which induces the dissociation of the GEF complex.^{68,69,319}

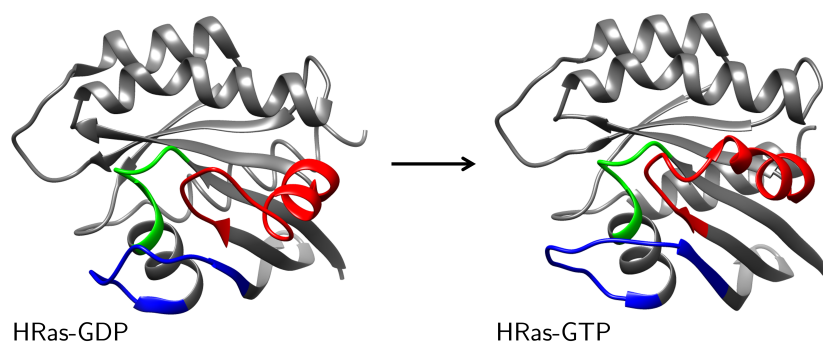


Figure 5.2.: **Structural GDP/GTP switch of HRas.** In the GDP-bound form the switch 1 (blue) and switch 2 (red) regions are more flexible. The G1 is highlighted in green. PDB entry 4Q21 (HRas-GDP), 5P21 (HRas-GTP). Created with UCSF Chimera, adapted from Lukman et al.³²⁵

As their name suggests, small GTPases have a low molecular weight (20-40 kDa). They share a G domain that contains a six-stranded β leaflet surrounded by five α helices and four to five conserved sequence motifs (G1 - G5), also called G boxes or G loops (Fig. 5.2).^{69,211} The G1 loop (P loop) is involved in the recognition and interaction of α - and β -phosphates and Mg^{2+} -ions of target nucleotides. In addition, there are two functional loop regions that change their conformation depending on the bound nucleotide (switch I and switch II regions). The GEFs bind to the GTPase, induce conformational changes in the switch I loop (G2 loop, effector loop) and stabilize the complex by interacting with the switch II region

(G3 loop). The switch I region allows the GTPase to interact with the effector, in the GTP-bound conformation, affinity is increased.^{68,69,318} In addition, both regions are involved in the coordination of γ -phosphate and Mg^{2+} -ions.^{68,69,318,326} The G4 loop and the G5 loop are mainly responsible for distinguishing the guanine base from other nucleotides.^{69,326,327} The conformational change can be described as a loaded spring mechanism. Here, the two switch regions are strained by hydrogen bonds between the γ -phosphate and the side group of the conserved threonine (switch I region) or glycine (switch II region). Hydrolysis of GTP leads to relaxation and a conformational change to GDP-specific conformation.³¹⁸

As mentioned previously, an additional important biochemical function of many members of the GTPases is post-translational modification by lipids. Many of the small GTPases of the Ras subfamily, like Ras, and the Rho family, like Rac, contain a c-terminal CAAX tetrapeptide sequence (C = cysteine, A = aliphatic, X = any amino acid). This motif owns a membrane targeting sequence, when coupled together with residues immediately upstream. These mediate interactions with membrane compartments and subcellular sites. The CAAX motif is used as a recognition sequence for farnesyltransferase and geranylgeranyltransferase I. These catalyze the covalent addition of a farnesyl or geranylgeranyl isoprenoid to the cysteine residue of the motif.^{68,317}

5.1. Ras

Ras is a membrane-anchored small GTPase that, together with Ral and Rap, forms the Ras subfamily. The numerous associated GEFs of the Ras subfamily share a CDC25 homologous catalytic domain. Two unrelated families function as GAPs containing either a RasGAP domain active in all members or a Rap member-specific RapGAP domain.^{68,208,317}

In human cells, there are four Ras isoforms (~ 21 kDa) encoded by three genes. The gene HRAS (Harvey rat sarcoma viral oncogene homolog) encodes the isoform HRas, the gene NRAS (Neuroblastoma RAS viral oncogene homolog) encodes the isoform NRas, and, by alternative RNA splicing, the gene KRAS (Kirsten rat sarcoma viral oncogene homolog) encodes the two isoforms KRas4A and KRas4B.²¹¹ Hyperactivity of oncogenic Ras mutants leads to initiation and progression of a variety of human cancers ($\sim 25\%$ of human cancers) with KRas being the most common mutated isoform.^{208,211} The KRas protein is composed of 188 amino acids, while the other isoforms are composed of 189 amino acids. Ras proteins possess a C-terminal CAAX motif (HRas: CVLS), which is essential for subsequent post-translational modifications and successive targeting to membranes. All Ras isoforms have a highly conserved and nearly identical N-terminal domain (residues 1-165) that mediates nucleotide and effector binding. However, there are important differences in the C-terminal domain, the hypervariable region. This is post-translationally modified and is responsible for differential subcellular localization, resulting in differential signaling of Ras isoforms.²¹¹

5.1.1. SOS

The most common family of Ras-GEFs in metazoan cells is SOS (Son of Sevenless). There are two mammalian orthologues of SOS, SOS1 and SOS2. The primary structure of SOS1/2 consists of a conserved distribution of functional domains. The guanine-nucleoid exchange activity of SOS is autoinhibited in the native cytosolic state and is activated upon membrane recruitment.^{96,328,329} SOS can be divided into three regions: the C-terminal, the catalytic, and the N-terminal region.³²⁸

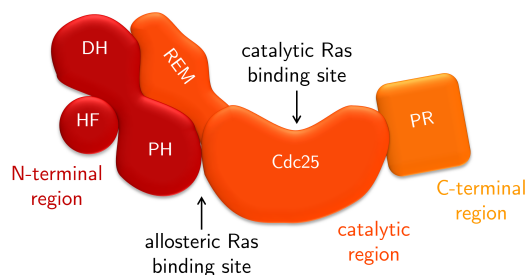


Figure 5.3.: **Schematic structure of the Ras-GEF SOS.** Adapted from Jun et al.²¹⁰

C-terminal region (~ 300 aa) contains a proline-rich domain (PR) that interacts with SH3 domains (Src homology 3) of proteins such as Grb2 for Ras or E3B1 for Rac.³²⁹ In addition to this classical interpretation of the function of GRB2-mediated membrane recruitment, numerous hints, for example using deletion mutants lacking the proline-rich domain, point to an additional inhibitory role of the C-terminal domain, where under unstimulated conditions the C-terminal exerts an autoinhibitory effect on the catalytic activity of GEF. Intermolecular interaction with adaptor proteins, such as GRB2 and E3B1, releases autoinhibition. Thus, site-specific activation of SOS-GEF activity occurs through the specific subcellular recruitment to and interaction with these adaptor proteins.^{208,328}

Catalytic region (residues ~550 to ~1050), also called SOS_{cat} , involves allosteric modulation and catalytic activity. It is centrally located and consists of the Ras Exchange Motif (REM) and the highly conserved Cell Division Cycle 25 (CDC25).³³⁰ The CDC25 catalytic domain has a hairpin structure and forms a hydrophobic pocket. This spiral hairpin structure is inserted as a molecular wedge between the Switch I and Switch II regions. This leads to a break-up of the active site of Ras, resulting in the release of the bound nucleotide. In the native state, the helical hairpin is tilted toward the active site of the SOS, narrowing the site where the SOS targets the Switch II region. Binding of GTP-bound Ras to the allosteric binding pocket of SOS, at the edge of the REM and CDC25 domain, results in rotation of the REM domain, leading to a rotation of the helical hairpin and release of the steric hindrance of the catalytic site. This enables Ras binding to the catalytic site and nucleotide exchange can occur. Therefore, a positive feedback loop of SOS activation is obtained (Fig. 5.4).^{328,329}

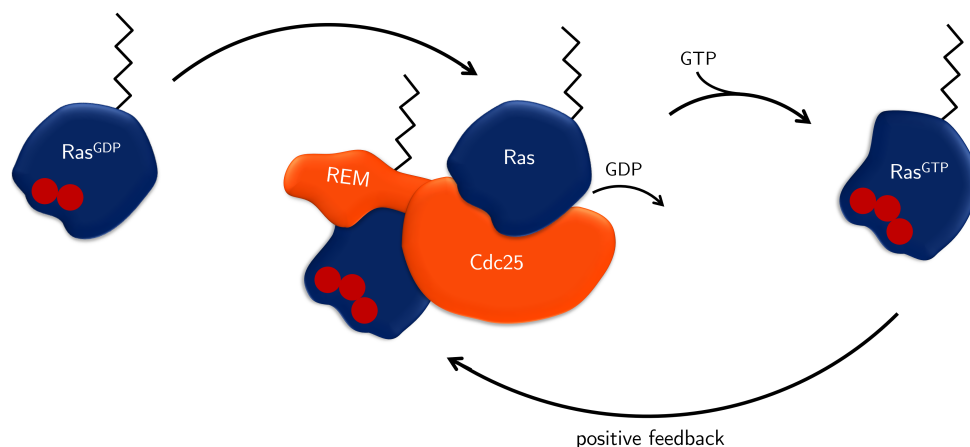


Figure 5.4.: **Schematic model of allosteric activation of SOS.** Adapted from Jun et al.²¹⁰

N-terminal region is responsible for autoinhibitory mechanisms and membrane localization. It consists of two tandem histone(-like) folds (HF), Dbl homology domain (DH), and pleckstrin homology domain (PH) and is approximately 550 amino acids long. The structural domains provide SOS-GEF autoinhibition and tight binding of the SOS protein to the plasma membrane and subsequent release of autoinhibition. HF (≈ 110 aa) has structural similarity to the histone 2 dimer, and mediates lipid interaction with negatively charged membrane phospholipids, such as phosphatidylinositol-4,5-bis-phosphate (PIP₂) or phosphatidic acid (PA). Furthermore, it is involved in the occlusion of the allosteric site and stabilizes the basal inhibitory conformation of the DH-PH tandem module (≈ 350 aa).^{210,328,331} The DH domain is common as a functional domain in GEFs of Rho GTPases, where it catalyzes nucleotide release, which indicates Rho-specific GEF activity of the SOS protein (see Chapter 5.2). PH domains mediate the interaction between lipids and proteins, with a higher affinity for PIP₃ (phosphatidylinositol(3,4,5)-trisphosphates) than for PIP₂. The HF and DH-PH units are conformationally coupled and their lipid interactions are critical for growth factor driven SOS membrane recruitment. Furthermore, these interactions with membrane lipids regulate the release of GEF autoinhibition.^{328,332} Under native conditions, the DH-PH unit blocks the allosteric binding site at the REM domain so that GEF activity is suppressed. This is released by the interaction of the N-terminal domains with membrane phospholipids. Thereby, interaction of the PH domain with membrane phosphoinositol phosphates and electrostatic interactions of the HF domain with negatively charged membranes leads to reorientation of the protein at the membrane, which increases the accessibility for Ras binding.^{328,333}

C-terminal as well as N-terminal regions play crucial roles in both functional membrane localization and self-inhibition of GEF activity. Crucial for catalytic GEF activity is the catalytic region, SOS_{cat}, consisting of the catalytic CDC25 domain and the regulatory REM domain. Therefore, in this thesis, the effective GEF activity of SOS_{cat}, without

the self-inhibition of the C-terminal and N-terminal region, was combined with magnetic manipulation of biofunctionalized nanoparticles, which allows translocation to the plasma membrane. Shi et al. examined the copy number of the proteins of the EGFR-MAPK pathway in different cell lines and observed a significantly lower copy number of the adaptor proteins compared to the core components, such as RAS, MAP2K, and MAPK. The mean ratio of the adaptor protein GBR2 to the receptor was $EGFR/GRB2 \approx 4:1$. The copy number of SOS1 and SOS2 was even lower. The mean ratio of the adaptor protein to the receptor was $EGFR/SOS \approx 40:1$, and to the small GTPase was $SOS/RAS \approx 1:35$. This indicates the limiting factor of the adaptor proteins, especially GEFs, and hints at the suitability of GEFs as a site for interfering into signaling pathways.³³⁴

5.1.2. Ras/Raf/MAPK pathway

There are 4 independent signaling families of MAPK pathways: the canonical MAPK/ERK, Big MAP kinase-1 (BMK-1), c-Jun N-terminal kinase (JNK), and p38 signaling family. These share the basic organization of two serine/threonine kinases and a dual-specificity threonine/tyrosine kinase. In downstream order to the nucleus, these are referred to as MAPK kinase kinase (MAPKKK), MAPK kinase (MAPKK), and MAPK. In the signaling pathway, in a kinase cascade, MAPKKK is activated whereupon it activates MAPKK by phosphorylation, followed by activation of MAPK by phosphorylation, which subsequently results in activation of various substrates.

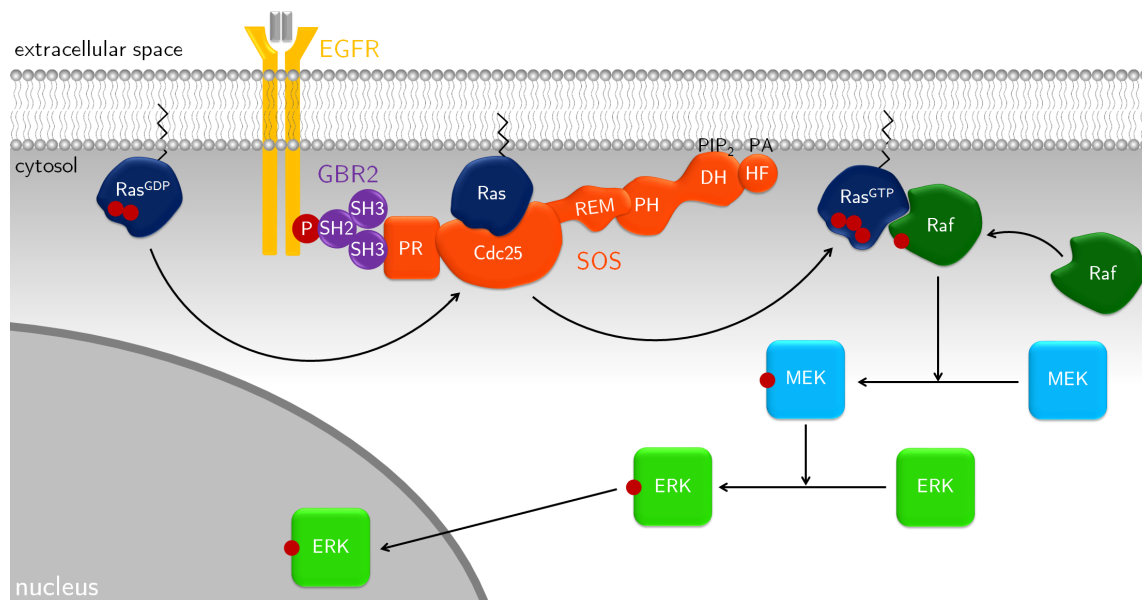


Figure 5.5.: **Schematic illustration of the Ras/Raf/MAPK pathway.** Adapted from Pierre et al.³²⁹

The Ras/Raf/MAPK pathway (Fig. 5.5) is highly conserved in evolution and plays a critical role in various processes such as proliferation, cell growth, embryogenesis, embryonic stem cell differentiation, and also T cell activation and development and early B cell

development.^{208,210,211} Overactivation of this pathway is often described in carcinogenesis.³²⁹

The Activation of this pathway is mediated by a wide variety of receptor tyrosine kinases, such as insulin receptor, EGFR, and PDGFR. Also, it can be mediated by B cell, T cell and monocyte colony-stimulating factor receptors. Binding of a ligand to its tyrosine kinase receptors activates auto-phosphorylation of the receptor. Subsequently, the adaptor protein Growth factor receptor-bound protein 2 (Grb2) binds this phosphotyrosine. Grb2 (25 kDa) is a ubiquitously expressed protein consisting of a central SH2 domain and two SH3 domains. Thereby, the interaction with the tyrosine kinase receptor occurs directly or indirectly mediated by docking proteins. The previously described binding of Grb2 to the proline-rich C-terminal domain of SOS recruits it. Resulting in translocation of cytosolic SOS to the cell membrane. In addition to the C-terminal domain, the N-terminal HD and PH domain is also involved in membrane relocalization as described before. Membrane relocalization enables the interaction of SOS with Ras.^{70,210,329} This results in the increased catalyzed release of the bound nucleotide due to positive feedback. Driven by the higher intracellular concentrations of GTP compared to GDP, the switch to the GTP-bound active Ras form occurs. Subsequently, the GTP-bound Ras activates the protein kinase activity of the MAPK kinase kinase Raf (A-RAF, B-RAF, and RAF-1), which starts the kinase cascade, followed by the MAPK kinase MEK1/2, and further downstream by MAPK ERK1/2. Phosphorylation of ERK results in the activation of cell proliferation-stimulating substrates, whereby the spatial localization of ERK determines the specific target substrates and associated subsequent cell effects. In the cytoplasm, ERK phosphorylates proteins involved in cell adhesion, cell movement and trafficking, or metabolism. Minutes after activation of the pathway, release of ERK from cytoplasmic anchoring proteins occurs whereupon ERK translocalizes to the nucleus. There, phosphorylation leads to activation of various transcription factors that stimulate cell proliferation. In addition to spatial activation, the duration, timing, and intensity of the signal also play an important role in modulating the final effect.³³⁵

The membrane localization of the SOS is maintained until it is actively removed by membrane endocytosis, for which the PR domain seems to be necessary. This makes membrane recruitment of SOS quasi-irreversible on signal-relevant time scales. This, supported by positive feedback, can lead to activation of thousands of Ras proteins by a single SOS protein.^{208,210,328,329}

The level of Ras activation is regulated on the one side by a control through the feedback mechanism of serine/threonine phosphorylation of SOS. This phosphorylation of the C-terminal region of SOS occurs by extracellular signal-regulated kinase (ERK) or ribosomal s6 kinase (RSK) and results in a change in association with GRB2 and thus inhibition of GEF function. On the other side, control of activity is regulated by reversible binding kinetics between SOS and GBR2 in conjunction with alternative binding of competitive

antagonists to Grb2. This can be promoted, for example, by oxidative stress, which can inhibit EGFR signaling by activating the binding of the p66 (SHC) protein to EGFR and Grb2, thereby increasing the dissociation of Grb2 and SOS.^{328,329}

5.2. Rac

Ras-related C3 botulinum toxin substrate (Rac) is a member of the Rho subfamily. Rho (Ras homologous) GTPases play an important role in the regulation of the actin cytoskeleton and is involved in the control of other cellular activities such as embryonic development, immune responses, wound healing, adhesion, and proliferation.^{68,322} This subfamily includes RhoA, mainly involved in stress fiber assembly and focal adhesions, Rac1, mainly involved in lamellipodia formation and membrane ruffling, and Cdc42, mainly involved in actin microtip and filopodia formation.²⁰⁵ Figure 5.6 schematically illustrates various Rac1 signaling pathways, focusing on signaling pathways known to affect tumor-related angiogenesis and metastasis.³³⁶

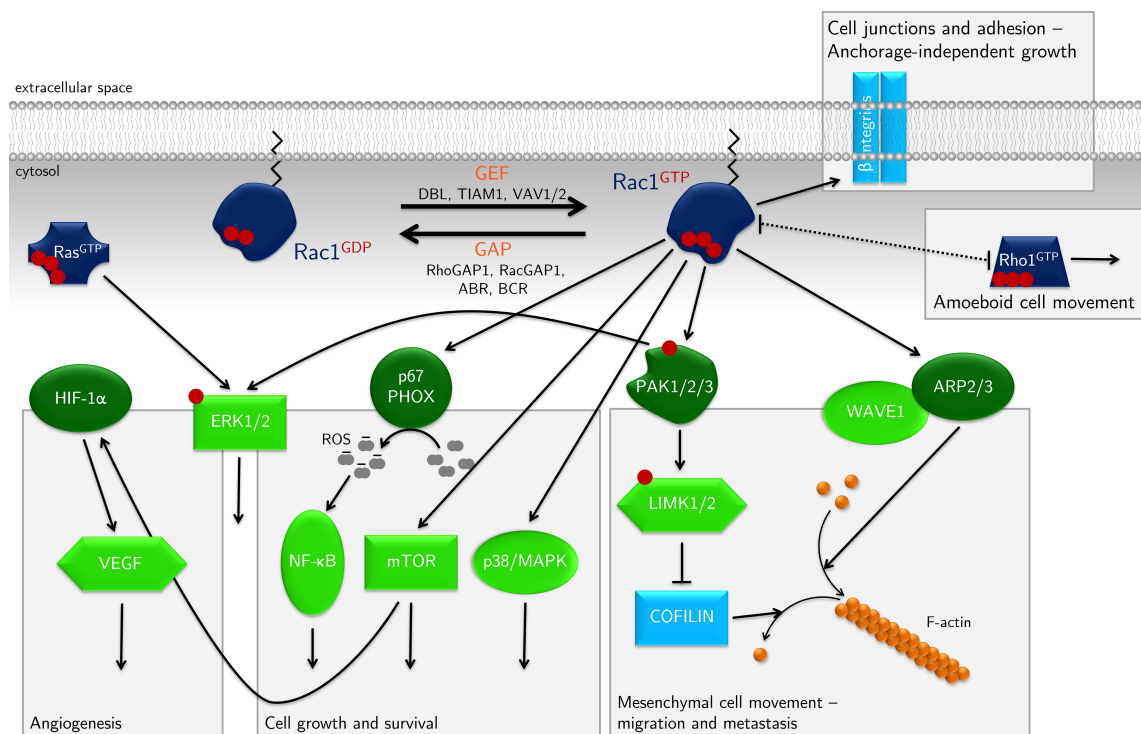


Figure 5.6.: **Schematic illustration of Rac1 signaling pathways.** Focus on pathways known to affect tumor-related angiogenesis and metastasis. Adapted from Bid et al.³³⁶

The actin cytoskeleton enables cells to respond to specific demands of the extracellular environment by changing their shape and forming protrusions. Thereby, monomeric globular actin is converted into filamentous (F)-actin and exerts a deforming force on the plasma membrane. Relevant to mesenchymal motility, the actin-based projections

are the lamellipodia, ruffles, and filopodia (Fig. 5.7). Lamellipodia and ruffles are veil-like, dynamic wave-like extensions of the plasma membrane composed of a tightly packed branched actin filament network assembled by the Arp2/3 complex and are free of organelles. Lamellipodia attach to the underlying substrate and mark the leading edge of the cell. They have a thin ($0.1\ \mu\text{m}$ - $0.3\ \mu\text{m}$) and usually long ($1\ \mu\text{m}$ - $5\ \mu\text{m}$) geometry. Ruffles are thin sheet-like structures and extend over the advancing lamellipodium or onto the dorsal plasma membrane. Circular dorsal ruffles (CDRs) form ring-like structures and project from the dorsal surface of the cells. Filopodia are tiny (about $200\ \text{nm}$ wide) micrometer long finger-like structures and can twist and bend. In contrast to the aforementioned, they consist of a bundle of 10-30 parallel linear actin filaments. They contain various receptors, including growth factor receptors and integrins, which are considered cellular antenna that can control the direction and persistence of movement, promote cell-matrix adhesiveness at the leading edge, and thus stabilize the advancing lamellipodium.^{337,338}

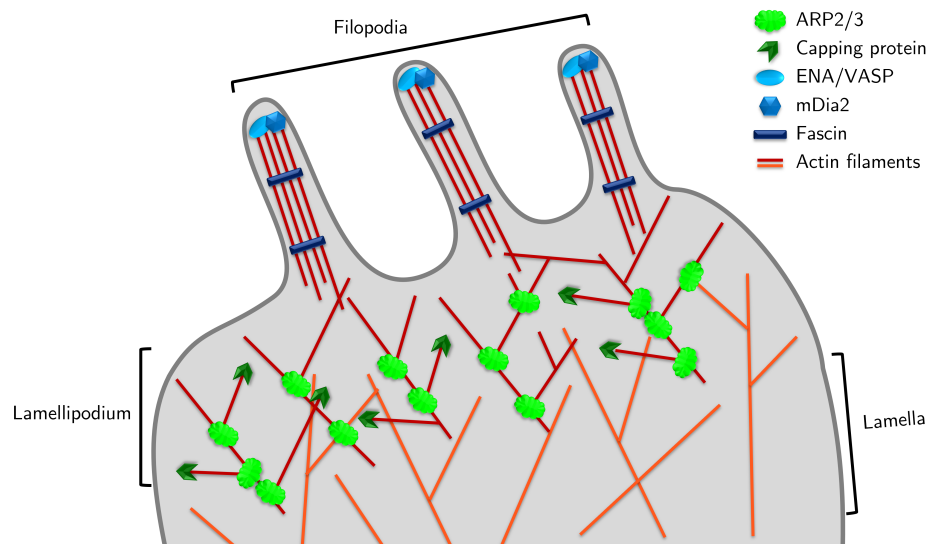


Figure 5.7.: **Schematic representation of lamellipodia and filopodia.** Lamellipodia are formed with dendritic networks of branched actin filaments at the anterior edge of the cell. Filopodia are thin protrusions containing parallel bundles of actin filaments extending from the leading edge. Adapted from Heasman et al.³³⁹

Three Rac isoforms are found in mammalian organisms, Rac1, which is ubiquitously expressed, Rac2, which is expressed mainly in the hematopoietic lineage, and Rac3, which is found only in the central nervous system.^{211,336} Rac1, by controlling the dynamics of the actin cytoskeleton, regulates many cellular processes associated with cell motility, such as migration and axonal growth, cell spreading, adhesion, phagocytosis, macropinocytosis, pinocytosis, and vesicular transport. Furthermore, Rac1 interacts with other cellular signaling pathways and is also involved in cellular processes independent of actin cytoskeleton dynamics, such as proliferation, cell differentiation, cell survival, and gene expression control.²¹¹ These RAC-1-mediated activities are also described as central mechanisms of ma-

ligniant transformation, including tumorigenesis, angiogenesis, invasion, and metastasis.³³⁶ Abnormal Rac1 signaling and associated deregulation of cell motility and invasion represents a hallmark of cancer metastases and is a major cause of death in cancer patients.^{338,340}

Rac1 possesses a C-terminal CAAX motif (CLLL) and adjacent to this motif a polybasic region in the hypervariable region that interacts with anionic membrane phospholipids and in this way determines localization in specific membrane domains. Adjacent, Rac1 contains a proline-rich domain that contributes to the targeting of Rac1 to cellular focal adhesions. The membrane stability of Rac1 is strongly enhanced by palmitoylation of the cysteine at position 178, which promotes localization and functionality in cholesterol-rich plasma membrane domains (lipid rafts).²¹¹

Activation of Rac1 leads to the interaction with a variety of effectors, including protein kinases and actin-binding proteins.³⁴¹ A key player in lamellipodia and ruffle formation and mesenchymal cell migration is the actin-related (Arp)2/3 complex. This complex, which consists of two actin-related proteins (Arp2 and Arp3) and five other subunits, is present inactivated. Activated RAC1, together with the adaptor protein NCK, induces separation of WAVE1 from its regulatory complex. This complex stimulates the activation of the ARP2/3 complex and thus catalyzes the polymerization of a new (daughter) actin filament to an existing (parent) filament, with an angle of about 70 degrees.³³⁶⁻³³⁸

Protein kinases activated by Rac1 include the p21-activated kinases (PAKs). These serine/threonine kinases are Cdc42/Rac-interacting proteins and are divided into two groups based on their structural homology and activation mechanism (group I: PAK1-3, group II: PAK4-6). They share a conserved C-terminal kinase domain and an N-terminal regulatory domain containing the p21 binding domain (PBD). In group I, the p21 binding domain overlaps with an autoinhibitory domain (AID). Due to the interaction of the AID with a kinase domain of a second PAK molecule, group I PAKs exist as cytosolic homodimers. Interaction of Rac or Cdc42 with the p21 protein-binding domain breaks this bond resulting in a conformational change that resolves this autophosphorylation of the activation loop and several C-terminal serine residues, leading to full kinase activity. Group II PAKs are constitutively phosphorylated and binding to Rac or Cdc42 does not lead to activation but affects subcellular localization.^{336,342,343} Activated PAK1 phosphorylates many substrates that control various aspects of cytoskeletal dynamics, such as LIM kinase, filamin A, myosin light chain kinase, and p41-ARC. For example, phosphorylation of actin-binding LIM kinases (LIMK1, LIMK2) causes them to phosphorylate cofilin resulting in the prevention of actin depolymerization. Phosphorylation of the p41-ARC subunit of the Apr2/3 complex results in the polymerization of a new (daughter) actin filament, as previously described, and thus in the branching of the network of actin filaments.^{336,338,343,344} In addition, PAKs can increase cell proliferation. In this regard, PAK1 acts downstream of Ras by phosphorylating Raf1 and MEK1 resulting in an enhanced RAF/MEK/ERK signaling pathway. PAK1

exerts a further influence on cell proliferation by phosphorylating β -cat. This stabilizes β -cat and facilitates its nuclear translocation resulting in transcriptional activity. This crosstalk between PAK1 and the RAF/MEK/ERK signaling pathway and Wnt signaling pathway is important in tumorigenesis. In addition, PAK is involved in many other cellular processes, such as cell cycle progression and cell survival.³⁴³

5.2.1. Tiam1

The GEFs of the Rho GTPases are classified into the Dbl or DOCK families according to their domain mediating GEF activity. In the Dbl GEF family, to which Tiam1 belongs, this activity mediates a Dbl homology (DH) domain. The Rac-specific GEF Tiam1 was initially described by its ability to induce T lymphoma cells to invade monolayers of fibroblasts, deriving its name T-lymphoma invasion and metastasis-inducing protein 1. In interplay with Rac1, Tiam1 is a deciding regulator of cadherin-mediated cell-cell adhesions. Destabilization of these adhesions is a prerequisite for cell movement.^{338,345}

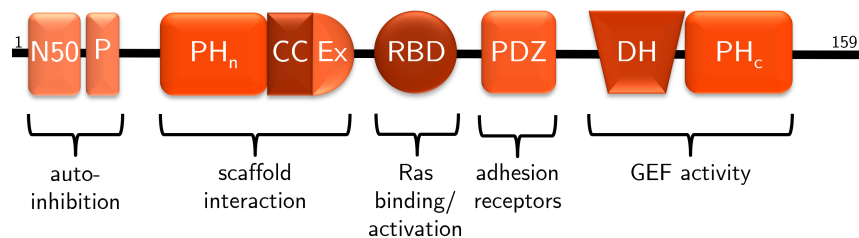


Figure 5.8.: **Schematic structure of the GEF Tiam1.** Adapted from Minard et al.³⁴⁶

Tiam1 consists of 1591 amino acids, with a molecular weight of 177 kDa. The previously mentioned Dbl homology (DH) domain carries the catalytic GEF activity, consists of approximately 150 amino acids, and is conserved. This catalytic Dbl homology (DH) domain is coupled to an adjacent pleckstrin homology (PH) domain in the family of Dbl GEFs. The DH-PH domain unit is the minimal region for the catalytic activity of nucleotide exchange through interaction with the switch I and II regions of the GTPase. In this context, the PH domain acts as a regulator of GEF activity through interactions with the DH domain, GTPase substrate, or phosphoinositides. Furthermore, Tiam1 contains several protein-protein binding domains that also contribute to the regulation of catalytic activity.^{346–348} In addition to the C-terminal PH domain coupled to the DH domain, Tiam1 has a further PH domain (PH_n) N-terminally. This PH_n domain, together with a coiled-coil region with adjacent sequence (CC-Ex), forms a functional PH_n-CC-Ex region that interacts with the scaffold. These interactions modulate the subcellular localization of Tiam1 and are required for membrane localization. Thus, GEF catalytic activity can be increased 2-3-fold. Furthermore, Tiam1 has adjacent to this region a Ras-binding domain (RBD) to which activated GTP-bound HRas can bind, resulting in activation of GEF activity. Adjacent to this is a PDZ domain (Post-Synaptic Density-95/Discs Large/Zonula Occludens-1), which binds cell adhesion molecules. In addition, Tiam1 has a myristylation site N-terminally at position 2 and two N-terminal PEST domains. PEST sequences are

proline, glutamate, serine, and threonine rich and result in a shorter half-life of the protein and faster degradation. Activity is regulated by phosphorylation of adjacent domains.³⁴⁶⁻³⁴⁸

The model for Tiam1 autoinhibition and activation is thought to be a combinatorial model representing a multistep process. According to this model, full-length Tiam1 is in an equilibrium between inactive and fully auto-inhibited forms, in which the N50 domain and PH_n-CC-Ex region assemble. Thus, Rac1 access to the catalytic DH-PH region is prevented. In the first step, phosphorylation of serine 29 and serine 33 which releases the PH_n-CC-Ex/N50 interaction occurs. In the second step, phosphorylation of tyrosine 829 and/or protein-protein interactions between the PH_n-CC-Ex region and/or the RBD domain with partner proteins occurs, which disrupts the PH_n-CC-Ex/DH-PH interaction. This leads to the fully activated form of Tiam1, which allows interaction with Rac1 and thus catalytic GEF activity.^{346,348}

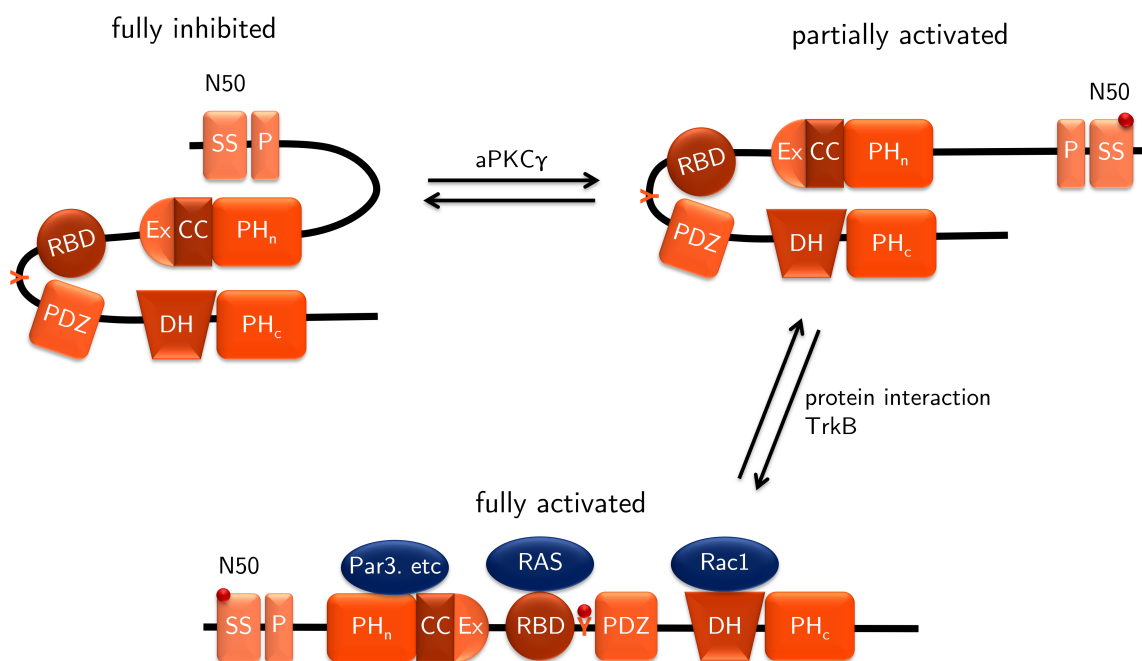


Figure 5.9.: **Schematic illustration of Tiam1 autoinhibition.** Adapted from Xu et al.³⁴⁸

In this thesis, the GEF activity of the catalytic DH-PH domain was exploited by presenting it on the NP surface and translocating the nano signaling actuator site-specific to the target region. The catalytic DH-PH domain lacks the membrane localization ability of the full-length protein, which is required for the induction of signaling and membrane ruffling.³⁴⁹

5.3. The Role of Rho and Ras GTPases in Axon Growth, Guidance, and Branching

Rho and Ras GTPases play a key role in regulating axon growth, guidance and branching.³⁵⁰ Coordination of various signaling pathways with precise spatial control by Rho and Ras GTPases is important in different processes. These include the interaction of the growing axon with the environment such as cells and the extracellular matrix, the dynamic assembly, remodeling, and disassembly of the actin and microtubule cytoskeleton, the exocytosis-driven delivery of lipids and proteins to the axon, and the endocytosis-triggered internalization of membranes and proteins at the tip of the growth cone. In this context, the Rho GTPases are particularly important for axon growth, guidance, and branching through their function in the assembly, reorganization, and degradation of the actin and microtubule cytoskeleton. Ras GTPases play a critical role in axonogenesis. Mediated by a variety of growth factor receptors and plasma membrane adhesion receptors, it activates important signal transduction pathways involving, for example, ERK, MAP kinase, and PI3 kinase.³⁵⁰

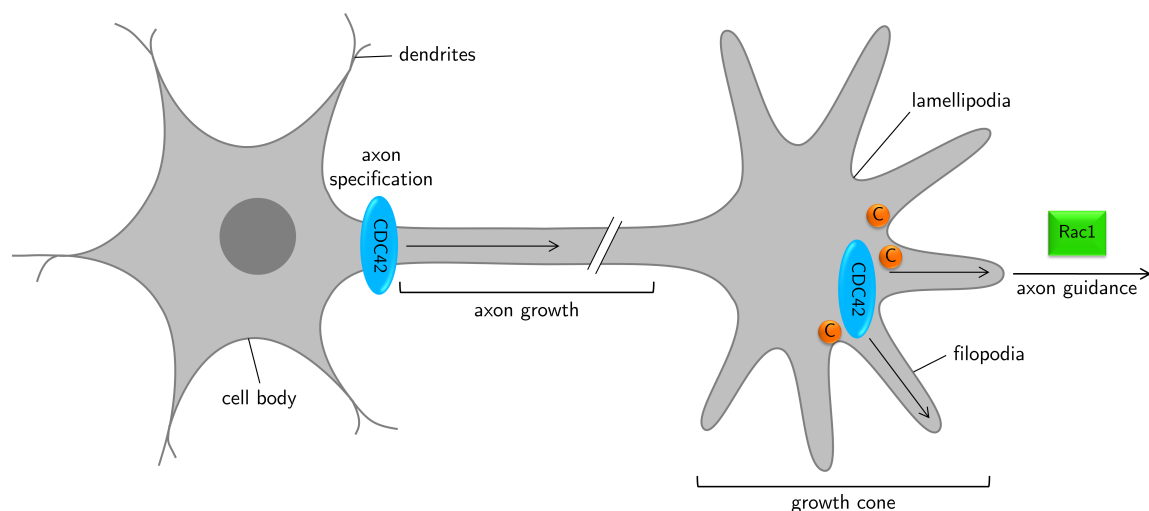


Figure 5.10.: **Schematic illustration of the roles of Rho GTPases in neuronal development.** Rac1 plays a critical role in lamellipodia formation and axon guidance, Cdc42 in filopodia formation, axon specification and elongation. Active cofilin (C) present in the growth cone where it is thought to regulate axonal growth and filopodia. Adapted from Heasman et al.³³⁹

To form synaptic contacts with other cells, the axon extends over long distances during neuronal development (Fig. 5.10). At the tip of the axon is the growth cone containing lamellipodia and filopodia. Rac1 plays a critical role in lamellipodia formation and expansion, membrane curling, and axon guidance.^{339,351,352} Cdc42 is required for filopodia formation, axon specification and extension. In addition, active cofilin (C) is present in the growth cone, where it is thought to regulate axonal growth and filopodia.³³⁹ Cofilin and other proteins that regulate actin cytoskeleton assembly, such as gelsolin and profilin, have been identified as downstream effectors of Rho GTPases. Many *in vitro* and *in vivo*

studies show marked changes in axon morphology, motility, and pathfinding following disruption of Rho GTPases, suggesting that Rac and Cdc42 are positive regulators that promote neurite elongation, whereas Rho is a negative regulator that causes inhibition or collapse of growth cones.^{339,350,353–358} Neuronal polarity plays an important role, in which symmetry breaking triggers the rapid ingrowth of one of several small neurites into an axon. Fivaz et al. showed increased HRas activity in the nascent axonal growth cone upon symmetry breaking. Phosphatidylinositol 3-kinase (PI3K) is a downstream effector that regulates axon formation by local reorganization of actin and microtubules. Here, the local increase in HRas activity results from a positive feedback loop between HRas and PI3K and is enhanced by vesicular transport of HRas to the axonal growth cone. This recruitment of HRas to the axonal growth cone leads to a decrease in HRas concentration in the remaining neurites, resulting in symmetry breaking and the formation of a single axon.³⁵⁹ The critical role of GTPase Rhas in neurotrophin signaling was demonstrated in transgenic mice expressing a constitutively active HRas mutant.^{206,209,212}

6 | Model systems - Wnt signaling

The Wnt signaling pathway is one of the most conserved pathways during evolution. This pathway plays essential roles in many biological processes of development, including stem cell differentiation, stem cell self-renewal, cell proliferation, polarity formation, embryonic development, and tissue homeostasis. Deregulation of Wnt signaling has been implicated in the pathogenesis of a variety of human cancers.^{360–369}

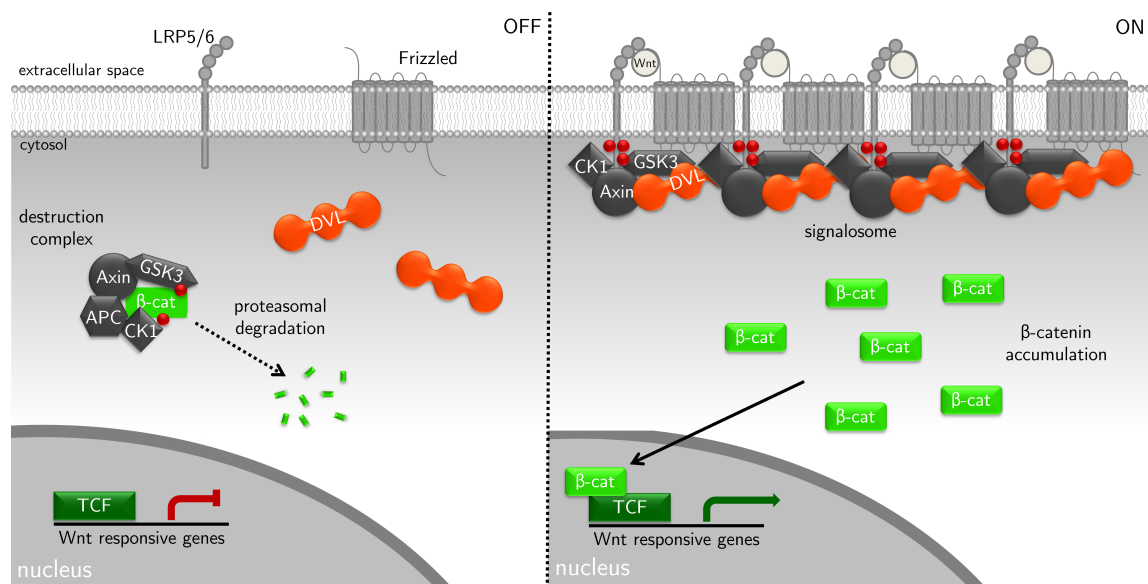


Figure 6.1.: **Schematic illustration of the canonical Wnt signaling pathway.** (left) In the absence of a Wnt ligand, tagging of β -catenin by the destruction complex (consisting of Axin, APC, CK1, and GSK3 β) leads to proteasomal degradation of β -catenin. The absence of β -catenin in the nucleus leads to binding of the repressor complex to the Wnt responsive gene. (right) Binding of the Wnt ligand to the Frizzled receptor and the LRP coreceptor dissolves the destruction complex and β -catenin is no longer degraded. This leads to the accumulation of β -catenin in the cytoplasm and its translocation to the nucleus, resulting in the transcription of Wnt responsive genes. Adapted from Patel et al.³⁷⁰

The canonical Wnt pathway differs from the non-canonical ones in its dependence on β -catenin (β -cat) and is therefore also called the Wnt/ β -catenin pathway (Fig. 6.1). In the absence of the Wnt ligand, a cytosolic β -catenin destruction complex is formed. It keeps low level of β -cat. The destruction complex is composed of the scaffold protein Axin, the Adenomatous Polyposis Coli (APC) tumor suppressor, and two serine-threonine kinases, glycogen synthase kinase 3 (GSK3) and casein kinase 1a (CK1).^{360,362–364,366–368,371} Increasing evidences suggest that this complex is a biomolecular condensate, so-called puncta, which is

not surrounded by a membrane and exhibits liquid-liquid phase-separated behavior. The non-enzymatic components APC and Axin are complex multidomain scaffold proteins. They contain domains that mediate protein-protein interaction and long intrinsically disordered regions that contain binding sites for proteins of the complex, including the β -cat.³⁶⁶ The C-terminal DIX domain of Axin, also called DAX domain, induces assembly of the complex by head-to-tail polymerization. The affinity is weak, so Axin polymerization does not occur spontaneously at the concentrations of Axin typically present in cells. Degradosome assembly is promoted by APC, which interacts with the N-terminal regulator of G-protein signaling (RGS) domain of Axin via multiple conserved motifs.^{360,366,371} The intrinsically disordered region of Axin contains binding sites for β -cat, kinases GSK-3 and CK1, and phosphatase PP2A. Thus, Axin may mediate spatial proximity of β -cat to the kinases GSK-3 and CK1 and a high local concentration of the enzymes. APC contains a conserved N-terminal region that promotes oligomerization with its self-association, an Armadillo repeat domain involved in binding of different partners, and a long intrinsically disordered region embedded in multiple binding sites for β -cat and Axin.^{364,366} Indirect interaction via β -cat also contributes to assembly of the destruction complex. Enabled by the previously described spatial proximity and high enzyme concentration, GSK3 effectively phosphorylates β -cat at the N-terminus, this results in ubiquitylation by a β -TrCP-containing SCF-E3 ubiquitin ligase and subsequent degradation by the proteasome.^{360,364,368,371}

In the canonical Wnt signaling pathway, Wnts (Wnt1, 2, 3, 3a, 8 or 8a) or engineered Wnt surrogate ligands crosslink Frizzled (Fzd) with co-receptor low-density lipoprotein receptor-related protein 5/6 (Lrp5/6) in the plasma membrane, followed by phosphorylation of the intracellular PPPSPxS/T motifs of Lrp5/6. This leads to recruitment of destruction complex to the cell membrane. Moreover, Dvl is consecutively binding to Fzd, thus facilitates the binding of Axin to Lrp5/6.²³³ Upon association with phosphorylated Lrp5/6, the ability of the destruction complex to promote β -cat degradation is impaired since the binding site for the ubiquitin ligase is blocked. Without ubiquitination, the newly formed β -cat accumulates in the cytosol, eventually transferring into the nucleus.³⁷² This allows β -cat to bind to the transcription complex with LEF-1/TCF (lymphoid enhancer binding factor-binding factor/T-cell factor). This switches the inhibitory state of LEF/TCF to the activating state, leading to transcription of Wnt target genes.^{360,362,364,368,369,373}

As with the degradosome, there is also increasing evidence that the complex formed by stimulation by the Wnt ligand is a phase-separated condensate called a signalosome. Upon stimulation with Wnt ligand, Dvl binds to Fzd via its DEP domain, leading to self-association of Dvl. This results in the formation of a high molecular weight assembly near the plasma membrane induced by dynamic head-to-tail polymerization of the DIX domains of Dvl proteins.^{362-364,368,369,371} Yamanishi et al. showed by structural studies and affinity measurements the strongest affinity for the homotypic DIX-DIX interaction, followed by the heterotypic DAX-DIX interaction and the homotypic DAX-DAX interaction.

By comparing the structure of merged DAX-DIX, DIX-DIX and DAX-DAX structures with a flexible linker between the domains, three different interaction sites were identified which conform to the different affinities. All three interactions form a parallel intermolecular bridge consisting of a hydrophobic cluster between $\beta 4$ of one partner and $\beta 2$ partner. The DIX-DIX interaction additionally forms a salt bridge and a hydrogen bond in a second interaction site. These hydrophilic and electrostatic interactions were not detected for the DAX-DIX and DAX-DAX interactions. Which is an indication of the high DIX-DIX affinity. In a third identified interaction site, the loop between $\beta 1$ and $\beta 2$ of the DIX domain shifts slightly toward the DAX domain in the DAX-DIX interaction, allowing hydrogen bonding to form.³⁶⁹ Kan et al, Schwarz-Romond et al, and Yamanishi et al. indicate a consistent affinity of the DIX-DIX interaction in the range of $K_D = 4.9\text{-}20 \mu\text{M}$.^{364,369,374} However, Kan et al. disagree with the lower affinity of the DAX-DIX and DAX-DAX interaction. They describe the affinity of the DAX-DIX interaction as being of the same order of magnitude as the DIX-DIX interaction, and the affinity between DAX-DAX as being an order of magnitude stronger, pointing out that the other studies only examined one head-tail interface through mutation experiments. Thus, possible effects with more than a single head-tail interface, energetically coupled and not independent of each other, were dismissed.³⁶⁴ The preference for heterotypic interaction over homotypic DAX-DAX interaction described by Yamanishi et al. could make the self-affinity of the Axin polymer susceptible to disruption by Dvl, and thus dynamic Dvl-DIX polymerization could lead to the recruitment of Axin and thus the β -catenin destruction complex to the plasma membrane.³⁶⁹

6.1. Dishevelled

Dishevelled (Dvl) is central branch point for the canonical Wnt signaling and non-canonical Wnt signaling pathways such as Wnt-GSK microtubules, Wnt-Calcium, Wnt-RYK (related to tyrosine kinase), Wnt-aPKC (atypical protein kinase C), Wnt-mTOR (Mammalian Target of Rapamycin), and planar cell polarity (PCP) signaling pathway (Fig. 6.3).^{362,367} Non-canonical Wnt signaling pathways are controlling for example cell polarity, actin and cytoskeletal dynamics, and cell movement. At the PCP signaling pathway, Wnt stimulation activate the small GTPase Rho. Dvl forms a complex with Daam1 (Dishevelled associated activator of morphogenesis 1) which forms WGEF (weak-similarity GEF) with Rho-GEF. This leads to activation of small GTPases, such as Rho, with subsequent activation of Rho-associated kinase (ROCK), and Cdc42. Independently, Daam1 and small GTPase Rac can also be activated mediated by Dvl, resulting in activation of downstream effector c-Jun N-terminal kinase (JNK).^{362,367,375,376}

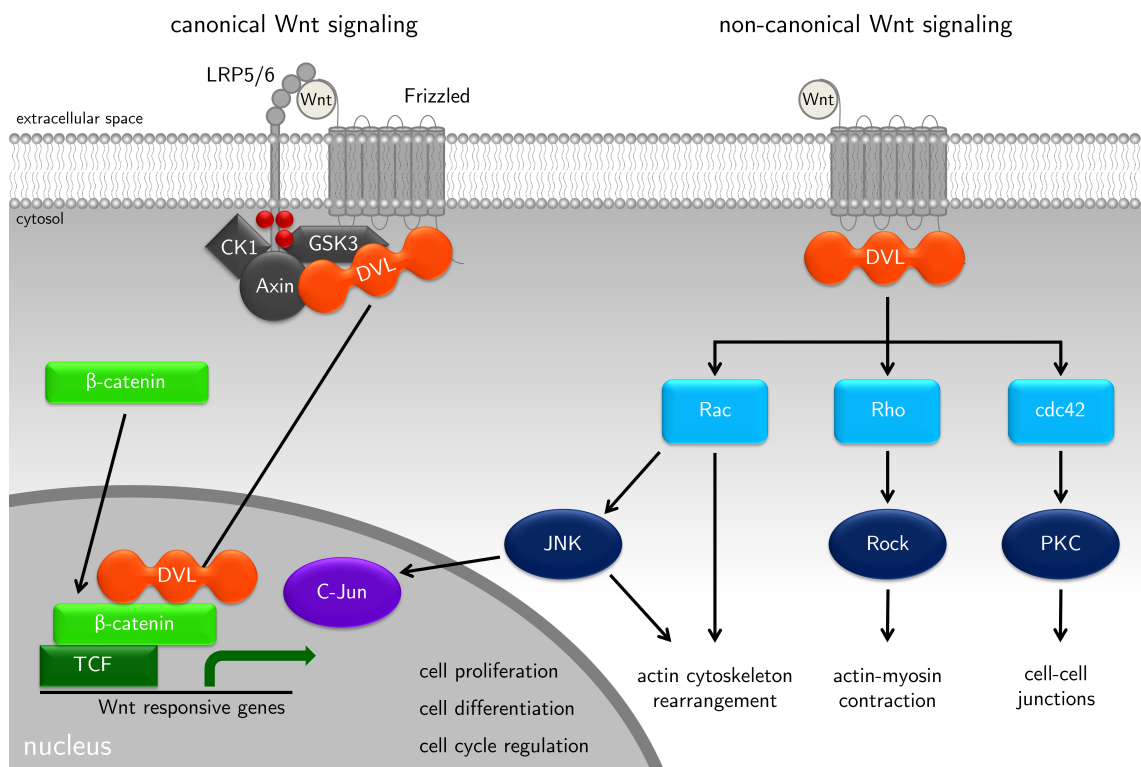


Figure 6.2.: **Schematic illustration of canonical and non-canonical Wnt signaling pathway and the role of Dvl.** These signaling pathways are involved in the regulation of many cellular functions such as cell proliferation, differentiation, cell cycle regulation, actin cytoskeleton rearrangement, actin-myosin contraction, and the formation of cell-cell junctions. Adapted from Sharma et al.³⁶⁷

All Dvl homologs (Dvl1, Dvl2, Dvl3) are conserved from *Drosophila* to humans. They show high sequence homology and consist of about 750 amino acids. Among them, Dvl2 is the most abundant member. The Dvls possess three conserved domains, an N-terminal DIX domain, a central PDZ, and a C-terminal DEP domain (Fig. 6.3). In addition to these domains, they possess two conserved regions with positively charged amino acid residues that mediate protein-protein interactions. These regions are a basic region, between the DIX and PDZ domains, consisting of serine and threonine residues, and a proline-rich region, downstream of the PDZ domain. Dvl also possesses a conserved nuclear export sequence (NES) and a nuclear localization sequence (NLS), which enables a shuttle between the cytoplasm and nucleus that appears to be critical for proper function of the canonical Wnt signaling pathway. In the nucleus, Dvl functions as a transcriptional activator of Wnt target genes.^{362,363,367,377-379}

The N-terminal DIX domain of human Dvl consists of 82-85 amino acids and is composed of a compact fold with five β -strands and a α -helix with highly conserved amino acid residues, which are critical for the structural and functional role of DVL. In addition to Dvl, this domain is also present in proteins such as Axin and the coiled-coil protein DIX-domain-containing 1 (DIXdc1 or Ccd1). Dvl has the ability to form cytoplasmic puncta

mediated by dynamic head-to-tail home-polymerization via the DIX domain. In addition to assembling Wnt signalosomes near the plasma membrane, DIX mediates protein-protein interactions, such as interaction with the DAX domain of Axin.^{362,363,367}

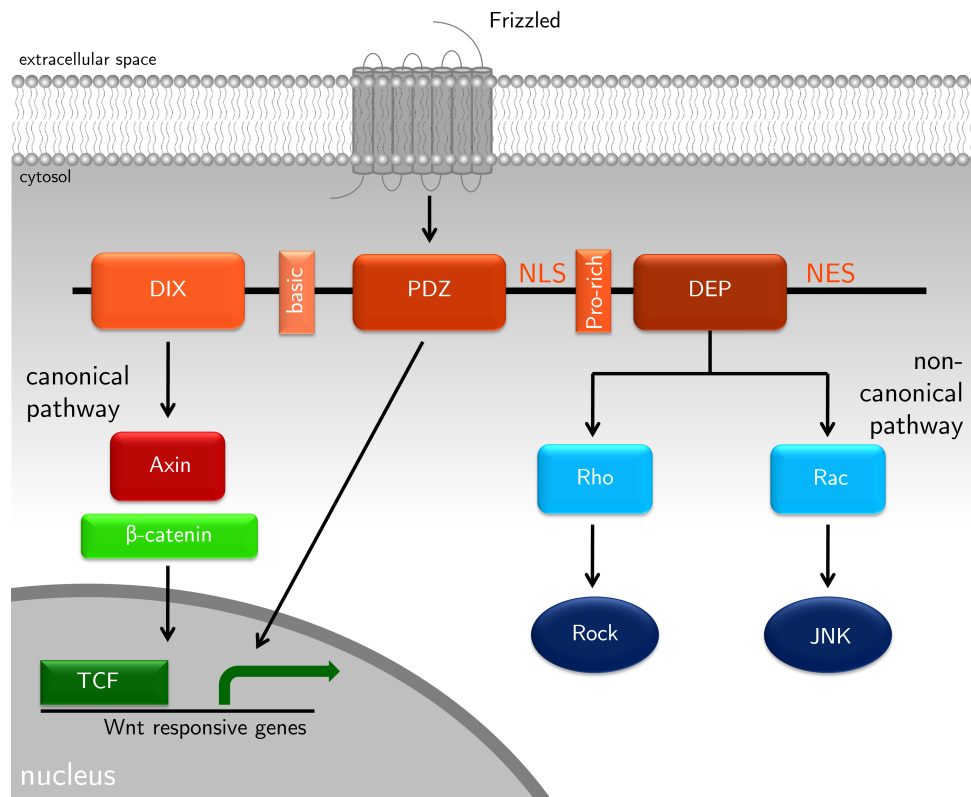


Figure 6.3.: **Schematic illustration of the structure and function of Dvl.** Dvl consists of three conserved motifs (N-terminal DIX domain, central PDZ, C-terminal DEP domain), two regions with positively charged amino acid residues (basic and proline-rich domains), a nuclear import signal (NLS) and a nuclear export signal (NES). DIX and PDZ domains are involved in transduction of signals to the canonical pathway, the DEP domain regulates membrane localization and non-canonical pathway. Adapted from Sharma et al.³⁶⁷

The central PDZ domain (Postsynaptic density 95, Discs Large, Zonula occludens-1) of human Dvl consists of approximately 73 amino acids. The PDZ contain 2 or 3 α -helices and 5 or 6 β -sheets, with a conserved motif (R/KXXXG ϕ G ϕ , X = any amino acid, ϕ = hydrophobic residues). The PDZ domain interacts with a conserved C-terminal region of Fzd (KTXXXW). This interaction plays a critical role in membrane localization of Dvl and activation of the Wnt signaling pathway.^{362,363,367}

The C-terminal DEP domain (Dvl, Egl-10, pleckstrin) of human Dvl consists of 75 amino acids. The DEP domain mediates interaction with DAAM1, which results in activation of the non-canonical signaling pathway. In addition, it is also involved in the targeting of Dvl to the membrane after Wnt stimulation. Studies show that the DEP domain contributes in signalosome assembly via strong electrical dipole mediated protein-protein interaction. The

DEP domain contains several arginines and lysines that promote membrane localization during planar epithelial polarization.^{362,363,367}

The diversity of Dvl interaction partners is the cause of diverse cellular functions. For activation of the canonical Wnt signaling pathway, the PDZ domain interacts with Fzd, casein kinase 1/2, β -arrestin, and protein phosphatase 2C. In the non-canonical Wnt pathway, the interaction of the DEP domain with activators (diversion, protein kinase C, and APC) and antagonists (e.g. $G\beta\gamma$) plays a crucial role. Dvl also interacts with a variety of other proteins, including c-Jun and Tiam1.³⁶⁷ Moreover, post-translational modifications of Dvl, such as phosphorylation, ubiquitination, and methylation, are also found to be the mechanism for the branching of Wnt signaling pathways.^{362,367} The interaction with the interaction partners Axin and Frodo occurs via the DIX domain and results in stabilization of the canonical and non-canonical Wnt signaling pathway.³⁶⁷

In this work, MNPs were biofunctionalized with Dvl. Using magnetic control, the Dvl-LLPS should be induced in a targeted manner to obtain a powerful tool to test hypotheses of the Wnt signaling pathway activation.

IV Results & Discussion

7 | Magnetic Remote Activation of small GTPase HRas using MagIcS

For initial proof-of-concept experiments of magnetic manipulation of signaling pathways, magnetic intracellular stealth MNPs (MagIcS) were used. They are based on natural ferritin as a highly stable and biocompatible protein cage and were developed in previous work by Liße et al.⁷⁵ The small GTPase HRas was chosen as the first model system. HRas plays a crucial role in different processes such as proliferation, differentiation, cell growth, embryogenesis, axonogenesis and neurotrophin signaling.^{206–212} To probe the spatiotemporal remote control of small GTPases activity, the catalytic region (SOS_{cat}) of the Ras-GEF SOS, containing the Rem domain and Cdc25 domain, was immobilized at the surface of MagIcS. Translocation of the biofunctionalized magnetic nanoparticles allows site-specific control of the spatial distribution of the catalytic region. Thus, the spatiotemporal controlled actuation of HRas activation is tested at a subcellular level. The first step was to test *in vitro* whether the catalytic region of the GEF still possesses guanine nucleotide exchange activity, even when bound to the surface of the MNPs. In the second step, it was tested whether this guanine nucleotide exchange activity is also present *in cellulo*, and whether this leads to activation of the small GTPase HRas. HRas activation was investigated using reengineered FRET biosensors.

7.1. Non-fluorescent MNPs with intracellular stealth properties (xMagIcS)

Non-fluorescent MagIcS ferritin has a crucial advantage for multicolor fluorescence experiments, as the distinguishability of the color channels is limited and the green fluorescence is often occupied by established fluorescent reporters. Therefore, MagIcS (see Chapter 4.5.1) were evolved and a non-fluorescent MagIcS ferritin was generated by a point mutation, consisting of non-fluorescent GFP (mXFP, meGFP Y66F) fused to the N-terminus of human heavy chain ferritin (HCF). At this point mutation, the tyrosine at position 66, which is known to form the GFP chromophore, was replaced by phenylalanine.

In a first try, mXFP::HCF was expressed in *E. coli* and purified according to the protocol previously used by Liße et al. consisting of thermal treatment followed by ammonium sulfate precipitation, ion exchange chromatography and, size exclusion chromatography.⁷⁵ The mXFP::HCF purification gave a significantly lower protein yield compared to mEGFP::HCF, which can be explained by a less efficient folding of GFP caused by the Y67F mutation. For this reason, the purification was optimized and a His6-Tag was genetically added (H6::mXFP::HCF). The resulting fusion construct H6::mXFP::HCF was produced in *E. coli* and purified to homogeneity by immobilized metal affinity chromatography (IMAC) followed by size exclusion chromatography. Compared to the previously used purification protocol, protein purification is less time consuming and results in a higher protein yield. This was followed by PEGylation (PEG₂₀₀₀, MW: 2000 Da) and further purification by size exclusion chromatography. The final step was the synthesis of the ferrimagnetic core at 65 °C as reported by Allen et al.,³⁸⁰ resulting in a non-fluorescent magnetic nanoparticle with intracellular stealth properties (xMagIcS).

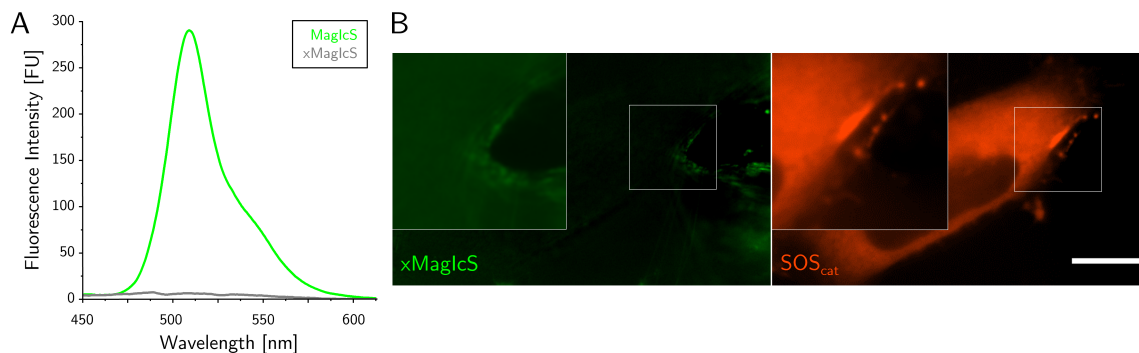


Figure 7.1.: **Characterization of non-fluorescent xMagIcS.** (A) Fluorescence spectra of mEGFP fused to heavy chain ferritin (green) and non-fluorescent mXFP fused to heavy chain ferritin (grey). (B) Magnetic manipulation of α GFP::mCherry::SOS_{cat} by utilizing xMagIcS in living cells. Scale bar: 5 μ m.

Fluorescence spectroscopy confirmed no fluorescence emission from xMagIcS *in vitro* (Fig. 7.1A). After microinjection into HeLa cells expressing α GFP::mCherry::SOS_{cat} and application of a magnetic field gradient, magnetic manipulation of functionalized xMagIcS to the plasma membrane was observed in the mCherry channel. xMagIcS did not show fluorescence in the cytoplasm or colocalization with the mCherry fluorescence (Fig. 7.1B). This demonstrates the successful production and application of xMagIcS for magnetic manipulation of proteins inside living cells.

7.2. *In vitro* MNP-GEF activity of biofunctionalized MNPs

To confirm the guanine nucleotide exchange activity of the catalytic region of the GEF, when bound to MNPs, an *in vitro* assay for probing SOS activity was used based on monitoring the exchange of fluorescent mant-GDP. Mant-GDP is fluorescent when bound to the GTPase, by the release of mant-GDP and with subsequent binding of GDP, due to

an excess of free GDP, a decrease in fluorescence occurs.

A fusion protein ($\alpha\text{GFPnb}::\text{mCherry}::\text{SOS}_{\text{cat}}::\text{H10}$) consisting of a nanobody against mEGFP for MNP functionalization, the fluorescent protein mCherry for visualization, the catalytic region of Ras-GEF mSOS (SOS_{cat}), and a His10-Tag (H10) for purification, was expressed in *E. Coli*. Purification was performed by IMAC followed by SEC. After *in vitro* functionalization to the surface of xMagIcS, excess of fusion protein was removed by size exclusion chromatography. Guanine nucleotide exchange activity of HRas premixed with mant-GDP was measured in a stop-flow apparatus without GEF or in presence of soluble $\alpha\text{GFPnb-mCherry-SOS}_{\text{cat}}$ fusion protein or with functionalized MNPs (Fig. 7.2A).

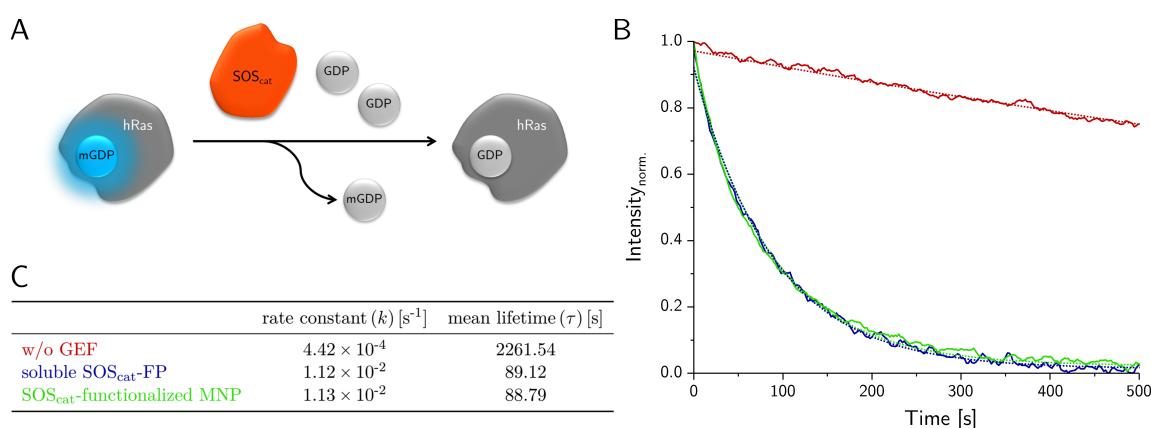


Figure 7.2.: **Probing the GEF activity of biofunctionalized MagIcS nanoparticles *in vitro*.** (A) Schematic of the guanine nucleotide exchange activity assay. Reduction of mant-GDP fluorescence by mant-GDP (mGDP) release and GDP exchange. (B) Measurement of fluorescence intensity as a function of time to quantify GEF activity. Comparison of spontaneous exchange of mant-GDP (red), with catalyzed exchange by soluble SOS_{cat} fusion protein (blue) and SOS_{cat} -functionalized MNPs (green). Cropped for illustration, measured time periods 75 min for spontaneous exchange and 25 min for catalyzed exchange. Exponential fits (dotted lines) with resulting (C) rate constants and mean lifetimes of guanine nucleotide exchange.

Spontaneous exchange of mant-GDP in the absence of SOS_{cat} showed a basal rate of $k_{w/o} = 4.42 \times 10^{-4} \text{ s}^{-1}$ (Fig. 7.2B-C). Strikingly, a dramatic increase in the exchange rate was observed in presence of either soluble fusion protein or functionalized MNPs. The same rates of $k_{FP} = 1.12 \times 10^{-2} \text{ s}^{-1}$ for the soluble fusion protein, and $k_{FP-MNPs} = 1.13 \times 10^{-2} \text{ s}^{-1}$ for the fusion protein functionalized MNPs confirm an intact GEF functionality of $\alpha\text{GFPnb-mCherry-SOS}_{\text{cat}}$ -modified MagIcS. The successful biofunctionalization of MagIcS opens an avenue of magnetic remote control in living cells, including untransfected native cells by injection of *in vitro* functionalized particles.

7.3. Reengineered FRET biosensors for probing GTPase activation

To monitor the activation of the small GTPases HRas and, tackled in later experiments, Rac1, two kinds of Förster resonance energy transfer (FRET) biosensors were reengineered. These FRET biosensors are based on the Raichu HRas and Raichu Rac1 FRET biosensor (Ras and interacting protein chimeric unit) developed by Kamatsu et al.³⁸¹

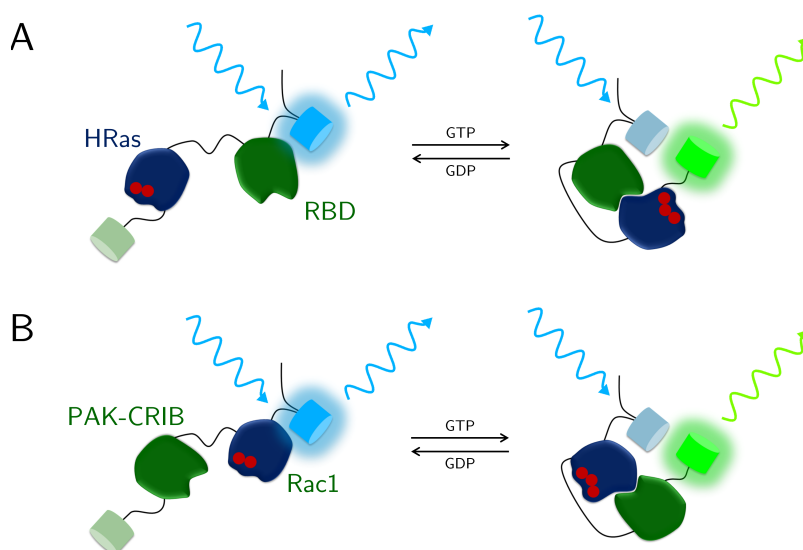


Figure 7.3.: **Reengineered FRET Biosensor.** A FRET biosensor based on (A) Raichu HRas and (B) Raichu Rac1 was reengineered by substitution of the FRET pair CFP/YFP for mTFP1/mNeonGreen. Activation of the small GTPase leads to a conformational change resulting in FRET.³⁸¹

The Raichu HRas FRET biosensor uses HRas as the sensing region and the Ras-binding domain of Raf (RBD) as the ligand region. The two regions are coupled with a flexible linker. Similarly, the Raichu Rac1 FRET biosensor uses Rac1 and the Cdc42/Rac1 interactive binding (CRIB) motif of PAK (PAK-CRIB). Both biosensors contain a CAAX box for plasma membrane anchoring. Fluorescent proteins CFP and YFP are used as FRET pairs to be donor and acceptor, respectively. Activation of GTPase into the GTP-bound state results in an interaction of GTPase with the binding domain of its effector. This leads to a conformational change of the FRET biosensor by bringing the two fluorescent proteins into close proximity and allowing FRET to be detected (Fig. 7.3). The original FRET pair CFP and YFP used by Komatsu et al. shares the same surface epitope of GFP. Therefore, they lack the orthogonality for syMagIcS targeting based on α GFPnb nanobody-GFP interaction. To gain the orthogonality of recombination, the fluorescent proteins were substituted with the GFP-orthogonal FRET pair mTFP1 and mNeonGreen. They were chosen due to their photophysical properties (Fig. 7.4).³⁸²⁻³⁸⁷

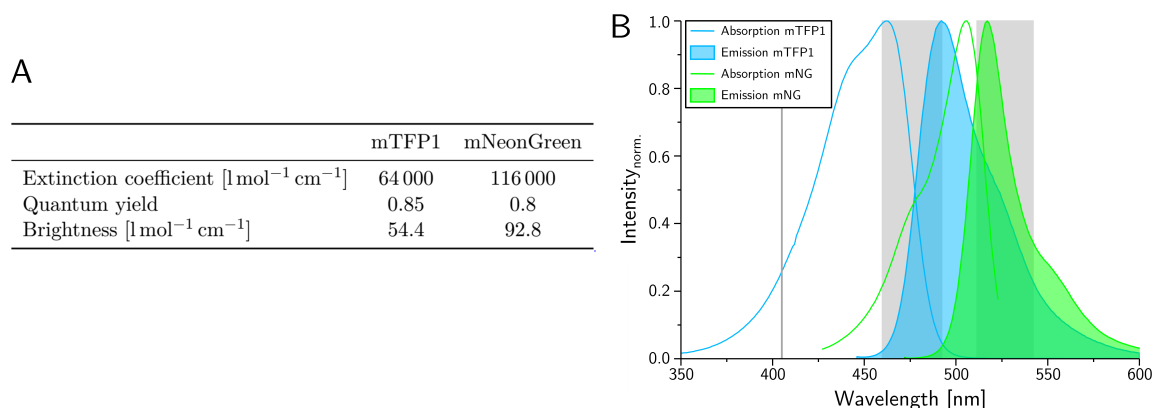


Figure 7.4.: **FRET pair mTFP1/mNeonGreen.** (A) Optical properties and (B) absorption/emission spectra of the FRET pair mTFP1/mNeonGreen.³⁸²⁻³⁸⁷

7.3.1. Characterization of the Raichu FRET biosensor

Prolonged exposure to excitation light can photochemically destroy a fluorescent protein and cause permanent loss of its fluorescence. To determine the photobleaching effect to the FRET biosensors, the Raichu Rac1 FRET biosensor was expressed in HeLa cells. Donor and acceptor fluorescence were monitored under constant excitation to calculate the acceptor/donor emission ratios as an indicator of FRET efficiency. Under this condition, strong donor bleaching could be observed as the donor intensity decreased rapidly while the acceptor/donor ratio increased (Fig. 7.5). Within the first 20s the increase was within the range of the deviation. Thus, for the acquisition of 80 images with an exposure time of 250 ms, the effect of bleaching is negligible.

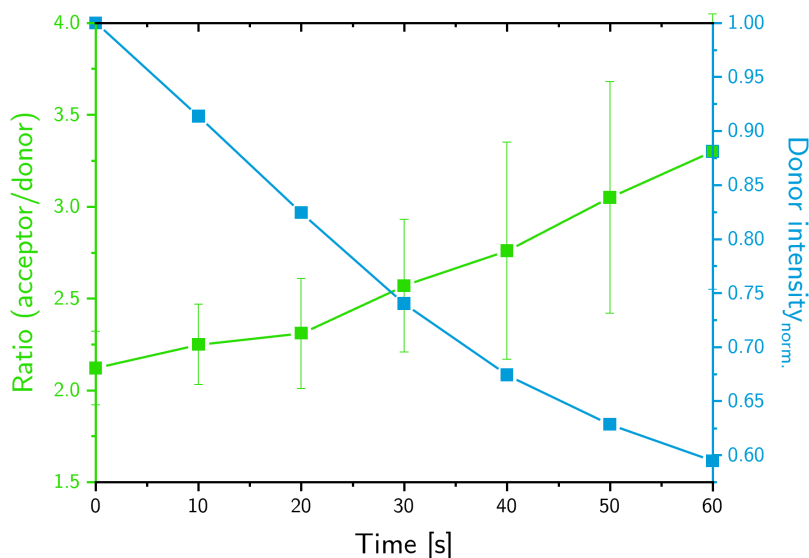


Figure 7.5.: **Photostability of Raichu Rac1.** Changes in normalized donor intensity (blue) and acceptor/donor ratio (green) under constant donor excitation. Simultaneous image acquisition by image splitter at an interval of 10s.

In the next step two variants with point mutations for each Raichu biosensor were cloned

and compared by ratiometric imaging. The Q61L mutation blocks the GTP-hydrolysis activities of the small GTPases Rac1 and Cdc42. This constitutively active mutant maintains a persistently active state. Meanwhile, a dominant-negative mutant of T17N was introduced, which prevents activation of the small GTPase as it is nucleotide-binding defective.³⁸⁸ Similarly, Raichu HRas G12V was introduced as the constitutively active mutant and Raichu HRas N116Y as the inactive mutant of the Raichu HRas biosensor.^{389,390} In addition, a fusion construct of the two fluorescent proteins connected to a flexible linker was constructed to explore the maximum intramolecular acceptor/donor ratio of the FRET pair. Figure 7.6 summarizes the ratiometric results of all the variations. As expected, the constitutively active mutant showed a higher ratio and the dominant-negative mutations had a lower ratio compared with the wild type. The result is more pronounced for the Raichu HRas biosensor. The FRET pair with a flexible linker shows the highest acceptor/donor ratio, indicating a tighter orientation of the biosensor compared to the positive control.

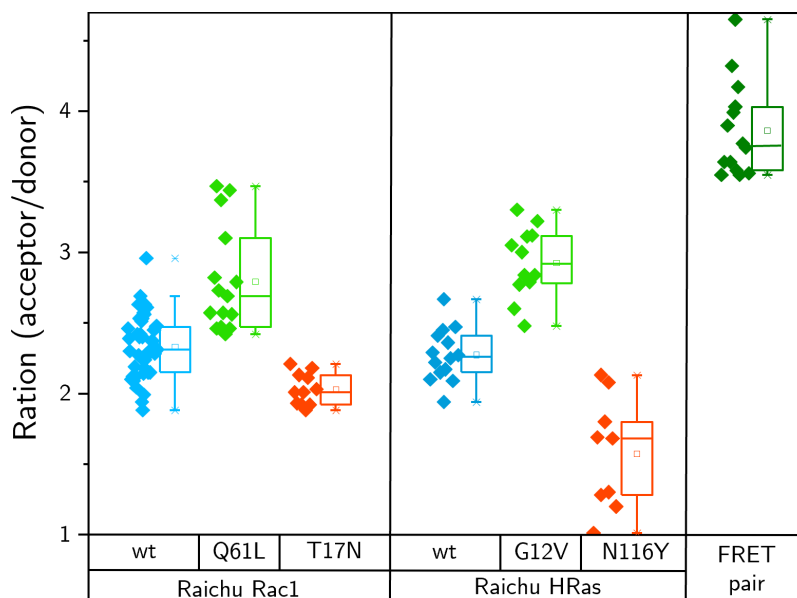


Figure 7.6.: **Characterization of Raichu Rac1 and Raichu HRas.** A constitutively active mutant (Q61L) and dominant-negative mutant (T17N) of Raichu Rac1, and respectively a constitutively active mutant (G12V) and dominant-negative mutant (N116Y) of Raichu HRas were investigated to determine the ratios of activated and inactivated FRET. This was compared to the ratio of the wild type Raichu biosensors and to the ratio of the FRET pair alone fused together via a flexible linker.

Time dependent activation of Rac1 and HRas was investigated using the Raichu FRET biosensors. For this purpose, HeLas were cultured under starved conditions with panexin. Activation was probed by the simultaneous addition of EGF and bradykinin. The epithelial growth factor (EGF) binds to the EGF receptor (EGFR), resulting in the activation of multiple signaling cascades that promote cell proliferation.²⁰⁷ Thus, the Ras/Raf/MEK

pathway³⁹¹ and also Rac1³⁹² is activated. Bradykinin is a tissue hormone of the kinin group that activates Rho GTPases, such as Rac1.³⁹³ Activation of the Ras/Raf/MEK pathway by bradykinin has been described.^{394–396} After addition of EGF and bradykinin, increased acceptor/donor ratios of both Raichu Rac1 and Raichu HRas were observed (Fig. 7.7). This indicates that the reengineered FRET biosensors are capable of monitoring the activation of the small GTPases Rac1 and HRas.

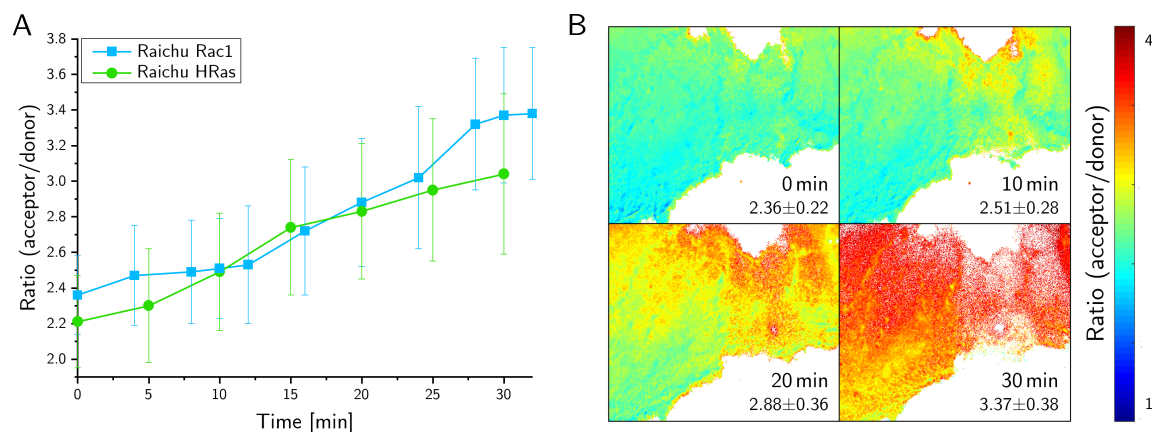


Figure 7.7.: **Probing activation of Raichu Rac1 and Raichu HRas.** Raichu biosensor transfected HeLa cells were activated by addition of 28 nM EGF and 20 μ M bradykinin. (A) Course of acceptor/donor ratio for representative cells during activation of Raichu Rac1 and HRas biosensors. (B) Distribution of the acceptor/donor ratio of Rac1 activation within the plasma membrane.

In summary, the reengineered FRET biosensors using the FRET pair of mTFP1/mNeonGreen are suitable for probing the activation of the small GTPases Rac1 and HRas inside living cells. They are implemented for detecting magnetogenetic GTPase activation in the following experiments.

7.4. Magnetic remote activation of the small GTPase HRas

With the reengineered FRET biosensor at hand, the magnetic activation of HRas by SOS_{cat} -functionalized MagIcS was investigated using the reengineered FRET biosensor Raichu HRas. It was probed whether the interaction of SOS (SOS_{cat}) bound to the functionalized syMagIcS leads to activation of the small GTPase HRas and consequently a conformational change of the biosensor to its active state.

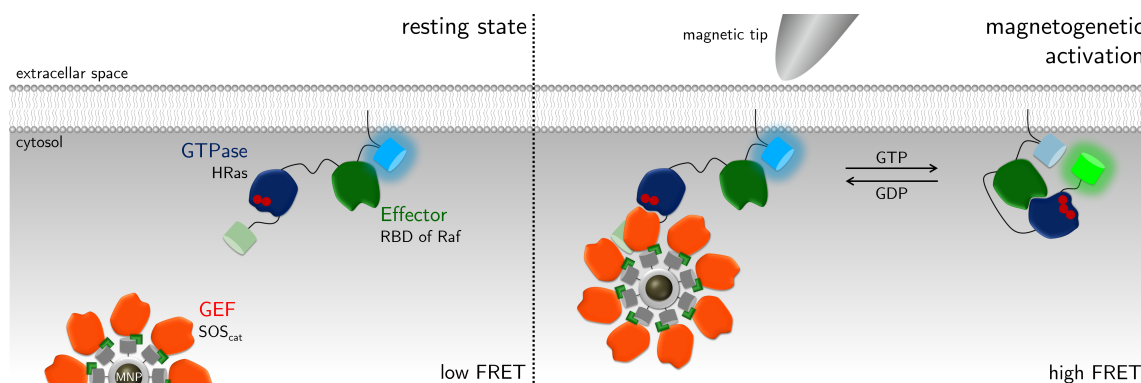


Figure 7.8.: **Concept of magnetic remote activation of a HRas Raichu FRET reporter system comprising HRas fused to the Ras binding domain of Raf (RBD) and the fluorescent proteins mTFP1 and mNeonGreen (mNG):** (left) Inactive GDP-bound state. (right) Translocating the catalytic region of the GEF protein mSOS (orange) captured to MagIcS to the plasma membrane. Interaction with HRas-GDP promotes GDP-GTP exchange resulting in a conformational change into the active state.

HeLa cells were cotransfected with $\alpha\text{GFP}::\text{mCherry}::\text{SOS}_{\text{cat}}$ and the FRET biosensor Raichu HRas. After microinjection of mEGFP-MagIcS, the SOS_{cat} -functionalized MagIcS were assembled *in situ* by specific, high affinity αGFP -GFP interaction. Magnetic manipulation of MagIcS particles at the plasma membrane was achieved by applying the magnetic tip close to the cell. Activation of HRas was observed with a strong activation signal of the Raichu HRas biosensor (Fig. 7.9 I). Most prominently, the activation signal colocalizes with the subcellular position of the MagIcS particles and constantly increases over the observation period of 45 min. After removal of the magnetic field gradient, however, the particles diffused back into the cytosol and the activation signal disappeared within a few minutes, demonstrating reversible magnetic control of HRas activation (Fig. 7.9 II).

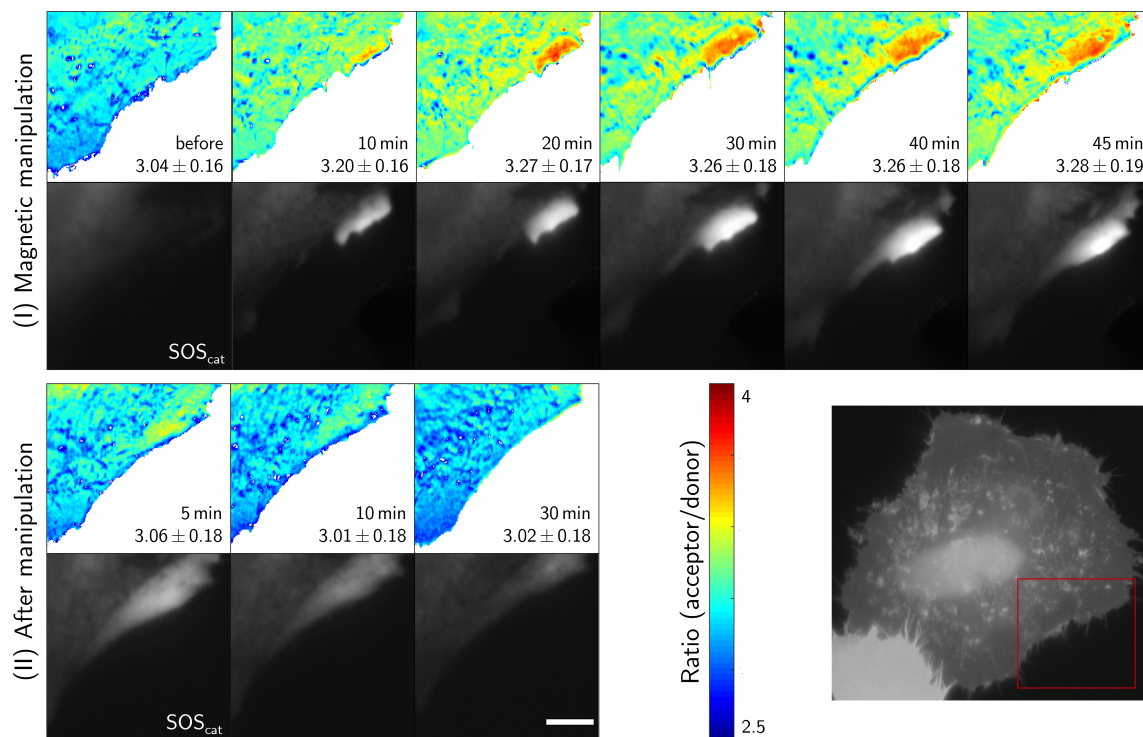


Figure 7.9.: **Magnetic remote activation of the HRas Raichu biosensor.** (I) Magnetically controlled HRas activation using SOS_{cat}-functionalized MagIcS monitored by Raichu HRas FRET biosensor activation (top row). MagIcS (non-fluorescent) was injected into cells expressing α GFP::mCherry::SOS_{cat} and mNeonGreen::HRas::Linker::RBD::mTFP1::CAAX. Time-lapse images during magnetic manipulation show an increase in the FRET signal colocalized with recruitment of the SOS_{cat} catalytic region. (II) After removal of the magnetic field gradient, the SOS_{cat}-functionalized MagIcS diffuse back resulting in a decrease of the FRET signal. (Bottom right) An Overview image of the cell (mTFP1 fluorescence) and the evaluated ROI (red) are shown. Scale bar: 10 μ m.

Despite the advantageous properties, such as excellent biocompatibility, the experiments revealed limitations in the magnetic properties of MagIcS. The limited magnetic response is due to the synthesis conditions by using the natural ferroxidase activity of ferritin and due to the restriction of the magnetic core to a maximum of 8 nm caused by the size of the ferritin protein cage. Furthermore, the encapsulation of the magnetic core into the protein cage represents a challenging, elaborate and sensitive process. For these reasons, a new approach was chosen and a fundamentally new system of magnetic nanoparticles was developed that overcomes these limitations and exhibits other advantageous properties.

Acknowledgement

The characterization of the Raichu HRas FRET biosensor was done by Anabelle Ludi as part of her bachelor's thesis. The Matlab routine for analyzing the FRET ratio was written by Christian P. Richter.

8 | Semi-synthetic Magnetic Intracellular Stealth Nanoparticles

There are high requirements for MNPs to be used in living cells. As previously described, nanoparticles must maintain their robust colloidal properties in complex biological environments, while the overall hydrodynamic diameter of fully assembled MNPs must be small enough (approx. <50 nm) to ensure efficient cellular delivery of nanoparticles for unhindered mobility in the cytosol. Other critical requirements are high magnetic response, special surface passivation to minimize toxicity and recognition by the cellular degradation machinery, and biofunctionalization for site-specific and efficient conjugation with target proteins by *in situ* capturing in cells. To meet the stringent requirements of MNPs for use in living cells, high-affinity iron oxide binding Mms6 protein from magnetotactic bacteria was utilized. For efficient, high-affinity binding to the MCP surface, mEGFP was fused to the C-terminal iron-binding domain of the Mms6 protein (amino acids 112-133, Mms6 Δ N). This approach resulted in semi-synthetic MNPs with intracellular stealth properties (syMagIcS). This strategy leads to densely coating of syMagIcS with the stable mEGFP- β -barrels in a single step. The versatility of the coating can be extended by replacing mEGFP with other GFP derivatives. To obtain a weakly fluorescent variant, the GFP was replaced by the mEGFP Y66F mutant (mXFP). Furthermore, mEGFP was replaced by the GFP derivatives to which the anti-GFP nanobody enhancer (α GFPnb) has different affinities. The affinity is tunable between $K_D = 0.3$ nM for mEGFP, $K_D = 450$ nM for mECFP (H164N), and $K_D > 10$ μ M mECFPm (E142K H164N). The different coating proteins and mixtures of them allow specific control over the multivalency of the biofunctionalization. The obtained syMagIcS show significant advantages by overcoming the limitations of previously used ferritin-based MagIcS in terms of magnetic properties and variability to control biofunctionalization.

In order to specify the properties and to demonstrate the suitability for intracellular applications in living cells, several characterization steps were performed. First, the synthesized maghemite nanoparticles were analyzed in terms of size and magnetic properties. This was followed by one-step biofunctional coating of the MCPs, resulting in syMagIcS. The *in vitro* characterization of the biofunctionalized syMagIcS was performed by analytical size-exclusion chromatography, TEM imaging and resulting size analysis and comparison with the hydrodynamic diameter determined by DLS, as well as ζ potential measurements. Furthermore, the stoichiometry of the functionalization was estimated and the long-term stability under different conditions was investigated. In the next step, *in cellulo* characteri-

zation was performed by stability studies, determination of cytosolic concentration after microinjection and characterization of magnetic response inside living cells. Crucial for the fulfillment of the functionality is a site-specific functionalization. This was verified by studying the interaction *in vitro* by solid phase detection and a site-specific *in cellulo* targeting. Furthermore, the magnetic response of protein-functionalized syMagIcS was demonstrated inside living cells.

8.1. Synthesis and *in vitro* characterization of maghemite core particles

As part of the MAGNEURON project (Horizon2020 FET open No. 686841), the PHENIX Laboratory (Sorbonne University) synthesized maghemite core particles (MCP) by an inverse co-precipitation method. Characterization by transmission electron microscopy (TEM), dynamic light scattering (DLS), and superconducting quantum interference device (SQUID) is shown in Figure 8.1. This characterization resulted in an average physical diameter of $d_p = (11.7 \pm 4.8)$ nm (TEM), an average hydrodynamic diameter of $d_{hydro} = (22.2 \pm 7)$ nm (DLS) and a saturation magnetization of $M_S = 62.5$ emu/g. These values are comparable to those in the literature. There the saturation magnetization at RT of bulk maghemite is given with $M_{S,bulk} = 80$ emu/g, for 9 nm maghemite nanoparticles with $M_{S,9nm} \sim 58$ emu/g and 12 nm maghemite nanoparticles $M_{S,12nm} \sim 65$ emu/g.^{397,398}

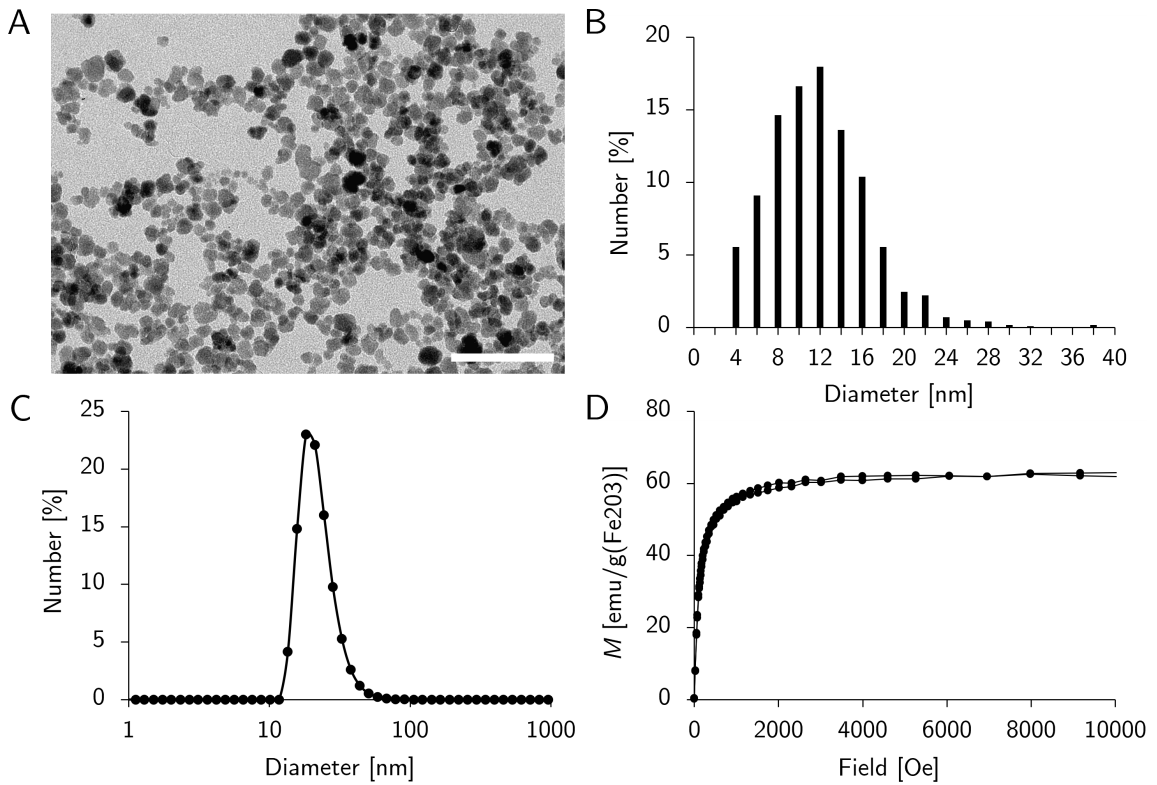


Figure 8.1.: **Characterization of the maghemite MCP.** (A) Transmission electron microscopy image of MCPs. Scale bar: 100 nm. (B) Physical size distribution of the MCPs determined by measuring over 1250 particles with ImageJ. The average diameter of the MCPs used in this study is $d_p = 11.7$ nm. (C) Hydrodynamic diameter distribution of the MCPs in water at pH=2, with an average hydrodynamic of $d_{hydro} = (22.2 \pm 7)$ nm. (D) Magnetization curve of the MCP dispersed in water at pH=2. The saturation magnetization is $M_S = 62.5$ emu/g.

8.2. One-step biofunctional coating of MCP

In order to create a dense biofunctional coating, a new fusion protein was developed. This coating should enable biocompatible and stealth behavior, provide a colloidal stable particle inside the cytosol and enable site-specific bio-orthogonal functionalization. For this purpose the iron-binding fragment of Mms6 comprising the C-terminal 22 amino acid residues (MKSRDIESA QSDEEVELRD ALA) of Mms6 (Mms6 Δ N) was genetically fused to the C-terminus of monomeric enhanced GFP (mEGFP). A His6-Tag (H6) was fused to the C-terminus of mEGFP for purification.

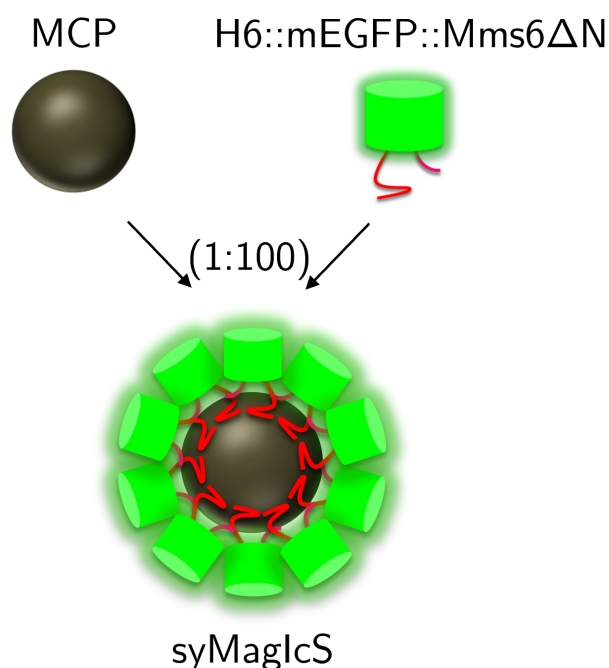


Figure 8.2.: **Strategy for one-step biofunctional coating of syMagIcS.** Coating MCP by mixing a 100-fold excess H6::mEGFP::Mms6 Δ N with MCPs.

The recombinant coating protein (H6::mEGFP::Mms6 Δ N) was produced in *E. coli* in high yields. Purification by IMAC under denaturing conditions to prevent proteolytic degradation followed by size exclusion chromatography lead to a high homogeneity of the protein (Fig. 8.3). After a buffer exchange of the protein solvation buffer to pure water, the MCPs (Fig. 8.2) dispersed in pH 2 water were added at a protein:MCP ratio of 100:1. The amount of added MCP solution was very low compared to the volume of the protein solution. Therefore the pH of the protein solution was maintained through the process. After incubation (> 1 h at RT), excess of unbound coating proteins was removed by ultrafiltration yielding mEGFP-Mms6 Δ N coated MCPs (syMagIcS).

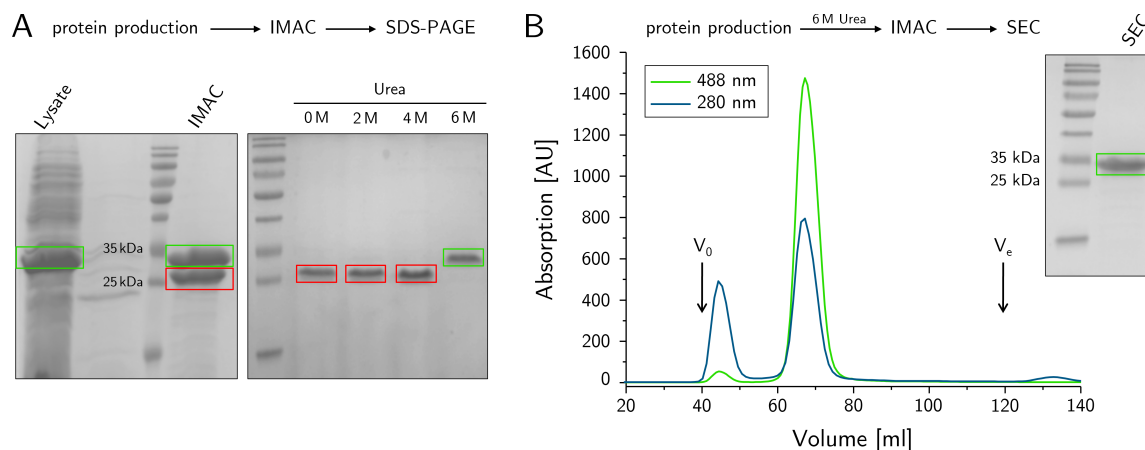


Figure 8.3.: **Purification of H6::mEGFP::Mms6 Δ N.** (A) Optimization of a standard protocol for purification of H6::mEGFP::Mms6 Δ N. Left: SDS-PAGE after immobilized metal affinity chromatography (IMAC) of H6::mEGFP::Mms6 Δ N according to a standard protocol for HIS-Tagged proteins. Full length protein is highlighted by the green rectangle and proteolytic products by the red rectangle. Right: optimization of the purification strategy by titration of different urea concentrations. Cells were lysed in presence of urea. (B) Final purification strategy: IMAC in presence of 6 M urea with subsequent size-exclusion chromatography (SEC). SDS-PAGE of H6::mEGFP::Mms6 Δ N after SEC.

8.3. *In vitro* characterization of syMagIcS

For characterization of mEGFP-Mms6 Δ N coated MCP, analytical size exclusion chromatography (SEC) in HBS (20 mM HEPES, 150 mM NaCl, pH 8.0) of the reaction mixture resulted in a brownish monodisperse elution at the volume expected for MCP coated with mEGFP monolayers (Fig. 8.4). While the non-coated MCPs precipitated under these conditions, the monodisperse elution profile indicates that the MCPs are effectively coated with mEGFP.

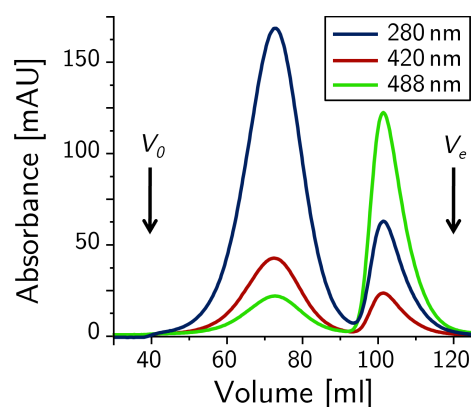


Figure 8.4.: **Analytical size-exclusion chromatography.** SEC (Sephacryl S500) of the reaction mix detected via absorbance at three different wavelengths. Column void volume (V_0) and bed volume (V_e) are indicated.

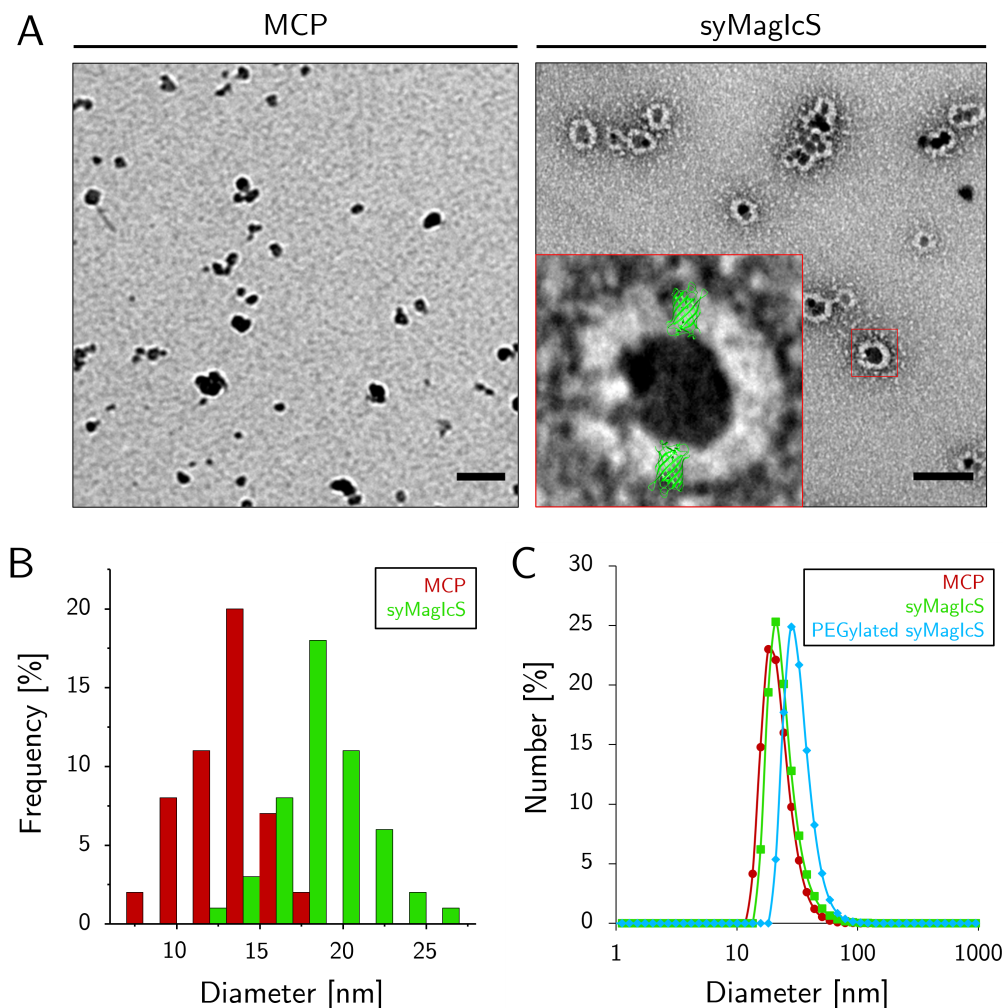


Figure 8.5.: **TEM analysis.** (A) Transmission electron micrographs of MCPs (left) and syMagIcS (right). Scale bar: 50 nm. (B) Particle size distribution of MCPs (red) and syMagIcS (green) obtained from TEM images; $n = 100$ particles for each species. (C) Hydrodynamic diameter of the particles quantified by DLS. Size distributions in number obtained for the bare MCP (red), MCP functionalized with non-PEGylated Mms6-GFP (green) and MCP functionalized with PEGylated Mms6-GFP (blue).

TEM images of syMagIcS by negative staining confirmed the complete coating of MCPs by a densely packed mEGFP coating (Fig.1.5A). These TEM images revealed an average physical diameter $d_{p,MCP} = (12.1 \pm 2.1)$ nm for MCPs. Strikingly, an increased size to $d_{p,syMagIcS} = (19.6 \pm 2.7)$ nm was observed for syMagIcS (Fig. 8.5B). This increased diameter of ~ 8 nm is in good agreement with the ~ 4 nm height of the mEGFP barrel. The height strongly suggests an upright orientation of mEGFP coated on MCP, which is expected for the C-terminal fusion of Mms6 Δ N peptide to mEGFP and monolayer coating (Fig. 8.5A, inset). Similarly, an increase of the hydrodynamic diameter was observed in DLS measurements due to the protein and an additional PEGylation (Fig. 8.5C), with an average hydrodynamic diameter of $d_{hydro,MCP} = (22.2 \pm 7)$ nm for MCP, $d_{hydro,syMagIcS} = (24.8 \pm 8.9)$ nm for syMagIcS, and $d_{hydro,syMagIcS,PEG} = (33.1 \pm 9.9)$ nm for PEGylated syMagIcS. The ζ

potential of syMagIcS was determined to be -25 mV in HEPES buffer pH 7.5. This slightly negative ζ potential is advantageous for stability in the predominantly negatively charged environment of the cell.²⁶⁵

In order to obtain effective shielding properties and thus biocompatibility, a dense, gapless coating of the MCP is required. To further confirm the dense coating previously shown on the TEM images, the stoichiometry of the functionalization was determined. This functionalization stoichiometry also plays a crucial role in the interaction and reactivity of the particles, as the valency of the functionalization determines the local concentration of the functional component. For this reason, the degree of multivalence is an important parameter, which must be known in order to control the interaction specifically. To estimate the functionalization stoichiometry, the concentration of coating protein bound on the particle surface was determined by denaturing SDS-PAGE and related to the concentration of syMagIcS measured by spectrophotometry. (Fig. 8.6). This Functionalization stoichiometry estimation revealed an average number of 66 mEGFP molecules per MCP, which corresponds to a dense monolayer coverage of the particle surface. The theoretical covered area of these 66 mEGFP molecules, with a diameter per molecule of $d_{mEGFP} = 4.2$ nm,³⁹⁹ is $A_{66 \times mEGFP} \approx 498$ nm², the particle surface $A_{MCP} \approx 450$ nm². The slightly larger surface area covered by the mEGFP molecules can be explained on the one hand by the error due to the estimation and experimental deviations, and on the other hand by the mEGFP molecules being located slightly above the particle surface. The difference in surface area corresponds to a radius difference of $\Delta r \approx 0.15$ nm.

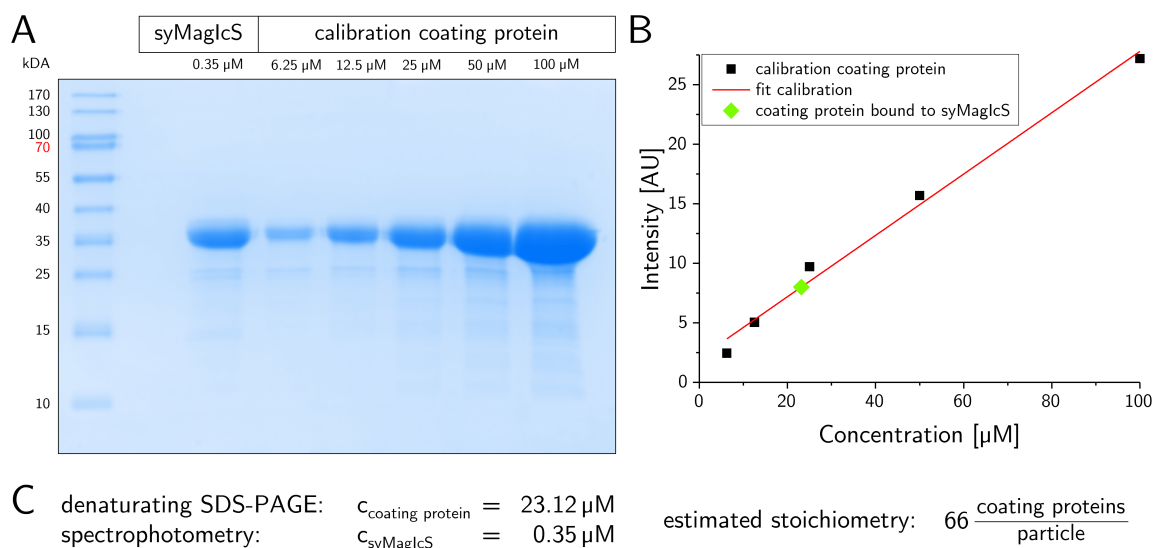


Figure 8.6.: **Estimation of functionalization stoichiometry.** (A) Denaturing SDS-PAGE of syMagIcS and increasing concentration of coating protein. Coomassie staining. (B) Intensity in dependence on coating protein concentration. (C) Concentration of Coating protein and syMagIcS, calculation of functionalization stoichiometry.

The *in vitro* long-term stability of syMagIcS was probed in HEPES buffer pH 7.5 (HB), Dulbecco's phosphate-buffered saline (DPBS) or minimal essential medium containing 10% fetal bovine serum (MEM⁺⁺) pH 7.5, to mimic the cellular environments (Fig 8.7A). After an initial drop, no significant loss of particles was detected in HB buffer over 14 days, demonstrating tight binding of H6::mEGFP::Mms6 Δ N in HB. The syMagIcS particles were stable in MEM⁺⁺ for several days, with a slow loss over the observation period. This lower stability of the particles in the culture medium compared to HB reflected that the multivalent binding of Mms6 Δ N to the maghemite surface is liable to be abolished by competing molecules (e.g. amino acids, proteins, salts etc.) in the culture medium.⁴⁰⁰ syMagIcS showed further reduced colloidal stability in DPBS. Over the time course of one hour, the majority of the particles in solution was lost (Fig 8.7B). This could be due to competitive binding of the contained phosphate ions, whose concentration in PBS is approximately 10-fold higher than in MEM.^{401,402} To increase stability, the coating proteins were cross-linked using paraformaldehyde (4% PFA in HB). The intermolecular cross-linking of coating proteins creates a closed protein cage (i.e. mEGFP shell) around the MCP, thus prevents dissociation of the coating proteins. After 4% PFA treatment, the syMagIcS showed comparable stability in DPBS as in HB (Fig 8.7A), indicating successful crosslinking to form a protein cage around MCP. The long-term stability is an important feature for applications in biomedicine where the maintenance of a protein gradient over a prolonged period is required. Moreover, stable protein coating of the syMagIcS will not cause undesirable reactions even when remaining in the organism.

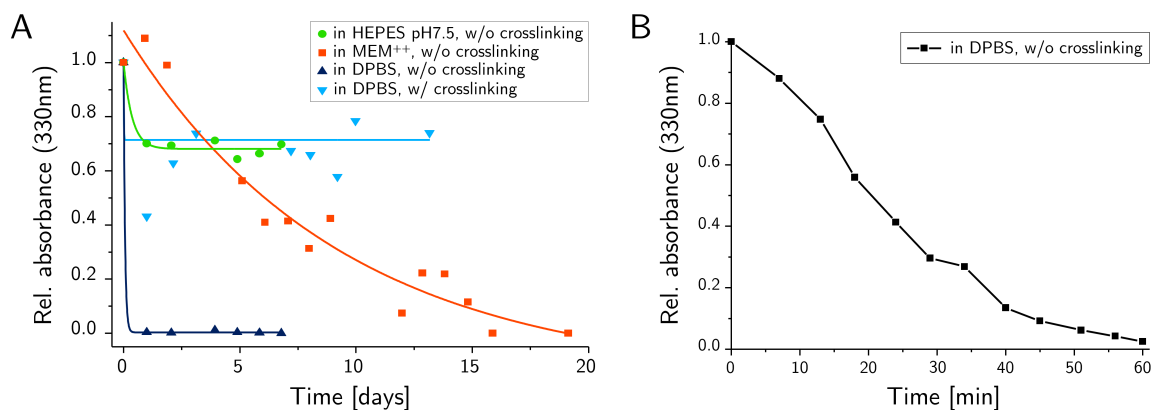


Figure 8.7.: **Long-term particle stability under different conditions.** (A) Stability of syMagIcS in different physiological solutions and crosslinking of the particle coating using 4% PFA. (B) Stability of syMagIcS in DPBS over 1 h.

8.4. *In cellulo* characterization of syMagIcS

Key challenges for the intracellular use of nanoparticles include the prevention of non-specific interactions with large biomolecules or organelles, as well as recognition by cellular degradation machineries. Previous studies showed the uptake of protein-based nanoparticles

into autophagosomes happens on a time scale of a few seconds.⁴⁰³ In order to investigate the cytosolic stability for intracellular applications, non-crosslinked syMagIcS were delivered into the cytosol by microinjection. Immediately after microinjection, the particles showed a homogeneous distribution, which was maintained over an observation period of 30 min. Neither clustering of the particles nor non-specific interaction with the intracellular environment was observed (Fig 8.8 and Supplementary Movie S1). This high intracellular stability indicates monolayer protein coating of the MCPs achieve intracellular stealth properties without additional modifications. Thus fulfilling a critical prerequisite for the following experiments, which require intracellular syMagIcS stability on a medium-long time scale. The following experiments will also investigate whether syMagIcS show an intracellular magnetic response. This is an important control whether the shown homogeneous distribution in this experiment refers to intact coated syMagIcS or whether only the coating protein was observed.

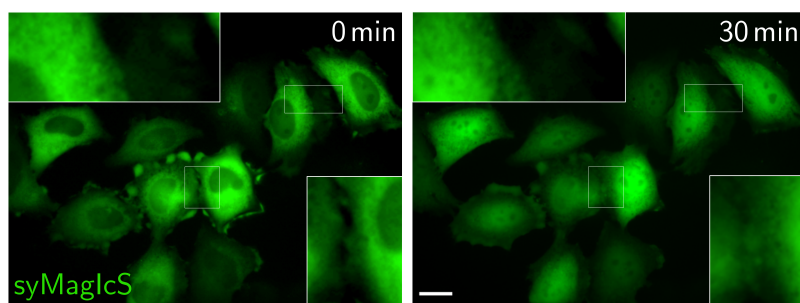


Figure 8.8.: **Stability of syMagIcS inside living cells.** Distribution of syMagIcS in the cytosol of wt HeLa cells. Scale bar: 30 μm .

The law of mass action implies that concentration is an important factor for interactions and reactions and thus the control of cellular processes (see Chapter 1.1). The local concentration of the functional protein bound on the syMagIcS surface depends on the one hand on the multivalence of the functionalization and on the other hand on the local concentration of the functionalized syMagIcS. In order to know the initial concentration, the cytosolic syMagIcS concentration delivered into the cell by microinjection was investigated. For this purpose, two differently concentrated syMagIcS solutions were microinjected into HeLa cells. Confocal laser scanning microscopy showed that intracellular syMagIcS concentrations are in the range of 35 nM for high load and 5 nM for low load after microinjection (Fig 8.9).

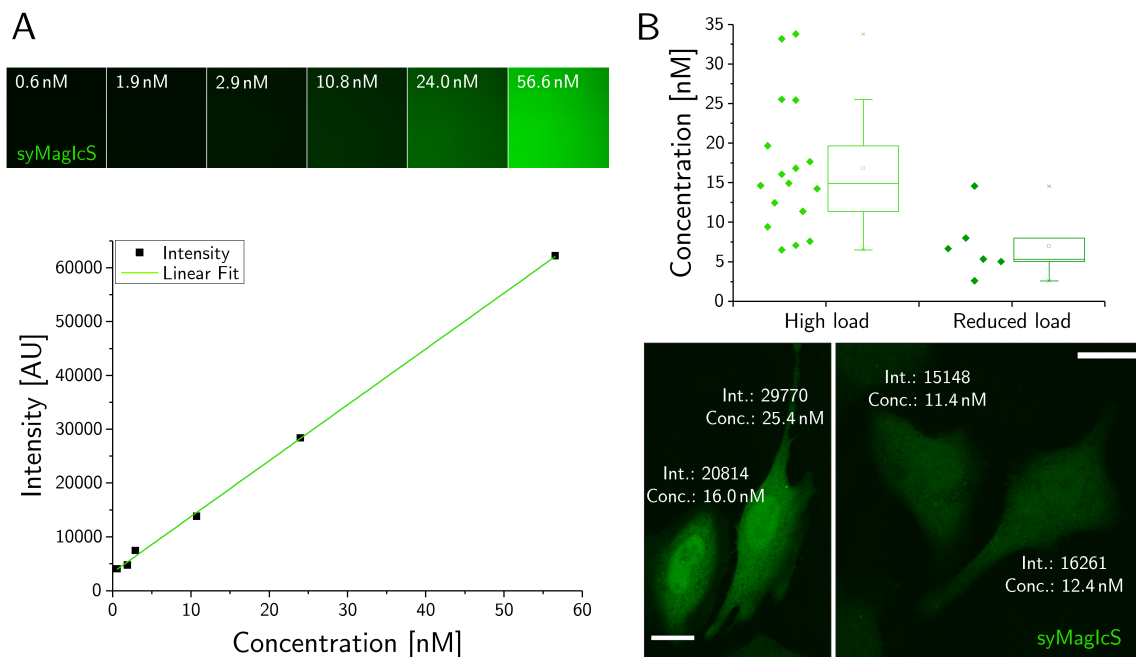


Figure 8.9.: **Quantification of syMagIcS concentrations inside cells.** (A) Confocal laser scanning microscopy images of syMagIcS solutions at different concentrations. Calibration curve is shown below. (B) Concentration measured inside HeLa cells. Scale bar: 20 μm in all images.

To obtain an estimate of the particle concentration required, the endogenous concentration of proteins involved in signal transduction was estimated using Ras-GEFs SOS1 and SOS2 as examples. Shi et al. investigated the copy number in human mammary epithelial cells. This resulted in a copy number of 3,671 copies/cell for SOS1, 1,635 copies/cell for SOS2. In contrast, the copy number of the corresponding small GTPases was significantly higher, 68,452 copies/cell for HRas, 95,735 copies/cell for KRas, and 82,045 copies/cell for NRas.³³⁴ In addition to these values, the literature value given by Alberts et al. for the volume of an average mammalian tissue culture cell of about 4 picoliters was used,⁴⁸ leading to an estimated concentration of about 0.7 nM SOS1 and 1.5 nM SOS2. Due to the multivalency of syMagIcS, a fraction of this concentration is estimated to be required to bind an endogenous amount of the GEF.

The most important requirement for intracellular manipulation of syMagIcS is the magnetic response. To probe the magnetic response of syMagIcS, the manipulation of freely diffusing syMagIcS within HeLa cells was investigated by applying a magnetic field gradient generated from a magnetic tip. syMagIcS showed rapid attraction to the magnetic tip approaching a cell. Fast response to the changed position of the magnetic tip was shown by recruiting the syMagIcS to different subcellular parts within a few seconds (Fig 8.10 and supplemental Movie S2).

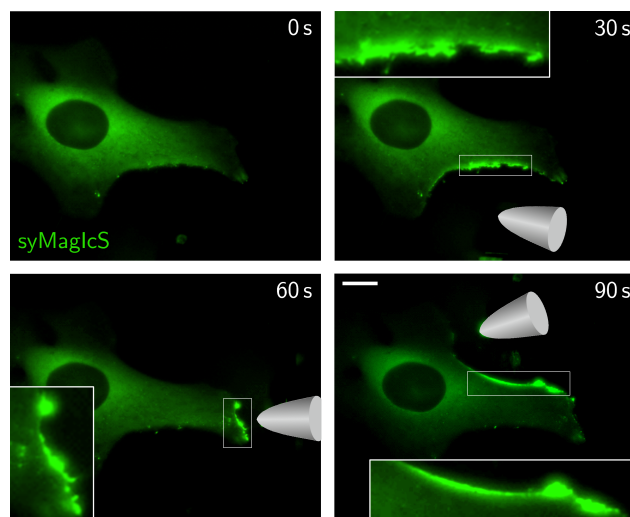


Figure 8.10.: **Magnetic manipulation of syMagIcS inside living cells.** Time lapse imaging of a magnetic tip approaching a HeLa cell loaded with syMagIcS (green) from different directions. Scale bar: 30 μm .

Reversible attraction to the plasma membrane and diffusion back into the cytosol were examined by applying and removing the magnetic tip at a distance of $\sim 45 \mu\text{m}$ from the plasma membrane (Fig. 8.11 and supplemental Movie S3). Repeated reversible attraction was shown over several cycles. Evaluation of the attraction time constant (τ_A) and relaxation time constant (τ_R) confirmed fast spatiotemporal magnetic control of syMagIcS with $\tau_A = (1.7 \pm 0.1) \text{ s}$ and $\tau_R = (1.0 \pm 0.2) \text{ s}$. This reversible attraction within seconds is suitable for the applications in magnetic remote control of the model systems, as it should be done on a time scale of several minutes.

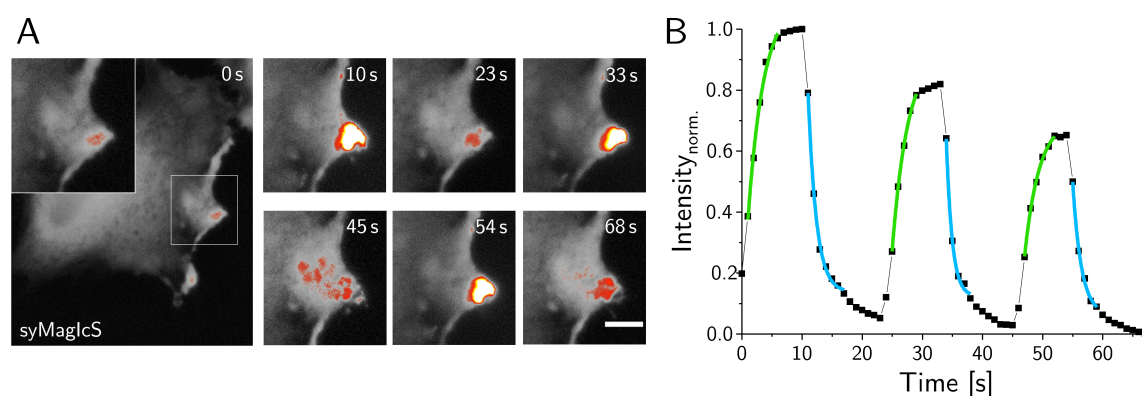


Figure 8.11.: **syMagIcS attraction and release kinetics in living cells.** (A) syMagIcS were injected into HeLa cells and repeatedly attracted and released with a micro-magnet to the plasma membrane. (B) Attraction and release kinetics of syMagIcS determined from the changes in fluorescence intensity in the area highlighted by the white square and exponential fit of the curve (green, blue). Scale bar: 10 μm .

The magnetic force applied to syMagIcS was determined in the cell cytosol at the steady-state of attraction. A distance-dependent decrease of the particle intensity $I(r)$ was fitted

exponentially under the assumption the theoretical profile follows the Boltzmann law:

$$I(r) = e^{-\frac{Fr}{k_B T}} \quad (8.1)$$

where k_B is the Boltzmann constant; T is the temperature; F is the applied force; r is the distance. The results show that micromagnets at a distance of 48 μm to 152 μm from the plasma membrane exerted a force in the femto-Newton range (Fig. 8.12). These values are comparable to those obtained by Liße et al. using MagIcS at a distance of the magnetic tip to the cell of 10 μm , which demonstrates an improved magnetic response.⁷⁵

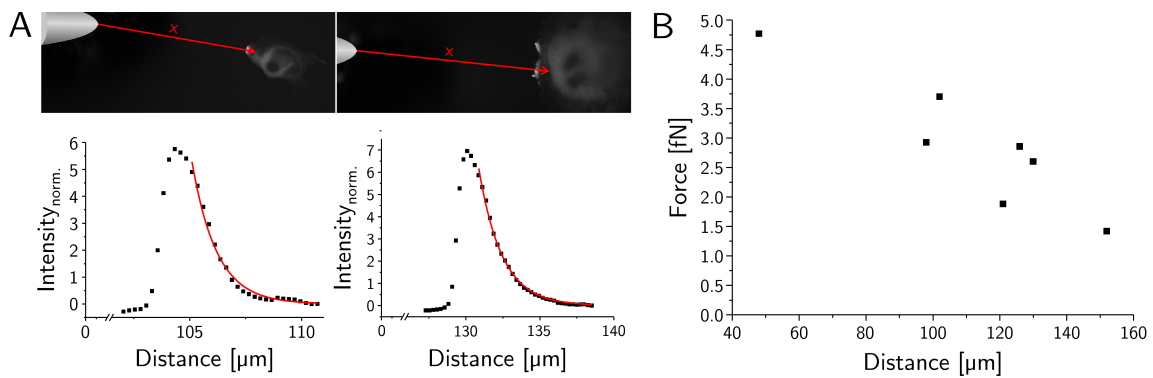


Figure 8.12.: **Quantification of the force exerted on syMagIcS.** (A) Microscopy images of the steady-state syMagIcS gradient profiles inside the cytosol of living cells under a magnetic gradient. Red curves are mono-exponential fittings according to equation 8.1 (B) Detected force as the function of the distance of the magnetic tip from the cell. Scale bar: 50 μm .

To overcome the limitations of magnetic control using magnetic tip on single cell experiments, a magnetic device based on Halbach array was constructed (Chapter 4.6.2). This array generates a strong magnetic gradient over an enlarged area, allowing parallel investigation of multiple cells. To test the custom-made magnetic device and demonstrate remote magnetic control over larger distances, the first step was to investigate the *in vitro* behavior of syMagIcS in solution (HB buffer). A rapid fluorescence increase was observed towards the magnetic device (Fig 8.13A-B). After two hours, most of the syMagIcS were assembled at the edge in the direction of the magnetic device; the next day, the solution was free of visible syMagIcS and the syMagIcS were densely accumulated at the edge (Fig 8.13C).

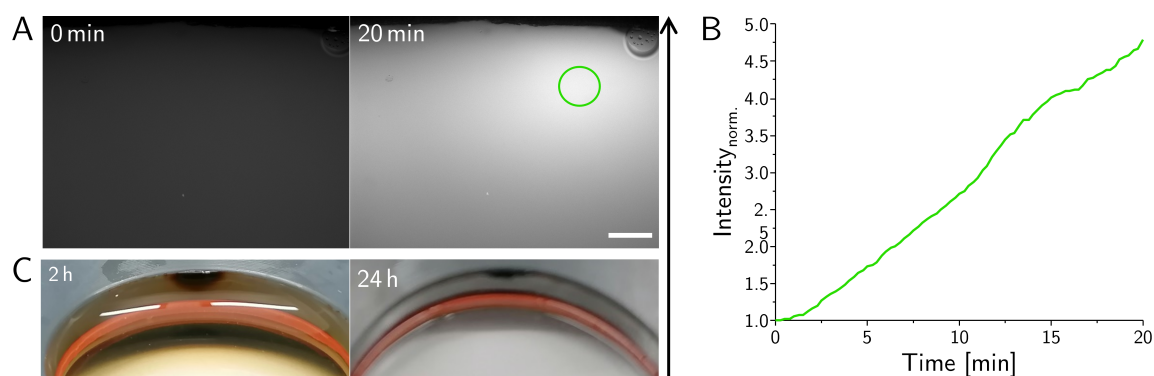


Figure 8.13.: ***In vitro* magnetic manipulation using a device based on a Halbach array.** Magnetic response of syMagIcS in solution (HB buffer). The arrow indicates the direction of the magnetic field gradient, the green circle the ROI. (A-B) Increase in fluorescence over a period of 20 min. (C) Accumulation of syMagIcS at the edge facing the magnetic device. Scale bar: 50 μm .

After demonstrating a strong magnetic response of syMagIcS in solution *in vitro*, the next step was to investigate the magnetic behavior inside living cells. syMagIcS were microinjected into HeLa cells and the cells were located at a distance of approximately 1 cm from the Halbach array. The magnetic response to the applied magnetic field gradient was successfully observed (Fig. 8.14). This preliminary experiment suggests the potential of the Halbach array and is a first step towards extending single cell experiments to a multi-cell scale. To further parallel the investigation, this magnetic device can be combined in the future with available methods which allow simultaneously delivery of nanoparticles to a large amount of cells. These methods include bead loading, electroporation, or cell-penetrating peptides.^{404–406}

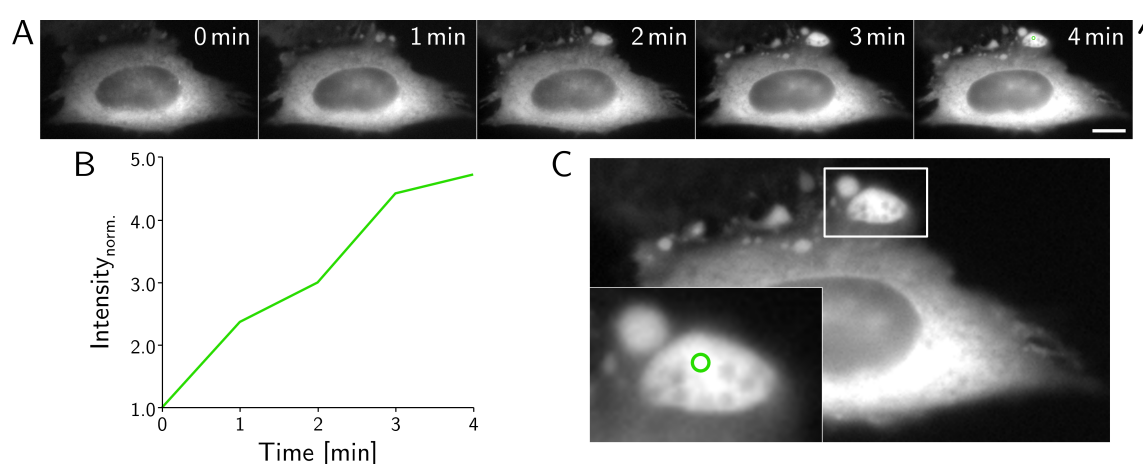


Figure 8.14.: **Magnetic manipulation using a device based on Halbach array inside living cells.** Magnetic response of syMagIcS after microinjection into HeLa cells. The arrow indicates the direction of the magnetic field gradient. (B) Normalized intensity as a function of time. (C) Investigated ROI indicated by the green circle. Scale bar: 10 μm .

8.5. Functionalization and site-specific targeting

Functionalized MNPs can be used as nano signaling actuators for modulating cell signaling pathways. This can be achieved by immobilizing biomolecule recognition entities on their surface. Here, mEGFP is immobilized on the surface of syMagIcS. Intracellular targeting proteins were genetically fused to α GFPnb-enhancer for high affinity binding to the mEGFP presented on the syMagIcS surface. The ability of *in cellulo* functionalization of proteins avoids the need for purification of large proteins or protein complexes, which are often challenging and time consuming. This site-specific targeting was investigated *in vitro* using solid phase detection of total internal reflectance fluorescence spectroscopy and reflectance interference (TIRFS-RIf).

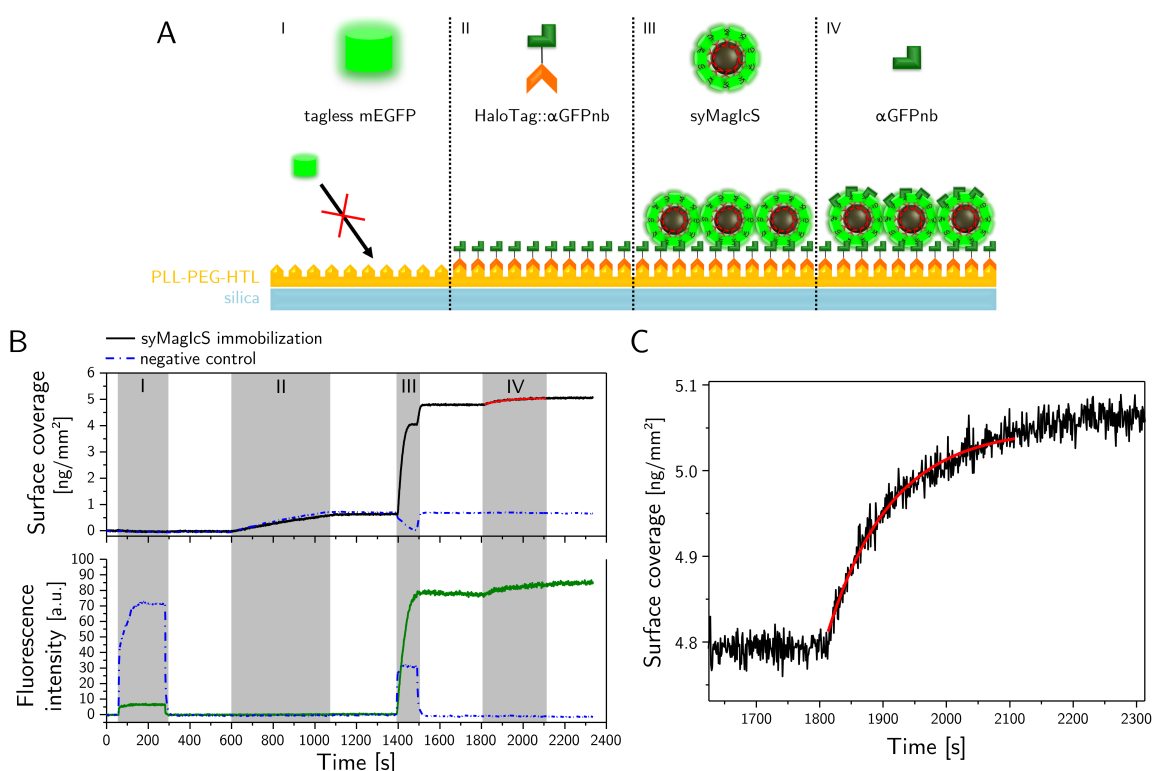


Figure 8.15.: **Interaction of α GFP with syMagIcS quantified by solid phase detection *in vitro*.** (A) Schematic illustration of the assay: (I) injection of tagless mEGFP as control for unspecific binding to the PLL-PEG-HTL-functionalized surface, (II) immobilization of HaloTag-H10- α GFPnb to HTL ligands at a concentration of 1 μ M; (III) binding of syMagIcS to immobilized α GFPnb; (IV) binding of α GFPnb to the toplayer of immobilized syMagIcS. (B) Mass signal (top) and fluorescence signal (bottom) acquired during the assay. (C) Zoom into the mass signal detected for α GFPnb binding to immobilized syMagIcS (iv) and fit of Langmuir model ($k_{on} = (4.0 \pm 0.1) \times 10^4 \text{ M}^{-1}\text{s}^{-1}$). The blue dashed line represents the negative control where a HaloTag without α GFPnb was immobilized.

TIRFS-RIf measurements were performed as previously described by Gavutis et al. using a homemade instrument.⁴⁰⁷ Glass substrates coated with a silica layer and functionalized with PLL-PEG-HTL were used. Mass signal and fluorescence signal is acquired during this assay. First, injection of a tagless mEGFP as a control confirmed absence of unspecific binding to the PLL-PEG-HTL-functionalized surface. After immobilization of HaloTag:: α GFPnb, PFA-crosslinked syMagIcS bound onto an α GFPnb-presenting surface in a diffusion-limited manner (Fig. 8.15, phase III). Additional α GFPnb was able to bind onto the syMagIcS surface, confirming the binding of a multivalent nanoparticle, which has free binding sites available (Fig. 8.15, phase IV). The Langmuir model fit of the mass signal results in an association rate constant $k_{on} = (4.0 \pm 0.1) \times 10^4 \text{ M}^{-1} \text{ s}^{-1}$ for the interaction of the α GFPnb to immobilized syMagIcS (phase IV). The negative control, where a HaloTag without α GFPnb was immobilized instead of the HaloTag:: α GFPnb, showed no significant binding of syMagIcS to the surface (blue dashed line). This confirmed the specific recognition of syMagIcS by α GFPnb even after the fixation of the mEGFP coating with PFA. The significantly reduced association rate constants compared with the pure interaction between mEGFP and α GFPnb ($k_{on} = (1.1 \pm 0.8) \times 10^6 \text{ M}^{-1} \text{ s}^{-1}$ ⁴⁰⁸) could be due to the dense packing of the coating proteins onto the particle surface or to the PFA-crosslinking. The tight packing could inhibit access to the binding epitope and thus sterically hinder the interaction.

In a proof of concept experiment, the feasibility of *in cellulo* targeting under the complex conditions in the cytosol was investigated. For this purpose, TOM20 fused with mCherry and α GFPnb (TOM20::mCherry:: α GFPnb) was transfected into HeLa cells. TOM20 is anchored in the mitochondrial outer membrane with α GFPnb directed towards the cytosol. Microinjection of substoichiometric amounts of PFA-crosslinked syMagIcS resulted in binding to TOM20::mCherry:: α GFPnb only in the vicinity of the microinjection site. This result confirmed fast and highly specific *in situ* conjugation of syMagIcS with target proteins (Fig. 8.16). Microinjection was repeated at different positions resulting in a very homogeneous co-localization of mEGFP (syMagIcS) and mCherry (TOM20) fluorescence. These results demonstrate the suitability of mEGFP-functionalized syMagIcS as an intracellular targeting system.

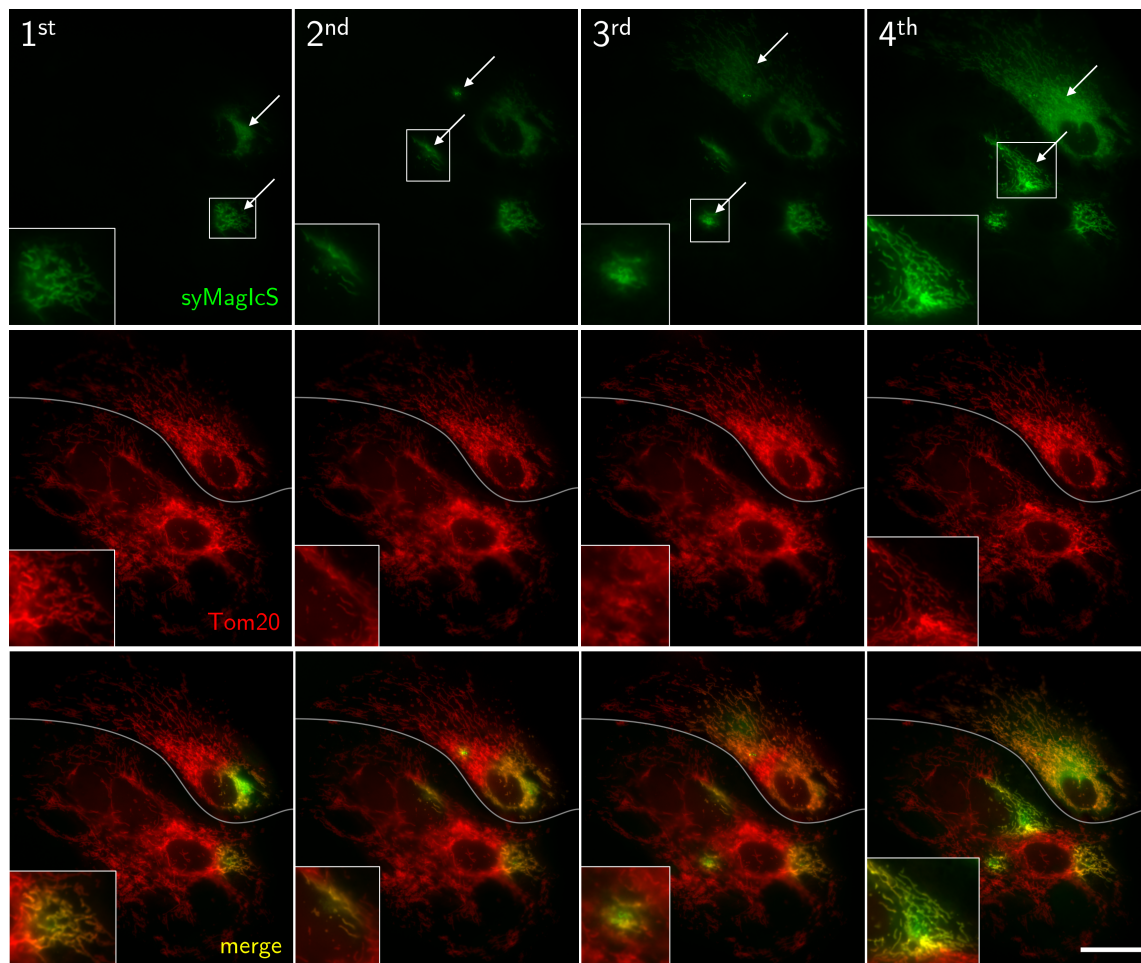


Figure 8.16.: **Site-specific targeting to mitochondria.** Rapid site-specific targeting of PFA-crosslinked syMagIcS (green) upon repeated microinjection into HeLa cell transiently overexpressing TOM20::mCherry:: α GFPnb (red). Scale bar: 30 μ m.

To demonstrate spatial control of proteins in a cellular cytosol, HeLa cells were transiently transfected with α GFPnb fused with mCherry (mCherry:: α GFPnb). After microinjection of syMagIcS, a magnetic field gradient was periodically applied by placing a magnetic tip at a distance of $\sim 30 \mu$ m from the plasma membrane. A rapid, reversible accumulation of mCherry:: α GFPnb was observed (Fig. 8.17A and Supplementary Movie S4). Evaluation of the attraction time constant (τ_A) and relaxation time constant (τ_R) revealed fast magnetic remote control with $\tau_A = (1.7 \pm 0.2) \text{ s}$ and $\tau_R = (1.5 \pm 0.1) \text{ s}$ (Fig. 8.17B+C). The increased relaxation time constants observed in the presence of mCherry:: α GFPnb can be explained by the increased hydrodynamic diameter due to the proteins bound to the syMagIcS surface. These results demonstrate a very robust, reversible, and rapid spatial control of proteins in the cytosol using syMagIcS.

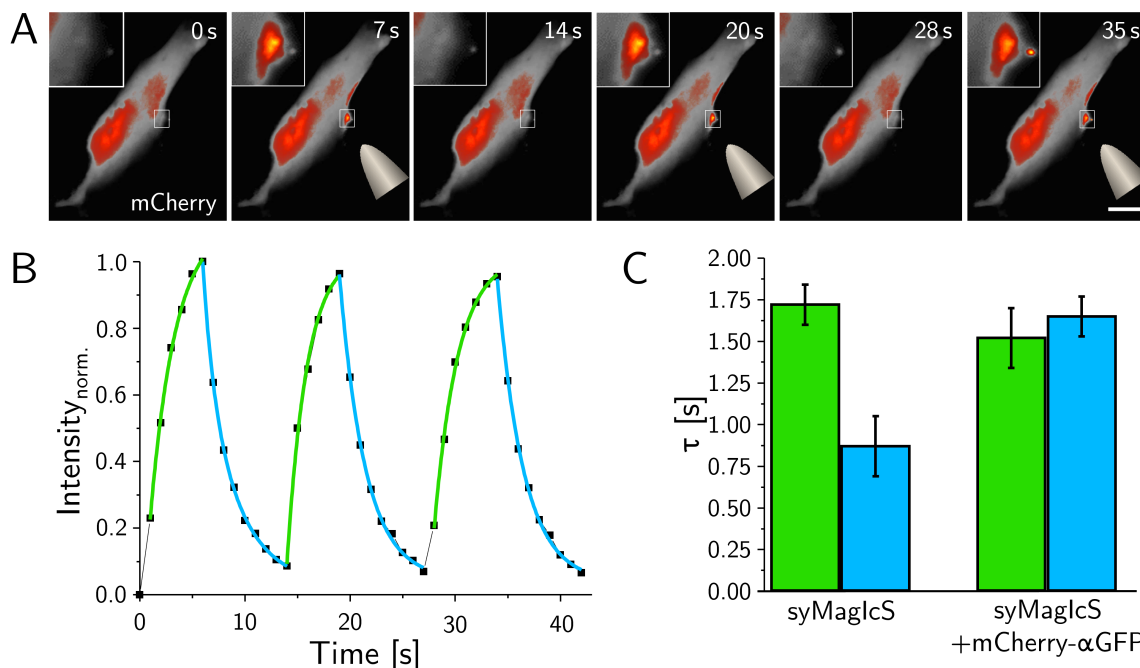


Figure 8.17.: **Spatial control of intracellular proteins.** syMagIcS was injected into HeLa cells expressing mCherry:: α GFPnb and repeatedly attracted and released with a micro-magnet positioned at a $\sim 30 \mu\text{m}$ distance to the plasma membrane. Only mCherry fluorescence is shown to demonstrate magnetic manipulation of a cytosolic protein. Scale bar: $30 \mu\text{m}$. (B) Attraction and release kinetics of mCherry-functionalized syMagIcS determined from the changes in fluorescence intensity in the area highlighted by the white square. Time constants were determined by fitting an exponential curve (green, cyan). (C) Comparison of the manipulation time constants of attraction and release observed for syMagIcS in the absence and presence of mCherry:: α GFPnb.

In conclusion, the surface coating of synthetic maghemite core nanoparticles with green fluorescent protein based on the iron binding site of Mms6 provided MNPs with intracellular stealth properties (syMagIcS) that could be readily biofunctionalized *in situ* and translocated within cells via magnetic field gradients.

Dense coating of MCPs was demonstrated *in vitro* using TEM images and estimation of functionalization stoichiometry by denaturing SDS-PAGE. The hydrodynamic radius and ζ potential of syMagIcS were determined. Intracellular application exhibited free dispersion of syMagIcS in the cytosol over the observation period; neither particle clustering nor nonspecific interactions with the intracellular environment were observed. Combined with the intracellular magnetic response, as a control whether the coating protein is still bound to the core, this demonstrates intracellular stability and obtaining intracellular stealth properties without the need for additional chemical surface modifications. In *in vitro* experiments using TIRFS-RIF and in intracellular experiments an ultrafast and highly specific conjugation with target proteins could be demonstrated. Both, MagIcS alone and *in-situ* conjugated with target proteins, showed rapid and reversible control in the cytosol by

magnetic forces. These results demonstrate a highly controllable relocalization of proteins in the cytosol using syMagIcS.

Furthermore, Chapter 10 demonstrates the control of biofunctionalization multivalency enabled by direct binding of individual coating proteins to the MCP surface. Various affinities of α GFPnb toward different GFP variants are utilized to selectively alter the degree of functionalization. In addition, by directly binding individual coating proteins to the MCP surface an extension of the versatility of functionalization is conceivable. The use of a mixture with different orthogonal targeting systems would allow site-specific binding of various proteins of interest to a single syMagIcS, or a combination of specific binding of a protein of interest and site-specific binding of this functionalized syMagIcS to a region of interest.

Demonstration of surface passivation to minimize toxicity and recognition by cellular degradation machineries, reversible magnetic response despite its small hydrodynamic radius and associated mobility in the cytosol, and biofunctionalization for selective and efficient *in situ* conjugation with target proteins reveal the suitability and potential of syMagIcS for magnetic manipulation in living cells.

Acknowledgements

Maghemite core particles were synthesized and characterized and DLS measurements were performed by Dr. Emilie Secret (PHENIX laboratory at Centre National de la Recherche Scientifique (CNRS) and Université Pierre et Marie Curie (UPMC), Sorbonne University). Optimization of the purification protocol for the coating protein and transmission electron imaging was performed by Annette Budke-Giesecking. ζ potential measurements and interaction analysis by TIRFS-RIf detection were done by Dr. Julia Flesch. Stability of syMagIcS under different conditions was tested by Hannah Klein as part of her bachelor thesis. Analytical size-exclusion chromatography, experiments on the *in cellulo* stability of the syMagIcS and the fast response to the application of a magnetic field gradient of syMagIcS and protein-biofunctionalized syMagIcS was performed by Dr. Domenik Liße. Dr. Dennis Meyer (University of Göttingen) contributed to the engineering of the magnetic device based on the Halbach Array. Fabrication of the 3D printed tray was done with the help of Dr. Felix Lager of the ultrafast physics research group led by Prof. Dr. Mirco Imlau at University of Osnabrück.

9 | Magnetic remote activation of small GTPase Rac1 using syMagIcS

To demonstrate the suitability and strength of the developed biofunctionalization of MCPs and the concept of magnetic space mode remote activation of biological processes using syMagIcS, the small GTPase Rac1 from the Rho family was chosen as another model system. Rho family GTPases regulate and coordinate cytoskeleton remodeling,^{409,410} where Rac1 is mainly involved in the formation of lamellipodia and membrane ruffling.^{203,204} This Rac1-induced actin remodeling provides a favorable readout of whether magnetic remote activation results in downstream signaling. The morphological changes can be observed using Lifeact, a peptide for staining filamentous actin (F-actin).⁴¹¹

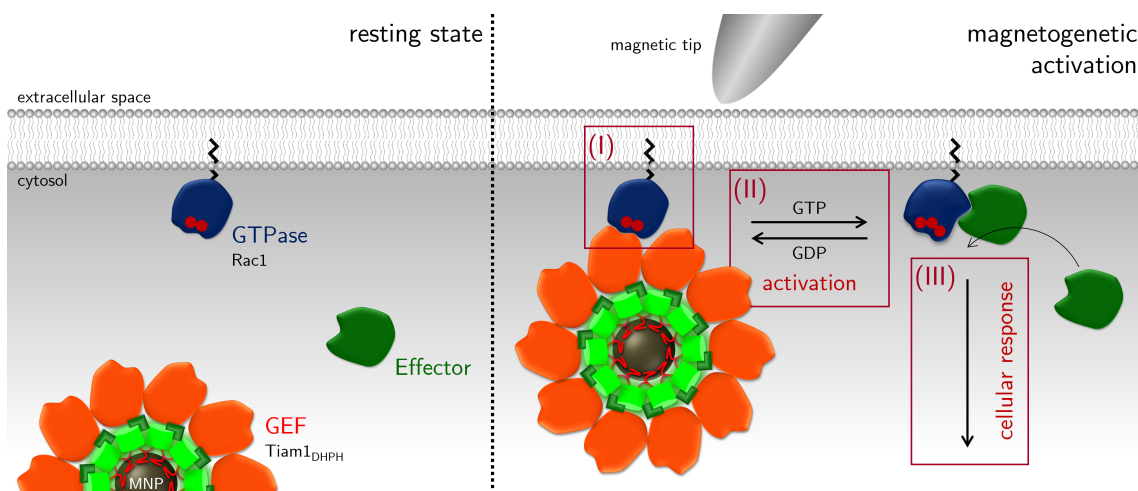


Figure 9.1.: **Magnetic remote activation of Rac1.** Schematic illustration depicting the strategy for magnetical control of Rac1: (left) Resting state. (right) Translocating the catalytic active region of the GEF protein Tiam1_{DHPH} captured to syMagIcS to the plasma membrane, interaction with Rac1-GDP (step I) promotes GDP-GTP exchange (step II). Rac1-GTP recruits the effector protein PAK to initiate downstream activity leading to formation of cell protrusions (step III).

Magnetically controlled activation of Rac1 was studied by translocating the catalytic region of guanine nucleotide exchange factor (GEF) Tiam1 to the plasma membrane via magnetic forces. The catalytic region of Tiam1, hereafter referred to as Tiam1_{DHPH}, comprises the DH and PH domains. Tiam1_{DHPH} lacks the ability of full-length Tiam1 to localize to the plasma membrane. This function is fulfilled by syMagIcS as a controllable nano signaling actuator. This allows magnetic remote control of site-specific, subcellular

localization and thus activity of Tiam1. The investigation of magnetic remote activation was performed in three steps: (I) interaction of GEF with small GTPase, (II) activation of small GTPase, and (III) downstream activity (Fig. 9.1).

9.1. *In cellulo* MNP-GEF activity

In the first step, it was probed whether Tiam1_{DHPH} is capable of interacting with the small GTPase Rac1 even when Tiam1_{DHPH} is immobilized to the surface of syMagIcS. To this end, the ability to recruit Rac1 to Tiam1_{DHPH} functionalized syMagIcS was investigated.

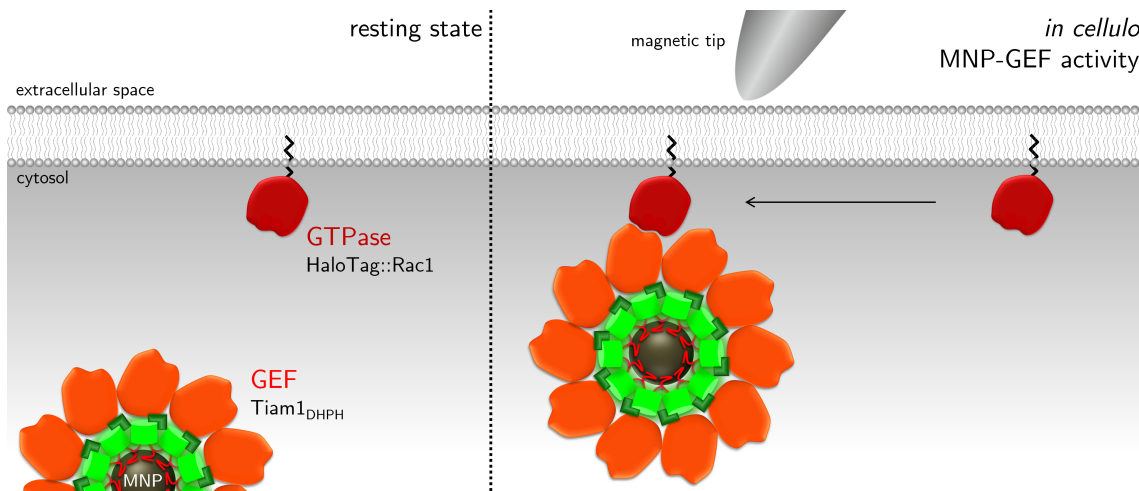


Figure 9.2.: **Schematic illustration of probing *in cellulo* MNP-GEF activity.** Recruitment of Rac1 by Tiam1_{DHPH}-functionalized syMagIcS translocated to the plasma membrane via magnetic forces.

To monitor Rac1 recruitment, Tiam1_{DHPH} fused to mCherry and α GFP (Tiam1_{DHPH}::mCherry:: α GFP) was expressed in COS7 cells along with Rac1 fused to HaloTag (HaloTag::Rac1). HaloTag::Rac1 was stained with far-red silicon rhodamine (SiR). By applying a magnetic field gradient, the *in situ* Tiam1_{DHPH} functionalized syMagIcS (Tiam1_{DHPH}-syMagIcS) were translocated to the plasma membrane. Recruitment of Rac1 to the Tiam1_{DHPH}-syMagIcS translocated to the plasma membrane was observed as the colocalization of green, orange and red fluorescence signals (Fig. 9.3 and Supplementary Movie S5). The Tiam1_{DHPH}-specific magnetically controlled Rac1 recruitment was robust and reproducible observed in 90% of the performed experiments. In control experiments without Tiam1_{DHPH} bound to syMagIcS, no Rac1 recruitment could be detected (Fig. 9.4).

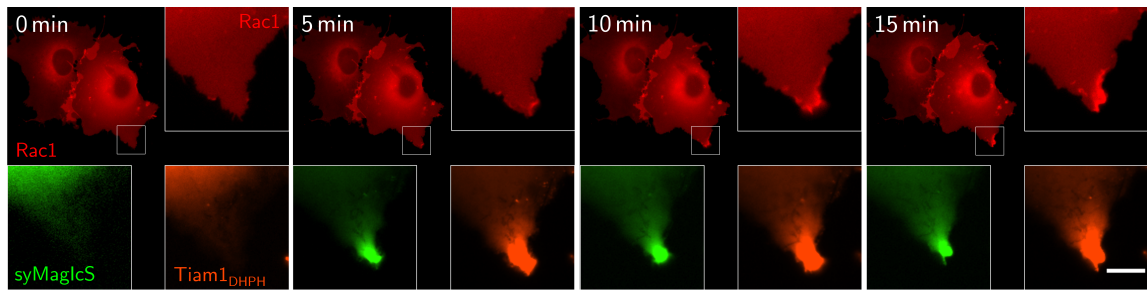


Figure 9.3.: **Recruitment of Rac1 by Tiam1_{DHPH}-functionalized syMagIcS translocated to the plasma membrane via magnetic forces.** syMagIcS (green) was injected into cells expressing HaloTag::Rac1 labeled with SiR (red) and Tiam1_{DHPH}::mCherry::αGFP (orange). Time-lapse imaging during magnetic manipulation showing Rac1 distribution in the entire cell and zoom into the zone enriched in syMagIcS for all three channels. Scale bar: 10 μm.

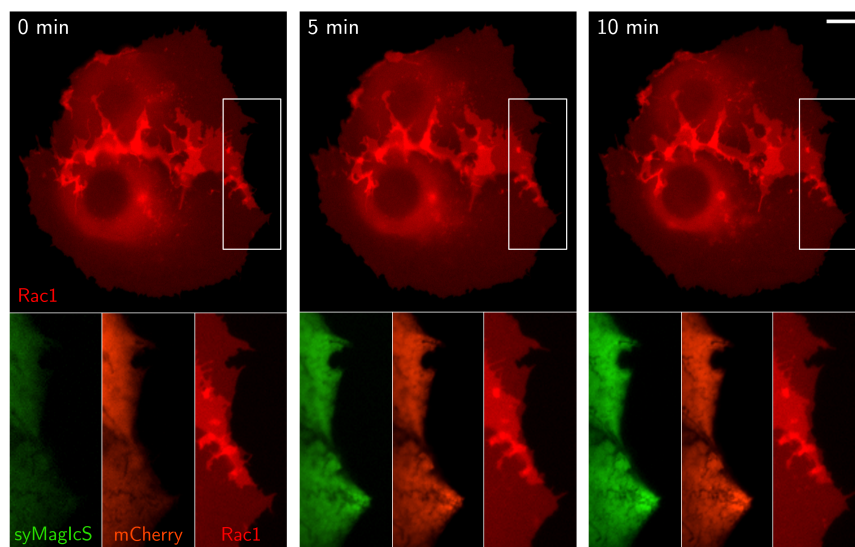


Figure 9.4.: **Negative control of Rac1 recruitment.** COS7 cell expressing SiR-labeled HaloTag::Rac1 (red) and αGFP::mCherry (orange) after injection of syMagIcS (green). Overview image (^{SIR}HaloTag::Rac1) and crop of syMagIcS (green), mCherry (orange) and Rac1 (red) at different time points during magnetic manipulation. Scale bar: 10 μm.

9.2. Magnetic remote activation of Rac1

Next, the signaling consequence of magnetic remote activation of the small GTPase Rac1 was explored, i.e. whether the interaction between Tiam1_{DHPH} results in an exchange of GDP for GTP and thus to the activation of Rac1. To this end, a fluorescent reporter protein consisting of the Rac1-binding domain CRIB of PAK (PAK-CRIB) fused to mNeonGreen and Rac1 fused to mTFP1 and the CAAX box was generated. The two parts were linked by the self-cleaving P2A peptide linker, which ensures equimolar protein production by proteolytic digestion (mNeonGreen::PAK-CRIB::P2A::Rac1::mTFP1::CAAX).⁴¹² The construct was produced by replacing the EV linker in the Raichu Rac1 biosensor with the P2A linker (see Chapter 7.3). In this way, studying the interaction between GEF and GTPase by monitoring Tiam1_{DHPH}-specific Rac1 recruitment (Rac1::mTFP1::CAAX), and small GTPase activation by monitoring effector recruitment (mNeonGreen::PAK-CRIB) can be obtained simultaneously. To avoid overlapping of the mEGFP fluorescence with mNeonGreen in the reporter, non-fluorescent H6::mXFP::Mms6ΔN (mEGFP Y67F) was used to coat the MCP for preparing the syMagIcS.

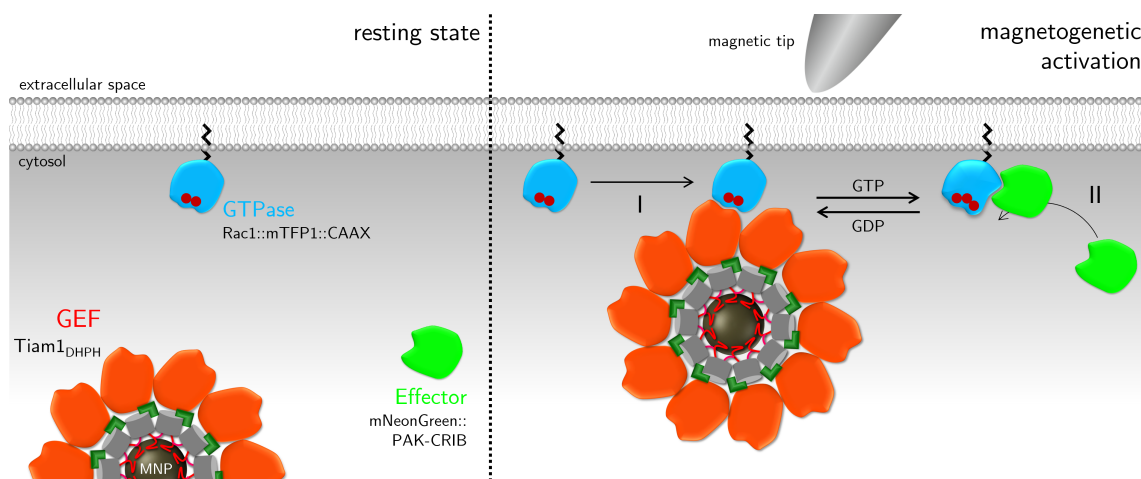


Figure 9.5.: **Probing magnetic remote activation of Rac1.** Schematic illustration of the strategy to study magnetically controlled activation of Rac1 using functionalized syMagIcS: (left) resting state. (right) Translocation of the syMagIcS-bound GEF protein Tiam1_{DHPH} to the plasma membrane using magnetic field gradients. Simultaneous investigation of the interaction of the GEF with the small GTPase through the recruitment of Rac1 (I) and whether this interaction leads to the activation of Rac1 into the GTP-bound state (II), observed by the interaction and recruitment of the Rac1-binding domain of the effector protein PAK (PAK-CRIB).

In COS7 cells, the reporter (mNeonGreen::PAK-CRIB::P2A::Rac1::mTFP1::CAAX) was co-expressed with Tiam1_{DHPH}::mCherry:: α GFP for *in situ* syMagIcS functionalization. After microinjection of mXFP::Mms6 Δ N-MagIcS, the Tiam1_{DHPH}-functionalized MagIcS (Tiam1_{DHPH}-syMagIcS in abbreviation) were assembled *in situ*. By placing a magnetic tip close to the cell, the Tiam1_{DHPH}-syMagIcS was translocated to the plasma membrane. Strikingly, simultaneous enrichment of Rac1 at the plasma membrane was observed, followed by local accumulation of PAK-CRIB in the cytosol (Fig. 9.6 and Supplementary Movie S6). In contrast, neither Rac1 nor PAK-CRIB recruitment was observed in control experiments lacking Tiam1_{DHPH} (Fig. 9.7). These results indicate successful specific subcellular magnetic remote activation of Rac1 by Tiam1_{DHPH}-functionalized syMagIcS.

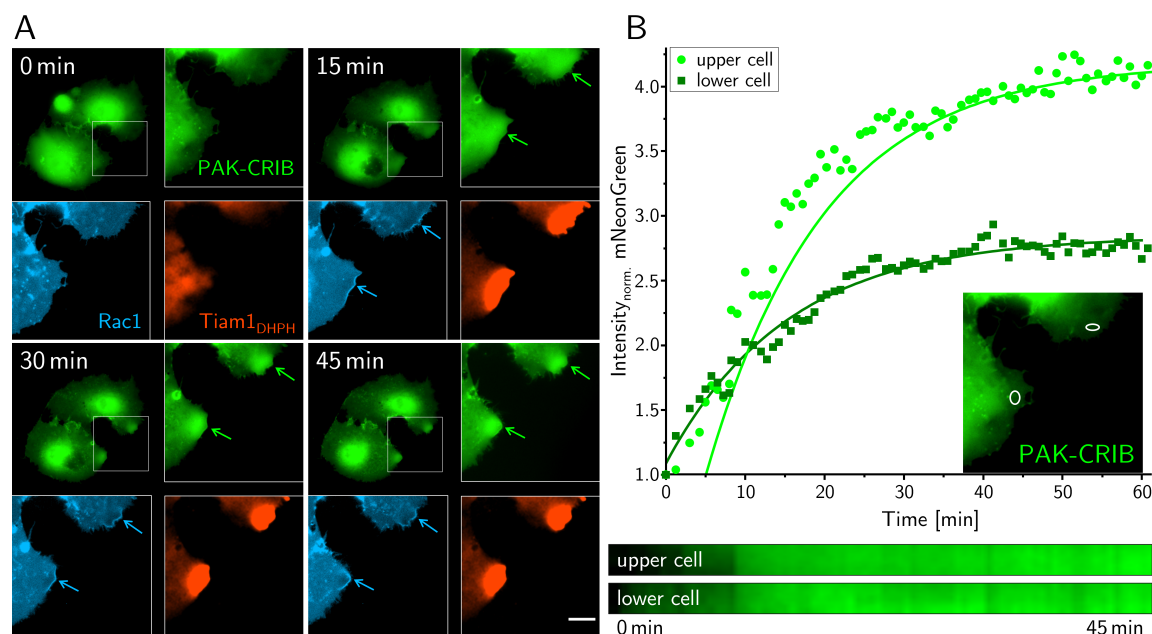


Figure 9.6.: **Magnetic remote activation of Rac1.** (A) Magnetically control of Rac1 GDP-GTP exchange detected by monitoring recruitment of PAK-CRIB: syMagIcS (non-fluorescent) was injected into cells expressing Tiam1_{DHPH}::mCherry:: α GFP (orange) and mNeonGreen::PAK-CRIB::P2A::Rac1::mTFP1::CAAX (green/cyan). Time-lapse imaging during magnetic manipulation showing PAK-CRIB distribution and zoom into the zone enriched in syMagIcS for all three channels. The kinetics of PAK-CRIB recruitment is shown by the intensity increase of mNeonGreen (top) and corresponding kymographs (bottom). (B) Kinetics of mNeonGreen::PAK-CRIB recruitment within the two white ROIs indicated in the inset and corresponding kymographs (bottom). Scale bar: 10 μ m in all images.

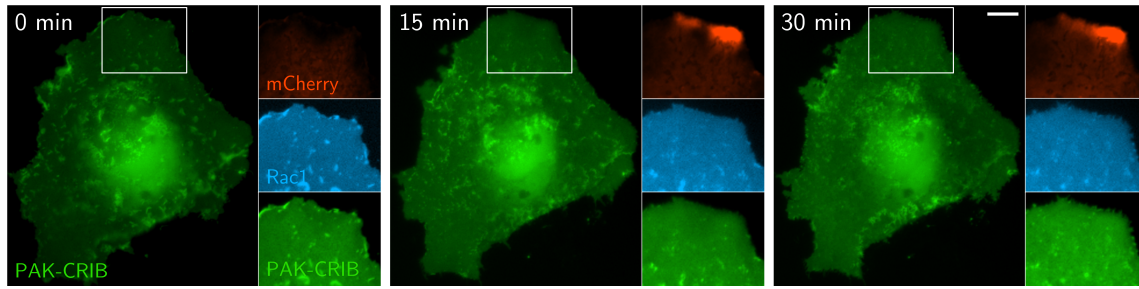


Figure 9.7.: **Negative control of magnetic remote Rac1 activation.** COS7 cell expressing α GFP::mCherry (orange) and mNeonGreen::PAK-CRIB::P2A::Rac1::mTFP1::CAAX Box (green/cyan) after injection of non-fluorescent syMagIcS. Overview image showing PAK and crop at the ROI indicated by a white rectangle for all three channels at different time points after initiating magnetic manipulation. Scale bar: 10 μ m.

9.3. Cellular response resulting upon magnetic remote activation of Rac1

In the final step, it was investigated whether our magnetic remote activation is sufficient to result in downstream activity. The downstream cellular responses of locally activated Rac1 was accessed by monitoring cell morphological changes. For this purpose, fluorescent mEGFP coated syMagIcS were microinjected into COS7 cells co-expressing Tiam1_{DHPH}::mCherry:: α GFP and Lifeact fused with iRFP (Lifeact::iRFP). Lifeact is a short peptide that binds to actin which reports the morphological changes of actin due to Rac1 signaling.

After *in situ* Tiam1_{DHPH}-functionalization, translocation of Tiam1_{DHPH}-syMagIcS to the plasma membrane was obtained by applying a magnetic gradient. Local enhancement of actin polymerization and protrusion formation was observed in COS7 cells with endogenous Rac1 (Fig. 9.8 and Supplementary Movie S7). Strikingly, a significant cellular response by Lamellipodia-like protrusion formation was observed only at low nanoparticle concentrations. No significant protrusion was observed at high particle concentrations, suggesting an autoinhibitory effect of Tiam1_{DHPH}-syMagIcS. These results indicate successful magnetic remote manipulation of the Rac1 signaling cascade.

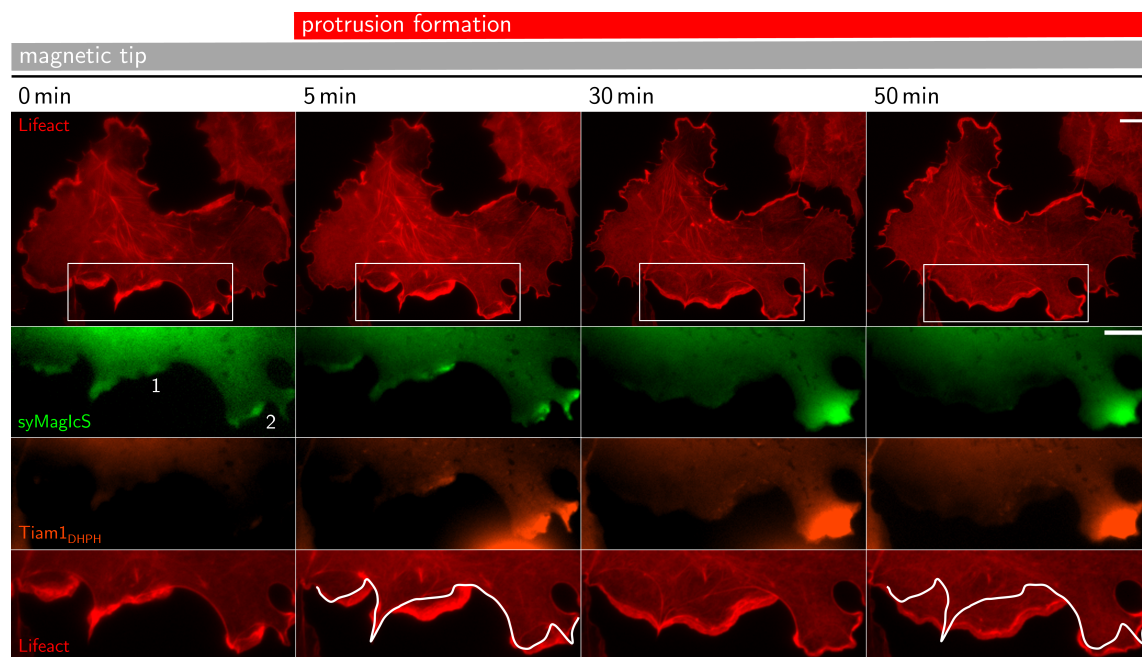


Figure 9.8.: **Downstream activity after magnetic remote activation of endogenous Rac1.** Magnetic syMagIcS (green) was injected into cells expressing Tiam1_{DHPH}::mCherry:: α GFP (orange) and Lifeact::iRFP (red, overview and crop) for staining f-actin. Time-lapse imaging during magnetic manipulation showing the actin cytoskeletal structure in regions with low (1) and high (2) syMagIcS densities. Scale bar: 10 μ m.

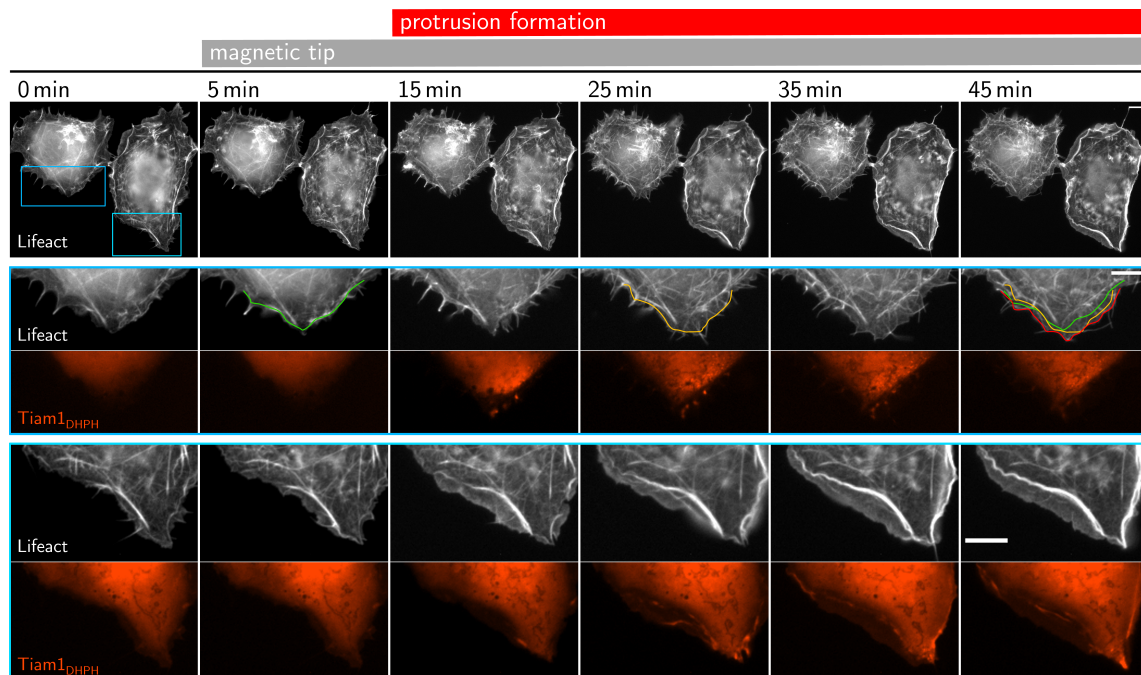


Figure 9.9.: **Downstream activity after magnetic remote activation of Rac1.** Magnetic remote activation of Rac1 downstream signal responses by monitoring protrusion formation (step III): syMagIcS was injected into cells expressing Tiam1_{DHPH}::mCherry:: α GFP (orange) and Lifeact::iRFP (white) for staining f-actin. Time-lapse imaging during magnetic manipulation showing the actin cytoskeletal structure. Zoom into the zone enriched in Tiam1_{DHPH} for both cells (light blue rectangles). Scale bar: 10 μ m in all images.

To confirm that the observed morphological change was magnetic remote activation-specific, the cells were monitored before the application of the magnetic gradient (Fig. 9.9 and Supplementary Movie S8). In these cases, Rac1 was co-expressed (HaloTag::Rac1). However, due to the limitation of fluorescence channels, Rac1 expression could not be labeled for fluorescent visualization. The results showed that no protrusion formation was observed over the 45 min observation period without a magnetic field gradient. Only upon application of a magnetic field gradient, significant formation of protrusions was observed in the upper cell on a time scale of a few minutes, starting with the formation of filopodia, followed by lamellipodia. The second cell, upon application of the magnetic field gradient, shows a long lamellipodia-like edge with strong membrane ruffling. These results thus confirm site-specific, magnetic remote activation of downstream cellular responses of a locally activated Rac1 signaling triggered by syMagIcS at a subcellular level. The formation of filopodia is a strong hint for activation of the Rho GTPase Cdc42. Compared to optogenetic activation of Rac1, the cellular responses of magnetic remote activation using syMagIcS is weaker.¹⁴⁵ The reasons could be the assembly of a dense cloud of multivalently functionalized syMagIcS at the plasma membrane. The dense enrichment of syMagIcS could have created a physical barrier that sterically hinders the diffusion of effectors and further downstream molecules to and from the plasma membrane. This assumption is supported by

the observation that low nanoparticle concentration results in larger morphological change (Fig. 9.8).

In conclusion, the potential of syMagIcS for magnetic remote manipulation of the small GTPase has been demonstrated. This remote control was successfully demonstrated at different levels, the recruitment of the small GTPase Rac1, its activation as well as resulting cellular response, in the form of morphological changes.

10 | Magnetic Remote Manipulation of LLPS to activate Wnt signaling pathway

Recently, liquid-liquid phase separation (LLPS) has emerged as a key principle in the spatiotemporal organization of basic cellular functions such as transcription and translation, cell division, and signal transduction.^{371,413,413,413–416} Furthermore, LLPS has been shown to be involved in several pathophysiological processes of complex diseases such as cancer and neurodegeneration.^{88,104,417}

To undergo phase separation, the system must exceed the saturation concentration (c_{sat}) (see Chapter 1.1.2, Fig. 1.3). syMagIcS enable to increase and control the local protein concentration at different levels: (I) Increase of local concentration by multivalent functionalization. (II) Interaction of functionalized syMagIcS by magnetization. (III) Site-specific concentration increase by spatial manipulation of the functionalized syMagIcS through magnetic field gradients. This, in addition to inducing LLPS, enables precise subcellular localization of LLPS to control site-specific biological processes.

To demonstrate the potential of the magnetic remote manipulation approach for basic biological research testing hypotheses of activation and thus gaining detailed understanding of signaling pathways, the Wnt signaling pathway was chosen as a model system. As described previously (see Chapter 6), the mechanism of the canonical Wnt signaling pathway is thought to be initiated by the formation of signalosomes, after stimulation with the Wnt ligand.^{364,369} This is characterized by the LLPS of Dvl2 with co-phase separation of Axin, and the recruitment of additional components of the destruction complex (GSK3, APC). Removal of these components resolves the destruction complex, stopping proteasomal degradation of β -catenin. This allows translocation of β -catenin and translation of Wnt responsive genes.³⁶⁰ To test the hypothesis whether Dvl2 phase separation at the plasma membrane is sufficient for the assembly of a functional signalosome and results in the activation of the Wnt signaling pathway, it is to be demonstrated that the concept of magnetic remote manipulation is suitable to induce site-specific Dvl2 LLPS in a controlled manner. Furthermore, induction of Dvl2-LLPS at different subcellular locations enables investigation of whether plasma membrane contact of Dvl2-LLPS is required for initiation of the Wnt signaling pathway, or whether LLPS also leads to initiation independently of the plasma membrane

and thus independently of membrane receptors. The concept is depicted in Figure 10.1: (I) Microinjection of syMagIcS into cells expressing Dvl2 fusion protein leads to (II) *in cellulo* self-assembly of Dvl2-functionalized syMagIcS. (III) Upon application of a magnetic field gradient, there is a local increase in concentration of Dvl2 due to enhanced interaction of magnetized syMagIcS and spatial translocation and therefore local enrichment. Here, we investigated whether this leads to an induction of Dvl2 liquid-liquid phase separation and whether it is feasible to specifically target these liquid droplets to the plasma membrane.

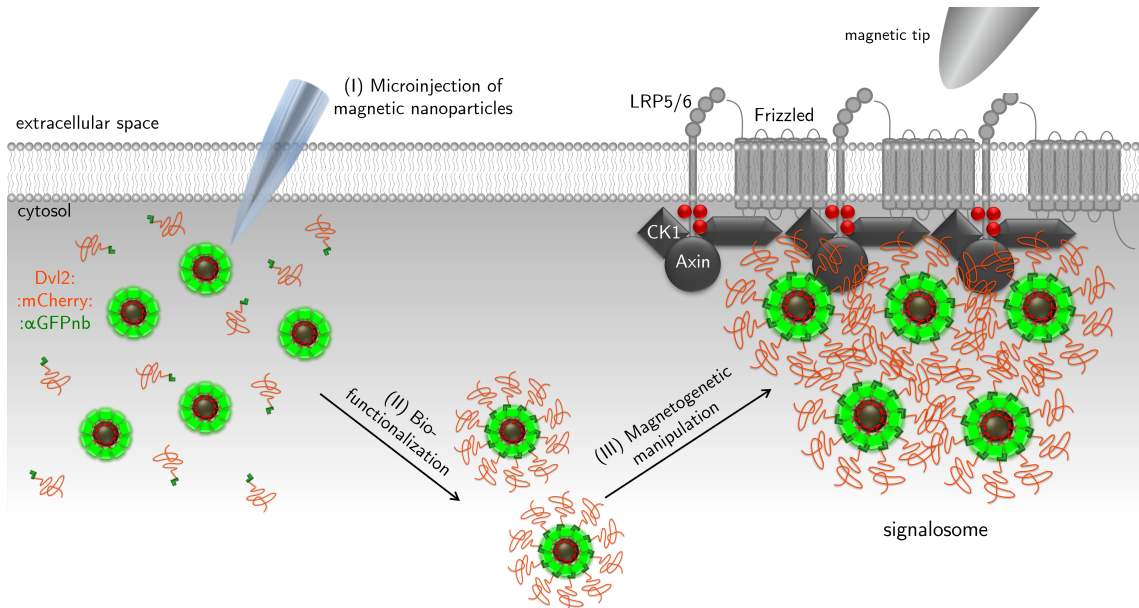


Figure 10.1.: **Schematic representation of the concept of magnetically controlled induction of Dvl2 LLPS.** (I) Microinjection of syMagIcS into cells containing a fusion protein consisting of Dvl2, the fluorescent protein mCherry for visualization, and α GFPnb for site-specific MNP functionalization. (II) Self-assembly of the Dvl2-functionalized syMagIcS. (III) Applying a magnetic field gradient results in translocation and therefore in locally increased concentration. This local concentration increase should lead to induction of Dvl2 LLPS. Thus, the suitability of the toolkit to test the hypothesis whether Dvl2 phase separation at the plasma membrane is sufficient for the assembly of a functional signalosome and results in the activation of the Wnt signaling pathway is to be demonstrated.

To obtain proof of concept, in the first step, DVL2 LLPS induced by increased intracellular protein concentrations was characterized and LLPS behavior was examined. The influence of the fused fluorescent protein and resulting additional interactions were also examined. Subsequently, the spontaneous LLPS behavior by functionalized syMagIcS with different multivalency was investigated and the multivalency was titrated to prevent spontaneous phase separation. This is a fundamental requirement for the subsequent controlled magnetic remote manipulation of LLPS using magnetic forces. In the final step, magnetically controlled induction of Dvl2 LLPS was probed and co-phase separation of Axin1 was inves-

tigated. Magnetical control of the concentration increase and resulting LLPS was achieved in two ways: (I) By the interaction of functionalized syMagIcS through magnetization. (II) By the spatial control of the functionalized syMagIcS through a magnetic field gradient.

10.1. Characterization of Dvl2 liquid-liquid phase separation

Preliminary results showed that transient transfection of Dvl2 fused with mCherry and α GFPnb (Dvl2::mCherry:: α GFPnb) in HeLa cells resulted in spontaneous phase separation (Fig 10.2 middle). The formation of spherical protein droplets depended on the protein expression level. mCherry is used for visualization and the α GFPnb is used for *in cellulo* site-specific functionalization on syMagIcS. It is known that mCherry has an intrinsic affinity to form trimers. To assess the effect due to additional interactions by the fluorescent protein, different Dvl2 fusion constructs including tandem-mCherry (Dvl2::tdm-mCherry:: α GFPnb) and a monomeric dsRed variant (dsRed.M1, Dvl2::dsRed:: α GFPnb) were designed. The tandem mCherry was engineered to avoid oligomerization due to strong self-dimerization of two closely linked mCherry. dsRed is known to form tetramers. The effects of additional interaction by fluorescence proteins to DVL2 LLPS were examined by epifluorescence microscopy (Fig. 10.2). Compared to the cells expressing Dvl2::mCherry:: α GFPnb, a significantly lower proportion of HeLa cells expressing Dvl2::tdm-mCherry:: α GFPnb showed LLPS. Only cells with extremely high expression levels had LLPS and the shape of protein condensate was dominated by small droplets. On the contrary, for cells expressing Dvl2::dsRed:: α GFPnb, LLPS was observed in a much higher proportion. In particular, the protein condensates due to LLPS showed highly expanded sizes with irregular geometry instead of spheres (Fig. 10.2). Based on the results, the tendency of LLPS for Dvl2 fusions is Dvl2::tdm-mCherry:: α GFPnb < Dvl2::mCherry:: α GFPnb < Dvl2::dsRed:: α GFPnb. The tendency correlated very well with the intrinsic affinity of protein interaction within the fluorescence proteins. These observations were reproducible, but an influence by different expression levels cannot be excluded without knowledge about intracellular concentrations. In the following, an attempt was made to substantiate this first subjective impression by quantifying and characterizing the LLPS.

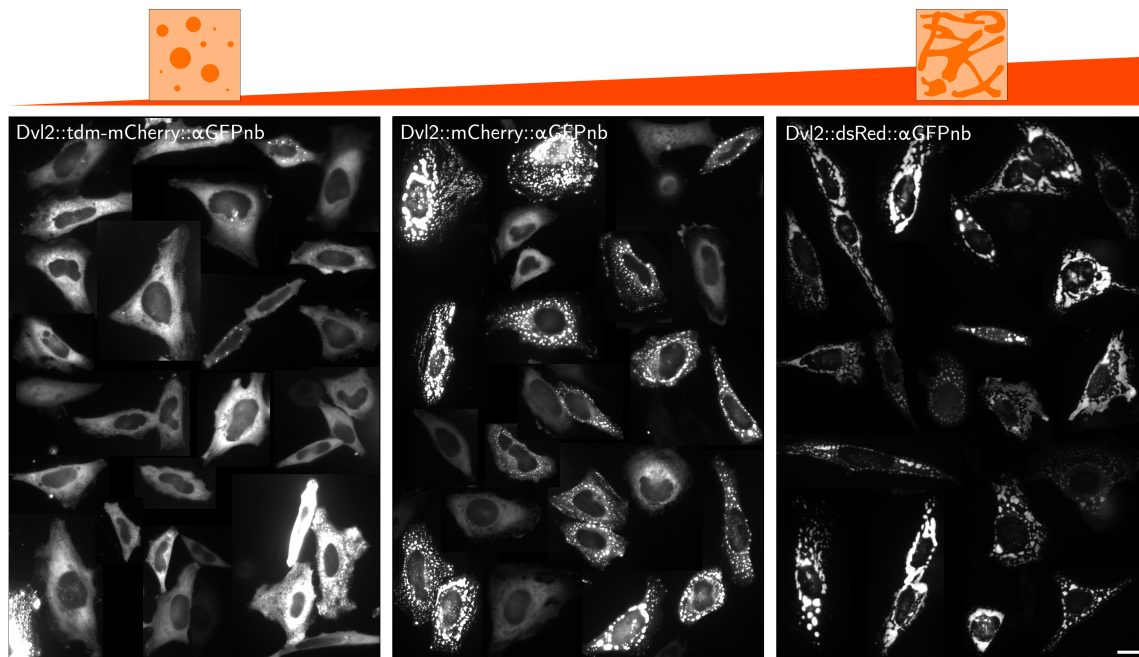


Figure 10.2.: **Comparison of the different Dvl2::FP::αGFPnb constructs.** HeLa cells were transiently transfected with Dvl2::tdm-mCherry::αGFPnb, Dvl2::mCherry::αGFPnb or Dvl2::dsRed::αGFPnb. Scale bar: 20 μm.

10.1.1. Dvl2 concentrations inside liquid droplets

To quantify the influence of the additional interaction by the fluorescent proteins, the environmental concentration and the droplet concentration were determined (Fig. 10.3A). For this purpose, HeLa cells were transfected with the three fusion constructs and the fluorescence intensity was determined using confocal laser scanning microscopy (cLSM). Calibration curves to correlate the fluorescent intensity with concentrations were obtained by using purified fluorescent proteins, i.e. mCherry, tandem mCherry and dsRed in solution.

Mean values of environmental concentration showed similarly low values ($c_{E,tdm-mCherry} = 28 \mu\text{M}$, $c_{E,mCherry} = 14 \mu\text{M}$, $c_{E,dsRed} = 12 \mu\text{M}$), whereas the resulting droplet concentrations showed a trend. The highest mean concentration was determined for tdm-mCherry ($c_{D,tdm-mCherry} = 267 \mu\text{M}$), followed by mCherry ($c_{D,mCherry} = 188 \mu\text{M}$), and dsRed ($c_{D,dsRed} = 158 \mu\text{M}$) (Fig. 10.3B). This result contradicts the expectations that the additional interactions should lead to a denser packing. This could be explained due to the additional interactions by the fluorescent protein promoting phase separation already at lower concentrations and leading to an increase in the size instead of the density of the LLPS.

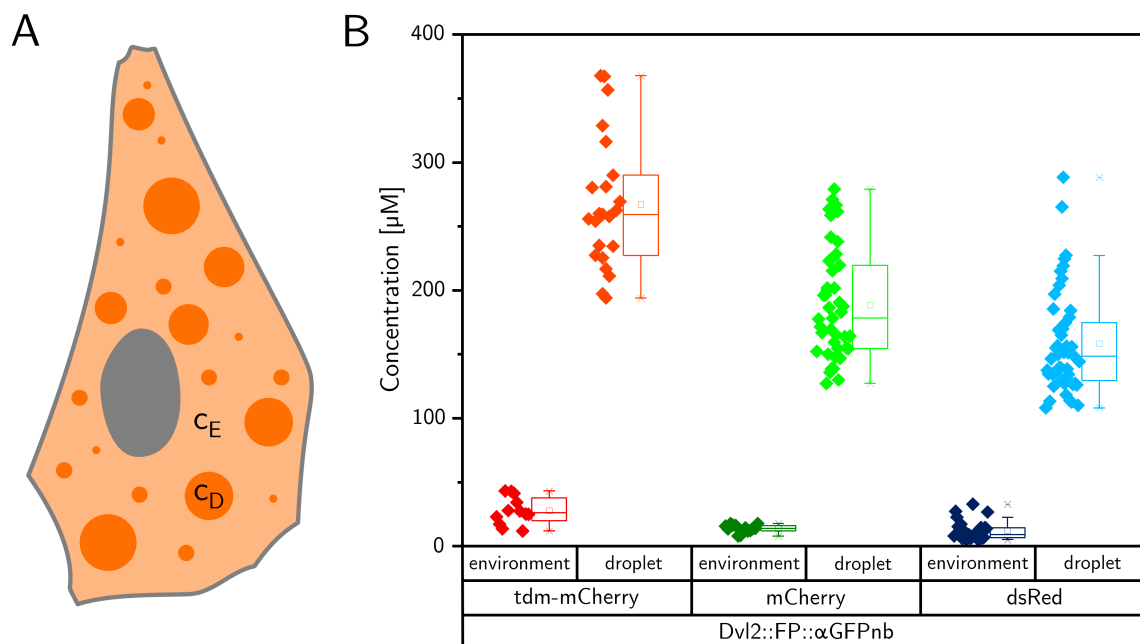


Figure 10.3.: **Quantification of environment and droplet concentration.** (A) Schematic illustration of LLPS in the cell with environmental concentration (c_E) and droplet concentration (c_D). (B) Comparison of the concentration inside and outside of the droplets for the three different fusion proteins consisting of Dvl2, the fluorescent protein (tdm-mCherry, mCherry, dsRed), and α GFPnb.

10.1.2. LLPS behavior of Dvl2 droplets

An important criterion for LLPS is the mobility between the light and dense phases. Therefore, to discriminate LLPS from protein aggregations, fluorescence recovery after photobleaching (FRAP) experiments were performed. Both, the entire droplet was bleached to investigate the mobility between the light and dense phases, and a subarea of the droplet was bleached to investigate internal mixing (Fig 10.4A). For this purpose, Dvl2::mCherry:: α GFPnb was transiently transfected into HeLa cells and FRAP measurements were performed at cLSM. Both the mobility between the light and dense phases and the mobility within the dense phase describe a comparable course (Fig 10.4B). Recovery after bleaching of the whole droplet showed a mean recovery of 69 % with a mean rate constant of $k_{\text{entire droplet}} = 0.029 \text{ s}^{-1}$, that of internal mixing 72 % with a mean rate constant of $k_{\text{internal mixing}} = 0.032 \text{ s}^{-1}$ (Fig 10.4C-D). Exemplary cells of a FRAP experiment of the entire droplet and a subarea are shown in Figure 10.4E-F. This demonstrates a similar behavior for the mobility between the environment and the droplet and internal mixing with a low proportion of immobile proteins.

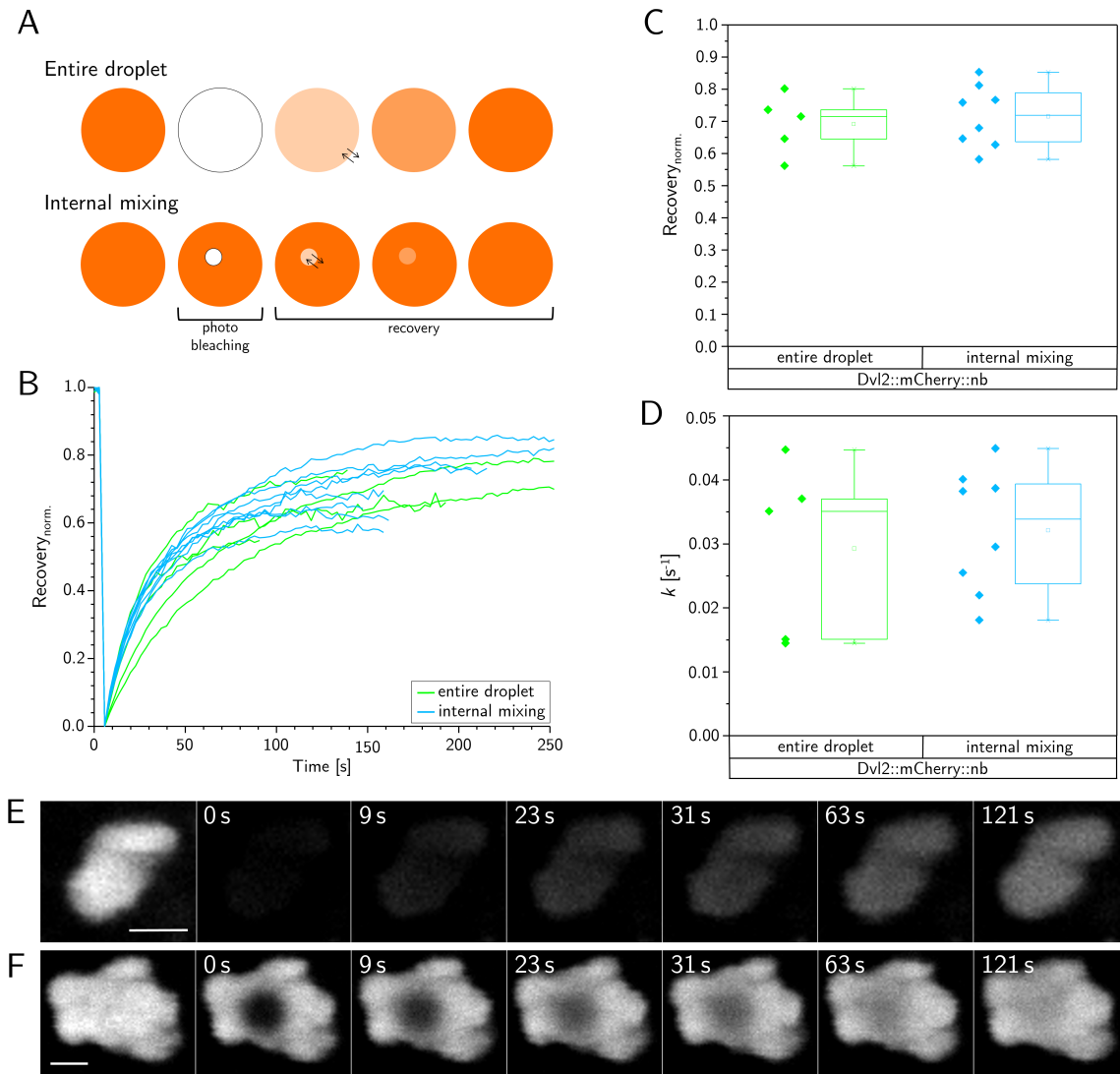


Figure 10.4.: **Fluorescence recovery after photobleaching (FRAP) to probe LLPS behavior.** (A) To investigate mobility between light and dense phase the entire droplet is bleached, to investigate internal mixing a subarea of the droplet is bleached. (B) Time course of the intensity. (C) Proportion recovery showing the proportion of mobile proteins. (D) Rate constants k of recovery. (E-F) Exemplary cell of a FRAP experiment of (E) entire droplet and (F) subarea. Scale bar: 2 μm in all images.

In the next step, the LLPS behavior and the influence of the fluorescent protein of the different Dvl2 fusion constructs were investigated using FRAP. In these experiments, the entire droplet was bleached to study the mobility between the environment and the droplet. For all Dvl2-FP constructs recovery could be observed (Fig. 10.5A), which confirms mobility and thus LLPS behavior. A mean recovery of 76 % was observed for Dvl2::tdm-mCherry:: αGFPnb , 59 % for Dvl2::mCherry:: αGFPnb , and 33 % for Dvl2::dsRed:: αGFPnb (Fig. 10.5B). This is in agreement with the higher additional interactions in dsRed, followed by mCherry and tdm-mCherry. Dvl2::dsRed:: αGFPnb showed the lowest recovery and thus the highest proportion of immobile proteins, while Dvl2::tdm-mCherry:: αGFPnb had the

lowest proportion of immobile proteins. The determined rate constants k did not show a clear trend (Fig. 10.5C). Moreover, a correlation with the concentration within the droplet and recovery was observed (Fig. 10.5A). The higher the concentration was, the lower the recovery was. This can be explained by the maturation of the droplets, which later change to a less mobile state.

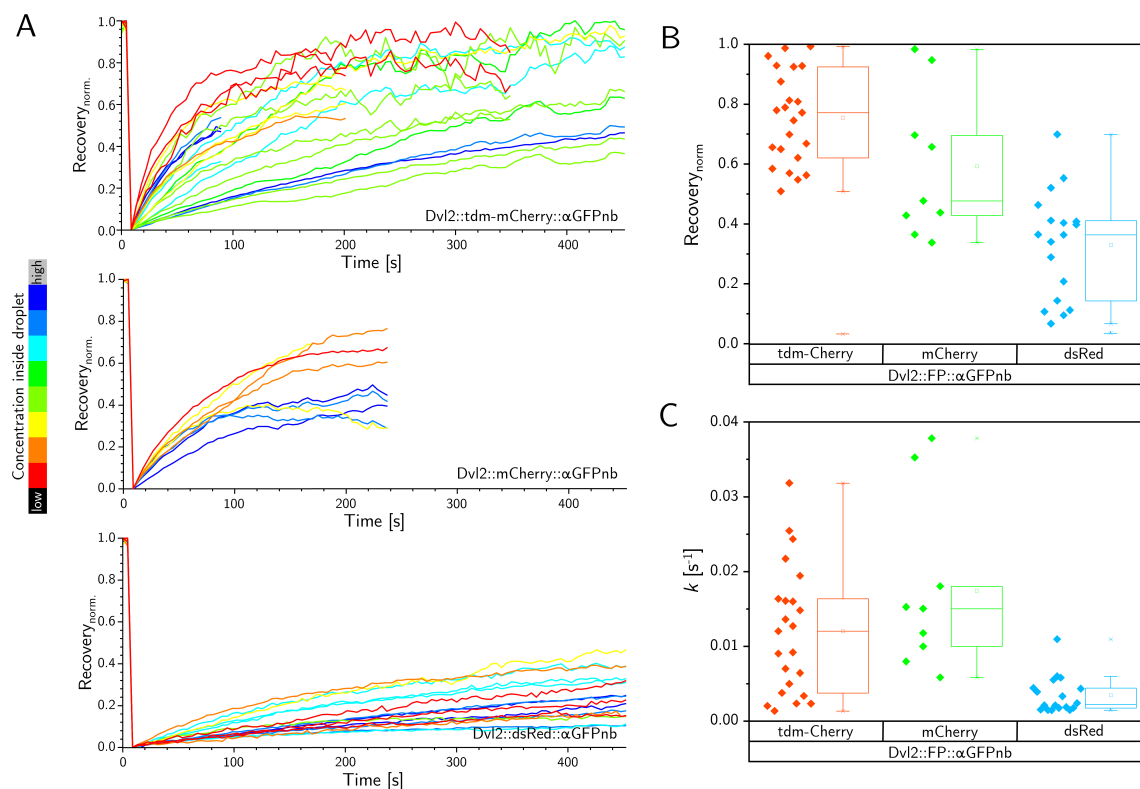


Figure 10.5.: **Investigation of LLPS behavior using FRAP for different DVL2-FP constructs.** (A) Time course of the intensity. The dependence on the droplet concentration is illustrated by color mapping. (B) Proportion recovery showing the proportion of mobile proteins. (C) Rate constants k of recovery.

Microscopic imaging observations of the Dvl2 droplets showed highly dynamic behavior. Fusion and splitting events could be observed, another important criterion for LLPS (Fig. 10.6). The dynamic behavior is particularly visible in Supplementary Movie S9, where the whole sequence is shown. In summary, the characterization confirms LLPS of Dvl2 droplets behavior.

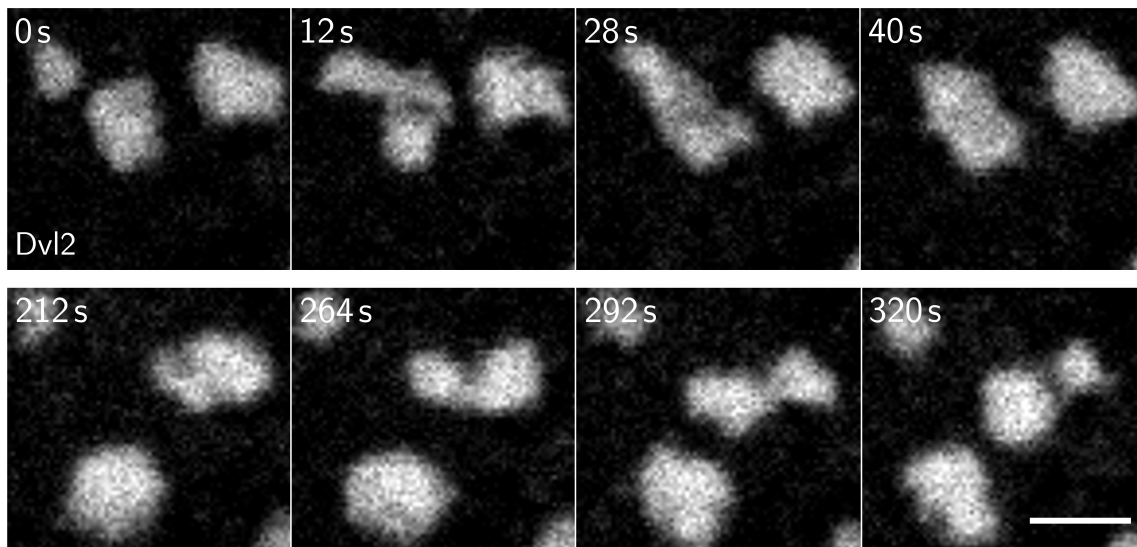


Figure 10.6.: **Dynamic behavior of Dvl2-LLPS.** (Upper row) Fusion event. (Bottom row) Splitting event. Scale bar: 3 μm .

10.1.3. Dvl LLPS dependent β -cat level

Next, it was examined whether phase separation of Dvl2 is linked to a higher cellular β -catenin level. An increased level may be indicative of an activated Wnt signaling pathway, as β -catenin is no longer degraded by the disruption of the destruction complex. To this end, HeLa cells were transiently transfected with Dvl2::mCherry:: α GFPnb or Dvl2::tdm-mCherry:: α GFPnb. The samples of the different Dvl2-FP constructs were not run at the same time, so the conditions may be different, and thus the results are not absolutely comparable. Subsequently, immunostaining of the transfected and wild-type HeLa cells was performed with an anti- β -catenin antibody (β -Catenin L54E2 Mouse mAb, Alexa Fluor 647 conjugate, Cell Signaling Technology). Consistent with expectations, a higher β -catenin level was detected in cells showing Dvl2 phase separation (Fig. 10.7). The mean measured intensity in HeLa cells transiently transfected with Dvl2::mCherry:: α GFPnb was without LLPS 378, with LLPS 578, in HeLa cells transiently transfected with Dvl2::tdm-mCherry:: α GFPnb without LLPS 464, with LLPS 689. This gives an indication that in cells with Dvl2 phase separation the Wnt signaling pathway is more active than in cells without phase separation. Without overexpression of Dvl2, a lower β -catenin level was detected.

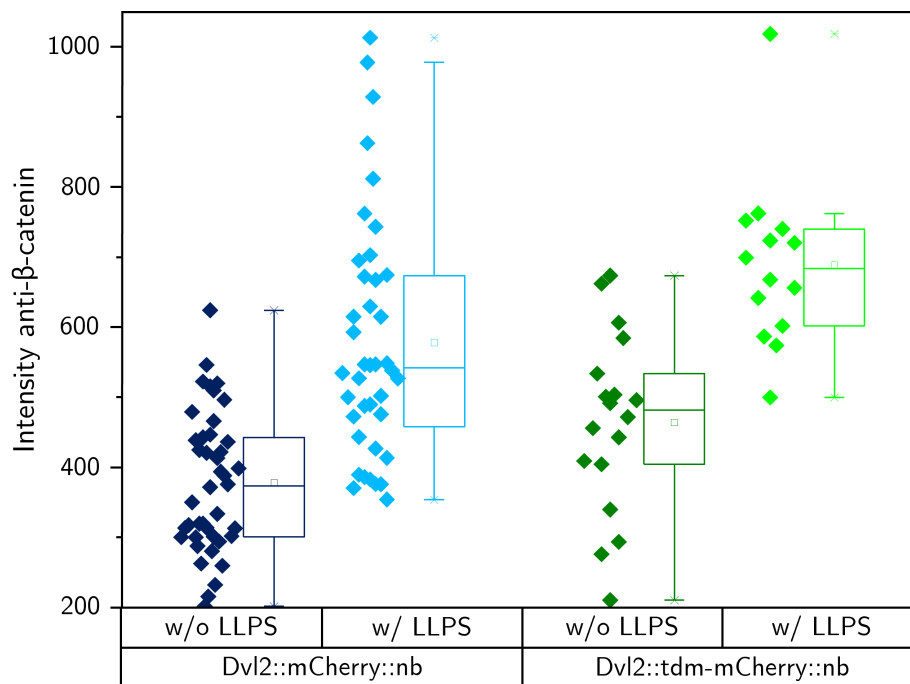


Figure 10.7.: **β -catenin immunostaining.** Examination of β -cat levels in cells with and without LLPS. Immunostaining was performed using Alexa Fluor 647 conjugated anti- β -catenin antibody.

10.2. Magnetic remote manipulation of Dvl2 liquid-liquid phase separation

After the characterization of the Dvl2 LLPS, syMagIcS were integrated. In the first step, the use of variously valent syMagIcS was investigated. For subsequent magnetic control of phase separation, it is important that multivalent binding at the particle surface, which increases the local concentration, is not sufficient to induce phase separation. Thereafter, LLPS behavior of induced Dvl2 droplets was investigated and finally proof-of-concept experiments on magnetic remote manipulation of Dvl2 LLPS were performed.

10.2.1. Titration of GFP binding affinities in order to prevent spontaneous phase separation

To prevent spontaneous phase separation due to multivalent binding on the particle surface, the valency was varied by using different GFP derivatives. The α GFPnb has varying affinities towards these derivatives (mEGFP $K_D = 0.3$ nM, mECFP (H164N) $K_D = 450$ nM, mECFPm (E142K H164N) $K_D > 10$ μ M). By using these GFP derivatives and mixtures of them, different degrees of Dvl2 functionalization can be achieved, and thus the local concentration can be varied. HeLa cells were transiently transfected with Dvl2::mCherry:: α GFPnb and MCP were coated with H6::mEGFP::Mms6 Δ N, H6::mECFP::Mms6 Δ N, H6::mECFPm::Mms6 Δ N or mixtures in various ratios.

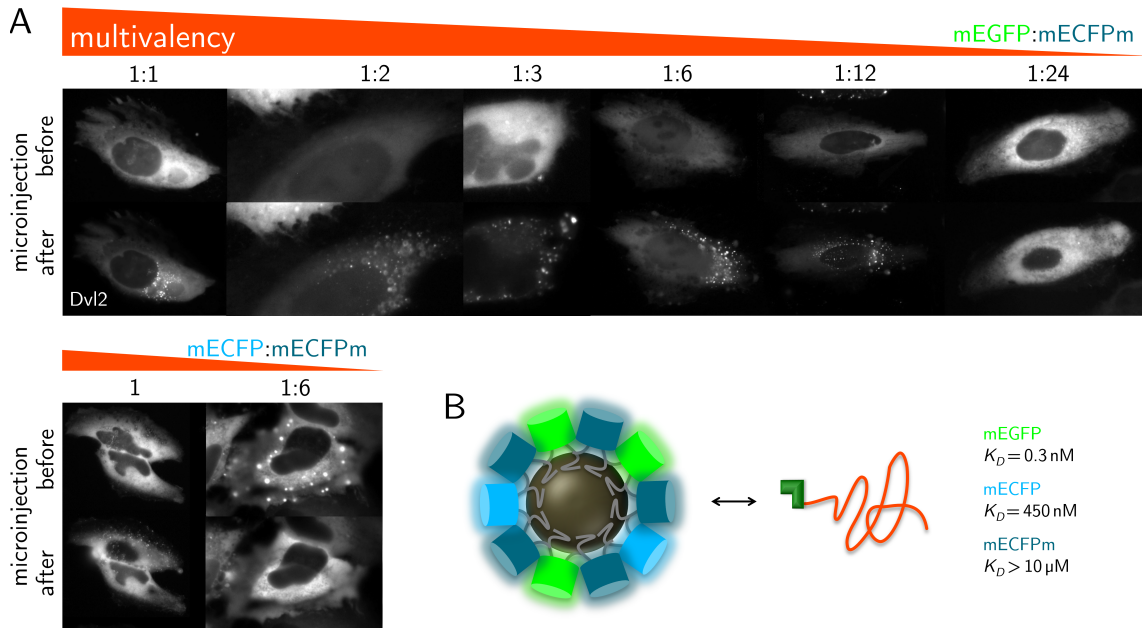


Figure 10.8.: **LLPS by multivalently functionalized syMagIcS.** (A) Spontaneous phase separation after microinjection of syMagIcS coated with different ratios of mEGFP and mECFP, and mECFPm in HeLa cells expressing Dvl2::mCherry::αGFPnb. (B) Schematic illustration of the interaction of the Dvl2-mCherry-αGFPnb fusion protein with coating proteins of syMagIcS.

Microinjection of high-valent functionalized syMagIcS (mixture of mEGFP and mCFPm coating protein, ratio 1:1 - 1:6) showed significant spontaneous phase separation starting from the injection site. With decreasing valency, a mixture of mEGFP and mCFPm coating protein, ratio 1:12 and mCFP coating protein, showed a decreasing trend of spontaneous phase separation (Fig. 10.8). Microinjection of syMagIcS coated with mEGFP and mCFPm coating protein, ratio 1:24 did not cause phase separation. In addition to the multivalency of the coating, spontaneous phase separation is also strongly dependent on other parameters, such as intracellular Dvl2 concentration and intracellular syMagIcS concentration, which is dependent on the volume and concentration of injected syMagIcS and the volume of the cell. These parameters can only be controlled to a limited extent, which makes it difficult to control the conditions for LLPS or the prevention of LLPS. Microinjection of syMagIcS with further reduced multivalency, mixture of mECFP and mCFPm coating protein, ratio 1:6, did not lead to phase separation in any of the observed cells. Injection into cells that had previously shown phase separation resulted in dissolving of the phase separation. This could be due to dilution by the additional volume injected and/or shear forces. This is supported by the control experiment on the volume/shear forces effect. For this purpose, HeLa cells were transiently transfected with Dvl2::mCherry::αGFPnb. In cells showing LLPS, HEPES buffer was microinjected. This resulted in dissolution of phase separation immediately after microinjection in all tested cells. Figure 10.9 demonstrates a specific dissolution of LLPS as a result of the increased volume and thereby decreased Dvl2 concentration around the microinjection site and/or applied shear forces. After a few minutes, the distribution of

concentrations within the cell resulted in recovery of phase separation. This reversible formation and dissolution of the structures also demonstrates LLPS behavior.

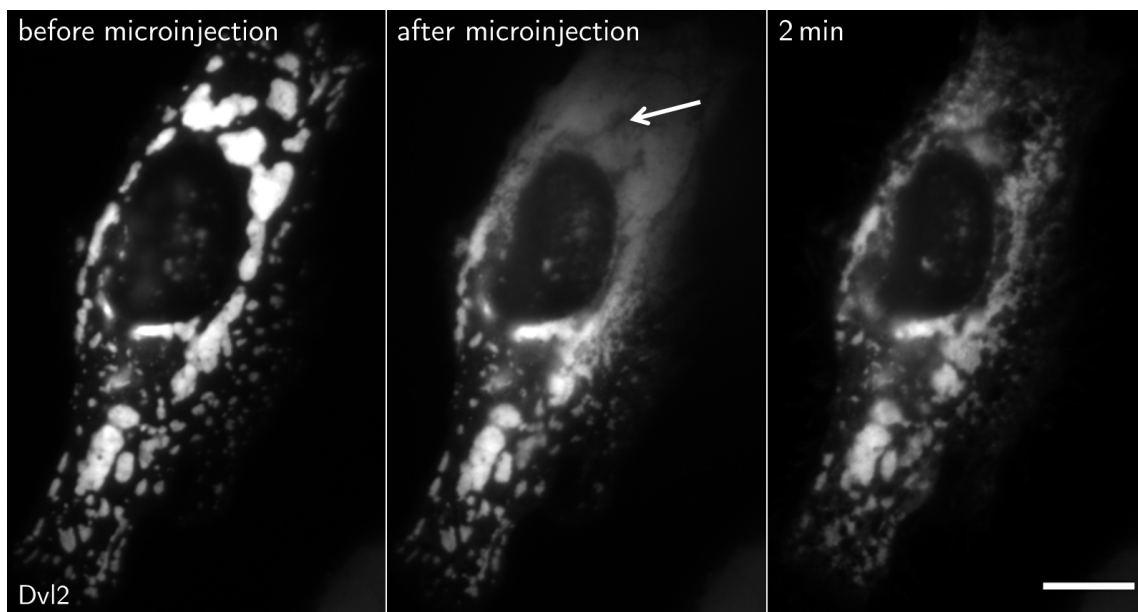


Figure 10.9.: **Control of volume effect and/or shear forces on LLPS and probing of LLPS behavior by dissolving Dvl2 phase separation.** Microinjection of HEPES buffer pH 7.5 into HeLa cell containing LLPS due to Dvl2::mCherry:: α GFPnb expression. The reduced Dvl2 concentration around the microinjection site (white arrow) and/or applied shear forces results in a reversible dissolution of LLPS. Scale bar: 20 μ m.

For magnetically controlled phase separation of Dvl2::mCherry:: α GFPnb, the mECFP coating protein was chosen in further experiments. Microinjection of the mCFP-coated syMagIcS resulted in low to no spontaneous phase separation, so the system appears to be at the border of phase separation and additional local concentration enhancement by magnetic remote manipulation may push the system over this border.

10.2.2. LLPS behavior of induced Dvl2 droplets

To further confirm the LLPS behavior indicated by the previously observed fusion of the droplets, the fluorescence recovery after photobleaching (FRAP) was investigated. This gives conclusions about the mobility of proteins between light and dense phases, a criterion for LLPS behavior.

HeLa cells were transiently transfected with Dvl2::mCherry:: α GFPnb and droplet formation was induced by microinjection of mEGFP-coated syMagIcS. The entire droplet was bleached to study the mobility between the environment and the droplet. Recovery was observed for the fluorescence of Dvl2::mCherry:: α GFPnb and that of syMagIcS (Fig 10.10A). The analysis showed a recovery for Dvl2::mCherry:: α GFPnb of 49%, and for syMagIcS of 61% (Fig 10.10B). This result is in good agreement with values previously obtained

for the system without syMagIcS (w/o syMagIcS, Dvl2::mCherry:: α GFPnb, Fig 10.5B) (Fig. 10.10B). This suggests that the use of syMagIcS and the binding of Dvl2 to the surface of the particles does not lead to a significant change in the fraction of immobile particles. The determined rate constants showed a faster recovery, for Dvl2::mCherry:: α GFPnb of $k_{Dvl2} = 0.04 \text{ s}^{-1}$, for syMagIcS of $k_{syMagIcS} = 0.067 \text{ s}^{-1}$, compared to LLPS without syMagIcS. These results confirm that both Dvl2::mCherry:: α GFPnb and the particles are mobile between the light and dense phases.

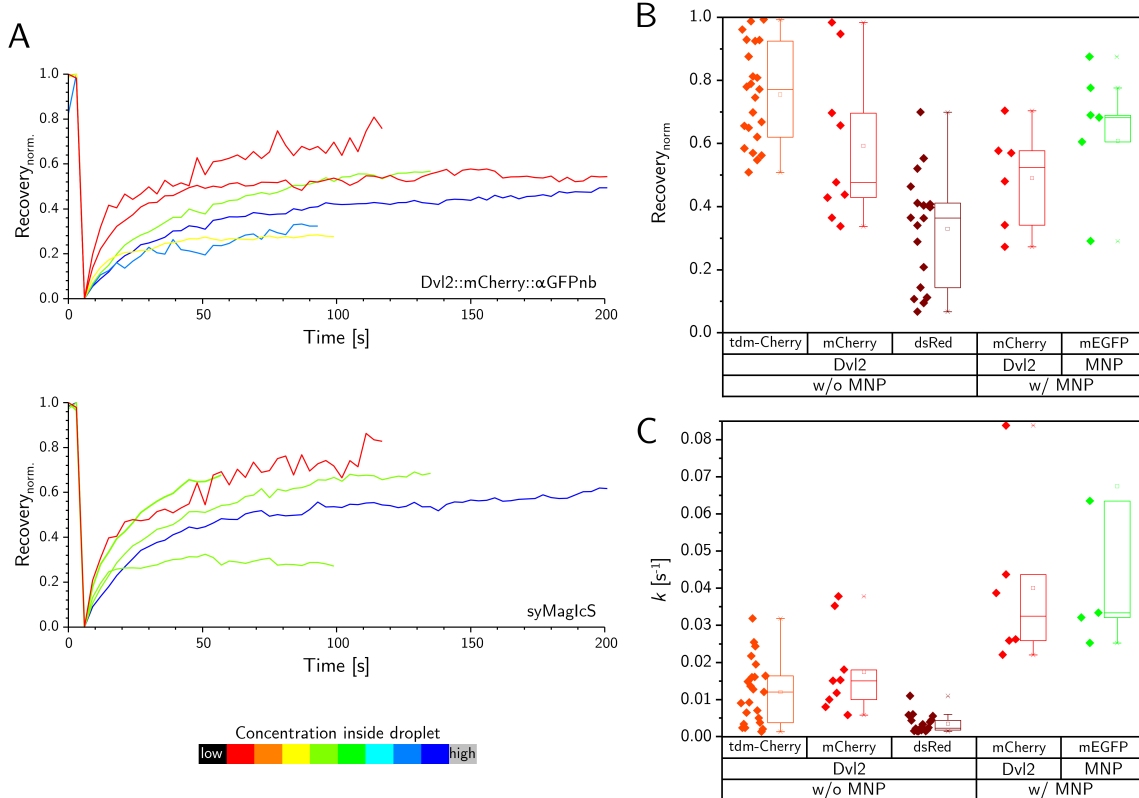


Figure 10.10.: **Investigation of LLPS behavior of induced LLPS using FRAP.** (A) Time course of the intensity. The dependence on the droplet concentration is illustrated by color mapping. (B) Proportion recovery showing the proportion of mobile proteins. (C) Rate constants k of recovery.

Fusion events could be observed for Dvl2 droplets containing MagIcS. In Figure 10.11 time series images of several consecutive fusion events in HeLa cell transiently transfected with Dvl2::mCherry:: α GFPnb are shown, after induction of LLPS by microinjection of mEGFP-coated MagIcS. The time offset between the two channels is due to the serial acquisition of the images. The entire sequence can be seen in Supplementary Movie S10. This demonstrates a highly dynamic behavior of the Dvl2 droplets.

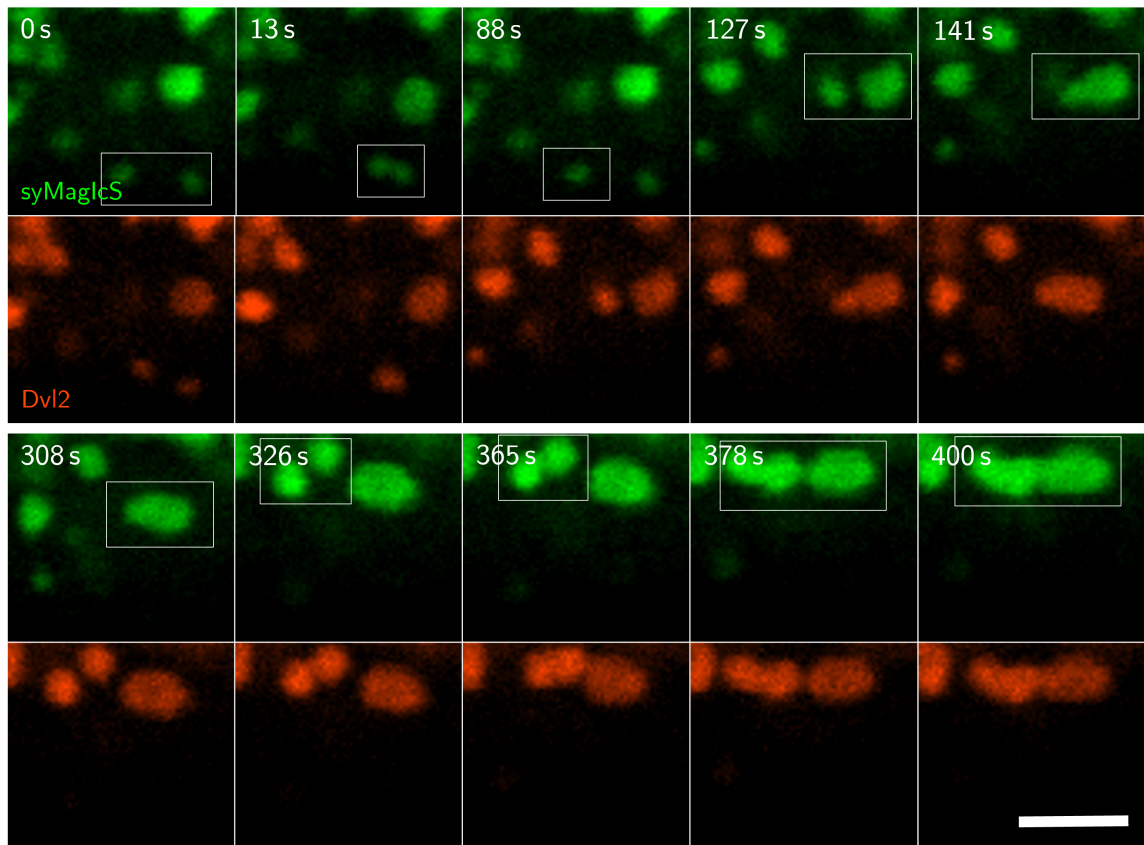


Figure 10.11.: **Dynamic behavior of induced LLPS.** syMagIcS are shown in green, Dvl2 in red. Scale bar: 3 μm .

10.2.3. Magnetic remote manipulation of Dvl2 LLPS using a magnetic field gradient

This proof-of-concept experiment aimed to find out whether our syMagIcS toolkit can be used to spatiotemporally control phase separation in living cells. In addition, it was investigated whether magnetically induced phase separation of Dvl2 also results in co-phase separation of Axin1. The induction of co-phase separation is another important step, which shows whether a component not bound to the particle can be recruited into the LLPS as well.

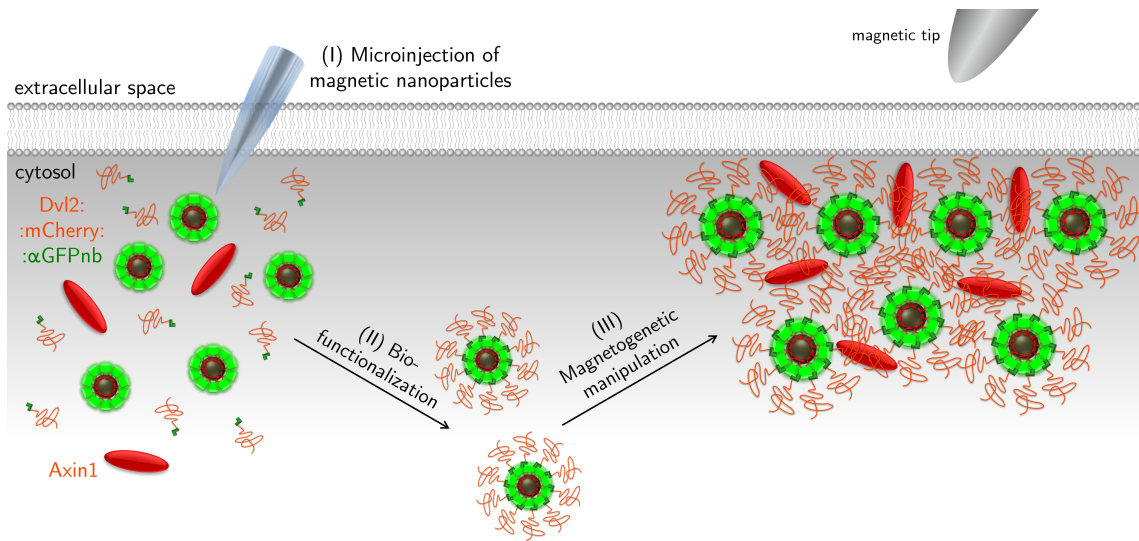


Figure 10.12.: **Magnetic remote manipulation of Dvl2 LLPS.** (I) Microinjection of syMagIcS into cells containing a fusion protein consisting of Dvl2, the fluorescent protein mCherry for visualization, and α GFPnb for site-specific MNP functionalization. (II) Self-assembly of the Dvl2-functionalized syMagIcS. (III) Application of a magnetic field gradient leading to locally increased concentration. Study of induction of Dvl2 LLPS due to this local increase in concentration and investigation of Axin1 recruitment and co-phase separation.

HeLa cells were cotransfected with Dvl2::mCherry:: α GFPnb and Axin-HaloTag stained with silicon rhodamine (SiR). This overexpression leads to a mostly homogeneous distribution of proteins in the cells; a few very faint droplets were already visible (Figure 10.13 and Supplementary Movie S11). Microinjection of mECFP-coated syMagIcS resulted in faintly seeded droplet formation in the upper cell. After applying a magnetic field gradient through a magnetic tip, a significant change was observed. The formation of small droplets was induced in the lower cell, which increased strongly over the observation period. Droplet formation in the upper cell, which was weak before the application of the magnetic field gradient, was significantly promoted. The induction of large droplets was observed. These large droplets could also be translocated inside the cell toward the magnetic tip by the magnetic field gradient. Some droplets could be enriched near to the plasma membrane. Also, the fusion of some droplets could be observed. This represents

an important criterion for LLPS. After removing the magnetic field gradient, continued dynamic behavior and further fusion events are observed (Supplementary Movie S11). In addition, the behavior of Axin1, which is not involved in the nanoparticle system, was investigated. A recruitment and co-phase separation of Axin1 could be observed. This is a key milestone for the assembly of a signalosome for future studies of the Wnt signaling pathway activation hypothesis. In addition, the potential for translocation of the droplets represents another important feature for targeted local placement of the signalosomes. This allows to investigate whether plasma membrane localization is required for Wnt signaling and whether Dvl2 LLPS at the plasma membrane is able to recruit the receptors Fzd and Lrp5/6.

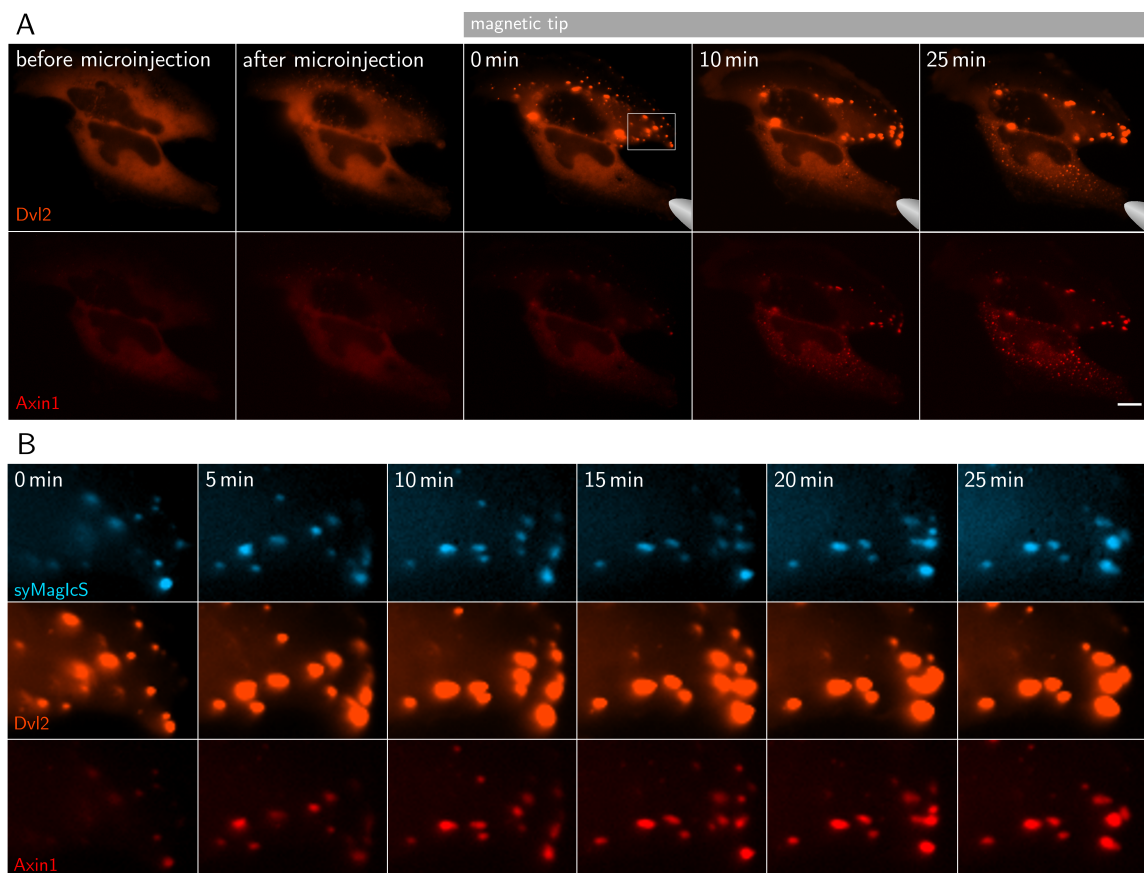


Figure 10.13.: **Magnetically controlled induction of LLPS using syMagIcS and demonstration of co-phase separation of Axin1.** (A) Microinjection of syMagIcS into Dvl2::mCherry:: α GFPnb and Axin-HaloTag overexpressing HeLa cells. Dvl2 Droplet formation and Axin1 co-phase separation was induced by the application of a magnetic field gradient. (B) Crop to the region marked by the white rectangle. Translocation of several droplets to the plasma membrane. Scale bar: 10 μ m.

10.2.4. Magnetic remote manipulation of Dvl2 LLPS due to magnetization

After investigating the behavior after microinjection of the multivalently functionalized syMagIcS, the next step was to remotely control Dvl2 phase separation in living cells. Superparamagnetic particles do not maintain magnetization even under the Curie temperature T_C after removal of the previously applied magnetic field. The property of being magnetic only when an external magnetic field is applied was used in a second proof-of-concept experiment of remote control of phase separation. Here, the aim was to investigate whether the additional interaction between the syMagIcS, due to magnetization by the application of a magnetic field, was sufficient to induce the droplet formation.

At a small distance above the cells transiently transfected with Dvl2::mCherry:: α GFPnb, two stacked strong magnets were placed. Each cube magnet with an edge length of 3 cm made of NdFeB (N52) material, has a holding force on iron of 736,24 N and can lift 75,05 kg. By applying these magnets, a very strong magnetic field was applied, resulting in magnetization of the syMagIcS as strong as possible. In contrast to the previous experiments, no sharp magnetic field gradient was applied, which is necessary for spatial control, but a strong magnetic field was applied, which resulted in the magnetization of the syMagIcS.

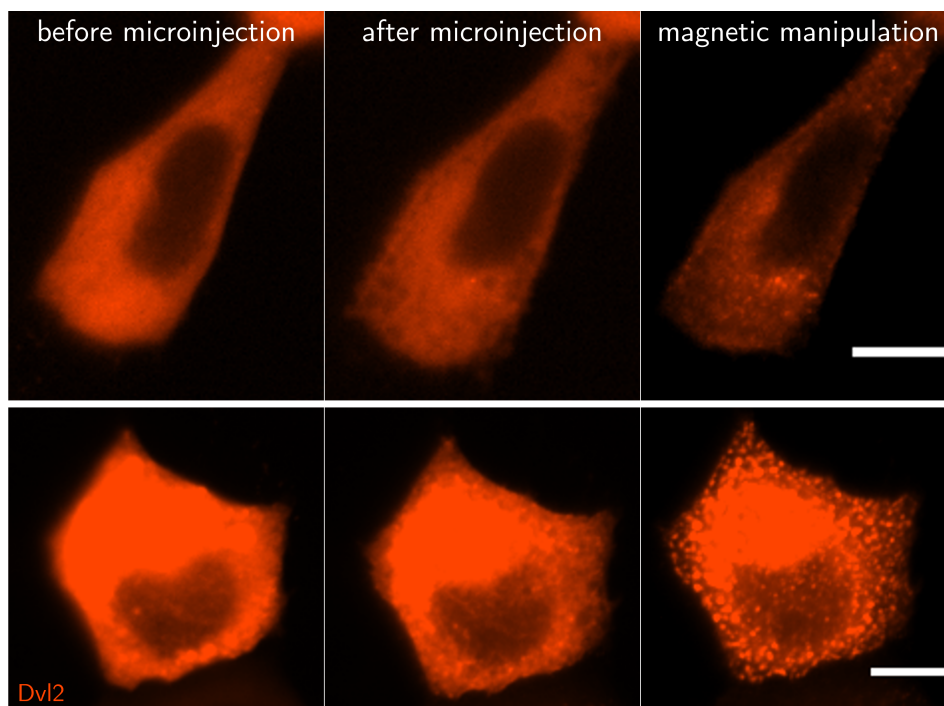


Figure 10.14.: **Magnetically controlled induction of LLPS due to magnetization of superparamagnetic syMagIcS.** Scale bar: 10 μ m.

After microinjection of syMagIcS, slight droplet formation was observed in some cases. The application of the magnetic field resulted in a significant enhancement of the droplet

formation (Fig. 10.14). This demonstrates that the additional interactions of the magnetized particles with each other is sufficient to drive the LLPS. This remote control of LLPS is limited to non-specific induction throughout the cytosol. Also, site-specific translocation of the induced droplets is not possible. For this reason, this concept is not suitable for site-specific control of LLPS, for example, targeted near the plasma membrane. However, remote control of cytosolic LLPS is a useful toolkit for addressing a wide field of biological questions, because LLPS can perform a variety of functions, as described previously (see Fig. 1.7).

To summarize this chapter, the LLPS behavior of Dvl2 fused with fluorescent proteins was characterized, afterwards syMagIcS was integrated into the system and the effect of multivalent binding of Dvl2 on the surface of the particle was investigated. It was shown that the droplets induced by multivalent syMagIcs exhibit LLPS behavior, such as intra and inter phase mobility, and fusion. Building on these characterizations, remote magnetically controlled induction of LLPS of Dvl2 was successfully demonstrated in proof-of-concept experiments. The induction could be achieved both by magnetizing the syMagIcS with associated attractive forces between the particles, and by applying a magnetic field gradient. The application of a magnetic field gradient, in addition to the attractive forces due to magnetization, leads to a site-specific translocation of the syMagIcS bound to Dvl2. This results in a local increase in concentration and thus local increase in interaction and induction of LLPS. In addition, remote translocation of the Dvl2-LLPS through the cytoplasm to the plasma membrane by the magnetic field gradient was observed. This offers the potential of remotely controlling the occurrence of LLPS at a desired target site, and thereby site-specifically inducing, manipulating, and monitoring cellular responses.

11 | Conclusion

The aim of this work was to develop biocompatible and biofunctional MNPs for magnetogenetic manipulation of downstream signal effector proteins at the plasma membrane and cytosol inside living cells. With this toolkit, proof-of-concept experiments aimed to magnetically remote control cellular functions and to gain detailed knowledge of the activation and regulatory mechanisms of signaling pathways by testing current hypotheses of activation. The intracellular application in the complex cytoplasmic environment places high requirements on the magnetic nanoparticles and their coating. One of the requirements is the biocompatibility of the nanoparticles, this includes colloidal stability and stealth behavior in living cells to avoid causing unwanted cellular reactions. In addition, there are requirements for size; the nanoparticles must be small enough not to exert mechanical forces on the crowded cell compartment, and to allow free diffusion in the cytosol. At the same time the particles must exhibit sufficient magnetic response to allow remote spatial control of the biofunctionalized nanoparticles. Moreover, a small size within the limits of superparamagnetism offers the advantage that the magnetization immediately disappears when the magnetic field is removed. This prevents unwanted magnetic forces between nanoparticles beyond magnetic remote manipulation. For targeted manipulation of cellular functions, the targeting system is critical, allowing site-specific functionalization of the nanoparticles with the protein of interest. A bio-orthogonal targeting system minimizes non-specific interactions and enables *in cellulo* functionalization.

In the initial experiments, the magnetic intracellular stealth nanoparticles, MagIcS, developed by Liße et al. in a previous work based on the natural ferritin protein cage fulfilled the requirements of intracellular application. However, despite the advantageous properties, such as excellent biocompatibility, MagIcS have certain limitations, especially in terms of magnetic properties and flexibility of functionalization, due to the fixed cage size and the construction from identical subunits. To overcome these limitations, a new generation of biofunctionalized magnetic nanoparticles was developed (syMagIcS). This one-step surface coating of synthetic magnetic core nanoparticles with green fluorescent proteins utilizes the iron binding site of Mms6 from magnetotactic bacteria to create a dense biofunctional coating of the MCP. The use of synthetic magnetic cores enables optimized magnetic properties, by synthesizing under optimized conditions and removing the limitation of a maximum diameter of 8 nm. Furthermore, the direct binding of fusion proteins to the surface and the application of various mixtures of fusion proteins enables control of the degree of functionalization and versatile functionalization. The dense coating of MCPs

and colloidal stability were demonstrated in *in vitro* experiments. The hydrodynamic radius and ζ potential of syMagIcS were determined and the functionalization stoichiometry was estimated. In intracellular experiments, free diffusion in the cytosol, intracellular stability, and stealth properties were confirmed without the need for additional chemical surface modifications. Ultrafast and highly specific conjugation with target proteins was demonstrated in *in vitro* by TIRFS-RIf and *in cellulo* experiments. Rapid and reversible control in the cytosol by magnetic forces was established for both MagIcS alone and *in cellulo* conjugated with target proteins. The characterization of syMagIcS demonstrated the suitability of syMagIcS for remote magnetic manipulation of target proteins inside living cells.

Furthermore, the use of these particles for magnetic remote control of cellular functions was investigated and the potential of the magnetic remote control approach for basic research and biomedicine was demonstrated. The intracellular applications of MagIcS and syMagIcS in pure space mode, realized in this work, represents a more advanced development to the widely known extracellular applications of magnetic nanoparticles in today's biomedical research. Previous applications are usually characterized by a thermal mode, a force mode or a mixture of space and force modes. The applicability of MagIcS and syMagIcS for intracellular magnetogenetic applications in space mode was explored at different levels. Efficient *in situ* MNP biofunctionalization with intracellular effector proteins by direct capture via α GFPnb was achieved, and intracellular translocation using magnetic field gradients was successfully performed for both MNP types. Activation of G proteins at the plasma membrane was achieved by magnetogenetic translocation of MNP-bound catalytically active region of GEF proteins, with syMagIcS showing significantly better performance compared to MagIcS.

Remote magnetic activation of Rho and Ras GTPases offers great potential for regenerative medicine. This dissertation was part of the MAGNEURON project, which developed an innovative therapeutic approach for neurodegenerative diseases such as Parkinson's disease. In 2016, neurological diseases accounted for 11.6% of disability-adjusted life years (DALYs) and 16.5% of deaths worldwide, making them the leading cause of DALYs and the second leading cause of death.⁴¹⁸ The number of people with Parkinson's disease is expected to more than double from 6.9 million in 2015 to 14.3 million by 2040.⁴¹⁹ In Parkinson's disease, selective degeneration of dopaminergic (DA) neurons in the substantia nigra occurs, with associated decreased dopamine levels in the striatum. This results in motor symptoms, such as bradykinesia, muscle tone rigidity, resting tremor, and postural instability, and non-motor symptoms, such as sleep disturbances, dementia, sensory abnormalities, and autonomic dysfunction.⁴²⁰⁻⁴²⁴ Cell therapy (CT), in which DA neurons are transplanted into the striatum or substantia nigra to replace degenerating neurons, represents a promising approach to treat Parkinson's disease.^{425,426} Despite good results, practical and ethical concerns limit the use of human fetal tissue. Through research advances, stem cell reprogramming technologies using induced pluripotent stem cells offer a promising alternative

source of DA progenitor neurons.^{427–431} Challenging in this regard is the need to minimize the risk of tumor development⁴³², promote survival of transplanted cells, control stem cell line development toward DA neurons, and control outgrowth of remote neurites from the substantia nigra into the striatum.⁴³³

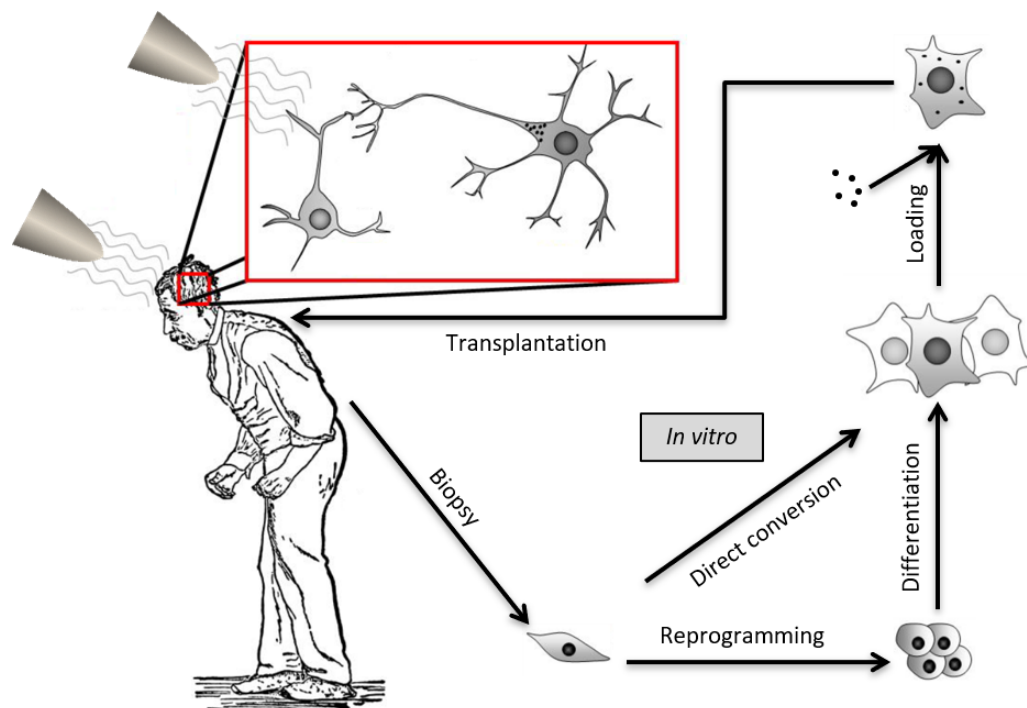


Figure 11.1.: **Concept of MAGNEURON approach to innovative therapy treatment of neurodegenerative diseases.** In a biopsy, patients' own body cells are taken and reprogrammed into dopamine precursor neurons by direct conversion or reprogramming into stem cells and differentiation. These neuronal cells get loaded with biofunctionalized MNPs and retransplanted into the target site. At the target site, controlled differentiation and directional outgrowth is achieved using a magnetic field gradient. Adapted from Gowers⁴³⁴ and Schöneborn et al.¹⁴⁷

The innovative therapeutic approach of MAGNEURON is to rewire the destroyed connections by controlling differentiation into DA neurons and directing axonal growth towards the denervated brain target tissue using biofunctionalized magnetic nanoparticles, thus opening up CT progression. For this purpose, somatic cells are taken from the patient and reprogrammed into dopamine precursor neurons by direct conversion or reprogramming into stem cells and differentiation. These neuronal cells are then loaded with the biofunctionalized MNPs and retransplanted into the substantia nigra. The application of a magnetic field gradient should be used to remotely control differentiation and directional axonal growth.¹⁴⁷ This should be accomplished by targeting signaling pathways to be magnetically controlled activated and exploiting the cells' ability to sense signals with great sensitivity, process the signaling information, and mobilize complex molecular machinery to control cellular functions.

Due to the key role of Rho and Ras GTPases in axon growth, guidance, and branching (Chapter 5.3), they were targeted in the MAGNEURON project. Magnetogenetic control of Rho and Ras GTPases activity offers a promising approach to induce asymmetric signaling activity within the cell and promote directed differentiation and growth. In addition, the ability to functionalize syMagIcS *in vitro* offers an advantage over optogenetics for CT in human patients, as it does not require genetic modification of the biological material. Using the developed magnetogenetic toolkit, this thesis demonstrated successful magnetic control of the small GTPases hRas and Rac1 activity in non-neuronal cells. The demonstration of magnetogenetically controlled morphological change and outgrowth of cells represents a key proof-of-concept for the MAGNEURON approach and demonstrates the potential of syMagIcS and the remote magnetic control approach for biomedical research.

The ability to target site-specifically different stages of signaling provides insights to understand these pathways and, for example, to test hypotheses of activation. Here, this approach was applied to test the hypothesis of activation of the Wnt signaling pathway. First, the LLPS behavior of Dvl2 was characterized and, based on this characterization, the remote magnetic controlled induction of LLPS from Dvl2 was successfully demonstrated in proof-of-concept experiments. This induction could be achieved both by magnetizing the syMagIcS with the associated attractive forces between the particles and by applying a magnetic field gradient. In addition, remote translocation of Dvl2-LLPS through the cytoplasm to the plasma membrane by the magnetic field gradient was observed, demonstrating the ability to remotely control the appearance of LLPS at a desired target site and thereby affect and monitor cellular responses in a site-specific manner. With this tool in hand, the more detailed understanding of the activation and regulation mechanisms of cellular signaling pathways and the exploration of spatiotemporal regulation of cellular processes in living cells can be acquired.

In basic biological research, GFP is often used to visualize intracellular proteins and to investigate structures and processes. For this reason, reversing the targeting system, i.e. presenting a GFP-binding protein on the surface of the nanoparticles, offers a crucial advantage for compatibility and straightforward integration into existing systems. This allows intracellular targeting of any GFP-tagged protein, including cytosolic proteins and structures. For this purpose, in a preliminary experiment, the binding protein DARPin CR7 developed by Hansen et al. was used as GFP-binding protein. DARPin CR7 binds GFP with high affinity ($K_D = 10\text{-}30\text{ pM}$).²⁹⁴ In addition to enabling interaction for functionalization, other functions of GFP in functional coating are to provide a dense and stable protein coverage and enable visualization. These functions must be fulfilled by fluorescent proteins which are orthogonal to the targeting system. Thus, mTFP1 was chosen, which similarly consists of a stable β -barrel, enabling a stable, dense protein shell. Initial experiments showed successful magnetic manipulation of the coated particles. However, the particles

failed to bind to GFP-tagged structures. This could be due to the fact that in the β -barrel structure of the fluorescent protein, both termini are on the same side. Thus, the DARPin could be located under the protein coating, directed toward the MCP surface. For this reason, the dense protein coat could sterically hinder binding to GFP. One possible solution is the use of a flexible linker, which could allow the orientation of the GFP-binding DARPin on the outside. This should be tested in future experiments to extend the versatility of the use of syMagIcS by enabling GFP-tagged protein binding and targeting of multiple proteins in a site-specific manner.

Direct binding of individual coating proteins offers enormous potential and versatility of functionalization. This variability was demonstrated in this thesis by controlling multivalency, but offers much more potential. The use of a mixture of coating proteins with different orthogonal targeting systems would allow site-specific binding of various proteins of interest to a single syMagIcS simultaneously. Also conceivable is a combination of specific binding of a protein and site-specific binding of this functionalized syMagIcS to the region of interest. Besides the possibility to use synthetic MCP, of any form, with potent magnetic properties, the highly versatile functionalization options opens up excellent opportunities for syMagIcS. This makes syMagIcS a powerful toolkit for magnetic control of protein localization and magnetogenetic manipulation of cellular functions in living cells.

V Appendix

12 | Materials and methods

12.1. Biofunctionalized magnetic nanoparticles

12.1.1. Protein purification

Plasmid generation

Table 12.1.: Plasmids for protein purification.

Plasmid	Vektor	Insert	MW
H6::mEGFP::Mms6 Δ N	pet21a	His6-Tag, 3aa-linker, mEGFP, 7aa-linker, Mms6 Δ N (112-133)	31.2 kDa
H6::mXFP::Mms6 Δ N (mEGFP Y67F)	pet21a	His6-Tag, 3aa-linker, mEGFP Y67F, 7aa-linker, Mms6 Δ N (112-133)	31.2 kDa
H6::mCFP::Mms6 Δ N (mEGFP H164N)	pet21a	His6-Tag, 3aa-linker, mEGFP H164N, 7aa-linker, Mms6 Δ N (112-133)	31.2 kDa
H6::mCFPm::Mms6 Δ N (mEGFP E142K H164N)	pet21a	His6-Tag, 3aa-linker, mEGFP E142K H164N, 7aa-linker, Mms6 Δ N (112-133)	31.2 kDa
H6::mEGFP::HCF	pet21a	His6-Tag, 3aa-linker, mEGFP, 6aa-linker, heavy chain ferritin (human, P02794)	49.8 kDa
mXFP::HCF (mEGFP Y67F)	pet21a	3aa-linker, mEGFP Y67F, 6aa-linker, heavy chain ferritin (human, P02794)	49.7 kDa
H6::mXFP::HCF (mEGFP Y67F)	pet21a	His6-Tag, 3aa-linker, mEGFP Y67F, 6aa-linker, heavy chain ferritin (human, P02794)	49.8 kDa

The *mms6*-based coating proteins for bacterial expression were cloned into the vector pET21a. The iron-binding fragment of Mms6 comprising the C-terminal 22 amino acid residues (MKSRDIESA QSDEEVELRD ALA) of Mms6 (Mms6 Δ N) was genetically fused to the C-terminus of monomeric enhanced GFP (mEGFP), the non-fluorescent mutant mEGFP Y66F (mXFP), mEGFP H164N (mCFP), or mEGFP E142K H164N (mCFPm), containing 7 amino acids as linker by cassette cloning. For purification, a His6-Tag (H6) was fused to the N-terminus of the respective GFP variant. In the case of MagIcS, the plasmid previously cloned by Liße et al. was used, which consists of monomeric enhanced GFP (mEGFP) fused to the N-terminus of HCF.⁷⁵ For purification by Immobilized metal affinity chromatography (IMAC), a His6-Tag (H6) was inserted using tag insertion. For a weakly fluorescent version, a point mutation was inserted by PCR (mEGFP Y67F). For bacterial expression in *E. coli* BL21-CodonPlus-RIL, the cDNA of the fusion protein was cloned into pET21a (Novagen).

Protein expression and cell lysis

E. coli BL21-CodonPlus-RIL (Agilent) were transformed with the respective plasmid and grown at 37 °C, at OD₆₀₀ = 0.6-0.8 protein expression was induced with 0.5 mM isopropyl β-D-1-thiogalactopyranoside (IPTG, Thermo Scientific) and subsequently cultured at 16 °C overnight. Harvested cells (6 500 g, 10 min) were resuspended in lysis buffer (50 mM HEPES, 150 mM NaCl, 8 M urea, pH 7.5-8.0). The cell lysate was lysed by sonication (4 × 3 min; 50 % duty cycle, Sonifier 250, Branson) and insoluble material was pelleted by centrifugation (20 000 g, 30 min, 4 °C).

Immobilized metal affinity chromatography (IMAC)

The first step of purification was performed using Immobilized metal affinity chromatography (IMAC) on an fast protein liquid chromatography (FPLC) system (Äkta Explorer + UNICORN software, GE Healthcare,). A 5 ml HiTrap chelating HP column was loaded with nickel (II) chloride (20mM, 5 × bed volume) and equilibrated with 20 mM HEPES, 150 mM NaCl, pH 7.5-8.0 (HBS). After filtration (0.2 μm cut-off) the supernatant was loaded to the column. To promote proper refolding the transition from 8 M to 0 M urea was performed optionally over a one-hour gradient. After a washing step (HBS + 15 mM imidazole) the protein was eluted with HBS complemented up to 500 mM imidazole, pH 7.5-8.0 using a linear gradient covering 10 × the bed volume. The sample was collected and 5 mM EDTA was added. Protein integrity and purity were confirmed by 12 % SDS-PAGE.

Size-exclusion chromatography (SEC)

Subsequently, an additional purification step using SEC was performed on an FPLC system (Äkta Explorer + UNICORN software, GE Healthcare). The corresponding column (see table 12.2) was equilibrated in HBS, the protein was loaded after filtration (0.2 μm cut-off) onto the SEC column and eluted. Protein integrity and purity were confirmed by 12 % SDS-PAGE.

Heat treatment, ammonium sulfate precipitation, anion-exchange chromatography

In the case of mXFP::HCF purification, heat treatment (70 °C, 15 min) of the harvested cell lysate was followed by ammonium sulfate precipitation in two steps (200 g/l, 300 g/l). The pellet was washed twice (300 g/l ammonium sulfate, 50 mM HEPES, 150 mM NaCl, pH 8.0) and dissolved in HBS (50 mM HEPES, 150 mM NaCl, pH 8.0). Subsequently, the protein was purified by anion-exchange chromatography (Q-Sepharose FF, 20 mM HEPES, gradient 100 mM - 1 M NaCl, pH 8.0) and size-exclusion chromatography.

Table 12.2.: Column - properties.

column	molecular weight (globular proteins)	max. pressure	max. flow rate	bed volume	sample volume
HiLoad 16/60 Superdex 75, prep grade	3 kDa - 70 kDa	0.3 MPa	1.0 ml/min	120 ml	<5 ml
HiLoad 26/60 Superdex 75, prep grade	3 kDa - 70 kDa	0.3 MPa	2.6 ml/min	320 ml	<13 ml
HiLoad 16/60 Superdex 200, prep grade	10 kDa - 600 kDa	0.3 MPa	1.0 ml/min	120 ml	<5 ml
HiLoad 26/60 Superdex 200, prep grade	10 kDa - 600 kDa	0.3 MPa	2.6 ml/min	320 ml	<13 ml
Superdex 200 10/300 GL	10 kDa - 600 kDa	1.5 MPa	0.75 ml/min	24 ml	25 μ l - 500 μ l
HiPrep 16/60 Sephacryl S-400 HR	20 kDa - 8000 kDa	0.15 MPa	0.5 ml/min	120 ml	<5 ml
HiPrep 26/60 Sephacryl S-400 HR	20 kDa - 8000 kDa	0.15 MPa	1.3 ml/min	320 ml	<13 ml
HiPrep 16/60 Sephacryl S-500 HR	40 kDa - 20000 kDa	0.15 MPa	0.5 ml/min	120 ml	<5 ml
HiPrep 26/60 Sephacryl S-500 HR	40 kDa - 20000 kDa	0.15 MPa	1.3 ml/min	320 ml	<13 ml

PEGylation

For PEGylation, the protein was incubated with a 30-fold excess of PEG₂₀₀₀ (α -Methoxy- ω -NHS esters, CH₃O-PEG-NHCO-C₂H₄-CONHS, 2000 Da, Rapp Polymere) for >1 h and afterwards purified using SEC (see previous section).

12.1.2. syMagIcS

Synthesis of maghemite MCP

MCPs were synthesized and characterized by Emilie Secret (PHENIX laboratory at Centre National de la Recherche Scientifique (CNRS) and Universität Pierre et Marie Curie (UPMC), Sorbonne University). Maghemite nanoparticles were synthesized by an inverse co-precipitation method. The acidic iron (II) and iron (III) ions solution (248.5 g of FeCl₂, 4 H₂O, 100 ml of HCl 37 %, 500 ml of DI water, 587 ml of FeCl₃ 27 %) was added dropwise over 30 h into 4 l of 5 % ammonia in water under agitation. After rinsing the obtained Fe₃O₄ nanoparticles with water, they were redispersed in 2 l of nitric acid (9.5 %). These nanoparticles were then oxidized into γ -Fe₂O₃ nanoparticles by boiling them with a solution of iron (III) nitrate (323 g of Fe(NO₃)₃ in 800 ml of DI water) for 30 min. After washing the nanoparticles with nitric acid once, acetone three times and diethyl ether twice, they were redispersed in 1 l of water. At this step the maghemite nanoparticles are polydispersed in size. To decrease the polydispersity, the nanoparticles were size-sorted by addition of nitric acid which increase the ionic strength of the solution, leading to the flocculation of the larger, thus less stable, nanoparticles. The final nanoparticles were size sorted in two

steps: first with 20 ml of nitric acid (68%), then with 5 ml of nitric acid. After each size sorting step, the nanoparticles were rinsed with acetone 3 × and with diethylether twice before being resuspended in DI water.

One-step biofunctional coating of maghemite core particles

Prior to MCP coating, PEGylated or non-PEGylated H6::mEGFP::Mms6ΔN was transferred into to water pH 7.0 using a buffer exchange column (NAP5, NAP10 or PD10). After sonication (Ultrasound bath, 10 min, 10-15 °C) MCP were added to a 100-fold molar excess of coating protein and incubated for > 1 h. Excess protein was washed out by ultrafiltration (Amicon UF-Tubes, cut-off: 100 kDa, for V ~ 1000 μl, 4 min, 4000 g, 20 mM HEPES pH 7.5, RT) until the filtrate was free of coating protein. For optional crosslinking of the coating protein shell, particles were incubated in paraformaldehyde (4% PFA in HB, > 1 h, RT). This was followed by a washing step using ultrafiltration (Amicon UF tubes, cut-off: 100 kDa, ~ 1000 μl, 4 min, 20 mM HEPES pH 7.5, > 3 ×, RT). Directly before use inside living cells, particles were centrifuged to remove aggregates at 6000 g for 5 min.

12.1.3. MagIcS

Synthesis/encapsulation of magnetite core into the HCF cage

Purified, non-PEGylated H6::mEGFP::HCF or H6::mXFP::HCF self-assembled into protein cages under non-denaturing conditions was transferred to 100 mM NaCl using a buffer exchange column (PD10). To synthesize the magnetic core inside the cage, the protein is added to 25 ml 100 mM NaCl with a final concentration of 250 nM. During the synthesis, the reaction vessel was kept constant at 65 °C under positive N₂ pressure, and the pH was maintained at 8.5 using an automatic titrator (Titration Excellence T5, Mettler-Toledo) by adding a 100 mM NaOH, 100 mM NaCl solution. At a constant rate (250 μl/min), 2500 μl each of a 5 mM H₂O₂ solution and a 12.5 mM ammonium iron(II) sulfate hexahydrate solution, serving as the iron source, were added simultaneously. After addition of the iron and oxidant solution, 20 mM HEPES and 2 mM EDTA, to chelate free iron, was added. Aggregates of proteins or metal oxides formed outside the protein cage were removed by centrifugation (20 000 g, 10 min - 30 min), followed by a concentration step (Amicon UF tubes, cut-off: 100 kDa). The concentrated supernatant was purified by SEC to obtain monomeric MagIcS. Optionally, PEGylation was performed prior to SEC, for this purpose MagIcS were transferred to HEPES buffer (20 mM HEPES, 150 mM NaCl, pH 7.5 - 8.0) using a buffer exchange column (PD10), followed by PEGylation as previously described.

12.2. *In vitro* MNP characterization

12.2.1. Transmission Electron Microscopy (TEM) images

Maghemite nanoparticles were characterized by transmission electron microscopy (TEM) on a JEOL 100CX2 instrument. syMagIcS were applied onto negatively glow-discharged carbon-coated grids (400 mesh, copper grid) for 1 min. Excess liquid was removed by blotting with filter paper. The grid was washed twice shortly with distilled water and stained 2 min with 1% uranyl acetate and blotted. Digital micrographs were collected using a Zeiss LEO 912 electron microscope operated at 80 kV equipped with a TRS sharp:eye dual speed 2k-on-axis Digital CCD Camera. Image analyzing was performed using Fiji-ImageJ (NIH, USA).

12.2.2. Dynamic Light Scattering (DLS)

The obtained maghemite nanoparticles were characterized by dynamic light scattering (DLS) on a Malvern Zetasizer NanoZS instrument and by superconducting quantum interference device (SQUID) magnetometry on a Quantum Design MPMS-XL instrument. Size distributions and ζ -potential of syMagIcS were using DLS with a Zetasizer (nano series, MALVERN Instruments). For size distribution, 500 μ l samples were measured in plastic cuvettes. A dip cell (ZEN 1002) was used for ζ -potential measurements. Data analysis was performed using the Malvern software accompanying the instrument and OriginPro9.0 (OriginLab Corporation).

12.2.3. Interaction analysis by TIRFS-RIf detection

In vitro quantification of the interaction of α GFPnb with syMagIcS were carried out by simultaneous total internal reflectance fluorescence spectroscopy and reflectance interference (TIRFS-RIf) detection using home-built setup described previously.⁴⁰⁷ Glass substrates coated with a 325-400 nm silica layer were used as transducers for RIf detection. Transducer slides were plasma cleaned (10 min) and then sandwich-incubated (10 min) with 6 μ l poly-L-lysine-graft-poly(ethylene glycol) functionalized with the HaloTag ligand (PLL-PEG-HTL)⁴⁰⁸ (1 mg/ml). The chips subsequently were rinsed in MilliQ, dried with nitrogen and optionally stored at -20 °C. Data analysis was performed using OriginPro9.1 (OriginLab) and BIAevaluation 3.1 (Cytiva).

12.2.4. GTP exchange factor activity measurement

To investigate the GTP exchange factor activity of the soluble SOS_{cat} fusion protein and SOS_{cat}-functionalized MNPs, fluorescence decrease was observed by exchanging fluorescent N-methylanthraniloyl (mant)-GDP on preloaded HRAS to unlabeled GDP at 37 °C. H-RAS loaded with mant-GDP at a concentration of 1 μ M was provided in a quartz cuvette with nucleotide exchange buffer (40 mM HEPES pH 7.4, 5 mM MgCl₂, 1 mM DTT) and premixed with 0.5 μ M soluble or MNP-bound SOS_{cat} fusion protein or without to

measure intrinsic nucleotide exchange activity, in total reaction volume of 150 μl . The $\alpha\text{GFPnb}::\text{mCherry}::\text{SOS}_{\text{cat}}::\text{H6}$ fusion protein was purified using IMAC and SEC by Annette Budke-Gieseking and provided for this experiment. Using a fluorescence spectrometer, fluorescence intensity was measured at an emission wavelength of 440 nm at an interval of 2 s. After a stable fluorescence signal was obtained, nucleotide exchange was started by adding 1.3 mM GDP. The data obtained were analyzed using OriginPro9.0 (OriginLab Corporation). The exponential curve of the decrease in fluorescence was fitted to pseudo-first order due to the large excess of GDP to HRAS.

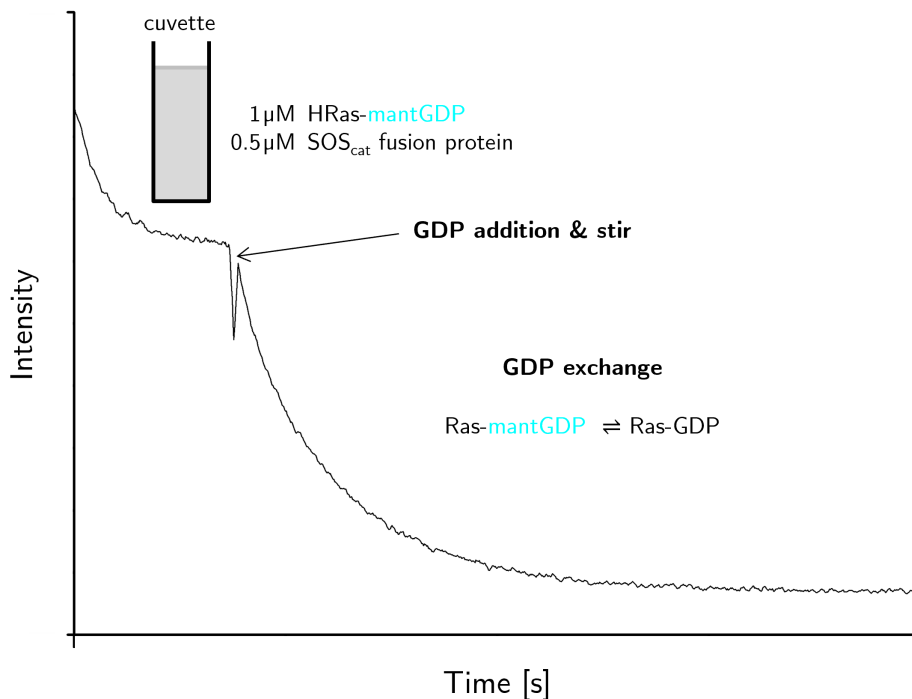


Figure 12.1.: Course of the GTP exchange factor activity measurement.

12.3. *In cellulo* experiments

12.3.1. Cell culture

HeLa and COS7 cells were cultivated at 37 °C, 5 % CO₂ in MEM (PAA) with 1.1 % HEPES (PAA), 1.1 % NEA (Biochrom/PAA), 10 % fetal bovine serum (Biochrom) (MEM⁺⁺) and seeded on sterilized glass coverslips in 35 mm cell culture dishes. After 6 h to 24 h cells were transfected using Viafect reagent (Promega, Madison, WI, USA, ratio: 1 μg DNA : 3 μl Viafect) according to the protocol. The next day cells were washed twice with DPBS buffer and media was exchanged for fresh MEM⁺⁺. In case of HaloTag an additional labeling step is needed (wash with preheated DPBS, incubate 20 min at 37 °C with 50 nM SIR-HTL in MEM⁺⁺, wash three times with DPBS, add fresh MEM⁺⁺) is needed. To increase the brightness of iRFP 25 μM biliverdin was added 16 h before the experiment (before imaging: 3 \times washing with DPBS, addition of fresh MEM⁺⁺).

Table 12.3.: Plasmids for transfection.

Plasmid	Vektor	Insert	MW
Tom20::mCherry:: α GFPnb	pSems	human Tom20 (Q15388), 16aa-linker, mCherry, 7aa-linker, α GFPnb (nanobody enhancer)	44.2 kDa
TIAM1 _{DHPH} ::mCherry:: α GFPnb	pSems	TIAM1 _{DHPH} (mouse TIAM1, amino acid 1033-1406, Q60610), 24aa-linker, mCherry, 7aa-linker, α GFPnb (nanobody enhancer)	91.7 kDa
α GFPnb::mCherry::SOS _{cat}	pSems	α GFPnb, 3aa-linker, mCherry, 8aa-linker, SOS _{cat} (human SOS1, amino acid 564-1049, Q07889)	104.0 kDa
HaloTag::Rac1	pSems	HaloTag, 17aa-linker, human Rac1 (P63000)	56.7 kDa
mNeonGreen::PAK-CRIB::P2A::Rac1::mTFP1::CAAX	pSems	mNeonGreen, 1aa-linker, PAK-CRIB (human PAK1, amino acid 68-150, Q13153), P2A, human Rac1 (amino acid 1-176, P63000), 2aa-linker, mTFP1, 2aa-linker, CAAX Box	100.2 kDa
mNeonGreen::PAK-CRIB::EV-linker::Rac1::mTFP1::CAAX	pSems	mNeonGreen, 1aa-linker, PAK-CRIB (human PAK1, amino acid 68-150, Q13153), 119aa-EV-linker, human Rac1 (amino acid 1-176, P63000), 2aa-linker, mTFP1, 2aa-linker, CAAX Box	100.2 kDa
mNeonGreen::HRas::EV-linker::RBD::mTFP1::CAAX	pSems	mNeonGreen, 2aa-linker, human HRas (amino acid 1-172, P01112), 119aa-EV-linker, Ras binding domain of Raf (human Raf1, amino acid 51-131, P04049), 2aa-linker, mTFP1, 2aa-linker, CAAX Box	100.0 kDa
Lifeact::iRFP	pIRES	Lifeact, 7aa-linker, iRFP713	35.9 kDa
α GFPnb::mCherry	pSems	mCherry, 7aa-linker, α GFPnb (nanobody enhancer)	40.2 kDa
Dvl2::mCherry:: α GFPnb	pSems	hDvl2 (human, O14641), 37aa-linker, mCherry, 7aa-linker, α GFPnb (nanobody enhancer)	128.2 kDa
Dvl2::tdm-mCherry:: α GFPnb	pSems	hDvl2 (human, O14641), mCherry, 27aa-linker, mCherry α GFPnb (nanobody enhancer)	157.1 kDa
Dvl2::dsRed:: α GFPnb	pSems	hDvl2 (human, O14641), dsRed.M1, α GFPnb (nanobody enhancer)	119.6 kDa
HaloTag::Axin1	pSems		

12.3.2. Microinjection

syMagIcS were microinjected into cells based on published protocols⁴³⁵ using a micro manipulation system (InjectMan NI2 and 10 FemtoJet Express, Eppendorf) and a capillary pressure between 15-25 hPa. Injection needles (GB100TF-10, 0.78 mm \times 1.00 mm \times 100 mm, Science Products GmbH) were pulled by a P97 micropipette puller (Sutter Instruments, Novato, CA, USA) using the following parameters: heat: 438; pull: 130; velocity: 38; time: 105. For microinjection the tip of the needle was slowly approached until it touched the cell membrane and a smooth flow of liquid entering the cell was observed. After injection, waiting for 5-10 minutes allowed the cells to recover.

12.3.3. Fluorescence Microscopy images

For Imaging cells were grown on 25 mm glass coverslips. Imaging and manipulation were performed, unless otherwise described, at Zeiss Axiovert 200 equipped with 40 \times water-objective and a Zeiss AxioCam. For the FRET experiments, images were acquired simultaneously using Cairn Research OptoSplit II.

Table 12.4.: Zeiss Axiovert 200 - Filter.

Fluorescence protein/Dye	Excitation	Dicroid	Emission
FRET	436/20	D455 LP	460-490, 510-540
mCherry	BP 545/25	565 CPXR	605/70
iRFP713, SIR	655/40-25	685	716/40-16
mEGFP	BP 450-490	FT 510	BP 515-565
mCFP	AT 435/20x	AT 455 DC	AT 480/30m

Confocal laser scanning microscopy images was taken at Olympus cLSM FV-1000 and FV-3000 equipped with 40 \times water-objective (sCMOS Camera Hamamatsu ORCAFlash 4.0 V3). Images for intracellular concentration determination were acquired at Olympus cLSM FV-1000 (syMagIcS) in the case of syMagIcS, whereas images of the other intracellular concentration determinations and FRAP measurements were acquired at Olympus cLSM FV-3000. The images of the various channels were taken sequentially.

Table 12.5.: Olympus cLSM FV-1000 - used lasers.

Fluorescence protein/Dye	Excitation
mCherry, tdm-mCherry, dsRed	561 nm
mEGFP	488 nm
SIR	640 nm

Image analyzing was done with Fiji-ImageJ (NIH, USA) and FRET was analyzed with self-written routines in Matlab (R2017a, The Mathworks Inc, Natick, MA). In the first step the channel alignment with horizontal and vertical shift is done, in the second step the off-set and the borders of the donor and acceptor channel are set. Finally, for the resulting ratio channel, the borders and a smoothing radius can be selected. The selected borders of the channels only influence the resulting image and represent the borders of the color scale. These borders do not affect the resulting ratio, the crucial paramters are the correct alignment and choice of the off-set of the donor and acceptor channels. The same parameters were chosen for compared images.

13 | References

- [1] E. Cao, J. F. Cordero-Morales, B. Liu, and others. TRPV1 channels are intrinsically heat sensitive and negatively regulated by phosphoinositide lipids. *Neuron* 77(4), 667–679 (2013).
- [2] Y.-R. Cheng, B.-Y. Jiang, and C.-C. Chen. Acid-sensing ion channels: dual function proteins for chemo-sensing and mechano-sensing. *Journal of Biomedical Science* 25(1), 46 (2018).
- [3] C. Engelhard, I. Chizhov, F. Siebert, and M. Engelhard. Microbial Halorhodopsins: Light-Driven Chloride Pumps. *Chemical reviews* 118(21), 10629–10645 (2018).
- [4] G. L. Fain. Mechanoreceptors and touch. In *Sensory transduction*, 76–98.
- [5] J. Moon. Design for Selective Remote Control of Cellular Signaling Using Magnetic Nanoparticles. PhD thesis, Massachusetts Institute of Technology, (2021).
- [6] A. Pires-da Silva and R. J. Sommer. The evolution of signalling pathways in animal development. *Nature reviews. Genetics* 4(1), 39–49 (2003).
- [7] L. A. Urry, M. L. Cain, S. A. Wasserman, and others. *Campbell Biologie*. Pearson Studium. Pearson, Hallbergmoos, 11th edition, (2019).
- [8] D. E. Sadava, D. M. Hillis, H. C. Heller, and others. *Purves Biologie*. Springer Spektrum, Berlin, 10. auflage (entspricht der 11. englischen auflage) edition, (2019).
- [9] N. C. Bauer, P. W. Doetsch, and A. H. Corbett. Mechanisms Regulating Protein Localization. *Traffic* 16(10), 1039–1061 (2015).
- [10] M. C. Good, J. G. Zalatan, and W. A. Lim. Scaffold proteins: hubs for controlling the flow of cellular information. *Science* 332(6030), 680–686 (2011).
- [11] T. Hunter. Signaling—2000 and Beyond. *Cell* 100(1), 113–127 (2000).
- [12] B. Jayanthi, B. Bachhav, Z. Wan, and others. A platform for post-translational spatiotemporal control of cellular proteins. *Synthetic Biology* 6(1), ysab002 (2021).
- [13] Q. Su, S. Mehta, and J. Zhang. Liquid-liquid phase separation: Orchestrating cell signaling through time and space. *Molecular cell* 81(20), 4137–4146 (2021).
- [14] B. D. Grant and J. G. Donaldson. Pathways and mechanisms of endocytic recycling. *Nature reviews. Molecular cell biology* 10(9), 597–608 (2009).

- [15] N. Hao, B. A. Budnik, J. Gunawardena, and E. K. O’Shea. Tunable signal processing through modular control of transcription factor translocation. *Science* 339(6118), 460–464 (2013).
- [16] J. Ryu and S.-H. Park. Simple synthetic protein scaffolds can create adjustable artificial MAPK circuits in yeast and mammalian cells. *Science signaling* 8(383), ra66–ra66 (2015).
- [17] D. A. Frank. Signal transduction in cancer, volume v. 115 of *Cancer treatment and research*. Kluwer Academic Publishers, (2003).
- [18] T. R. Geiger and D. S. Peeper. Metastasis mechanisms. *Biochimica et Biophysica Acta (BBA) - Reviews on Cancer* 1796(2), 293–308 (2009).
- [19] N. A. Mack, H. J. Whalley, S. Castillo-Lluva, and A. Malliri. The diverse roles of Rac signaling in tumorigenesis. *Cell Cycle* 10(10), 1571–1581 (2011).
- [20] S. Mehta and J. Zhang. Liquid–liquid phase separation drives cellular function and dysfunction in cancer. *Nature Reviews Cancer* 22(4), 239–252 (2022).
- [21] M. Yilmaz and G. Christofori. Mechanisms of Motility in Metastasizing Cells. *Molecular Cancer Research* 8(5), 629–642 (2010).
- [22] R. Sever and J. S. Brugge. *Signal Transduction in Cancer*. Cold Spring Harbor Perspectives in Medicine 5(4), a006098–a006098 (2015).
- [23] A. G. Stephen, D. Esposito, R. K. Bagni, and F. McCormick. Dragging Ras Back in the Ring. *Cancer Cell* 25(3), 272–281 (2014).
- [24] T. Zhan, N. Rindtorff, and M. Boutros. Wnt signaling in cancer. *Oncogene* 36(11), 1461–1473 (2017).
- [25] C. Monzel, C. Vicario, J. Piehler, and others. Magnetic control of cellular processes using biofunctional nanoparticles. *Chemical Science* 8(11), 7330–7338 (2017).
- [26] B. Alberts and L. Jaenicke. *Molekularbiologie der Zelle: Mit Cell biology interactive*. Wiley-VCH, 4th edition, (2004).
- [27] E. U. Azeloglu and R. Iyengar. Signaling networks: information flow, computation, and decision making. *Cold Spring Harbor perspectives in biology* 7(4), a005934 (2015).
- [28] C. Brun, F. Chevenet, D. Martin, and J. Wojcik. Functional classification of proteins for the prediction of cellular function from a protein-protein interaction network. *Genome Biology* 5(1) (2003).
- [29] S. Charbonnier, O. Gallego, and A.-C. Gavin. The social network of a cell: Recent advances in interactome mapping. *Biotechnology Annual Review* 14, 1–28.

- [30] J. D. Scott and T. Pawson. Cell signaling in space and time: where proteins come together and when they're apart. *Science* 326(5957), 1220–1224 (2009).
- [31] M. Vidal, M. E. Cusick, and A.-L. Barabási. Interactome networks and human disease. *Cell* 144(6), 986–998 (2011).
- [32] G. Weng, U. S. Bhalla, and R. Iyengar. Complexity in Biological Signaling Systems. *Science* 284(5411), 92–96 (1999).
- [33] J. Yang, S. A. Wagner, and P. Beli. Illuminating Spatial and Temporal Organization of Protein Interaction Networks by Mass Spectrometry-Based Proteomics. *Frontiers in Genetics* 6 (2015).
- [34] R. E. Ferner and J. K. Aronson. Cato Guldberg and Peter Waage, the history of the Law of Mass Action, and its relevance to clinical pharmacology. *British journal of clinical pharmacology* 81(1), 52–55 (2016).
- [35] C. E. Mortimer and U. Müller. *Chemie: Das Basiswissen der Chemie ; 128 Tabellen*. Thieme, 10th. edition, (2010).
- [36] R. Jin, S. McCallen, C.-C. Liu, and others. Identifying dynamic network modules with temporal and spatial constraints. *Pacific Symposium on Biocomputing* (14), 203–214 (2009).
- [37] I. Arozarena, F. Calvo, and P. Crespo. Ras, an Actor on Many Stages: Posttranslational Modifications, Localization, and Site-Specified Events. *Genes & Cancer* 2(3), 182–194 (2011).
- [38] N. Ausmees and C. Jacobs-Wagner. Spatial and Temporal Control of Differentiation and Cell Cycle Progression in *Caulobacter crescentus*. *Annual Review of Microbiology* 57(1), 225–247 (2003).
- [39] J. Collier and L. Shapiro. Spatial complexity and control of a bacterial cell cycle. *Current Opinion in Biotechnology* 18(4), 333–340 (2007).
- [40] A. Harding, T. Tian, E. Westbury, and others. Subcellular Localization Determines MAP Kinase Signal Output. *Current biology* 15(9), 869–873 (2005).
- [41] B. N. Kholodenko, J. F. Hancock, and W. Kolch. Signalling ballet in space and time. *Nature reviews. Molecular cell biology* 11(6), 414–426 (2010).
- [42] J. Krishnan, L. Lu, and A. Alam Nazki. The interplay of spatial organization and biochemistry in building blocks of cellular signalling pathways. *Journal of The Royal Society Interface* 17(166), 20200251 (2020).
- [43] L. J. Sweetlove and A. R. Fernie. The Spatial Organization of Metabolism Within the Plant Cell. *Annual Review of Plant Biology* 64(1), 723–746 (2013).

- [44] Y. Wu, H. Zhang, and E. E. Griffin. Coupling between cytoplasmic concentration gradients through local control of protein mobility in the *Caenorhabditis elegans* zygote. *Molecular biology of the cell* 26(17), 2963–2970 (2015).
- [45] S. Schmid, T. Hugel, M. Spies, and others. Controlling protein function by fine-tuning conformational flexibility. *eLife* 9, e57180 (2020).
- [46] A. Bah and J. D. Forman-Kay. Modulation of Intrinsically Disordered Protein Function by Post-translational Modifications. *The Journal of biological chemistry* 291(13), 6696–6705 (2016).
- [47] I. Owen and F. Shewmaker. The Role of Post-Translational Modifications in the Phase Transitions of Intrinsically Disordered Proteins. *International journal of molecular sciences* 20(21) (2019).
- [48] B. Alberts, A. Johnson, J. Lewis, and others. *Molecular biology of the cell*. Garland Science Taylor and Francis Group, 6th edition, (2015).
- [49] O. Dagliyan and K. M. Hahn. Controlling protein conformation with light. *Current opinion in structural biology* 57, 17–22 (2019).
- [50] S. E. Bondos, A. K. Dunker, and V. N. Uversky. On the roles of intrinsically disordered proteins and regions in cell communication and signaling. *Cell Communication and Signaling* 19(1), 88 (2021).
- [51] P. E. Wright and H. J. Dyson. Intrinsically disordered proteins in cellular signalling and regulation. *Nature reviews. Molecular cell biology* 16(1), 18–29 (2015).
- [52] A. A. M. André and E. Spruijt. Liquid-Liquid Phase Separation in Crowded Environments. *International journal of molecular sciences* 21(16) (2020).
- [53] A. K. Dunker, C. J. Brown, J. D. Lawson, and others. Intrinsic Disorder and Protein Function. *Biochemistry* 41(21), 6573–6582 (2002).
- [54] Z. Feng, B. Jia, and M. Zhang. Liquid–Liquid Phase Separation in Biology: Specific Stoichiometric Molecular Interactions vs Promiscuous Interactions Mediated by Disordered Sequences. *Biochemistry* 60(31), 2397–2406 (2021).
- [55] E. Korkmazhan, P. Tompa, and A. R. Dunn. The role of ordered cooperative assembly in biomolecular condensates. *Nature reviews. Molecular cell biology* 22(10), 647–648 (2021).
- [56] Y. Shin, J. Berry, N. Pannucci, and others. Spatiotemporal Control of Intracellular Phase Transitions Using Light-Activated optoDroplets. *Cell* 168(1-2), 159–171.e14 (2017).

- [57] P. E. Wright and H. Dyson. Intrinsically unstructured proteins: re-assessing the protein structure-function paradigm. *Journal of molecular biology* 293(2), 321–331 (1999).
- [58] H. Zhang, X. Ji, P. Li, and others. Liquid-liquid phase separation in biology: mechanisms, physiological functions and human diseases. *Science China. Life sciences* 63(7), 953–985 (2020).
- [59] S. Bhattacharya and X. Lin. Recent Advances in Computational Protocols Addressing Intrinsically Disordered Proteins. *Biomolecules* 9(4) (2019).
- [60] S. E. Bondos, A. K. Dunker, and V. N. Uversky. Intrinsically disordered proteins play diverse roles in cell signaling. *Cell Communication and Signaling* 20(1), 20 (2022).
- [61] P. M. Kim, A. Sboner, Y. Xia, and M. Gerstein. The role of disorder in interaction networks: a structural analysis. *Molecular systems biology* 4, 179 (2008).
- [62] F. Hucho and C. Weise. Ligand-Gated Ion Channels. *Angew. Chem. Int. Ed.* 40(17), 3100–3116 (2001).
- [63] N. L. Absalom, V. W. Liao, and M. Chebib. Ligand-gated ion channels in genetic disorders and the question of efficacy. *The international journal of biochemistry & cell biology* 126, 105806 (2020).
- [64] H. Lodish, A. Berk, C. Kaiser, and others. *Molecular cell biology*. Macmillan International Higher Education, 9th edition, (2021).
- [65] R. T. Dorsam and J. S. Gutkind. G-protein-coupled receptors and cancer. *Nature reviews. Cancer* 7(2), 79–94 (2007).
- [66] S. R. Neves, P. T. Ram, and R. Iyengar. G protein pathways. *Science* 296(5573), 1636–1639 (2002).
- [67] W. I. Weis and B. K. Kobilka. The Molecular Basis of G Protein-Coupled Receptor Activation. *Annual review of biochemistry* 87, 897–919 (2018).
- [68] J. Cherfils and M. Zeghouf. Regulation of small GTPases by GEFs, GAPs, and GDIs. *Physiological reviews* 93(1), 269–309 (2013).
- [69] S. Toma-Fukai and T. Shimizu. Structural Insights into the Regulation Mechanism of Small GTPases by GEFs. *Molecules* 24(18) (2019).
- [70] S. Pudewell, C. Wittich, N. S. Kazeminejad, and others. Accessory proteins of the RAS-MAPK pathway: moving from the side line to the front line. *Communications Biology* 4(1), 696 (2021).
- [71] M. R. Schiller. Coupling receptor tyrosine kinases to Rho GTPases—GEFs what’s the link. *Cellular signalling* 18(11), 1834–1843 (2006).

- [72] S. de Beco, K. Vaidžiulytė, J. Manzi, and others. Optogenetic dissection of Rac1 and Cdc42 gradient shaping. *Nature communications* 9(1), 4816 (2018).
- [73] F. Etoc, D. Lisse, Y. Bellaïche, and others. Subcellular control of Rac-GTPase signalling by magnetogenetic manipulation inside living cells. *Nature nanotechnology* 8(3), 193–198 (2013).
- [74] P. Hannanta-Anan, S. T. Glantz, and B. Y. Chow. Optically inducible membrane recruitment and signaling systems. *Current opinion in structural biology* 57, 84–92 (2019).
- [75] D. Liße, C. Monzel, C. Vicario, and others. Engineered Ferritin for Magnetogenetic Manipulation of Proteins and Organelles Inside Living Cells. *Advanced Materials* 29(42) (2017).
- [76] A. Akinleye, P. Avvaru, M. Furqan, and others. Phosphatidylinositol 3-kinase (PI3K) inhibitors as cancer therapeutics. *Journal of Hematology & Oncology* 6(1), 88 (2013).
- [77] M. V. Sundaram. Canonical RTK-Ras-ERK signaling and related alternative pathways. *WormBook*, 1–38 (2013).
- [78] T. Regad. Targeting RTK Signaling Pathways in Cancer. *Cancers* 7(3), 1758–1784 (2015).
- [79] O. Brandman and T. Meyer. Feedback Loops Shape Cellular Signals in Space and Time. *Science* 322(5900), 390–395 (2008).
- [80] B. N. Kholodenko. Cell-signalling dynamics in time and space. *Nature reviews. Molecular cell biology* 7(3), 165–176 (2006).
- [81] W. Dubitzky, O. Wolkenhauer, K.-H. Cho, and H. Yokota, editors. *Encyclopedia of Systems Biology*. Springer, (2013).
- [82] A. Whitty. Cooperativity and biological complexity. *Nature chemical biology* 4(8), 435–439 (2008).
- [83] S. F. Banani, H. O. Lee, A. A. Hyman, and M. K. Rosen. Biomolecular condensates: organizers of cellular biochemistry. *Nature reviews. Molecular cell biology* 18(5), 285–298 (2017).
- [84] P. A. Chong and J. D. Forman-Kay. Liquid-liquid phase separation in cellular signaling systems. *Current opinion in structural biology* 41, 180–186 (2016).
- [85] A. Jimenez Salinas and Y. K. Lee. In unity, there is strength: Phase separation controls receptor tyrosine kinase signal transduction. *Molecular cell* 82(6), 1081–1083 (2022).

- [86] A. S. Lyon, W. B. Peeples, and M. K. Rosen. A framework for understanding the functions of biomolecular condensates across scales. *Nature reviews. Molecular cell biology* 22(3), 215–235 (2021).
- [87] W. Peeples and M. K. Rosen. Mechanistic dissection of increased enzymatic rate in a phase-separated compartment. *Nature chemical biology* 17(6), 693–702 (2021).
- [88] Y. Shin and C. P. Brangwynne. Liquid phase condensation in cell physiology and disease. *Science* 357(6357) (2017).
- [89] Q. Xiao, C. K. McAtee, and X. Su. Phase separation in immune signalling. *Nature reviews. Immunology* (2021).
- [90] T. Schwarz-Romond, C. Merrifield, B. J. Nichols, and M. Bienz. The Wnt signalling effector Dishevelled forms dynamic protein assemblies rather than stable associations with cytoplasmic vesicles. *Journal of cell science* 118(Pt 22), 5269–5277 (2005).
- [91] R. P. Sear. Dishevelled: a protein that functions in living cells by phase separating. *Soft matter* 3(6), 680–684 (2007).
- [92] Q. Shi, K. Kang, and Y.-G. Chen. Liquid–liquid phase separation drives the b-catenin destruction complex formation. *BioEssays: news and reviews in molecular, cellular and developmental biology* 43(10), 2100138 (2021).
- [93] S. Banjade and M. K. Rosen. Phase transitions of multivalent proteins can promote clustering of membrane receptors. *eLife* 3 (2014).
- [94] L. B. Case, X. Zhang, J. A. Ditlev, and M. K. Rosen. Stoichiometry controls activity of phase-separated clusters of actin signaling proteins. *Science* 363(6431), 1093–1097 (2019).
- [95] P. Li, S. Banjade, H.-C. Cheng, and others. Phase transitions in the assembly of multivalent signalling proteins. *Nature* 483(7389), 336–340 (2012).
- [96] W. Y. C. Huang, S. Alvarez, Y. Kondo, and others. A molecular assembly phase transition and kinetic proofreading modulate Ras activation by SOS. *Science* 363(6431), 1098–1103 (2019).
- [97] A. K. Dunker, M. S. Cortese, P. Romero, and others. Flexible nets. The roles of intrinsic disorder in protein interaction networks. *The FEBS journal* 272(20), 5129–5148 (2005).
- [98] S. Alberti, A. Gladfelter, and T. Mittag. Considerations and Challenges in Studying Liquid-Liquid Phase Separation and Biomolecular Condensates. *Cell* 176(3), 419–434 (2019).

- [99] A. P. Jalihal, A. Schmidt, G. Gao, and others. Hyperosmotic phase separation: Condensates beyond inclusions, granules and organelles. *The Journal of biological chemistry* 296, 100044 (2021).
- [100] A.-O. Vweza, C.-G. Song, and K.-T. Chong. Liquid-Liquid Phase Separation in the Presence of Macromolecular Crowding and State-dependent Kinetics. *International journal of molecular sciences* 22(13) (2021).
- [101] G. L. Dignon, R. B. Best, and J. Mittal. Biomolecular Phase Separation: From Molecular Driving Forces to Macroscopic Properties. *Annual review of physical chemistry* 71, 53–75 (2020).
- [102] D. T. McSwiggen, M. Mir, X. Darzacq, and R. Tjian. Evaluating phase separation in live cells: diagnosis, caveats, and functional consequences. *Genes & Development* 33(23-24), 1619–1634 (2019).
- [103] S. Boeynaems, S. Alberti, N. L. Fawzi, and others. Protein Phase Separation: A New Phase in Cell Biology. *Trends in cell biology* 28(6), 420–435 (2018).
- [104] S. Alberti and D. Dormann. Liquid-Liquid Phase Separation in Disease. *Annual review of genetics* 53, 171–194 (2019).
- [105] S. Elbaum-Garfinkle. Matter over mind: Liquid phase separation and neurodegeneration. *The Journal of biological chemistry* 294(18), 7160–7168 (2019).
- [106] G. A. P. de Oliveira, Y. Cordeiro, J. L. Silva, and T. C. R. G. Vieira. Liquid-liquid phase transitions and amyloid aggregation in proteins related to cancer and neurodegenerative diseases. *Advances in protein chemistry and structural biology* 118, 289–331 (2019).
- [107] T. Vanderweyde, K. Youmans, L. Liu-Yesucevitz, and B. Wolozin. Role of stress granules and RNA-binding proteins in neurodegeneration: a mini-review. *Gerontology* 59(6), 524–533 (2013).
- [108] R. Koningsveld and A. J. Staverman. Liquid-liquid phase separation in multicomponent polymer solutions. *Kolloid-Zeitschrift und Zeitschrift für Polymere* 218(2), 114–124 (1967).
- [109] J.-M. Choi, A. S. Holehouse, and R. V. Pappu. Physical Principles Underlying the Complex Biology of Intracellular Phase Transitions. *Annual review of biophysics* 49, 107–133 (2020).
- [110] E. W. Martin, A. S. Holehouse, I. Peran, and others. Valence and patterning of aromatic residues determine the phase behavior of prion-like domains. *Science* 367(6478), 694–699 (2020).

- [111] C. P. Brangwynne, P. Tompa, and R. V. Pappu. Polymer physics of intracellular phase transitions. *Nature Physics* 11(11), 899–904 (2015).
- [112] Z. Feng, X. Chen, X. Wu, and M. Zhang. Formation of biological condensates via phase separation: Characteristics, analytical methods, and physiological implications. *The Journal of biological chemistry* 294(40), 14823–14835 (2019).
- [113] Y.-H. Lin, J. D. Forman-Kay, and H. S. Chan. Theories for Sequence-Dependent Phase Behaviors of Biomolecular Condensates. *Biochemistry* 57(17), 2499–2508 (2018).
- [114] A. E. Posey, A. S. Holehouse, and R. V. Pappu. Phase Separation of Intrinsically Disordered Proteins. *Methods in enzymology* 611, 1–30 (2018).
- [115] K. K. Turoverov, I. M. Kuznetsova, A. V. Fonin, and others. Stochasticity of Biological Soft Matter: Emerging Concepts in Intrinsically Disordered Proteins and Biological Phase Separation. *Trends in Biochemical Sciences* 44(8), 716–728 (2019).
- [116] R. M. Vernon, P. A. Chong, B. Tsang, and others. Pi-Pi contacts are an overlooked protein feature relevant to phase separation. *eLife* 7 (2018).
- [117] J. Li, M. Zhang, W. Ma, and others. Post-translational modifications in liquid-liquid phase separation: a comprehensive review. *Molecular Biomedicine* 3(1), 13 (2022).
- [118] S. Alberti. The wisdom of crowds: regulating cell function through condensed states of living matter. *Journal of cell science* 130(17), 2789–2796 (2017).
- [119] P. Thandapani, T. R. O’Connor, T. L. Bailey, and S. Richard. Defining the RGG/RG motif. *Molecular cell* 50(5), 613–623 (2013).
- [120] T. P. Dao and C. A. Castañeda. Ubiquitin-Modulated Phase Separation of Shuttle Proteins: Does Condensate Formation Promote Protein Degradation? *BioEssays: news and reviews in molecular, cellular and developmental biology* 42(11), 2000036 (2020).
- [121] L. D. Gallego, M. Schneider, C. Mittal, and others. Phase separation directs ubiquitination of gene-body nucleosomes. *Nature* 579(7800), 592–597 (2020).
- [122] C. Garcia-Cabau and X. Salvatella. Regulation of biomolecular condensate dynamics by signaling. *Current opinion in cell biology* 69, 111–119 (2021).
- [123] C. Xia, Y. Tao, M. Li, and others. Protein acetylation and deacetylation: An important regulatory modification in gene transcription (Review). *Exp Ther Med* 20(4), 2923–2940 (2020).
- [124] S. B. Zimmerman and A. P. Minton. Macromolecular crowding: biochemical, biophysical, and physiological consequences. *Annual review of biophysics and biomolecular structure* 22, 27–65 (1993).

- [125] K. K. Nakashima, M. A. Vibhute, and E. Spruijt. Biomolecular Chemistry in Liquid Phase Separated Compartments. *Frontiers in molecular biosciences* 6, 21 (2019).
- [126] B. G. O’Flynn and T. Mittag. The role of liquid-liquid phase separation in regulating enzyme activity. *Current opinion in cell biology* 69, 70–79 (2021).
- [127] X. Su, J. A. Ditlev, E. Hui, and others. Phase separation of signaling molecules promotes T cell receptor signal transduction. *Science* 352(6285), 595–599 (2016).
- [128] J. A. Riback, C. D. Katanski, J. L. Kear-Scott, and others. Stress-Triggered Phase Separation Is an Adaptive, Evolutionarily Tuned Response. *Cell* 168(6), 1028–1040.e19 (2017).
- [129] T. Inobe and N. Nukina. Rapamycin-induced oligomer formation system of FRB-FKBP fusion proteins. *Journal of bioscience and bioengineering* 122(1), 40–46 (2016).
- [130] K. Krawczyk, S. Xue, P. Buchmann, and others. Electrogenetic cellular insulin release for real-time glycemic control in type 1 diabetic mice. *Science* 368(6494), 993–1001 (2020).
- [131] S. Mangal, J. Zielich, E. Lambie, and E. Zanin. Rapamycin-induced protein dimerization as a tool for *C. elegans* research. *microPublication biology* 2018 (2018).
- [132] Y. Pan, S. Yoon, J. Sun, and others. Mechanogenetics for the remote and noninvasive control of cancer immunotherapy. *Proceedings of the National Academy of Sciences* 115(5), 992–997 (2018).
- [133] S. M. Sternson and B. L. Roth. Chemogenetic tools to interrogate brain functions. *Annual review of neuroscience* 37, 387–407 (2014).
- [134] M. C. Walker and D. M. Kullmann. Optogenetic and chemogenetic therapies for epilepsy. *Neuropharmacology* 168, 107751 (2020).
- [135] F. Etoc, C. Vicario, D. Lisse, and others. Magnetogenetic control of protein gradients inside living cells with high spatial and temporal resolution. *Nano letters* 15(5), 3487–3494 (2015).
- [136] J. E. Toettcher, O. D. Weiner, and W. A. Lim. Using optogenetics to interrogate the dynamic control of signal transmission by the Ras/Erk module. *Cell* 155(6), 1422–1434 (2013).
- [137] L. Dehmelt and P. I. H. Bastiaens. Spatial organization of intracellular communication: insights from imaging. *Nature reviews. Molecular cell biology* 11(6), 440–452 (2010).
- [138] A. Kinkhabwala and P. I. H. Bastiaens. Spatial aspects of intracellular information processing. *Current opinion in genetics & development* 20(1), 31–40 (2010).

- [139] N. Vartak and P. Bastiaens. Spatial cycles in G-protein crowd control. *The EMBO journal* 29(16), 2689–2699 (2010).
- [140] Z. Liu, Y. Liu, Y. Chang, and others. Nanoscale optomechanical actuators for controlling mechanotransduction in living cells. *Nature methods* 13(2), 143–146 (2016).
- [141] J. M. Harris, A. Y.-D. Wang, J. Boulanger-Weill, and others. Long-Range Optogenetic Control of Axon Guidance Overcomes Developmental Boundaries and Defects. *Developmental cell* 53(5), 577–588.e7 (2020).
- [142] B. Hu, A. J. El Haj, and J. Dobson. Receptor-targeted, magneto-mechanical stimulation of osteogenic differentiation of human bone marrow-derived mesenchymal stem cells. *International journal of molecular sciences* 14(9), 19276–19293 (2013).
- [143] D. Seo, K. M. Southard, J.-W. Kim, and others. A Mechanogenetic Toolkit for Interrogating Cell Signaling in Space and Time. *Cell* 165(6), 1507–1518 (2016).
- [144] S. A. Stanley, J. Sauer, R. S. Kane, and others. Remote regulation of glucose homeostasis in mice using genetically encoded nanoparticles. *Nature medicine* 21(1), 92–98 (2015).
- [145] Y. I. Wu, D. Frey, O. I. Lungu, and others. A genetically encoded photoactivatable Rac controls the motility of living cells. *Nature* 461(7260), 104–108 (2009).
- [146] P. van Bergeijk, M. Adrian, C. C. Hoogenraad, and L. C. Kapitein. Optogenetic control of organelle transport and positioning. *Nature* 518(7537), 111–114 (2015).
- [147] H. Schöneborn, F. Raudzus, M. Coppey, and others. Perspectives of RAS and RHEB GTPase Signaling Pathways in Regenerating Brain Neurons. *International journal of molecular sciences* 19(12) (2018).
- [148] G. Spagnuolo, F. Genovese, L. Fortunato, and others. The Impact of Optogenetics on Regenerative Medicine. *Applied Sciences* 10(1), 173 (2020).
- [149] G. C. R. Ellis-Davies. Caged compounds: photorelease technology for control of cellular chemistry and physiology. *Nature Methods* 4(8), 619–628 (2007).
- [150] J.H. Kaplan and A.P. Somlyo. Flash photolysis of caged compounds: New tools for cellular physiology. *Trends in Neurosciences* 12(2), 54–59 (1989).
- [151] D. Tischer and O. D. Weiner. Illuminating cell signalling with optogenetic tools. *Nature reviews. Molecular cell biology* 15(8), 551–558 (2014).
- [152] A. Gautier, C. Gauron, M. Volovitch, and others. How to control proteins with light in living systems. *Nature chemical biology* 10(7), 533–541 (2014).

- [153] G. Guntas, R. A. Hallett, S. P. Zimmerman, and others. Engineering an improved light-induced dimer (iLID) for controlling the localization and activity of signaling proteins. *Proceedings of the National Academy of Sciences of the United States of America* 112(1), 112–117 (2015).
- [154] F. Kawano, H. Suzuki, A. Furuya, and M. Sato. Engineered pairs of distinct photo-switches for optogenetic control of cellular proteins. *Nature communications* 6, 6256 (2015).
- [155] M. J. Kennedy, R. M. Hughes, L. A. Peteya, and others. Rapid blue-light-mediated induction of protein interactions in living cells. *Nature methods* 7(12), 973–975 (2010).
- [156] S. T. Glantz, E. E. Berlew, Z. Jaber, and others. Directly light-regulated binding of RGS-LOV photoreceptors to anionic membrane phospholipids. *Proceedings of the National Academy of Sciences* 115(33), E7720–E7727 (2018).
- [157] L. He, J. Jing, L. Zhu, and others. Optical control of membrane tethering and interorganellar communication at nanoscales. *Chemical Science* 8(8), 5275–5281 (2017).
- [158] S. Shimizu-Sato, E. Huq, J. M. Tepperman, and P. H. Quail. A light-switchable gene promoter system. *Nature biotechnology* 20(10), 1041–1044 (2002).
- [159] L. J. Bugaj, A. T. Choksi, C. K. Mesuda, and others. Optogenetic protein clustering and signaling activation in mammalian cells. *Nature Methods* 10(3), 249–252 (2013).
- [160] X. X. Zhou, H. K. Chung, A. J. Lam, and M. Z. Lin. Optical control of protein activity by fluorescent protein domains. *Science* 338(6108), 810–814 (2012).
- [161] S. Beck, J. Yu-Strzelczyk, D. Pauls, and others. Synthetic Light-Activated Ion Channels for Optogenetic Activation and Inhibition. *Frontiers in neuroscience* 12, 643 (2018).
- [162] A. Guru, R. J. Post, Y.-Y. Ho, and M. R. Warden. Making Sense of Optogenetics. *The international journal of neuropsychopharmacology* 18(11), pyv079 (2015).
- [163] B. R. Rost, F. Schneider-Warme, D. Schmitz, and P. Hegemann. Optogenetic Tools for Subcellular Applications in Neuroscience. *Neuron* 96(3), 572–603 (2017).
- [164] M. Ni, J. M. Tepperman, and P. H. Quail. Binding of phytochrome B to its nuclear signalling partner PIF3 is reversibly induced by light. *Nature* 400(6746), 781–784 (1999).
- [165] Y. Uda, Y. Goto, S. Oda, and others. Efficient synthesis of phycocyanobilin in mammalian cells for optogenetic control of cell signaling. *Proceedings of the National Academy of Sciences of the United States of America* 114(45), 11962–11967 (2017).

- [166] E. E. Berlew, I. A. Kuznetsov, K. Yamada, and others. Optogenetic Rac1 engineered from membrane lipid-binding RGS-LOV for inducible lamellipodia formation. *Photochemical & photobiological sciences: Official journal of the European Photochemistry Association and the European Society for Photobiology* 19(3), 353–361 (2020).
- [167] W. Benman, E. E. Berlew, H. Deng, and others. Temperature-responsive optogenetic probes of cell signaling. *Nature chemical biology* 18(2), 152–160 (2022).
- [168] M. Bongaerts, K. Aizel, E. Secret, and others. Parallelized Manipulation of Adherent Living Cells by Magnetic Nanoparticles-Mediated Forces. *International journal of molecular sciences* 21(18) (2020).
- [169] S. Del Sol-Fernández, P. Martínez-Vicente, P. Gomollón-Zueco, and others. Magnetogenetics: remote activation of cellular functions triggered by magnetic switches. *Nanoscale* 14(6), 2091–2118 (2022).
- [170] X. Long, J. Ye, Di Zhao, and S.-J. Zhang. Magnetogenetics: remote non-invasive magnetic activation of neuronal activity with a magnetoreceptor. *Science Bulletin* 60(24), 2107–2119 (2015).
- [171] S. Nimpf and D. A. Keays. Is magnetogenetics the new optogenetics? *The EMBO journal* 36(12), 1643–1646 (2017).
- [172] M. I. Brier and J. S. Dordick. Remote activation of cellular signaling. *Science* 368(6494), 936–937 (2020).
- [173] S. Chen, A. Z. Weitemier, X. Zeng, and others. Near-infrared deep brain stimulation via upconversion nanoparticle-mediated optogenetics. *Science* 359(6376), 679–684 (2018).
- [174] N. Yu, L. Huang, Y. Zhou, and others. Near-Infrared-Light Activatable Nanoparticles for Deep-Tissue-Penetrating Wireless Optogenetics. *Advanced healthcare materials* 8(6), e1801132 (2019).
- [175] C. Wu, Y. Shen, M. Chen, and others. Recent Advances in Magnetic-Nanomaterial-Based Mechanotransduction for Cell Fate Regulation. *Advanced Materials* 30(17), 1705673 (2018).
- [176] P. Anikeeva and A. Jasanoff. Problems on the back of an envelope. *eLife* 5 (2016).
- [177] M. Meister and D. E. Clapham. Physical limits to magnetogenetics. *eLife* 5, e17210 (2016).
- [178] T. J. Gahl and A. Kunze. Force-Mediating Magnetic Nanoparticles to Engineer Neuronal Cell Function. *Frontiers in neuroscience* 12 (2018).

- [179] H. Huang, S. Delikanli, H. Zeng, and others. Remote control of ion channels and neurons through magnetic-field heating of nanoparticles. *Nature nanotechnology* 5(8), 602–606 (2010).
- [180] R. Munshi, S. M. Qadri, Q. Zhang, and others. Magnetothermal genetic deep brain stimulation of motor behaviors in awake, freely moving mice. *eLife* 6, e27069 (2017).
- [181] Sarah A Stanley, Jeremy Sauer, Ravi S Kane, and others. Remote regulation of glucose homeostasis in mice using genetically encoded nanoparticles. *Nature medicine* (21), 92–98 (2014).
- [182] S. A. Stanley, J. E. Gagner, S. Damanpour, and others. Radio-wave heating of iron oxide nanoparticles can regulate plasma glucose in mice. *Science* 336(6081), 604–608 (2012).
- [183] L. Fenno, O. Yizhar, and K. Deisseroth. The Development and Application of Optogenetics. *Annual review of neuroscience* 34(1), 389–412 (2011).
- [184] A. Pekarsky and O. Spadiut. Intrinsically Magnetic Cells: A Review on Their Natural Occurrence and Synthetic Generation. *Frontiers in bioengineering and biotechnology* 8, 573183 (2020).
- [185] A. Tajik, Y. Zhang, F. Wei, and others. Transcription upregulation via force-induced direct stretching of chromatin. *Nature materials* 15(12), 1287–1296 (2016).
- [186] M. A. Wheeler, C. J. Smith, M. Ottolini, and others. Genetically targeted magnetic control of the nervous system. *Nature neuroscience* 19(5), 756–761 (2016).
- [187] C. Cao, L. Tian, Q. Liu, and others. Magnetic characterization of noninteracting, randomly oriented, nanometer-scale ferrimagnetic particles. *Journal of Geophysical Research* 115(B7), 589 (2010).
- [188] Le Xue, D. Deng, and J. Sun. Magnetoferritin: Process, Prospects, and Their Biomedical Applications. *International journal of molecular sciences* 20(10) (2019).
- [189] T. L. Li, Z. Wang, H. You, and others. Engineering a Genetically Encoded Magnetic Protein Crystal. *Nano letters* 19(10), 6955–6963 (2019).
- [190] F. C. Meldrum, B. R. Heywood, and S. Mann. Magnetoferritin: in vitro synthesis of a novel magnetic protein. *Science* 257(5069), 522–523 (1992).
- [191] K. K. W. Wong, T. Douglas, S. Gider, and others. Biomimetic Synthesis and Characterization of Magnetic Proteins (Magnetoferritin). *Chemistry of Materials* 10(1), 279–285 (1998).
- [192] M. G. Walls, C. Cao, K. Yu-Zhang, and others. Identification of ferrous-ferric Fe₃O₄ nanoparticles in recombinant human ferritin cages. *Microscopy and microanalysis*:

- the official journal of Microscopy Society of America, Microbeam Analysis Society, Microscopical Society of Canada 19(4), 835–841 (2013).
- [193] H. Schöneborn, F. Raudzus, E. Secret, and others. Novel Tools towards Magnetic Guidance of Neurite Growth: (I) Guidance of Magnetic Nanoparticles into Neurite Extensions of Induced Human Neurons and In Vitro Functionalization with RAS Regulating Proteins. *Journal of functional biomaterials* 10(3) (2019).
- [194] T. T. T. N’Guyen, H. T. T. Duong, J. Basuki, and others. Functional iron oxide magnetic nanoparticles with hyperthermia-induced drug release ability by using a combination of orthogonal click reactions. *Angew. Chem. Int. Ed.* 52(52), 14152–14156 (2013).
- [195] A. Riedinger, P. Guardia, A. Curcio, and others. Subnanometer local temperature probing and remotely controlled drug release based on azo-functionalized iron oxide nanoparticles. *Nano letters* 13(6), 2399–2406 (2013).
- [196] Q. Yang, M. Gong, S. Cai, and others. Combining hard and soft magnetism into a single core-shell nanoparticle to achieve both hyperthermia and image contrast. *Therapeutic delivery* 6(10), 1195–1210 (2015).
- [197] S. Chakraborti and P. Chakrabarti. Self-Assembly of Ferritin: Structure, Biological Function and Potential Applications in Nanotechnology. *Advances in experimental medicine and biology* 1174, 313–329 (2019).
- [198] A. A. Bharde, R. Palankar, C. Fritsch, and others. Magnetic nanoparticles as mediators of ligand-free activation of EGFR signaling. *PloS one* 8(7), e68879 (2013).
- [199] M. H. Cho, E. J. Lee, M. Son, and others. A magnetic switch for the control of cell death signalling in in vitro and in vivo systems. *Nature materials* 11(12), 1038–1043 (2012).
- [200] C. Hoffmann, E. Mazari, S. Lallet, and others. Spatiotemporal control of microtubule nucleation and assembly using magnetic nanoparticles. *Nature nanotechnology* 8(3), 199–205 (2013).
- [201] H. Kagiwada, C. Nakamura, T. Kihara, and others. The mechanical properties of a cell, as determined by its actin cytoskeleton, are important for nanoneedle insertion into a living cell. *Cytoskeleton* 67(8), 496–503 (2010).
- [202] K. Murase, T. Fujiwara, Y. Umemura, and others. Ultrafine membrane compartments for molecular diffusion as revealed by single molecule techniques. *Biophysical Journal* 86(6), 4075–4093 (2004).
- [203] A. Mehidi, O. Rossier, M. Schaks, and others. Transient Activations of Rac1 at the Lamellipodium Tip Trigger Membrane Protrusion. *Current biology: CB* 29(17), 2852–2866.e5 (2019).

- [204] C. D. Nobes and A. Hall. Rho GTPases control polarity, protrusion, and adhesion during cell movement. *The Journal of cell biology* 144(6), 1235–1244 (1999).
- [205] A. J. Ridley. Rho family proteins: coordinating cell responses. *Trends in cell biology* 11(12), 471–477 (2001).
- [206] T. Arendt, U. Gärtner, G. Seeger, and others. Neuronal activation of Ras regulates synaptic connectivity. *The European journal of neuroscience* 19(11), 2953–2966 (2004).
- [207] R. Avraham and Y. Yarden. Feedback regulation of EGFR signalling: decision making by early and delayed loops. *Nature reviews. Molecular cell biology* 12(2), 104–117 (2011).
- [208] S. M. Christensen, H.-L. Tu, J. E. Jun, and others. One-way membrane trafficking of SOS in receptor-triggered Ras activation. *Nature structural & molecular biology* 23(9), 838–846 (2016).
- [209] R. Heumann, C. Goemans, D. Bartsch, and others. Transgenic activation of Ras in neurons promotes hypertrophy and protects from lesion-induced degeneration. *Journal of Cell Biology* 151(7), 1537–1548 (2000).
- [210] J. E. Jun, I. Rubio, and J. P. Roose. Regulation of Ras exchange factors and cellular localization of Ras activation by lipid messengers in T cells. *Frontiers in immunology* 4, 239 (2013).
- [211] C. Lamaze and I. Prior. *Endocytosis and Signaling*, volume 57. Springer International Publishing, Cham, (2018).
- [212] G. Seeger, U. Gärtner, and T. Arendt. Transgenic activation of Ras in neurons increases synapse formation in mouse neocortex. *Journal of neural transmission* 112(6), 751–761 (2005).
- [213] A. A. Belanova, N. Gavalas, Y. M. Makarenko, and others. Physicochemical Properties of Magnetic Nanoparticles: Implications for Biomedical Applications In Vitro and In Vivo. *Oncology research and treatment* 41(3), 139–143 (2018).
- [214] J. T. Kemshead and J. Ugelstad. Magnetic separation techniques: their application to medicine. *Molecular and cellular biochemistry* 67(1), 11–18 (1985).
- [215] G. M. Whitesides, R. J. Kazlauskas, and L. Josephson. Magnetic separations in biotechnology. *Trends in biotechnology* 1(5), 144–148 (1983).
- [216] M. Kuhara, H. Takeyama, T. Tanaka, and T. Matsunaga. Magnetic cell separation using antibody binding with protein a expressed on bacterial magnetic particles. *Analytical chemistry* 76(21), 6207–6213 (2004).

- [217] K. E. McCloskey, J. J. Chalmers, and M. Zborowski. Magnetic cell separation: characterization of magnetophoretic mobility. *Analytical chemistry* 75(24), 6868–6874 (2003).
- [218] E. Tombácz, R. Turcu, V. Socoliuc, and L. Vékás. Magnetic iron oxide nanoparticles: Recent trends in design and synthesis of magnetoresponsive nanosystems. *Biochemical and biophysical research communications* 468(3), 442–453 (2015).
- [219] M. Zborowski and J. J. Chalmers. Rare cell separation and analysis by magnetic sorting. *Analytical chemistry* 83(21), 8050–8056 (2011).
- [220] F. Dilnawaz, A. Singh, C. Mohanty, and S. K. Sahoo. Dual drug loaded superparamagnetic iron oxide nanoparticles for targeted cancer therapy. *Biomaterials* 31(13), 3694–3706 (2010).
- [221] C. Heneweer, S. E. M. Gendy, and O. Peñate-Medina. Liposomes and inorganic nanoparticles for drug delivery and cancer imaging. *Therapeutic delivery* 3(5), 645–656 (2012).
- [222] J. Huang, Y. Li, A. Orza, and others. Magnetic Nanoparticle Facilitated Drug Delivery for Cancer Therapy with Targeted and Image-Guided Approaches. *Advanced functional materials* 26(22), 3818–3836 (2016).
- [223] A. Avasthi, C. Caro, E. Pozo-Torres, and others. Magnetic Nanoparticles as MRI Contrast Agents. *Topics in current chemistry (Cham)* 378(3), 40 (2020).
- [224] J. W. M. Bulte. Superparamagnetic iron oxides as MPI tracers: A primer and review of early applications. *Advanced drug delivery reviews* 138, 293–301 (2019).
- [225] P. Das, M. Colombo, and D. Prosperi. Recent advances in magnetic fluid hyperthermia for cancer therapy. *Colloids and surfaces. B, Biointerfaces* 174, 42–55 (2019).
- [226] J. Jose, R. Kumar, S. Harilal, and others. Magnetic nanoparticles for hyperthermia in cancer treatment: an emerging tool. *Environmental science and pollution research international* 27(16), 19214–19225 (2020).
- [227] D. Liu, Y. Hong, Y. Li, and others. Targeted destruction of cancer stem cells using multifunctional magnetic nanoparticles that enable combined hyperthermia and chemotherapy. *Theranostics* 10(3), 1181–1196 (2020).
- [228] I. M. Obaidat, B. Issa, and Y. Haik. Magnetic Properties of Magnetic Nanoparticles for Efficient Hyperthermia. *Nanomaterials* 5(1), 63–89 (2015).
- [229] V. F. Cardoso, A. Francesko, C. Ribeiro, and others. Advances in Magnetic Nanoparticles for Biomedical Applications. *Advanced Healthcare Materials* 7(5), 1700845 (2018).

- [230] J.-H. Lee, E. S. Kim, M. H. Cho, and others. Artificial control of cell signaling and growth by magnetic nanoparticles. *Angew. Chem. Int. Ed.* 49(33), 5698–5702 (2010).
- [231] G. Ali Mansoori and T. A. Fauzi Soelaiman. Nanotechnology – An Introduction for the Standards Community. *Journal of ASTM International* 2(6) (2005).
- [232] ISO/TS 80004-2:2015. Nanotechnologies - Vocabulary - Part 2: Nano-objects.
- [233] G. Hodes. When Small Is Different: Some Recent Advances in Concepts and Applications of Nanoscale Phenomena. *Advanced Materials* 19(5), 639–655 (2007).
- [234] M. Kopp, S. Kollenda, and M. Epple. Nanoparticle-Protein Interactions: Therapeutic Approaches and Supramolecular Chemistry. *Accounts of chemical research* 50(6), 1383–1390 (2017).
- [235] A. Gnach, T. Lipinski, A. Bednarkiewicz, and others. Upconverting nanoparticles: assessing the toxicity. *Chemical Society reviews* 44(6), 1561–1584 (2015).
- [236] S. Sasidharan, S. Raj, S. Sonawane, and others. Nanomaterial Synthesis: Chemical and Biological Route and Applications. In *Nanomaterials synthesis*, Y. B. Pottathara, editor, Micro & nano technologies series, 27–51. Elsevier (2019).
- [237] M. Faraji, Y. Yamini, and M. Rezaee. Magnetic nanoparticles: Synthesis, stabilization, functionalization, characterization, and applications. *Journal of the Iranian Chemical Society* 7(1), 1–37 (2010).
- [238] T. D. Schladt, K. Schneider, H. Schild, and W. Tremel. Synthesis and bio-functionalization of magnetic nanoparticles for medical diagnosis and treatment. *Dalton Transactions* 40(24), 6315–6343 (2011).
- [239] W. Wu, Q. He, and C. Jiang. Magnetic iron oxide nanoparticles: synthesis and surface functionalization strategies. *Nanoscale research letters* 3(11), 397–415 (2008).
- [240] J. Fresnais, J.-F. Berret, B. Frka-Petesic, and others. Electrostatic Co-Assembly of Iron Oxide Nanoparticles and Polymers: Towards the Generation of Highly Persistent Superparamagnetic Nanorods. *Advanced materials (Deerfield Beach, Fla.)* 20(20), 3877–3881 (2008).
- [241] J. Fresnais, C. Lavelle, and J. F. Berret. Nanoparticle aggregation controlled by desalting kinetics. *Journal of Physical Chemistry C* 113 (2009).
- [242] M. Mahmoudi, H. Hofmann, B. Rothen-Rutishauser, and A. Petri-Fink. Assessing the in vitro and in vivo toxicity of superparamagnetic iron oxide nanoparticles. *Chemical reviews* 112(4), 2323–2338 (2012).

- [243] H. Bannwarth, B. P. Kremer, and A. Schulz. *Basiswissen Physik, Chemie und Biochemie: Vom Atom bis zur Atmung ; für Biologen, Mediziner und Pharmazeuten*. Springer, (2007).
- [244] W. Bergmann. *Werkstofftechnik 2: Werkstoffherstellung, Werkstoffverarbeitung, Werkstoffanwendung*. Carl Hanser Fachbuchverlag, s.l., 4., aktualisierte Aufl. edition, (2009).
- [245] D. Halliday, R. Resnick, and J. Walker. *Halliday Physik*. 3th edition, (2018).
- [246] W. W. Seidel and F. Hahn. *Werkstofftechnik: Werkstoffe - Eigenschaften - Prüfung - Anwendung*. Lernbücher der Technik. Hanser, 11th edition, (2018).
- [247] A. Akbarzadeh, M. Samiei, and S. Davaran. Magnetic nanoparticles: preparation, physical properties, and applications in biomedicine. *Nanoscale research letters* 7(1), 144 (2012).
- [248] J. N. Israelachvili. *Intermolecular and surface forces*. Academic Press, Burlington, MA, 3. ed. edition, (2011).
- [249] Y. Min, M. Akbulut, K. Kristiansen, and others. The role of interparticle and external forces in nanoparticle assembly. *Nature materials* 7(7), 527–538 (2008).
- [250] A. E. Nel, L. Mädler, D. Velegol, and others. Understanding biophysicochemical interactions at the nano-bio interface. *Nature materials* 8(7), 543–557 (2009).
- [251] W. Zhang. Nanoparticle aggregation: principles and modeling. *Advances in experimental medicine and biology* 811, 19–43 (2014).
- [252] K. Binder, P. Virnau, and A. Statt. Perspective: The Asakura Oosawa model: a colloid prototype for bulk and interfacial phase behavior. *The Journal of chemical physics* 141(14), 140901 (2014).
- [253] M. A. Brown, Z. Abbas, A. Kleibert, and others. Determination of Surface Potential and Electrical Double-Layer Structure at the Aqueous Electrolyte-Nanoparticle Interface. *Physical Review X* 6(1) (2016).
- [254] M. Hermansson. The DLVO theory in microbial adhesion. *Colloids and Surfaces B: Biointerfaces* 14(1), 105–119 (1999).
- [255] E. M. V. Hoek and G. K. Agarwal. Extended DLVO interactions between spherical particles and rough surfaces. *Journal of colloid and interface science* 298(1), 50–58 (2006).
- [256] M. Jiao, P. Zhang, J. Meng, and others. Recent advancements in biocompatible inorganic nanoparticles towards biomedical applications. *Biomaterials science* 6(4), 726–745 (2018).

- [257] S. Schöttler, K. Landfester, and V. Mailänder. Controlling the Stealth Effect of Nanocarriers through Understanding the Protein Corona. *Angewandte Chemie (International ed. in English)* 55(31), 8806–8815 (2016).
- [258] J. Wolfram, M. Zhu, Y. Yang, and others. Safety of Nanoparticles in Medicine. *Current drug targets* 16(14), 1671–1681 (2015).
- [259] J. Conde, J. T. Dias, V. Grazú, and others. Revisiting 30 years of biofunctionalization and surface chemistry of inorganic nanoparticles for nanomedicine. *Frontiers in chemistry* 2, 48 (2014).
- [260] R. Thiruppathi, S. Mishra, M. Ganapathy, and others. Nanoparticle Functionalization and Its Potentials for Molecular Imaging. *Advanced science* 4(3), 1600279 (2017).
- [261] F. Zhang, E. Lees, F. Amin, and others. Polymer-coated nanoparticles: a universal tool for biolabelling experiments. *Small* 7(22), 3113–3127 (2011).
- [262] A. H. El-Sagheer and T. Brown. Click chemistry with DNA. *Chemical Society reviews* 39(4), 1388–1405 (2010).
- [263] H. Häkkinen. The gold-sulfur interface at the nanoscale. *Nature chemistry* 4(6), 443–455 (2012).
- [264] B. Derjaguin and L. Landau. Theory of the stability of strongly charged lyophobic sols and of the adhesion of strongly charged particles in solutions of electrolytes. *Progress in Surface Science* 43(1), 30–59 (1993).
- [265] R. D. Requião, L. Fernandes, H. J. A. de Souza, and others. Protein charge distribution in proteomes and its impact on translation. *PLoS computational biology* 13(5), e1005549 (2017).
- [266] Z. Amoozgar and Y. Yeo. Recent advances in stealth coating of nanoparticle drug delivery systems. *Wiley interdisciplinary reviews. Nanomedicine and nanobiotechnology* 4(2), 219–233 (2012).
- [267] S. Y. Fam, C. F. Chee, C. Y. Yong, and others. Stealth Coating of Nanoparticles in Drug-Delivery Systems. *Nanomaterials* 10(4) (2020).
- [268] T. Kopac. Protein corona, understanding the nanoparticle-protein interactions and future perspectives: A critical review. *International journal of biological macromolecules* 169, 290–301 (2021).
- [269] D. E. Owens and N. A. Peppas. Opsonization, biodistribution, and pharmacokinetics of polymeric nanoparticles. *International Journal of Pharmaceutics* 307(1), 93–102 (2006).

- [270] G. Sanità, B. Carrese, and A. Lamberti. Nanoparticle Surface Functionalization: How to Improve Biocompatibility and Cellular Internalization. *Frontiers in molecular biosciences* 7, 587012 (2020).
- [271] S. Schöttler, G. Becker, S. Winzen, and others. Protein adsorption is required for stealth effect of poly(ethylene glycol)- and poly(phosphoester)-coated nanocarriers. *Nature nanotechnology* 11(4), 372–377 (2016).
- [272] W. Xie, Z. Guo, F. Gao, and others. Shape-, size- and structure-controlled synthesis and biocompatibility of iron oxide nanoparticles for magnetic theranostics. *Theranostics* 8(12), 3284–3307 (2018).
- [273] Z. Hussain, S. Khan, M. Imran, and others. PEGylation: a promising strategy to overcome challenges to cancer-targeted nanomedicines: a review of challenges to clinical transition and promising resolution. *Drug delivery and translational research* 9(3), 721–734 (2019).
- [274] M. Schlapschy, U. Binder, C. Börger, and others. PASylation: a biological alternative to PEGylation for extending the plasma half-life of pharmaceutically active proteins. *Protein engineering, design & selection: PEDS* 26(8), 489–501 (2013).
- [275] Y. Zhang, Q. Yin, H. Lu, and others. PEG-Polypeptide Dual Brush Block Copolymers: Synthesis and Application in Nanoparticle Surface PEGylation. *ACS macro letters* 2(9), 809–813 (2013).
- [276] J. V. Jokerst, T. Lobovkina, R. N. Zare, and S. S. Gambhir. Nanoparticle PEGylation for imaging and therapy. *Nanomedicine* 6(4), 715–728 (2011).
- [277] L. Dai, Y. Liu, Z. Wang, and others. One-pot facile synthesis of PEGylated superparamagnetic iron oxide nanoparticles for MRI contrast enhancement. *Materials science & engineering. C, Materials for biological applications* 41, 161–167 (2014).
- [278] C. Lourenco, M. Teixeira, S. Simões, and R. Gaspar. Steric stabilization of nanoparticles: Size and surface properties. *International Journal of Pharmaceutics* 138(1), 1–12 (1996).
- [279] G. V. Los, L. P. Encell, M. G. McDougall, and others. HaloTag: a novel protein labeling technology for cell imaging and protein analysis. *ACS chemical biology* 3(6), 373–382 (2008).
- [280] A. Juillerat, T. Gronemeyer, A. Keppler, and others. Directed Evolution of O6-Alkylguanine-DNA Alkyltransferase for Efficient Labeling of Fusion Proteins with Small Molecules In Vivo. *Chemistry & Biology* 10(4), 313–317 (2003).
- [281] A. Keppler, S. Gendreizig, T. Gronemeyer, and others. A general method for the covalent labeling of fusion proteins with small molecules in vivo. *Nature biotechnology* 21(1), 86–89 (2003).

- [282] Y. Gong and L. Pan. Recent advances in bioorthogonal reactions for site-specific protein labeling and engineering. *Tetrahedron Letters* 56(17), 2123–2132 (2015).
- [283] C. A. Hoelzel and X. Zhang. Visualizing and Manipulating Biological Processes by Using HaloTag and SNAP-Tag Technologies. *Chembiochem: a European journal of chemical biology* 21(14), 1935–1946 (2020).
- [284] R. D’Agata, P. Palladino, and G. Spoto. Streptavidin-coated gold nanoparticles: critical role of oligonucleotides on stability and fractal aggregation. *Beilstein journal of nanotechnology* 8, 1–11 (2017).
- [285] Y. You, S. Lim, and S. Gunasekaran. Streptavidin-Coated Au Nanoparticles Coupled with Biotinylated Antibody-Based Bifunctional Linkers as Plasmon-Enhanced Immunobiosensors. *ACS Applied Nano Materials* 3(2), 1900–1909 (2020).
- [286] J. Helma, M. C. Cardoso, S. Muyldermans, and H. Leonhardt. Nanobodies and recombinant binders in cell biology. *The Journal of cell biology* 209(5), 633–644 (2015).
- [287] S. Muyldermans. Single domain camel antibodies: current status. *Reviews in Molecular Biotechnology* 74(4), 277–302 (2001).
- [288] S. Muyldermans. Nanobodies: natural single-domain antibodies. *Annual review of biochemistry* 82, 775–797 (2013).
- [289] P. C. Fridy, Y. Li, S. Keegan, and others. A robust pipeline for rapid production of versatile nanobody repertoires. *Nature methods* 11(12), 1253–1260 (2014).
- [290] A. Kirchhofer, J. Helma, K. Schmidhals, and others. Modulation of protein properties in living cells using nanobodies. *Nature structural & molecular biology* 17(1), 133–138 (2010).
- [291] M. H. Kubala, O. Kovtun, K. Alexandrov, and B. M. Collins. Structural and thermodynamic analysis of the GFP:GFP-nanobody complex. *Protein science: a publication of the Protein Society* 19(12), 2389–2401 (2010).
- [292] P. Kunz, K. Zinner, N. Mücke, and others. The structural basis of nanobody unfolding reversibility and thermoresistance. *Scientific reports* 8(1), 7934 (2018).
- [293] M. N. Mendoza, M. Jian, M. T. King, and C. L. Brooks. Role of a noncanonical disulfide bond in the stability, affinity, and flexibility of a VHH specific for the *Listeria* virulence factor InlB. *Protein science: a publication of the Protein Society* 29(4), 1004–1017 (2020).
- [294] S. Hansen, J. C. Stüber, P. Ernst, and others. Design and applications of a clamp for Green Fluorescent Protein with picomolar affinity. *Scientific reports* 7(1), 16292 (2017).

- [295] A. Plückthun. Designed ankyrin repeat proteins (DARPs): binding proteins for research, diagnostics, and therapy. *Annual review of pharmacology and toxicology* 55, 489–511 (2015).
- [296] E. Moeendarbary, L. Valon, M. Fritzsche, and others. The cytoplasm of living cells behaves as a poroelastic material. *Nature materials* 12(3), 253–261 (2013).
- [297] F. Etoc, E. Balloul, C. Vicario, and others. Non-specific interactions govern cytosolic diffusion of nanosized objects in mammalian cells. *Nature materials* 17(8), 740–746 (2018).
- [298] A. S. Verkman. Solute and macromolecule diffusion in cellular aqueous compartments. *Trends in Biochemical Sciences* 27(1), 27–33 (2002).
- [299] R. Swaminathan, C. P. Hoang, and A. S. Verkman. Photobleaching recovery and anisotropy decay of green fluorescent protein GFP-S65T in solution and cells: cytoplasmic viscosity probed by green fluorescent protein translational and rotational diffusion. *Biophysical Journal* 72(4), 1900–1907 (1997).
- [300] P. Arosio, R. Ingrassia, and P. Cavadini. Ferritins: a family of molecules for iron storage, antioxidation and more. *Biochimica et biophysica acta* 1790(7), 589–599 (2009).
- [301] M. Truffi, L. Fiandra, L. Sorrentino, and others. Ferritin nanocages: A biological platform for drug delivery, imaging and theranostics in cancer. *Pharmacological research* 107, 57–65 (2016).
- [302] I. Yamashita. Biosupramolecules for nano-devices: biomineralization of nanoparticles and their applications. *Journal of Materials Chemistry* 18(32), 3813 (2008).
- [303] Perrett. *Biological and Bio-inspired Nanomaterials*, volume 1174. Springer Singapore, Singapore, (2019).
- [304] S. Kim, J.-O. Jeon, E. Jun, and others. Designing Peptide Bunches on Nanocage for Bispecific or Superaffinity Targeting. *Biomacromolecules* 17(3), 1150–1159 (2016).
- [305] A. Arakaki, J. Webb, and T. Matsunaga. A novel protein tightly bound to bacterial magnetic particles in *Magnetospirillum magneticum* strain AMB-1. *The Journal of biological chemistry* 278(10), 8745–8750 (2003).
- [306] A. Arakaki, H. Nakazawa, M. Nemoto, and others. Formation of magnetite by bacteria and its application. *Journal of the Royal Society, Interface* 5(26), 977–999 (2008).
- [307] A. Arakaki, F. Masuda, Y. Amemiya, and others. Control of the morphology and size of magnetite particles with peptides mimicking the Mms6 protein from magnetotactic bacteria. *Journal of colloid and interface science* 343(1), 65–70 (2010).

- [308] H. Nudelman and R. Zarivach. Structure prediction of magnetosome-associated proteins. *Frontiers in microbiology* 5, 9 (2014).
- [309] H. Nudelman, Y.-Z. Lee, Y.-L. Hung, and others. Understanding the Biomineralization Role of Magnetite-Interacting Components (MICs) From Magnetotactic Bacteria. *Frontiers in microbiology* 9, 2480 (2018).
- [310] S. S. Staniland and A. E. Rawlings. Crystallizing the function of the magnetosome membrane mineralization protein Mms6. *Biochemical Society Transactions* 44(3), 883–890 (2016).
- [311] M. Tanaka, E. Mazuyama, A. Arakaki, and T. Matsunaga. MMS6 protein regulates crystal morphology during nano-sized magnetite biomineralization in vivo. *The Journal of biological chemistry* 286(8), 6386–6392 (2011).
- [312] A. E. Rawlings, P. Liravi, S. Corbett, and others. Investigating the ferric ion binding site of magnetite biomineralisation protein Mms6. *PloS one* 15(2), e0228708 (2020).
- [313] L. Wang, T. Prozorov, P. E. Palo, and others. Self-assembly and biphasic iron-binding characteristics of Mms6, a bacterial protein that promotes the formation of superparamagnetic magnetite nanoparticles of uniform size and shape. *Biomacromolecules* 13(1), 98–105 (2012).
- [314] A. E. Rawlings, J. P. Bramble, A. M. Hounslow, and others. Ferrous Iron Binding Key to Mms6 Magnetite Biomineralisation: A Mechanistic Study to Understand Magnetite Formation Using pH Titration and NMR Spectroscopy. *Chemistry* 22(23), 7885–7894 (2016).
- [315] V. O. Shipunova, P. A. Kotelnikova, U. F. Aghayeva, and others. Self-assembling nanoparticles biofunctionalized with magnetite-binding protein for the targeted delivery to HER2/neu overexpressing cancer cells. *Journal of Magnetism and Magnetic Materials* 469, 450–455 (2019).
- [316] K. Halbach. Design of permanent multipole magnets with oriented rare earth cobalt material. *Nuclear Instruments and Methods* 169(1), 1–10 (1980).
- [317] K. Wennerberg, K. L. Rossman, and C. J. Der. The Ras superfamily at a glance. *Journal of cell science* 118(Pt 5), 843–846 (2005).
- [318] I. R. Vetter and A. Wittinghofer. The guanine nucleotide-binding switch in three dimensions. *Science* 294(5545), 1299–1304 (2001).
- [319] J. L. Bos, H. Rehmann, and A. Wittinghofer. GEFs and GAPs: Critical elements in the control of small G proteins. *Cell* 129(5), 865–877 (2007).

- [320] J. L. Gray, F. von Delft, and P. E. Brennan. Targeting the Small GTPase Superfamily through Their Regulatory Proteins. *Angewandte Chemie (International ed. in English)* 59(16), 6342–6366 (2020).
- [321] G. W. Reuther and C. J. Der. The Ras branch of small GTPases: Ras family members don't fall far from the tree. *Current opinion in cell biology* 12(2), 157–165 (2000).
- [322] S. Etienne-Manneville and A. Hall. Rho GTPases in cell biology. *Nature* 420(6916), 629–635 (2002).
- [323] J. D. Moore. The Ran-GTPase and cell-cycle control. *BioEssays: news and reviews in molecular, cellular and developmental biology* 23(1), 77–85 (2001).
- [324] Z. Nie, D. S. Hirsch, and P. A. Randazzo. Arf and its many interactors. *Current opinion in cell biology* 15(4), 396–404 (2003).
- [325] S. Lukman, B. J. Grant, A. A. Gorfe, and others. The distinct conformational dynamics of K-Ras and H-Ras A59G. *PLoS computational biology* 6(9) (2010).
- [326] J. Colicelli. Human RAS superfamily proteins and related GTPases. *Science's STKE: signal transduction knowledge environment* 2004(250), RE13 (2004).
- [327] S. Jenrich. Biophysikalische Untersuchungen an Biophysikalische Untersuchungen an GTPasen und ihren Interaktionspartnern. PhD thesis, Ruhr-Universität, Bochum, (2015).
- [328] F. C. Baltanás, N. Zarich, J. M. Rojas-Cabañeros, and E. Santos. SOS GEFs in health and disease. *Biochimica et biophysica acta. Reviews on cancer* 1874(2), 188445 (2020).
- [329] S. Pierre, A.-S. Bats, and X. Coumoul. Understanding SOS (Son of Sevenless). *Biochemical pharmacology* 82(9), 1049–1056 (2011).
- [330] S. M. Margarit, H. Sondermann, B. E. Hall, and others. Structural evidence for feedback activation by Ras.GTP of the Ras-specific nucleotide exchange factor SOS. *Cell* 112(5), 685–695 (2003).
- [331] H. Sondermann, S. M. Soisson, D. Bar-Sagi, and J. Kuriyan. Tandem histone folds in the structure of the N-terminal segment of the ras activator Son of Sevenless. *Structure* 11(12), 1583–1593 (2003).
- [332] J. Gureasko, O. Kuchment, D. L. Makino, and others. Role of the histone domain in the autoinhibition and activation of the Ras activator Son of Sevenless. *Proceedings of the National Academy of Sciences of the United States of America* 107(8), 3430–3435 (2010).
- [333] H. Sondermann, S. M. Soisson, S. Boykevisch, and others. Structural analysis of autoinhibition in the Ras activator Son of sevenless. *Cell* 119(3), 393–405 (2004).

- [334] T. Shi, M. Niepel, J. E. McDermott, and others. Conservation of protein abundance patterns reveals the regulatory architecture of the EGFR-MAPK pathway. *Science signaling* 9(436), rs6–rs6 (2016).
- [335] M. Burotto, V. L. Chiou, J.-M. Lee, and E. C. Kohn. The MAPK pathway across different malignancies: a new perspective. *Cancer* 120(22), 3446–3456 (2014).
- [336] H. K. Bid, R. D. Roberts, P. K. Manchanda, and P. J. Houghton. RAC1: an emerging therapeutic option for targeting cancer angiogenesis and metastasis. *Molecular cancer therapeutics* 12(10), 1925–1934 (2013).
- [337] M. Innocenti. New insights into the formation and the function of lamellipodia and ruffles in mesenchymal cell migration. *Cell adhesion & migration* 12(5), 401–416 (2018).
- [338] H. Marei and A. Malliri. GEFs: Dual regulation of Rac1 signaling. *Small GTPases* 8(2), 90–99 (2017).
- [339] S. J. Heasman and A. J. Ridley. Mammalian Rho GTPases: new insights into their functions from in vivo studies. *Nature reviews. Molecular cell biology* 9(9), 690–701 (2008).
- [340] A. Hall. Rho GTPases and the control of cell behaviour. *Biochemical Society Transactions* 33(5) (2005).
- [341] S.-T. Sit and E. Manser. Rho GTPases and their role in organizing the actin cytoskeleton. *Journal of cell science* 124(Pt 5), 679–683 (2011).
- [342] M. C. Parrini, M. Matsuda, and J. de Gunzburg. Spatiotemporal regulation of the Pak1 kinase. *Biochemical Society Transactions* 33(Pt 4), 646–648 (2005).
- [343] H. He and N. Huynh. p21-activated kinase family: promising new drug targets. *Research and Reports in Biochemistry* (5), 119 (2015).
- [344] T. Y. Prudnikova, S. J. Rawat, and J. Chernoff. Molecular pathways: targeting the kinase effectors of RHO-family GTPases. *Clinical cancer research: an official journal of the American Association for Cancer Research* 21(1), 24–29 (2015).
- [345] F. G. Buchanan, C. M. Elliot, M. Gibbs, and J. H. Exton. Translocation of the Rac1 guanine nucleotide exchange factor Tiam1 induced by platelet-derived growth factor and lysophosphatidic acid. *The Journal of biological chemistry* 275(13), 9742–9748 (2000).
- [346] M. E. Minard, L.-S. Kim, J. E. Price, and G. E. Gallick. The role of the guanine nucleotide exchange factor Tiam1 in cellular migration, invasion, adhesion and tumor progression. *Breast cancer research and treatment* 84(1), 21–32 (2004).

- [347] A. E. Mertens, R. C. Roovers, and J. G. Collard. Regulation of Tiam1-Rac signalling. *FEBS Letters* 546(1), 11–16 (2003).
- [348] Z. Xu, L. Gakhar, F. E. Bain, and others. The Tiam1 guanine nucleotide exchange factor is auto-inhibited by its pleckstrin homology coiled-coil extension domain. *The Journal of biological chemistry* 292(43), 17777–17793 (2017).
- [349] F. Michiels, J. C. Stam, P. L. Hordijk, and others. Regulated membrane localization of Tiam1, mediated by the NH2-terminal pleckstrin homology domain, is required for Rac-dependent membrane ruffling and C-Jun NH2-terminal kinase activation. *Journal of Cell Biology* 137(2), 387–398 (1997).
- [350] A. Hall and G. Lalli. Rho and Ras GTPases in axon growth, guidance, and branching. *Cold Spring Harbor perspectives in biology* 2(2), a001818 (2010).
- [351] L. Chen, G. Liao, R. R. Waclaw, and others. Rac1 controls the formation of midline commissures and the competency of tangential migration in ventral telencephalic neurons. *The Journal of neuroscience: the official journal of the Society for Neuroscience* 27(14), 3884–3893 (2007).
- [352] Z. L. Hua, F. E. Emiliani, and J. Nathans. Rac1 plays an essential role in axon growth and guidance and in neuronal survival in the central and peripheral nervous systems. *Neural development* 10, 21 (2015).
- [353] G. J. Bashaw, H. Hu, C. D. Nobes, and C. S. Goodman. A novel Dbl family RhoGEF promotes Rho-dependent axon attraction to the central nervous system midline in *Drosophila* and overcomes Robo repulsion. *The Journal of cell biology* 155(7), 1117–1122 (2001).
- [354] N. Kaufmann, Z. P. Wills, and D. van Vactor. *Drosophila* Rac1 controls motor axon guidance. *Development* 125(3), 453–461 (1998).
- [355] J. Ng, T. Nardine, M. Harms, and others. Rac GTPases control axon growth, guidance and branching. *Nature* 416(6879), 442–447 (2002).
- [356] M. L. Ruchhoeft, S.-i. Ohnuma, L. McNeill, and others. The Neuronal Architecture of *Xenopus* Retinal Ganglion Cells Is Sculpted by Rho-Family GTPases In Vivo. *The Journal of Neuroscience* 19(19), 8454–8463 (1999).
- [357] X.-b. Yuan, M. Jin, X. Xu, and others. Signalling and crosstalk of Rho GTPases in mediating axon guidance. *Nature cell biology* 5(1), 38–45 (2003).
- [358] I. D. Zipkin, R. M. Kindt, and C. J. Kenyon. Role of a New Rho Family Member in Cell Migration and Axon Guidance in *C. elegans*. *Cell* 90(5), 883–894 (1997).
- [359] M. Fivaz, S. Bandara, T. Inoue, and T. Meyer. Robust neuronal symmetry breaking by Ras-triggered local positive feedback. *Current biology: CB* 18(1), 44–50 (2008).

- [360] M. Gammons and M. Bienz. Multiprotein complexes governing Wnt signal transduction. *Current opinion in cell biology* 51, 42–49 (2018).
- [361] M. V. Gammons, M. Renko, C. M. Johnson, and others. Wnt Signalosome Assembly by DEP Domain Swapping of Dishevelled. *Molecular cell* 64(1), 92–104 (2016).
- [362] C. Gao and Y.-G. Chen. Dishevelled: The hub of Wnt signaling. *Cellular signalling* 22(5), 717–727 (2010).
- [363] A. Kafka, S. Bašić-Kinda, and N. Pećina-Šlaus. The cellular story of dishevelleds. *Croatian medical journal* 55(5), 459–467 (2014).
- [364] W. Kan, M. D. Enos, E. Korkmazhan, and others. Limited dishevelled/Axin oligomerization determines efficiency of Wnt/b-catenin signal transduction. *eLife* 9 (2020).
- [365] C. Y. Logan and R. Nusse. The Wnt signaling pathway in development and disease. *Annual review of cell and developmental biology* 20, 781–810 (2004).
- [366] K. N. Schaefer and M. Peifer. Wnt/Beta-Catenin Signaling Regulation and a Role for Biomolecular Condensates. *Developmental cell* 48(4), 429–444 (2019).
- [367] M. Sharma, I. Castro-Piedras, G. E. Simmons, and K. Pruitt. Dishevelled: A masterful conductor of complex Wnt signals. *Cellular signalling* 47, 52–64 (2018).
- [368] X. Song, S. Wang, and L. Li. New insights into the regulation of Axin function in canonical Wnt signaling pathway. *Protein & cell* 5(3), 186–193 (2014).
- [369] K. Yamanishi, M. Fiedler, S.-I. Terawaki, and others. A direct heterotypic interaction between the DIX domains of Dishevelled and Axin mediates signaling to b-catenin. *Science signaling* 12(611) (2019).
- [370] S. Patel, A. Alam, R. Pant, and S. Chattopadhyay. Wnt Signaling and Its Significance Within the Tumor Microenvironment: Novel Therapeutic Insights. *Frontiers in immunology* 10, 2872 (2019).
- [371] L. B. Case, J. A. Ditlev, and M. K. Rosen. Regulation of Transmembrane Signaling by Phase Separation. *Annual review of biophysics* 48, 465–494 (2019).
- [372] S. Bayda, M. Adeel, T. Tuccinardi, and others. The History of Nanoscience and Nanotechnology: From Chemical-Physical Applications to Nanomedicine. *Molecules* 25(1) (2019).
- [373] M. Bienz. Signalosome assembly by domains undergoing dynamic head-to-tail polymerization. *Trends in Biochemical Sciences* 39(10), 487–495 (2014).
- [374] T. Schwarz-Romond, M. Fiedler, N. Shibata, and others. The DIX domain of Dishevelled confers Wnt signaling by dynamic polymerization. *Nature structural & molecular biology* 14(6), 484–492 (2007).

- [375] S.-L. Lai, A. J. Chien, and R. T. Moon. Wnt/Fz signaling and the cytoskeleton: potential roles in tumorigenesis. *Cell Research* 19(5), 532–545 (2009).
- [376] I. Spaan, R. A. Raymakers, A. van de Stolpe, and V. Peperzak. Wnt signaling in multiple myeloma: a central player in disease with therapeutic potential. *Journal of Hematology & Oncology* 11(1), 67 (2018).
- [377] X.-q. Gan, J.-y. Wang, Y. Xi, and others. Nuclear Dvl, c-Jun, beta-catenin, and TCF form a complex leading to stabilization of beta-catenin-TCF interaction. *The Journal of cell biology* 180(6), 1087–1100 (2008).
- [378] K. Itoh, B. K. Brott, G.-U. Bae, and others. Nuclear localization is required for Dishevelled function in Wnt/beta-catenin signaling. *Journal of biology* 4(1), 3 (2005).
- [379] W. Wang, X. Li, M. Lee, and others. FOXKs promote Wnt/b-catenin signaling by translocating DVL into the nucleus. *Developmental cell* 32(6), 707–718 (2015).
- [380] M. Allen, D. Willits, J. Mosolf, and others. Protein Cage Constrained Synthesis of Ferrimagnetic Iron Oxide Nanoparticles. *Advanced materials (Deerfield Beach, Fla.)* 14(21), 1562–1565 (2002).
- [381] N. Komatsu, K. Aoki, M. Yamada, and others. Development of an optimized backbone of FRET biosensors for kinases and GTPases. *Molecular biology of the cell* 22(23), 4647–4656 (2011).
- [382] H.-w. Ai, J. N. Henderson, S. J. Remington, and R. E. Campbell. Directed evolution of a monomeric, bright and photostable version of *Clavularia cyan* fluorescent protein: Structural characterization and applications in fluorescence imaging. *The Biochemical journal* 400(3), 531–540 (2006).
- [383] B. Bajar, E. Wang, S. Zhang, and others. A Guide to Fluorescent Protein FRET Pairs. *Sensors* 16(9), 1488 (2016).
- [384] T. J. Lambert. FPbase: a community-editable fluorescent protein database. *Nature Methods* 16(4), 277–278 (2019).
- [385] R. S. Molina, T. M. Tran, R. E. Campbell, and others. Blue-Shifted Green Fluorescent Protein Homologues Are Brighter than Enhanced Green Fluorescent Protein under Two-Photon Excitation. *The journal of physical chemistry letters* 8(12), 2548–2554 (2017).
- [386] N. C. Shaner, G. G. Lambert, A. Chamma, and others. A bright monomeric green fluorescent protein derived from *Branchiostoma lanceolatum*. *Nature methods* 10(5), 407–409 (2013).

- [387] F. Steiert, E. P. Petrov, P. Schultz, and others. Photophysical Behavior of mNeon-Green, an Evolutionarily Distant Green Fluorescent Protein. *Biophysical Journal* 114(10), 2419–2431 (2018).
- [388] P. Aspenström. The Intrinsic GDP/GTP Exchange Activities of Cdc42 and Rac1 Are Critical Determinants for Their Specific Effects on Mobilization of the Actin Filament System. *Cells* 8(7) (2019).
- [389] X. Guo, K. A. Schrader, Y. Xu, and J. W. Schrader. Expression of a constitutively active mutant of M-Ras in normal bone marrow is sufficient for induction of a malignant mastocytosis/mast cell leukemia, distinct from the histiocytosis/monocytic leukemia induced by expression of activated H-Ras. *Oncogene* 24(14), 2330–2342 (2005).
- [390] M. Takeuchi, T. Shichinohe, N. Senmaru, and others. The dominant negative H-ras mutant, N116Y, suppresses growth of metastatic human pancreatic cancer cells in the liver of nude mice. *Gene therapy* 7(6), 518–526 (2000).
- [391] G. Carpenter and S. Cohen. Epidermal growth factor. *The Journal of biological chemistry* 265(14), 7709–7712 (1990).
- [392] S. Lewis-Saravalli, S. Campbell, and A. Claing. ARF1 controls Rac1 signaling to regulate migration of MDA-MB-231 invasive breast cancer cells. *Cellular signalling* 25(9), 1813–1819 (2013).
- [393] B. Wojciak-Stothard and A. J. Ridley. Rho GTPases and the regulation of endothelial permeability. *Vascular Pharmacology* 39(4-5), 187–199 (2002).
- [394] A. Dendorfer, S. Wolfrum, M. Wagemann, and others. Pathways of bradykinin degradation in blood and plasma of normotensive and hypertensive rats. *American journal of physiology. Heart and circulatory physiology* 280(5), H2182–8 (2001).
- [395] A. Graness, S. Hanke, F. D. Boehmer, and others. Protein-tyrosine-phosphatase-mediated epidermal growth factor (EGF) receptor transinactivation and EGF receptor-independent stimulation of mitogen-activated protein kinase by bradykinin in A431 cells. *The Biochemical journal* 347(Pt 2), 441–447 (2000).
- [396] C.-M. Yang, C.-S. Chien, Y.-H. Ma, and others. Bradykinin B2 Receptor-Mediated Proliferation via Activation of the Ras/Raf/MEK/MAPK Pathway in Rat Vascular Smooth Muscle Cells. *Journal of Biomedical Science* 10(2), 208–218 (2003).
- [397] P. Kucheryavy, J. He, V. T. John, and others. Superparamagnetic iron oxide nanoparticles with variable size and an iron oxidation state as prospective imaging agents. *Langmuir* 29(2), 710–716 (2013).

- [398] P. Tartaj, M. Del Puerto Morales, S. Veintemillas-Verdaguer, and others. The preparation of magnetic nanoparticles for applications in biomedicine. *Journal of Physics D: Applied Physics* 36(13), R182–R197 (2003).
- [399] M. A. Hink, R. A. Griep, J. W. Borst, and others. Structural Dynamics of Green Fluorescent Protein Alone and Fused with a Single Chain Fv Protein*. *Journal of Biological Chemistry* 275(23), 17556–17560 (2000).
- [400] A. Yamagishi, K. Narumiya, M. Tanaka, and others. Core Amino Acid Residues in the Morphology-Regulating Protein, Mms6, for Intracellular Magnetite Biomineralization. *Scientific reports* 6, 35670 (2016).
- [401] T. L. Moore, L. Rodriguez-Lorenzo, V. Hirsch, and others. Nanoparticle colloidal stability in cell culture media and impact on cellular interactions. *Chemical Society reviews* 44(17), 6287–6305 (2015).
- [402] A. Plan Sangnier, A. B. van de Walle, A. Curcio, and others. Impact of magnetic nanoparticle surface coating on their long-term intracellular biodegradation in stem cells. *Nanoscale* 11(35), 16488–16498 (2019).
- [403] D. Liße, C. P. Richter, C. Drees, and others. Monofunctional stealth nanoparticle for unbiased single molecule tracking inside living cells. *Nano letters* 14(4), 2189–2195 (2014).
- [404] I. Gessner and I. Neundorf. Nanoparticles Modified with Cell-Penetrating Peptides: Conjugation Mechanisms, Physicochemical Properties, and Application in Cancer Diagnosis and Therapy. *International journal of molecular sciences* 21(7), 2536 (2020).
- [405] K. Kim and W. G. Lee. Electroporation for nanomedicine: a review. *Journal of Materials Chemistry B* 5(15), 2726–2738 (2017).
- [406] P. Mcneil and E. Warder. Glass beads load macromolecules into living cells. *Journal of cell science* 88(5), 669–678 (1987).
- [407] M. Gavutis, S. Lata, P. Lamken, and others. Lateral ligand-receptor interactions on membranes probed by simultaneous fluorescence-interference detection. *Biophysical Journal* 88(6), 4289–4302 (2005).
- [408] T. Wedeking, S. Löchte, O. Birkholz, and others. Spatiotemporally Controlled Reorganization of Signaling Complexes in the Plasma Membrane of Living Cells. *Small* 11(44), 5912–5918 (2015).
- [409] M. Machacek, L. Hodgson, C. Welch, and others. Coordination of Rho GTPase activities during cell protrusion. *Nature* 461(7260), 99–103 (2009).

- [410] O. Pertz. Spatio-temporal Rho GTPase signaling - where are we now? *Journal of cell science* 123(Pt 11), 1841–1850 (2010).
- [411] J. Riedl, A. H. Crevenna, K. Kessenbrock, and others. Lifeact: a versatile marker to visualize F-actin. *Nature Methods* 5(7), 605–607 (2008).
- [412] A. L. Szymczak-Workman, K. M. Vignali, and D. A. A. Vignali. Design and construction of 2A peptide-linked multicistronic vectors. *Cold Spring Harbor Protocols* 2012(2), 199–204 (2012).
- [413] E. M. Hildebrand and J. Dekker. Mechanisms and Functions of Chromosome Compartmentalization. *Trends in Biochemical Sciences* 45(5), 385–396 (2020).
- [414] D. L. J. Lafontaine, J. A. Riback, R. Bascetin, and C. P. Brangwynne. The nucleolus as a multiphase liquid condensate. *Nature reviews. Molecular cell biology* 22(3), 165–182 (2021).
- [415] K. Rhine, V. Vidaurre, and S. Myong. RNA Droplets. *Annual review of biophysics* 49, 247–265 (2020).
- [416] X. Wu, Q. Cai, Z. Feng, and M. Zhang. Liquid-Liquid Phase Separation in Neuronal Development and Synaptic Signaling. *Developmental cell* 55(1), 18–29 (2020).
- [417] R.-S. Nozawa, T. Yamamoto, M. Takahashi, and others. Nuclear microenvironment in cancer: Control through liquid-liquid phase separation. *Cancer science* 111(9), 3155–3163 (2020).
- [418] V. L. Feigin, E. Nichols, T. Alam, and others. Global, regional, and national burden of neurological disorders, 1990–2016: a systematic analysis for the Global Burden of Disease Study 2016. *The Lancet Neurology* 18(5), 459–480 (2019).
- [419] E. R. Dorsey and B. R. Bloem. The Parkinson Pandemic-A Call to Action. *JAMA neurology* 75(1), 9–10 (2018).
- [420] S. J. Chia, E.-K. Tan, and Y.-X. Chao. Historical Perspective: Models of Parkinson’s Disease. *International journal of molecular sciences* 21(7) (2020).
- [421] G. DeMaagd and A. Philip. Parkinson’s Disease and Its Management: Part 1: Disease Entity, Risk Factors, Pathophysiology, Clinical Presentation, and Diagnosis. *P & T: a peer-reviewed journal for formulary management* 40(8), 504–532 (2015).
- [422] J. Jankovic and E. K. Tan. Parkinson’s disease: etiopathogenesis and treatment. *Journal of Neurology, Neurosurgery & Psychiatry* 91(8), 795–808 (2020).
- [423] J. A. Obeso, M. C. Rodriguez-Oroz, C. G. Goetz, and others. Missing pieces in the Parkinson’s disease puzzle. *Nature medicine* 16(6), 653–661 (2010).

- [424] W. Poewe, K. Seppi, C. M. Tanner, and others. Parkinson disease. *Nature reviews. Disease primers* 3, 17013 (2017).
- [425] H. Braak and K. Del Tredici. Assessing fetal nerve cell grafts in Parkinson’s disease. *Nature medicine* 14(5), 483–485 (2008).
- [426] C. R. Freed, P. E. Greene, R. E. Breeze, and others. Transplantation of embryonic dopamine neurons for severe Parkinson’s disease. *The New England journal of medicine* 344(10), 710–719 (2001).
- [427] I. J. Fox, G. Q. Daley, S. A. Goldman, and others. Stem cell therapy. Use of differentiated pluripotent stem cells as replacement therapy for treating disease. *Science* 345(6199), 1247391 (2014).
- [428] G. Hargus, O. Cooper, M. Deleidi, and others. Differentiated Parkinson patient-derived induced pluripotent stem cells grow in the adult rodent brain and reduce motor asymmetry in Parkinsonian rats. *Proceedings of the National Academy of Sciences* 107(36), 15921–15926 (2010).
- [429] S. Kriks, J.-W. Shim, J. Piao, and others. Dopamine neurons derived from human ES cells efficiently engraft in animal models of Parkinson’s disease. *Nature* 480(7378), 547–551 (2011).
- [430] M. Sundberg, H. Bogetofte, T. Lawson, and others. Improved cell therapy protocols for Parkinson’s disease based on differentiation efficiency and safety of hESC-, hiPSC-, and non-human primate iPSC-derived dopaminergic neurons. *Stem cells* 31(8), 1548–1562 (2013).
- [431] M. Wernig, J.-P. Zhao, J. Pruszak, and others. Neurons derived from reprogrammed fibroblasts functionally integrate into the fetal brain and improve symptoms of rats with Parkinson’s disease. *Proceedings of the National Academy of Sciences* 105(15), 5856–5861 (2008).
- [432] N. S. Roy, C. Cleren, S. K. Singh, and others. Functional engraftment of human ES cell-derived dopaminergic neurons enriched by coculture with telomerase-immortalized midbrain astrocytes. *Nature medicine* 12(11), 1259–1268 (2006).
- [433] R. Heumann, R. Moratalla, M. T. Herrero, and others. Dyskinesia in Parkinson’s disease: mechanisms and current non-pharmacological interventions. *Journal of neurochemistry* 130(4), 472–489 (2014).
- [434] W. R. Gowers. *A manual of diseases of the nervous system*. P. Blakiston’s Son & Co., Philadelphia, (1899).
- [435] M. R. Capecchi. High efficiency transformation by direct microinjection of DNA into cultured mammalian cells. *Cell* 22(2), 479–488 (1980).

14 | Abbreviations

α GFPnb	anti-GFP nanobody enhancer
aa	amino acids
AID	autoinhibitory domain
ATP	adenosine triphosphate
B	magnetic flux density
B_s	saturation flux density
B_r	remanence flux density
χ	magnetic susceptibility
c	concentratin
C	conserved domain
CAAX	C = cysteine, A = aliphatic, X = any amino acid
CDR	circular dorsal ruffles
CIB1	Calcium and integrin-binding protein 1
cLSM	confocal laser scanning microscope
CT	cell replacement therapy
d	diameter
d_{hydro}	hydrodynamic diameter
DA	dopaminergic
DALYs	disability-adjusted life years
DARPin	designed ankyrin repeat protein
DH	Dbl homology domain
DLS	dynamic light scattering
DMEM	Dulbecco's Modified Eagle's Medium
DMSO	Dimethylsulfoxid
DNA	deoxyribonucleic acid
Dvl	Dishevelled
DVLO	named after Derjaguin, Landau, Verwey, and Overbeek
<i>E. coli</i>	<i>Escherichia coli</i>
EDC	1-ethyl-3-(3-dimethylaminopropyl)carbodiimide
EDL	electric double layer
EGF	epithelial growth factor
ERK	extracellular signal-regulated kinase
F	filamentous

F	force
F_s	surface fraction
Fab	antigen-binding fragment
Fc	crystallizable fragment
FCS	fluorescence correlation spectroscopy
FP	fluorescent protein
FPLC	fast protein liquid chromatography
FRAP	fluorescence recovery after photobleaching
FRET	Förster resonance energy transfer
Fv	variable fragment
Fzd	Frizzled
GAP	GTPase-activating protein
Grb2	Growth factor receptor-bound protein 2
GDI	GDP dissociation inhibitor
GDP	guanosine diphosphate
GEF	guanine nucleotide exchange factor
GFP	green fluorescent protein
GTP	guanosine triphosphate
GPCR	G protein-coupled receptor
H	magnetic field strength
H	heavy
H6	His6-Tag
<i>H. Sapiens</i>	<i>Homo Sapiens</i>
HB	20 mM HEPES, pH 7.5
HBS	20 mM HEPES, 150 mM NaCl, pH 7.5-8.0
HCAbs	heavy-chain antibodies
HF	histone(-like) folds
HTL	HaloTag ligand
I	intensity
IDP	intrinsic disordered protein
IDR	intrinsic disordered region
IgG	immunoglobulin γ
IMAC	immobilized metal affinity chromatography
IPTG	isopropyl β -D-1-thiogalactopyranoside
k_B	Boltzmann constant
K_A	equilibrium association constant
k_a	association rate constant
K_D	equilibrium dissociation constant
k_d	dissociation rate constant
L	light
μ_0	permeability of the vacuum

μ_B	Bohr magneton
μ_r	relative magnetic permeability
m	magnetic moment
M	magnetization
MACS	magnet-assisted cell separation
MagIcS	Magnetic Intracellular Stealth nanoparticles
MAPK	mitogen-activated protein kinase
MCP	maghemite core particles
mEGFP	monomeric enhanced GFP
MNP	magnetic nanoparticle
MPI	magnetic particle imaging
MRI	magnetic resonance imaging
MW	molecular weight
n	number
NES	nuclear export sequence
NIR	near-infrared
NLS	nuclear localization sequence
NP	nanoparticle
PA	phosphatidic acid
PAK-CRIB	Cdc42/Rac1 interactive binding motif of PAK
PBD	p21 binding domain
PCP	planar cell polarity
PCR	polymerase chain reaction
PEG	Polyethylene glycol
PFA	paraformaldehyde
PIP ₂	phosphatidylinositol-4,5-bis-phosphate
PIP ₃	phosphatidylinositol(3,4,5)-trisphosphates
PH	pleckstrin homology domain
pH	potential of hydrogen
PLL	poly-L-lysine
POI	proteins of interest
PR	proline-rich domain
PTM	post-translational modification
Q	quantum yield
r	radius
RBD	Ras binding domain
REM	Ras Exchange Motif
RGD	Arginine, Glycine, Aspartate
RIf	Reflectance interferometry
ROI	region of interest
RT	room temperature

RTK	Receptor tyrosine kinases
SEC	size-exclusion chromatography
SPION	Superparamagnetic iron oxide nanoparticle
SQUID	superconducting quantum interference device
SOS	Son of Sevenless
SOS _{cat}	catalytic region of SOS
scFv	single-chain variable fragment
syMagIcS	Synthetic Magnetic Intracellular Stealth nanoparticles
τ_A	attraction time constant
τ_R	relaxation time constant
T	temperature
TEM	transmission electron microscopy
TIRF	total internal reflection fluorescence
TIRFS	total internal reflection fluorescence spectroscopy
UCNP	upconversion nanoparticle
UV	ultraviolet
V	variable domain
V	volume
VIS	visible

15 | Acknowledgements

My thanks go to my supervisor Prof. Dr. Jacob Piehler for the opportunity to work on an exciting and highly interdisciplinary topic. For his helpful ideas and discussions, and the freedom and technical equipment, which made it possible to try out many techniques and approaches and to be tinkerers. It has been a pleasure to be able to follow my interdisciplinary interest also in the context of my doctoral studies. I am very grateful to have had the opportunity to learn an incredible amount in the Biophysics Department.

I thank our small subgroup, the Team for Cellular Nanobiotechnology. Dr. Domenik Liße for supervising my work, for the knowledge and expertise he imparted to me, and working together on these exciting research topic. Many thanks for the scientific discussions and private conversations. I would like to thank Annette Budke-Giesecking for her great support in the lab work and for keeping everything running in the CellNanOs lab.

Besides Annette Budke-Giesecking, I would also like to thank the other Biophysics Technical Assistants Hella Kenneweg, Gabriele Hikade and Wladislaw Kohl for their diligent and indispensable lab work, and Elli Olaru, Carmen Larberg and Dr. Uli Kunze for their organizational work. Without you, the biophysics department would not work. I would also like to thank my bachelor students Anabelle Ludi and Hannah Klein for their great work, the scientific exchange and the collaboration were very enjoyable.

For supervising the LLPS topic, I would like to thank Dr. Changjiang You. Thanks for opening another exciting avenue for application of magnetic nanoparticles and for the many exciting discussions. The more intense collaboration towards the end of my lab work was a great pleasure.

A big thanks to all current and former members of the biophysics group and for the great atmosphere. You have made the last years an unforgettable and wonderful time. Among them Dr. Julia Flesch, Dr. Sara Löchte, Dr. Christoph Drees, Dr. Junel Sotolongo-Bellón, Thomas Meyer, Dr. Michael Holtmannspötter, Dr. Michael Philippi, Julia Dohle, Florian Eull, Tim Wedeking, Hauke Winkelmann, Dr. Max Hafer, Isabelle Watrinet, Christian Richter, Shirin Kappelhoff, Dr. Domenik Liße, Dr. Christine Knies, Dr. Rainer Kurre, Dr. David Richter, Dr. Oliver Birkholz, Janosch Bajorath. I am grateful for many hours together in the lab and the exciting scientific exchange, and also for many private hours and conversations, such as the long barbecue evenings. I am grateful that I could get to

know them and share (non-)scientific interests.

Thanks to my office colleagues from the CellNanOs research building for the great time. I thank Dr. Rainer Kurre and Dr. Michael Holtmannspötter for their supervision of the microscopy facility and for always being there with advice and support.

I would like to thank the members of the MAGNEURON project at the Institut Curie in Paris, the PHENIX laboratory at the Sorbonne University in Paris, Keele University, the University of Birmingham and the Ruhr-University Bochum for their collaboration on this very fascinating topic and the great time I had at project meetings, workshops and laboratory visits with great people in different places.

For the support and the new exciting and inspiring work in a pleasant atmosphere I would like to thank my colleagues at b.value AG.

Hugh thanks for proofreading go to Dr. Christoph Drees, Dr. Julia Flesch und Markus Müller.

I would especially like to thank my family, my partner Markus Müller, my friends, and most of all my parents. For their loving support throughout my life, for always being there for me, and for the wonderful time I spend with them. I owe them everything that I am.

16 | Curriculum Vitae

Personal information

Name Marie Kappen
Date, Place of Birth 09.06.1991 in Winterberg

Education

04/2017 - present Doctoral Candidate
Department of Biology/Chemistry of the University of Osnabrück
Division of Biophysics - Prof. Dr. Jacob Piehler
Team for Cellular Nanobiotechnology
MAGNEURON Project Horizon2020 FET open No. 686841

03/2014 - 09/2016 Master of Science (M.Sc.) - Bio- and Nanotechnologies (1,4)
University of Applied Sciences Südwestfalen
Specialization: Biomedical engineering
Master thesis: Characterization of the interaction of α -taxilin with
cellular and viral proteins of the hepatitis B and hepatitis C viruses.
Paul Ehrlich Institute, Division of Virology, Prof. Dr. Eberhard Hildt

09/2010 - 05/2014 Bachelor of Science (B.Sc.) - Bio- and Nanotechnologies (2,0)
University of Applied Sciences Südwestfalen
Specialization: Biomedical engineering
Bachelor thesis: Optimization of plasma depyrogenation on catheter
systems using undulating vacuum.
Prof. Dr. Kilian Hennes

08/2001 - 06/2010 Abitur
Geschwister - Scholl - Gymnasium, Winterberg

08/1997 - 07/2001 Katholische Grundschule Züschen

Work experience

- 04/2021 - present b.value AG - Investment Manager
- 04/2017 - 09/2021 Research assistant
Department of Biology/Chemistry of the University of Osnabrück
Division of Biophysics - Prof. Dr. Jacob Piehler
- 01/2017 - 02/2017 botiss biomaterials GmbH - Product Manager
- 03/2016 - 09/2016 Internship - Paul-Ehrlich-Institut
Division of Virology, Prof. Dr. Eberhard Hildt

Publications, Conferences, Award

J. Flesch, M. Kappen, C. Drees, C. You, J. Piehler. Self-assembly of robust gold nanoparticle monolayer architectures for quantitative protein interaction analysis by LSPR spectroscopy. *Analytical and Bioanalytical Chemistry* 412(14), 3413–3422 (2020).

M. Philippi, C. P. Richter, M. Kappen, I. Watrinet, Y. Miao, M. Runge, L. Jorde, S. Korneev, M. Holtmannspötter, R. Kurre, J.C. Holthuis, K. C. Garcia, A. Plückthun, M. Steinhart, J. Piehler, C. You. Biofunctional Nanodot Arrays in Living Cells Uncover Synergistic Co-Condensation of Wnt Signalodroplets. *Small* 18(50), 2203723 (2022).

G. Xiong, D. Huang, L. Lu, X. Luo, Y. Wang, S. Liu, M. Chen, S. Yu, M. Kappen, C. You, S. Lu, Y. Yu, J. Lu, F. Lin. Near-Infrared-II Light Induced Mild Hyperthermia Activate Cisplatin-Artemisinin Nanoparticle for Enhanced Chemo/Chemodynamic Therapy and Immunotherapy. *Small Methods* 6(9), 2200379 (2022).

M. Kappen, E. Secret, J. Gemperle, J. Flesch, M. Coppey, C. Menager, D. Liße, J. Piehler. Biofunctional coating of synthetic magnetic nanoparticles enables magnetogenetic control of protein functions inside cells (in progress).

MagMeet, Copenhagen. 12th International Conference on the Scientific and Clinical Applications of Magnetic Carriers. Poster presentation (05/2018).

Symposium tribute to Maxime Dahan. Poster presentation (10/2019).

Project meetings and workshop - MAGNEURON Project (Horizon2020), participation in the Integrated Research Training Group (IRTG) - SFB 944. Aussois, Berlin, Brussels, Keele, Paris, Tübingen, Osnabrück. Talk and poster presentation.

1st place HKCM Magnet Award - M. Kappen, A. Budke-Giesecking, D. Liße - Project: Magnetic manipulation of human cell functions using magnetic nanobiomaterials (2018).

17 | Declaration

I hereby declare that the presented thesis ‘Magnetogenetic Control of Cellular Functions using Biofunctionalized Magnetic Nanoparticles Inside Living Cells’ was prepared entirely on my own and I have not used outside sources without declaration in the text. Any concepts or quotations applicable to these sources are clearly attributed to them. I have not attempted a doctorate before.

Place, date

Marie Kappen